

Aus der Abteilung „Molekulare Genetik“ am
Deutschen Institut für Ernährungsforschung

Elucidation of the epithelial sodium channel as
a salt taste receptor candidate and search for
novel salt taste receptor candidates

Dissertation

zur Erlangung des akademischen Grades
“doctor rerum naturalium”
(Dr. rer. nat.)
in der Wissenschaftsdisziplin „Molekulare Genetik“

eingereicht an der
Mathematisch-Naturwissenschaftlichen Fakultät
der Universität Potsdam

von
Katja Riedel

Potsdam, den 10.10.2011

Parts of this thesis were published:

Stahler, F.; Riedel, K.; Demgensky, S.; Neumann, K.; Dunkel, A.; Taubert, A.; Raab, B.; Behrens, M.; Raguse, J.-D.; Hofman, T.; Meyerhof, W. (2008): **A role of the epithelial sodium channel in human salt taste transduction?** *Chem Percept* 1 (1), 78-90

Riedel, K. (2008): **Characterization of the human lingual epithelial sodium channel.** 18th European Chemoreception Research Organization Congress (ECRO), Portorož, Slowenien

Published online at the
Institutional Repository of the University of Potsdam:
URL <http://opus.kobv.de/ubp/volltexte/2012/5876/>
URN <urn:nbn:de:kobv:517-opus-58764>
<http://nbn-resolving.de/urn:nbn:de:kobv:517-opus-58764>

1	INTRODUCTION.....	6
1.1	ANATOMY OF THE HUMAN TASTE SYSTEM.....	6
1.2	PHYSIOLOGY OF HUMAN SALT PERCEPTION.....	9
1.3	MOLECULAR MECHANISM OF SALT TASTE TRANSDUCTION.....	10
1.3.1	<i>Amiloride-sensitive, Na⁺-specific, salt taste transduction in rodents.....</i>	<i>11</i>
1.3.2	<i>Amiloride-insensitive, cation unspecific, salt taste transduction in rodents.....</i>	<i>12</i>
1.3.3	<i>Proposed mechanism of rodent salt taste transduction.....</i>	<i>12</i>
1.4	HUMAN SALT TASTE TRANSDUCTION.....	13
1.5	ENAC, AMILORIDE-SENSITIVE SALT TASTE RECEPTOR IN MICE.....	14
1.6	AIM OF THIS THESIS.....	16
2	MATERIAL AND METHODS.....	17
2.1	CHEMICALS.....	17
2.2	CULTURE MEDIA FOR BACTERIA AND BACTERIOPHAGES.....	17
2.3	BACTERIAL STRAINS, STORAGE AND GROWTH CONTROL.....	17
2.3.1	<i>Strains.....</i>	<i>17</i>
2.3.2	<i>Frozen bacterial stocks.....</i>	<i>18</i>
2.3.3	<i>Growth control.....</i>	<i>18</i>
2.4	BACTERIOPHAGES.....	18
2.5	EUKARYOTIC CELLS.....	18
2.5.1	<i>Cell line and culture medium.....</i>	<i>18</i>
2.5.2	<i>Cultivation and passaging of HEK293T cells.....</i>	<i>19</i>
2.6	PLASMIDS.....	19
2.7	STANDARD MOLECULAR BIOLOGICAL METHODS: DNA.....	19
2.7.1	<i>Isolation of DNA.....</i>	<i>19</i>
2.7.2	<i>Synthesis of cDNA from RNA.....</i>	<i>20</i>
2.7.2.1	<i>DNase digestion and standard cDNA synthesis from RNA.....</i>	<i>20</i>
2.7.2.2	<i>Synthesis of RACE ready cDNA using SMART RACE.....</i>	<i>20</i>
2.7.2.3	<i>Synthesis of RACE ready cDNA using First Choice®RLM-RACE.....</i>	<i>20</i>
2.7.3	<i>Quantification.....</i>	<i>21</i>
2.7.4	<i>Restriction digest of DNA.....</i>	<i>21</i>
2.7.5	<i>DNA agarose gel electrophoresis.....</i>	<i>21</i>
2.7.6	<i>Polymerase chain reaction (PCR).....</i>	<i>22</i>
2.7.6.1	<i>PCR using FIREPol DNA polymerase.....</i>	<i>22</i>
2.7.6.2	<i>Colony PCR using FIREPol DNA polymerase.....</i>	<i>22</i>
2.7.6.3	<i>PCR using Pfu DNA polymerases.....</i>	<i>23</i>
2.7.6.4	<i>PCR using Advantage® 2 PCR Kit.....</i>	<i>23</i>
2.7.6.5	<i>Correction of point mutations of a plasmid by PCR.....</i>	<i>23</i>
2.7.6.6	<i>Preparation of digoxigenin-labeled DNA probes.....</i>	<i>24</i>
2.7.7	<i>Purification of DNA fragments.....</i>	<i>24</i>
2.7.7.1	<i>Isolation using agarose gel electrophoresis.....</i>	<i>24</i>
2.7.7.2	<i>Isolation using column purification.....</i>	<i>24</i>
2.7.8	<i>Cloning of DNA fragments.....</i>	<i>24</i>
2.7.8.1	<i>Cloning of DNA polymerase amplicons into a T-overhang vector.....</i>	<i>24</i>
2.7.8.2	<i>Cloning of restricted DNA fragments into dephosphorylated plasmids.....</i>	<i>25</i>
2.7.8.3	<i>Transformation by heat shock.....</i>	<i>25</i>
2.7.9	<i>Nucleotide sequence analysis.....</i>	<i>25</i>
2.8	STANDARD MOLECULAR BIOLOGICAL METHODS: RNA.....	26
2.8.1	<i>Isolation of total RNA.....</i>	<i>26</i>
2.8.2	<i>Isolation of mRNA/Poly(A) RNA.....</i>	<i>26</i>
2.8.3	<i>Quantification.....</i>	<i>26</i>
2.8.4	<i>Synthesis of cRNA for injection in Xenopus laevis oocytes.....</i>	<i>26</i>
2.8.5	<i>Preparation of digoxigenin-labeled cRNA probes.....</i>	<i>27</i>

2.8.6	<i>Purification by precipitation with ammonium acetate</i>	27
2.8.7	<i>Denaturing agarose gel electrophoresis</i>	27
2.9	IN SITU HYBRIDIZATION OF DIGOXIGENIN LABELED RNA PROBES	28
2.9.1	<i>Buffers</i>	28
2.9.2	<i>Tissue sample origin</i>	28
2.9.3	<i>Cryo sections</i>	29
2.9.4	<i>In situ hybridization procedure</i>	29
2.9.5	<i>Colorimetric detection</i>	29
2.9.6	<i>Data analysis</i>	30
2.10	FILTER HYBRIDIZATION OF DNA PROBES: SOUTHERN BLOT, COLONY BLOT AND DOT BLOT	30
2.10.1	<i>Reagents and equipment</i>	30
2.10.2	<i>Dot Blot</i>	30
2.10.3	<i>Southern Blot</i>	31
2.10.4	<i>Colony Blot</i>	31
2.10.5	<i>Plaque lift</i>	31
2.10.6	<i>Hybridization and stringency washes</i>	32
2.10.7	<i>Chromogenic detection</i>	32
2.10.8	<i>Chemiluminescent detection of southern blots</i>	32
2.11	IMMUNOHISTOCHEMISTRY.....	33
2.11.1	<i>Reagents and equipment</i>	33
2.11.2	<i>Paraffin sections</i>	33
2.11.3	<i>Procedure for immunoperoxidase labeling</i>	34
2.11.4	<i>Detection with DAB</i>	34
2.11.5	<i>Detection with fluorescent dyes</i>	35
2.11.6	<i>Data analysis</i>	35
2.12	IMMUNOCYTOCHEMISTRY.....	35
2.12.1	<i>Cultivation of HEK293T-cells for immunocytochemistry</i>	35
2.12.2	<i>Transient transfection in 24-well plates for immunocytochemistry</i>	35
2.12.3	<i>Procedure</i>	36
2.12.4	<i>Data analysis</i>	36
2.13	IN VITRO TRANSLATION.....	36
2.14	WESTERN BLOT	37
2.14.1	<i>Reagents for SDS polyacrylamide gel electrophoresis</i>	37
2.14.2	<i>Reducing SDS polyacrylamide gel electrophoresis (SDS-PAGE)</i>	38
2.14.3	<i>Semi-dry blot of proteins from SDS-polyacrylamide gels</i>	38
2.14.4	<i>Immunolabeling of transferred proteins</i>	39
2.15	BACTERIOPHAGE CDNA LIBRARY OF MACACA FOLIATE PAPILLAE.....	39
2.15.1	<i>Sample origin and process status of the library</i>	39
2.15.2	<i>Plating and titering of the cDNA library λ-phages</i>	40
2.15.3	<i>Large scale in vivo excision of pBK-CMV phagemid vector</i>	40
2.15.4	<i>Scaling down the size of cDNA library pools of macaca foliate papillae</i>	41
2.16	ELECTROPHYSIOLOGY	41
2.16.1	<i>Preparation of Xenopus laevis oocytes and cRNA injection</i>	41
2.16.1.1	<i>Buffers and culture media</i>	41
2.16.1.2	<i>Isolation of Xenopus laevis oocytes</i>	42
2.16.1.3	<i>Microinjection of cRNA</i>	42
2.16.2	<i>Two electrode voltage clamp (TEVC) using OpusXpress 6000A</i>	43
2.16.3	<i>Data recording</i>	44
2.16.4	<i>Data analysis</i>	44
2.17	DATABASE SEARCH, MULTIPLE SEQUENCE ALIGNMENT AND PHYLOGNETIC TREE CONSTRUCTION	44
3	RESULTS	46
3.1	POSSIBLE INVOLVEMENT OF ENAC IN HUMAN SALT TASTE PERCEPTION.....	46
3.1.1	<i>Localization of ENaC subunit mRNAs in lingual taste tissue</i>	46

3.1.2	<i>Localization of ENaC subunit proteins in lingual taste tissue</i>	48
3.1.3	<i>Validation of δ-ENaC protein localization in taste pores</i>	50
3.2	A ROLE FOR DELTA-ENaC IN RODENT TASTE TRANSDUCTION?	54
3.3	EVOLUTION OF EPITHELIAL SODIUM CHANNEL SUBUNIT DELTA IN MICE	55
3.3.1	<i>Vertebrate δ-ENaC proteins and genetic organization of the mouse ortholog</i>	56
3.3.2	<i>Comparative gene mapping of human SCNN1D to mouse chromosome 4</i>	58
3.3.3	<i>Scnn1d evolution by repetitive elements and identification of retroviral sequences</i>	61
3.3.3.1	Evolution of endogenous retrovirus insertion disrupting mouse Scnn1d.....	61
3.3.3.2	Analysis of mutagenicity of Scnn1d disrupting endogenous retroviruses	62
3.3.4	<i>Expression analysis and characterization of mouse Scnn1d</i>	64
3.3.4.1	RT-PCR analysis.....	64
3.3.4.2	Identification of Scnn1d transcripts by rapid amplification of cDNA ends	65
3.3.4.3	Analysis of Scnn1d transcripts for coding competence.....	68
3.3.4.4	Analysis Scnn1d derived polypeptides for ion channel like function.....	73
3.4	TASTE TISSUE CDNA LIBRARY SCREENING FOR ENaC INTERACTION PARTNERS & NOVEL SALT TASTE RECEPTOR CANDIDATES	77
3.4.1	<i>Characterization of cDNA library from Macaca mulatta foliate papillae</i>	77
3.4.2	<i>Development of functional expression assay for cDNA library screening</i>	81
3.4.3	<i>Screening for interaction partners of human $\beta\gamma$-ENaC and novel ion channels potential involved in salt taste transduction</i>	83
3.4.4	<i>Screening for novel interaction partners of human δ-ENaC potential involved in human salt taste transduction</i>	90
4	DISCUSSION	97
4.1	INVOLVEMENT OF EPITHELIAL SODIUM CHANNEL IN HUMAN SALT TASTE TRANSDUCTION	97
4.2	TASTE TISSUE CDNA LIBRARY SCREENING FOR SALT TASTE RECEPTOR CANDIDATES	101
4.3	EVOLUTION OF DELTA-ENaC IN MICE	103
5	SUMMARY	110
6	ZUSAMMENFASSUNG	111
7	APPENDIX	112
7.1	ABBREVIATIONS.....	112
7.2	PLASMIDS	113
7.3	PRIMERS.....	114
7.4	RIBOPROBES FOR <i>IN SITU</i> HYBRIDIZATION.....	115
7.5	<i>MACACA MULATTA</i> CDNA LIBRARY POOLS	116
7.6	ANTISERA, BLOCKING PEPTIDES AND AVIDIN REAGENTS	117
7.7	MULTIPLE SEQUENCE ALIGNMENT	118
7.8	COMPANIES AND KIT SPECIFICATIONS.....	121
8	LITERATURE	122
9	ACKNOWLEDGEMENT/DANKSAGUNG	133
10	STATUTORY DECLARATION/EIDESSTÄTTLICHE ERKLÄRUNG	134

1 Introduction

1.1 Anatomy of the human taste system

The human gustatory system is able to distinguish between different basic taste qualities. So far, we know the aversive bitter taste, the attractive sweet- and umami-taste as well as the predominant aversive but also attractive sour taste. Similarly, the generally appetitive salty taste can be perceived as an aversive taste stimulus as well, serving as a detector for salt containing food. Currently, fatty taste sensation is discussed as additional basic taste quality (Khan & Besnard, 2009; Galindo *et al.*, 2011). All taste categories have evolved to ensure the supply with essential nutrients as well as the protection against rotten food and toxic substances. Taste qualities are detected by specialized epithelial taste receptor cells (TRCs) located within the oral cavity. Polarized TRCs are organized in taste buds, which are directly innervated by afferent nerve fibers transmitting taste information to the brain. A vertebrate taste bud consists of approximately 100 cells, forming an onion-like structure as shown in Fig. 1.1 (Lindemann, 2001). At the apical site of the bud a taste pore is formed by elongated taste bud cells, which are sealed by tight junctions from the extracellular space (Fig. 1.1; Jahnke & Baur, 1979; Simon, 1992). The pore enables direct contact of TRCs to tastants in the oral cavity, which are solved and transported by saliva (Spielman, 1990) supplied by parotid, submandibular, sublingual glands and von Ebner glands (Baum, 1993). A classification of mammalian taste bud cells was established by electron microscopy of rabbit taste bud cells (Murray *et al.*, 1969), while structural studies of human and primate taste bud cells strongly suggest similar organization in humans (Azzali *et al.*, 1996; Farbman *et al.*, 1985; Paran *et al.*, 1975). According to distinct optical appearance and morphological properties, taste bud cells were classified into dark (type I), light (type II) and intermediate (type III) cells (Fig. 1.1, Witt *et al.*, 2003; Murray *et al.*, 1969; Murray, 1973; Reutter & Witt, 1993; Royer & Kinnamon, 1991; Finger, 2005). In extension to Murray's nomenclature basal cells were designated as type IV and V cells (Fig. 1.1; Murray *et al.*, 1969; Reutter & Witt, 1993). Subsequent biochemical analyses confirmed distinct physiological functions of morphologic individual cell types I-IV and revealed complex interactions of cells within a taste bud unit (reviewed in Chaudhari & Roper, 2010). Biochemical analyses identified unexcitable (Medler *et al.*, 2003) and most frequent type I cells as glial-like supporting cells, competent for clearance of taste bud neurotransmitters (Lawton *et al.*, 2000, Bartel *et al.*, 2006; Dvoryanchikov *et al.*, 2007) as well as for K⁺ homeostasis (Dvoryanchikov *et al.*, 2009). In addition to glial function,

possible role of type I cells in salt taste transduction is discussed (Vandenbeuch *et al.*, 2008). Compounds perceived as sweet, bitter and umami are recognized by G-protein coupled taste receptors, which are restricted to distinct populations of type II cells (Margolskee, 2002, DeFazio *et al.*, 2006, Chandrashekar *et al.*, 2006, Tomchik *et al.*, 2007). Thus, type II cells are often termed as receptor cells, transmitting gustatory signals to the nervous system. Latter is achieved by release of neurotransmitters with complex autocrine and paracrine activity (Chaudhari & Roper, 2010, Dvoryanchikov *et al.*, 2011). In particular ATP stimulates afferent nerve fibers and presynaptic type III cells as well as type II cells (Finger *et al.*, 2005, Huang, Y. J. *et al.*, 2007, Romanov *et al.*, 2007). Excitable type III cells, are the solely cell type within a taste bud possessing synapses as well as synaptosome associated proteins, enabling synaptic signaling to the brain (Murray *et al.*, 1969, DeFazio *et al.*, 2006, Nelson, G. M. & Finger, 1993). However, beside serotonergic synaptic signaling, paracrine cell to cell communication with type II cells via secretion of further neurotransmitter is evident (Huang, Y. J. *et al.*, 2007, Herness & Zhao, 2009). In addition to neuronal function, type III cells are directly involved in detection of gustatory sour stimuli (Huang, Y. A. *et al.*, 2008).

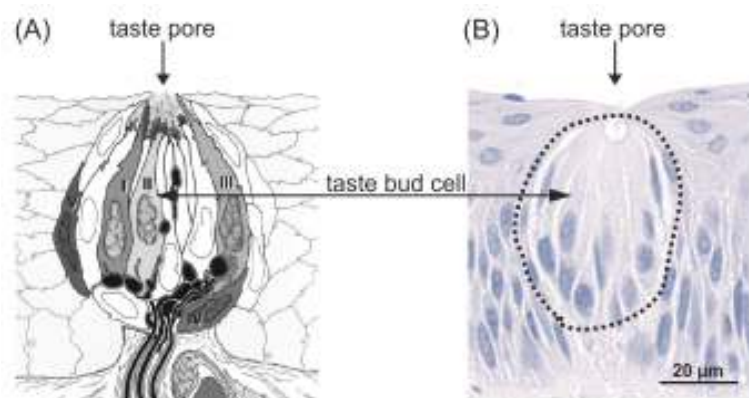


Fig. 1.1: Mammalian taste bud. **A** Idealized schematic view of a mammalian taste bud, showing one representative cell of type I, II, III, IV and V cells (see text for details, Witt *et al.*, 2003). **B** Hematoxylin-eosin staining of human circumvallate papillae showing one taste bud encircled with a dotted line (Behrens *et al.*, 2011).

Strikingly, cells harboring taste signaling components, like PLC β 2, α -gustducin and taste receptors, are not confined to oral taste buds but were also identified in respiratory as well as gastrointestinal epithelium (Shah *et al.*, 2009, Bezencon *et al.*, 2007, Margolskee *et al.*, 2007; Behrens & Meyerhof, 2010). In airways, these solitary chemosensory receptor cells were shown to sense noxious stimuli via bitter taste receptors, mediating defense responses (Shah *et al.*, 2009). Moreover, a role in metabolic regulation is likely, as an

influence on secretion of incretin hormones like glucagon-like peptide 1 is evident (Jang *et al.*, 2007, Rozengurt & Sternini, 2007, Behrens & Meyerhof, 2010). However, future studies will clarify functions of extra oral taste cells.

Mammalian oral taste cells are spread within the oral epithelium of the tongue, soft palate, larynx, pharynx and epiglottis, where they are assembled into taste buds (Lalonde & Eglitis, 1961). Taste buds of the dorsal tongue epithelium are distributed within three types of gustatory papillae, namely fungiform-, foliate- and circumvallate papillae (Fig. 1.2).

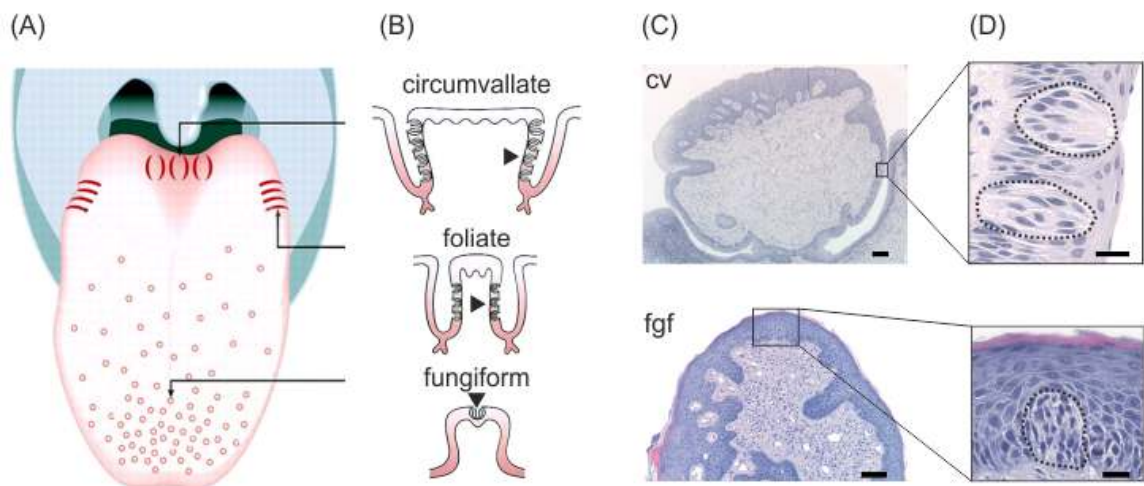


Fig. 1.2: Human tongue anatomy. **A** Idealized schematic drawing, showing the localization of circumvallate-, foliate- and fungiform papillae (according to Hoon *et al.*, 1999). **B** Structure of the gustatory papillae in expanded scale. Foliate and circumvallate taste buds are orientated close to lateral trenches (►). Fungiform taste buds locate at top of fungiform papillae, facing the oral cavity (▼). **C** Hematoxylin-eosin staining of human circumvallate (cv) and fungiform (fgf) papillae. Scale bar represents 100 μm . Rectangles mark representative regions shown in larger magnification in D (Behrens *et al.*, 2011). **D** Magnification of C. Taste bud(s) are encircled with a dotted line. Scale bar represents 20 μm .

The anatomy of taste papillae is similar among humans and other mammals (reviewed by Witt and colleagues (Witt *et al.*, 2003)). The mushroom-shaped fungiform papillae are unevenly distributed over the anterior part of the human tongue with a total amount of about 320 papillae (Fig. 1.2). They contain an average of approximately 3.5 taste buds each (Witt *et al.*, 2003) and are innervated by nerve fibers of the chorda tympani (CT), a branch of the VII. cranial nerve (Whitehead *et al.*, 1987; Miller & Reedy, 1990a, b; Witt *et al.*, 2003). At the lateral posterior borders of the human tongue the leaf-like foliate papillae are located, consisting of up to 20 clefts. Numerous taste buds are spread within the epithelium inbetween the ridges, with a total of about 1300 taste buds (Fig. 1.2; Mochizuki, 1939). Foliate taste buds are predominantly innervated by the

glossopharyngeal nerve (NG), which is the IX. cranial nerve (Guth, 1957). Further, innervation by CT was observed for anterior parts of foliate papillae (Oakley, 1970; Oakley *et al.*, 1993). In the posterior part of the tongue, the circumvallate papilla is located (Fig. 1.2). This largest gustatory papilla is surrounded by a deep trench and exclusively innervated by the NG (Guth, 1957). Humans possess three to eighteen circumvallate papillae with approximately 250 taste buds each (Munch, 1896, Arey *et al.*, 1935; Mochizuki, 1939). Foliate papillae and circumvallate are supplied with saliva, directly secreted into the trenches by van Ebner glands (Riva *et al.*, 1999).

1.2 Physiology of human salt perception

Evolutionary transition of organisms from saline marine water to land came along with the need for mechanisms maintaining water and electrolyte balance. Ions or electrolytes play crucial roles in cell physiology, in particular the major ions of extra- and intracellular fluids, K^+ , Na^+ and Cl^- , respectively (Jensen, 1980). Electrochemical gradients are constituted between K^+ -rich intracellular fluids and Na^+ - and Cl^- -rich extracellular fluids, maintained by the Na^+/K^+ -pump (Rapoport, 1970, 1971). This ion imbalance generates resting membrane potential and osmotic equilibrium, which is essential for water homeostasis and plasma volume (Diamond, 1965, 1966; Mahnensmith & Aronson, 1985). Moreover, entry of Na^+ -ions through membranes of excitable cells and opposite flux of K^+ -ions is the essential driving force of action potentials. Thus enabling nerve conductance and muscle contraction by changing the resting potential of membranes (Hodgkin & Huxley, 1952). Furthermore, Na^+ - and Cl^- -ions are involved in pH regulation, maintaining the acid-base balance of cells via Na^+/H^+ -exchange and Na^+ -dependent Cl^-/HCO_3^- -exchange (Simchowicz & Roos, 1985). The mammalian body loses major electrolytes by excretion and secretion, while the loss of Na^+ - and Cl^- -ions is approximately five times higher than the loss of K^+ (Schuster *et al.*, 1990). This reasonably shows the need for ingestion of more NaCl than other salts and suggests that salt perception has evolved to maintain electrolyte homeostasis stimulating the ingestion of Na^+ - and Cl^- -rich food (Daniels & Fluharty, 2004). However, our daily diet distinguishes markedly from the diet of our ancestors, which evolved in a nutrient-poor environment (Morris *et al.*, 2008; O'Shaughnessy & Karet, 2006). Today we ingest more carbohydrates, proteins and salt due to their unlimited availability, while our metabolism has not comparably changed. The daily salt intake, mostly ingested by common table salt (> 99 % NaCl), is increased at least 10 fold in our modern society (O'Shaughnessy & Karet, 2006). Clinical trials and epidemiological studies showed the association of high Na^+ -intake with raised blood

pressure in hypertensive as well as in normotensive individuals (Brown *et al.*, 2009; Frost *et al.*, 1991; Intersalt, 1988; Law *et al.*, 1991b, a Law *et al.*, 1991b, a ; Weinberger, 1996). Hypertension by itself was shown to be a predominant risk for cardiovascular diseases (Prospective study, 1995; Lawes *et al.*, 2003), which is the worlds leading cause of death (Rodgers *et al.*, 2002). Therefore the World Health Organization (WHO) recommends the reduction of daily Na⁺ intake to less than 85 mmol (WHO/FAO, 2003). However, the mean daily Na⁺ intake reaches up to 294 mmol in some populations, which is more than three times than recommended (Brown *et al.*, 2009). Unfortunately, reduction of NaCl content within food is not well accepted by consumers (Breslin & Beauchamp, 1997).

1.3 Molecular mechanism of salt taste transduction

As NaCl is the purest salt stimulus to humans early studies addressed the perception of NaCl. First evidence for an ion channel mediated Na⁺-ion transport in salt taste transduction was given by DeSimone and colleagues, showing inward directed Na⁺-currents through isolated dog tongue epithelium (DeSimone *et al.*, 1981). Psychophysical studies confirmed crucial role of chloride in salt perception of NaCl, revealing Na⁺ in combination with larger anions as for example acetate or sulphate as less salty (Murphy *et al.*, 1981; van der Klaauw & Smith, 1995). This anion effect was also evident in rat CT and NG nerve recordings, showing that gustatory nerve responses by Na⁺ are most prominent when chloride was the anion (Ye *et al.*, 1991, 1993, Kitada *et al.*, 1998). Small chloride ions are permeable to tight junctions allowing electro neutral para- and transcellular diffusion of Na⁺, which is achieved by minimizing the emerging electropositive potential (Ye *et al.*, 1991). Larger anions are less permeable and might inhibit the Na⁺ entry to prevent a charge separation (Ye *et al.*, 1993, 1994; Elliott & Simon, 1990; Roper, 2007). Nevertheless, also Na₂SO₄, NaHCO₃, KCl, NH₄Cl, (NH₄)₂SO₄, LiCl, MgCl₂ and CaCl₂ are perceived as salty with sour and bitter side tastes (Perty, 1838; von Skramlik, 1933; Cardello, 1978; van der Klaauw & Smith, 1995). Insight into the nature of ion channels mediating the Na⁺-flux was found using amiloride, an inhibitor of voltage-insensitive Na⁺ channels (Baer *et al.*, 1967), which is itself tasteless to rats (Bernstein & Hennessy, 1987). Thereby, studies in rodents showed that salty taste involves at least two transduction mechanisms: a Na⁺-specific, amiloride-sensitive pathway as well as an amiloride-insensitive, cation unspecific pathway triggered by various cations including Na⁺ (reviewed by Gilbertson, 1993; Lindemann, 1996; Gilbertson & Margolskee, 2003; DeSimone & Lyall, 2006).

1.3.1 Amiloride-sensitive, Na⁺-specific, salt taste transduction in rodents

Behavioral studies showed that mucosal applied amiloride abolished the ability of rats to discriminate NaCl from other salts, pointing to a dominant role of amiloride-sensitive Na⁺-taste in rodent salt taste transduction (Hill *et al.*, 1990; Spector *et al.*, 1996). Further, amiloride inhibited the response of a rat CT nerve fiber population, which was specific for Na⁺-ions (Schiffman *et al.*, 1983; Brand *et al.*, 1985; Heck *et al.*, 1984). Consistent with that, whole cell patch clamp recordings of isolated rat fungiform taste bud cells showed amiloride-sensitive currents in response to NaCl (Avenet & Lindemann, 1988; Doolin & Gilbertson, 1996; Yoshida *et al.*, 2009b). In anterior fungiform taste buds Na⁺ taste transduction is most likely mediated by amiloride-sensitive Na⁺-channels. Thus, the amiloride-sensitive epithelial Na⁺ channel (ENaC) became a candidate as the rodent Na⁺-specific salt taste receptor, which was verified by multiple lines of evidences. On the one hand ion channels of isolated taste buds and taste bud cells possess ENaC-like electrophysiological properties. These include the inhibition by amiloride in a nanomolar range (DeSimone *et al.*, 1984), the remarkable cationic selectivity to Na⁺- and Li⁺-ions over K⁺-ions (DeSimone *et al.*, 1984; Gilbertson *et al.*, 1992) as well as the small single channel conductance (Avenet, 1992). On the other hand, presence of ENaC subunit mRNAs and proteins was shown in rodent fungiform taste bud cells (Kretz *et al.*, 1999; Lin *et al.*, 1999; Shigemura *et al.*, 2005). Finally, conditional knock out of α -ENaC subunit led to loss of amiloride-sensitive salt taste in mice, verifying a crucial role of ENaC in rodent salt taste transduction (Chandrashekar *et al.*, 2010). However, exact subunit composition of ENaC in salt taste sensing cells was not subject of this study, lacking co-localization data for fungiform taste bud cells (Chandrashekar *et al.*, 2010). Notably, presence of all essential α -, β - and γ -ENaC subunits is necessary to assemble into a functional Na⁺ channel *in vitro* (Canessa *et al.*, 1994).

Gustatory NaCl responses of NG nerve fibers, innervating posterior taste buds, are not suppressed by amiloride, revealing topographic differences of Na⁺-specific taste transduction (Formaker & Hill, 1991; Frank, 1991). Thus $\alpha\beta\gamma$ -ENaC is not a candidate for transduction of Na⁺-taste mediated by posterior taste bud cells. However, ENaC mRNAs were found in vallate taste buds of rat, pointing to a role in posterior taste transduction (Kretz *et al.*, 1999, Chandrashekar *et al.*, 2010). However, lack of functional ENaC channels in vallate taste buds might be explained by non-overlapping expression pattern of ENaC subunits as shown for mice vallate taste bud cells (Chandrashekar *et al.*, 2010).

1.3.2 Amiloride-insensitive, cation unspecific, salt taste transduction in rodents

Amiloride-insensitive salt taste transduction, triggered by various cations including Na⁺, is less well studied. Gustatory responses of rodent NG nerve fibers to various salts including NaCl, KCl, NH₄Cl, CaCl₂ were shown to be unaffected by amiloride (Formaker & Hill, 1991, Frank, 1991, Kitada *et al.*, 1998). However, also amiloride insensitive CT nerve fibers are evident, implying a second, amiloride-insensitive salt taste transduction pathway (Brand *et al.*, 1985; Geran & Spector, 2007, Sollars & Bernstein, 1994, Formaker & Hill, 1988, Doolin & Gilbertson, 1996). Consistent with amiloride-insensitive gustatory responses of NG and CT, amiloride-insensitive currents of isolated rodent fungiform and vallate taste bud cells were evident (Avenet & Lindemann, 1988; Doolin & Gilbertson, 1996; Yoshida *et al.*, 2009b). Modulation of rat amiloride-insensitive CT-responses by cetylpyridinium chloride (CPC) as well as by transient receptor potential vanilloid receptor 1 (TRPV1) agonists pointed to TRPV1 as a candidate for amiloride-insensitive Na⁺-taste receptor (DeSimone *et al.*, 2001, Lyall *et al.*, 2004). However, CPC acts ambivalent, as high concentrations block entire CT-response to NaCl, while low concentrations show enhancing effects (DeSimone *et al.*, 2001). Minor CPC-sensitivity was observed for CT-responses evoked by KCl, NH₄Cl and CaCl₂ (DeSimone *et al.*, 2001; Lyall *et al.*, 2004). Contradictory, TRPV1 knockout mice lacking NaCl induced amiloride-insensitive CT responses (Lyall *et al.*, 2004), were able to taste NaCl in the presence of amiloride in an independent study (Ruiz *et al.*, 2006). Moreover, CPC was without effect on NaCl recognition in a conditioned taste aversion experiment with rats (St John & Hallagan, 2005). Thus, TRPV1 variant might be involved in rodent amiloride-insensitive Na⁺ taste transduction, but cannot account for entire amiloride-insensitive NaCl, KCl, NH₄Cl or CaCl₂ gustatory CT-responses. Notably, no data are available about CPC-sensitivity of rodent amiloride-insensitive NG cation responses. Thus, data suggest contribution of distinct, so far unknown, amiloride-insensitive ion channels, mediating rodent cation unspecific gustatory CT-response.

1.3.3 Proposed mechanism of rodent salt taste transduction

Based on the presented data a salt taste transduction mechanism was proposed for fungiform taste receptor cells (reviewed in DeSimone & Lyall, 2006; Gilbertson, 1993; Gilbertson & Margolskee, 2003; Lindemann, 1996). Thereby, Na⁺-ions enter taste cells via amiloride-sensitive and -insensitive ion channels (see Fig. 1.3). K⁺-, NH₄⁺- and Ca²⁺-ions enter via amiloride-insensitive ion channels located in apical membranes of taste cells

(Fig. 1.3). Salt sensing taste cells are possibly type I taste bud cells (Vandenbeuch *et al.*, 2008), which has not been shown undoubtedly. Transcellular ion current could depolarize the cell, which results in calcium influx via voltage-dependent calcium channels (Fig. 1.3). Subsequent neurotransmitter release and activation of afferent nerve fibers would lead to further signal transduction to the brain. Furthermore, Na^+ , K^+ , NH_4^+ and Ca^{2+} and Cl^- ions can diffuse through paracellular shunts of taste cells (Fig. 1.3). Basolateral amiloride-sensitivity of taste tissue has been shown by submucosal application of amiloride (Mierson *et al.*, 1996). Thus, it is likely that Na^+ -ions can enter taste cells also via basolateral amiloride-sensitive ion channels. The resting membrane potential is reconstituted by active ion channels at the basolateral membrane, as Na^+/K^+ ATPase (Fig. 1.3).

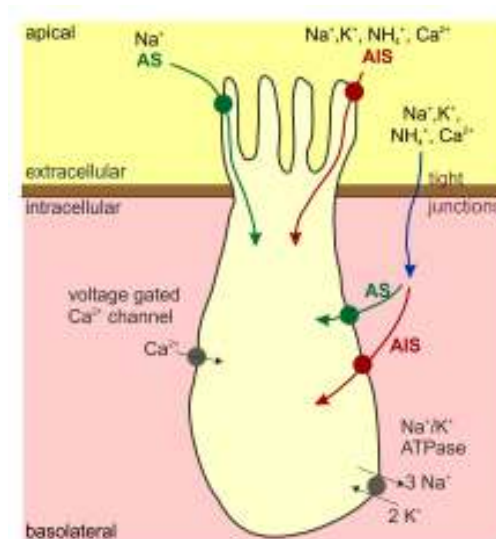


Fig. 1.3: Simplified illustration of proposed salt taste transduction mechanism in fungiform papillae. Schematically shown is ion influx via apical and basolateral amiloride-sensitive (AS, green) and amiloride-insensitive (AIS, red) ion channels. Paracellular ion flux through tight junctions of a taste bud is illustrated in blue (see text for details).

1.4 Human salt taste transduction

In contrast to rodents, human salt taste perception is dominated by amiloride-insensitive transduction pathway, while involvement of amiloride-sensitive pathway was also evident in some psychophysical studies (Feldman *et al.*, 2003; Feldman *et al.*, 2009; Halpern, 1998; Ossebaard & Smith, 1995; Schiffman *et al.*, 1983). However, CT nerve recordings in closely related primates revealed amiloride-sensitive as well as amiloride insensitive components mediating salt taste perception (Hellekant *et al.*, 1997b; Hellekant *et al.*, 1997a; Sato *et al.*, 1975). Thus, human salt taste transduction mechanisms likely involve amiloride-sensitive as well as -insensitive salt taste receptors. However, an

involvement of the rodent Na⁺ selective amiloride-sensitive salt taste receptor ENaC in human salt taste transduction has not been studied so far. Moreover, modulatory effects of CPC on primate Na⁺ taste responses were not investigated, yet. Thus, irrespective of unclear molecular basis of Na⁺ selective amiloride-sensitive salt taste perception in humans, identity of amiloride-insensitive salt taste receptor is unknown, as well.

1.5 ENaC, amiloride-sensitive salt taste receptor in mice

Rodent amiloride-sensitive salt taste receptor ENaC is a heteromultimeric, voltage gated, constitutive active Na⁺ channel, belonging to the metazoan ENaC/DEG ion channel superfamily (Kellenberger, S. & Schild, 2002). ENaC/DEG channel subunits share highly conserved protein domains as well as subunit topology with two hydrophobic transmembrane domains, a large extracellular loop and short intracellular N- and C-termini (Benos & Stanton, 1999). Four paralogous ENaC subunits (α , β , γ , and δ) have been identified in mammals, sharing an amino acid identity of approximately 27-37 % (McDonald *et al.*, 1994; McDonald *et al.*, 1995; Voilley *et al.*, 1994; Waldmann *et al.*, 1995; Canessa *et al.*, 1993; Canessa *et al.*, 1994; Lingueglia *et al.*, 1993; Lingueglia *et al.*, 1994; Ahn *et al.*, 1999). Alpha, β - and γ -ENaC subunits are widely expressed in polarized epithelial cells of kidney, lung, gastrointestinal tract and skin (Kellenberger, S. & Schild, 2002). However, δ -ENaC, originally cloned from human kidney, shows highest expression levels in testis, brain, pancreas and ovary (Waldmann *et al.*, 1995, Lingueglia *et al.*, 1996, Yamamura *et al.*, 2004). With 37 % amino acid identities, δ -ENaC is phylogenetically closely related to its α -ENaC paralog (Waldmann *et al.*, 1995). Interestingly mouse δ -ENaC was classified as pseudogene by automated genome annotation (Wheeler *et al.*, 2008), while parts of δ -ENaC mRNAs were detected by RT-PCR in BALB/c and CD-1 mice (Hernandez-Gonzalez *et al.*, 2006; Nie *et al.*, 2009). However, no experimental data about possible function of mouse δ -ENaC or its evolutionary origin are available (Sayers *et al.*, 2011). Thus, it is not clear if δ -ENaC is a gene, coding for a functional protein product, or a transcribed pseudogene in mice. Studies concerning salt taste perception concentrated on α -, β -, and γ -ENaC subunits, strongly suggesting an involvement of $\alpha\beta\gamma$ -ENaC in rodent amiloride-sensitive Na⁺ taste transduction (see 1.3.1). A possible role of δ -ENaC in rodent salt taste transduction has not been studied, so far.

In heterologous expression systems α -ENaC as well as human δ -ENaC are able to form an amiloride-sensitive Na⁺ channels with low Na⁺ conductance (Canessa *et al.*, 1994, Garty, 1994, McDonald *et al.*, 1995). Maximal channel activity is reached by co-expression of

$\beta\gamma$ -ENaC subunits, which potentiate Na^+ currents *in vitro* (Canessa *et al.*, 1994, Waldmann *et al.*, 1995). In contrast, β - and γ -ENaC alone are not able to form a functional Na^+ channel, emphasizing the profound role of α -ENaC or δ -ENaC for channel assembly (Canessa *et al.*, 1994, McDonald *et al.*, 1995, Waldmann *et al.*, 1995). In addition to functional replacement of human α -ENaC by δ -ENaC and *vice versa*, $\alpha\delta\beta\gamma$ -ENaC channels assembled by a all four subunits were evident *in vitro* (Ji, H. L. *et al.*, 2006). Heterologously expressed human $\alpha\beta\gamma$ - and $\delta\beta\gamma$ -ENaC differ significantly in their pharmacological properties, while $\alpha\delta\beta\gamma$ -ENaC shows intermediate properties (Ji, H.-L. *et al.*, 2004; Ji, H. L. *et al.*, 2006; Waldmann *et al.*, 1995). The amiloride sensitivity of $\delta\beta\gamma$ -ENaC is much less pronounced, showing inhibition by micro molar concentrations, while $\alpha\beta\gamma$ -ENaC is sensitive to nano molar amounts of the diuretic. Further distinctive properties of $\delta\beta\gamma$ -ENaC are higher permeability to Na^+ -ions than to Li^+ -ions, higher single channel conductance for Na^+ as well as activation by protons (Ji, H.-L. & Benos, 2004; Yamamura *et al.*, 2004), emphasizing critical role of subunit composition for ion channel function. Physiological relevance and regulation of $\alpha\beta\gamma$ -ENaC is intensively studied *in vivo*, verifying its crucial role in Na^+ transport in lung and kidney (reviewed in Rossier, B. C. *et al.*, 2002). Disorders of either α -, β - or γ -ENaC affect renal Na^+ transport and cause severe disease patterns as Liddle's syndrome or type I pseudohypoaldosteronism in humans (Chang *et al.*, 1996; Lingueglia *et al.*, 1996). Moreover, knock out of either α -, β - or γ -ENaC leads to neonatal or early postnatal death in mice and underlines the need for the presence of all three subunits to form a functional Na^+ channel *in vivo* (Hummler *et al.*, 1996; Merillat *et al.*, 2009). In contrast to well characterized $\alpha\beta\gamma$ -ENaC, little is known about physiological role of $\delta\beta\gamma$ -ENaC. Currently, a possible role of δ -ENaC in Na^+ regulation of human respiratory epithelium (Bangel-Ruland *et al.*, 2010) and in proton sensing in human brain, skin and esophagus (Yamamura *et al.*, 2004, Yamamura *et al.*, 2008b, Yamamura *et al.*, 2008a) are discussed.

1.6 Aim of this thesis

The need for Na⁺ reduction in our food is evident and recommended by WHO, while reduction of NaCl content within food is not well accepted by consumers. Strikingly, molecular basis of human salt taste transduction remains elusive. Strong amiloride-sensitivity of rodent salt taste perception revealed $\alpha\beta\gamma$ -ENaC as amiloride-sensitive Na⁺ taste receptor. However, situation in humans is unclear. On the one hand human psychophysical studies point to largely amiloride-insensitive Na⁺ taste perception. On the other hand primates possess amiloride-sensitive as well as amiloride-insensitive gustatory responses to NaCl, implying a role of both salt taste transduction pathways in humans. A role of $\alpha\beta\gamma$ -ENaC and in particular a role of less amiloride-sensitive $\delta\beta\gamma$ -ENaC in human Na⁺ taste perception was not shown, so far. Expression analyses, carried out in our group, showed the presence of all ENaC subunit mRNAs in fungiform papillae, circumvallate papillae and non-chemosensory lingual epithelium ($\alpha \sim \beta > \gamma \gg \delta$) with highest expression levels in non-chemosensory epithelium. Presence of α -, β -, γ - and δ -ENaC in human taste bud cells, which is a prerequisite for an involvement of ENaC in human Na⁺ taste transduction, was not analyzed so far.

In this study, cellular localization of ENaC mRNAs and proteins will be evaluated in human fungiform and circumvallate taste bud cells to elucidate a potential involvement of α -, β -, γ - and δ -ENaC in human salt taste transduction. Additionally, expression and evolution of mouse *Scnn1d* gene will be investigated in order to clarify a role for δ -ENaC in rodent taste transduction. Moreover, novel amiloride-insensitive and cation unspecific human salt taste receptor candidates should be identified by screening of a taste tissue cDNA library. Taken together this study aims to validate and to identify salt taste receptor candidates, which will provide novel insights in mechanisms of human salt taste transduction. This knowledge would enable further research concerning suitable salt substitutes and/or enhancer to reduce pathophysiology of high salt intake.

2 Material and methods

2.1 Chemicals

Chemicals were purchased from Merck (Darmstadt, GER), Roth (Karlsruhe, GER), Sigma-Aldrich (Munich, GER) and VWR (Darmstadt, GER) or otherwise indicated.

2.2 Culture media for bacteria and bacteriophages

Media were prepared with deionized water and adjusted to neutral pH of 7 to 7.5. All media were heat-sterilized for 20 min at 120 °C. Heat sensitive supplements as antibiotics, maltose and glucose were added filter-sterilized after autoclaving. Over night cultures of all *E. coli* strains were incubated at 37 °C. Liquid cultures were shaken at 200 rpm using a standard shaking incubator.

LB-medium

LB-broth 10 g/l tryptone or peptone; 5 g/l yeast extract; 10 g/l NaCl
LB-broth + LB-broth supplemented with 10 mM MgSO₄; 0.2 % (w/v) maltose
LB-agar LB-broth supplemented with 15 g/l agar; poured into petri dishes and stored at 4 °C

For selected growth of bacteria or bacteriophages media were supplemented with 100 µg/ml ampicillin, 50 µg/ml kanamycin or 15 µg/ml tetracycline.

2xYT-broth

16 g/l tryptone or peptone; 10 g/l yeast extract; 5 g/l NaCl

SOC-broth

20 g/l tryptone or peptone; 5 g/l yeast extract; 10 mM NaCl; 2.5 mM KCl; added after sterilization: 10 mM MgCl₂; 20 mM glucose. SOC-broth was stored in aliquots at -20 °C.

NZY-medium

NZY-broth 10 g/l NZ-amine (caseine hydrolysate); 5 g/l yeast extract;
5 g/l NaCl; 2 g/l MgSO₄ * 7 H₂O
NZY-agar NZY-broth incl. 15 g/l agar
NZY-top agar NZY-broth incl. 0.7 % (w/v) agarose

Filter-sterilized supplements

Ampicillin (100 mg/ml in dH ₂ O)	Kanamycin (50 mg/ml in dH ₂ O)
Tetracyclin (15 mg/ml in dH ₂ O)	Glucose (1 M in dH ₂ O)
Maltose (20 % (w/v) in dH ₂ O)	MgSO ₄ (1 M in dH ₂ O)

2.3 Bacterial strains, storage and growth control

2.3.1 Strains

E. coli BIOBlue 10⁹ chemically competent cells (Bioline)

genotype: recA1 endA1 gyrA96 thi-1 hscR17(r_km_k⁺) supE44 relA1 lac [F' proAB lacI^qZΔM15 TN10(Tet^r)]

application: routine cloning

E. coli One Shot® chemically competent cells (Invitrogen)

genotype: F- *mcrA* Δ (*mrr-hsdRMS-mcrBC*) ϕ 80*lacZ* Δ M15 Δ *lacX74* *recA1* *araD139* Δ (*araleu*)
7697 *galU galK rpsL* (StrR) *endA1 nupG*

application: routine cloning

E. coli XL1-Blue MRF' (Stratagene)

genotype: *recA1* Δ (*mcrA*)183 Δ (*mcrCB-hsdSMR-mrr*)173 *endA1 gyrA96 thi-1 supE44*
relA1 lac [F' *proAB lacI^qZ* Δ M15 TN10(Tet^r)]

application: host strain for λ -phages

E. coli XL0LR (Stratagene)

genotype: *recA1* Δ (*mcrA*)183 Δ (*mcrCB-hsdSMR-mrr*)173 *endA1 gyrA96 thi-1 relA1 lac* [F'
proAB lacI^qZ Δ M15 TN10(Tet^r)] Su⁻ (nonsuppressing) λ_r (lambda resistant)

application: host strain for phagemids, *in vivo* excision

2.3.2 Frozen bacterial stocks

Genetically modified bacteria were stored as frozen bacterial stocks using the cryoprotectant glycerole. Therefore aliquots of over night cultures were supplemented with 15 % (v/v) glycerole and immediately frozen at -80 °C.

2.3.3 Growth control

Growth control of E. coli strains was performed by turbidity measurements at 600 nm in the standard spectrophotometer Ultrospec 3100pro (Biochrom). Sterile media served as a blank control.

2.4 Bacteriophages

Packaging extract λ -phages (Stratagene)

HsdR⁻ McrA⁻ McrBC⁻ McrF⁻ Mrr⁻ (restriction minus)

application: cDNA library construction from highly methylated DNA.

ExAssist® interference-resistant helper phage (Stratagene)

application: generation of filamentous phages, which are used for subsequent *in vivo* excision of pBK-CMV vector from λ -ZAP®II library phages.

2.5 Eukaryotic cells

2.5.1 Cell line and culture medium

cell line: HEK293T G α 16gust 44 (in the following abbreviated as "HEK293T cells")

culture medium:

Dulbecco's Modified Eagle Medium incl. 4.5 g/l glucose ('DMEM^{plus}', Invitrogen)

supplemented with: 10 % (v/v) fetal bovine serum (Biochrom);

2 mM glutamine (200 mM; Invitrogen);

100 U/ml penicillin (10000 U/ml; Sigma-Aldrich);

100 μ g/ml streptomycin (10 mg/ml; Sigma-Aldrich);

200 μ g/ml G418 (100 mg/ml; Calbiochem)

transfection medium: 'DMEM'

Dulbecco's Modified Eagle Medium incl. 4.5 g/l glucose (Invitrogen)

2.5.2 Cultivation and passaging of HEK293T cells

Cells were maintained in disposable 10 cm cell culture dishes, suitable for adherent cell culture. Incubation at 37 °C, 5 % CO₂ partial pressure and water saturated atmosphere was carried out in a standard cell incubator. HEK293T cells grown to 90 % confluence were passaged by detaching the cells with trypsin. Therefore the culture medium was removed and cells were washed with 5 ml prewarmed 1 x PBS (10 x stock: 0.2 M NaHPO₄; 0.8 M Na₂HPO₄; 0.65 M NaCl; pH 7.4). Thereafter the cells were incubated with 3 ml prewarmed trypsin (0.05 % (w/v) trypsin; 0.5 mM EDTA in 1 x PBS; filter sterilized) for 2 to 3 minutes at room temperature. Afterwards 3 ml of prewarmed DMEM^{plus} was added to stop the reaction and the cells were detached and separated by pipetting up and down. Cells were centrifuged for 5 minutes at 900 g and resuspended in 10 ml DMEM^{plus}. An appropriate amount was used to seed the cells in new culture dishes to a confluence of 10 to 15 %. HEK293T cells were used upon passages 25 to 30. Cells maintained cryoprotected with 10 % DMSO at -80 °C were thawed quickly at 37 °C and transferred into a culture dish with DMEM^{plus} without antibiotics. Cells were allowed to adhere for 2 to 4 hours before medium was removed by aspiration and fresh medium was added. After 24 hours DMEM^{plus} was exchanged by DMEM^{plus} supplemented with geneticin 418, which is used to maintain the stable expression of the G-protein G α _{16gust 44}.

2.6 Plasmids

See appendix 7.2, Tab. 7.1.

2.7 Standard molecular biological methods: DNA

2.7.1 Isolation of DNA

Small amounts of plasmid DNA from *E. coli* was prepared using Jetquick Plasmid Miniprep Spin Kit (GENOMED) according to recommendations of the supplier. Preparations were carried out using two to four milliliters of a 2xYT-overnight culture. Plasmid DNA was eluted in 50 μ l dH₂O preheated to 70 °C and stored at -20 °C.

Large scale plasmid preparations were carried out using the NukleoBond PC 500 Kit (Macherey-Nagel). Preparations were carried out using 200 ml LB- or 100 ml 2xYT-overnight cultures. Plasmid DNA was resuspended in an adequate amount (100 to 1000 μ l) of dH₂O preheated to 70 °C and stored at -20 °C.

2.7.2 Synthesis of cDNA from RNA

2.7.2.1 DNase digestion and standard cDNA synthesis from RNA

Total RNA or Poly(A) RNA prepared according to 2.8.1 was used for synthesis of complementary DNA (cDNA). To remove genomic DNA from the samples, a DNase digestion was carried out using 1.5 µg total RNA or 2.5 µl of Poly(A) RNA, 1 x DNase I reaction buffer (10 x, Invitrogen), 10 mM DTT (0.1 M, Invitrogen), 20 U RiboLock™ Ribonuclease Inhibitor (40 U/µl, Fermentas) and 1 U DNase I Amp Grade (1 U/µl, Invitrogen) in a final volume of 15 µl. The reaction was incubated one hour at room temperature. DNase I was then inactivated by addition of 2 mM EDTA (25 mM, Invitrogen) and incubation for 15 minutes at 68 °C. Two third (1µg) of DNA free RNA was supplemented with 3 µg random primers (3 µg/µl, Invitrogen) and incubated at 72 °C for 5 minutes. The reaction was then chilled on ice for 5 minutes and completed by the addition of 1 x First Strand Buffer (10 x, Invitrogen), 0.5 mM dNTPs (100 mM each, Fermentas), 3 mM MgCl₂ (25 mM, Invitrogen), 10 U RiboLock™ Ribonuclease Inhibitor (40 U/µl, Fermentas) and 200 U Superscript™ II Reverse Transcriptase (200 U/µl, Invitrogen) in a final volume of 21 µl. After incubation at 42 °C for 60 minutes 200 U of reverse transcriptase was added and incubation was extended for additional 30 minutes. The reaction was inactivated by incubation at 72 °C for 15 minutes and designated as +RT. One third (0.5 µg) of DNA free RNA served as a negative control and was incubated without reverse transcriptase and designated as -RT. The volume of the +RT and -RT reactions were adjusted to 25 ng initially used RNA per µl and stored at -20 °C. Routinely two µl of synthesized cDNA was used for RT-PCR analysis (see 2.7.6.1).

2.7.2.2 Synthesis of RACE ready cDNA using SMART RACE

RACE ready cDNA from 1 µg DNA free total RNA or 2.5 µl DNA free Poly(A) RNA was prepared according to 2.7.2.1. Instead of random primers 5'-CDS primer A; SMART II A oligo and 3'-CDS primer were used to generate 5' and 3' ready cDNA. Five prime RACE ready cDNA was obtained by incubating the DNase digested RNA with 0.6 µM 5'-CDS primer A (12 µM, Clontech) and 0.6 µM SMART II A oligo (12 µM, Clontech) at 72 °C for 5 minutes. Three prime RACE ready cDNA was obtained by incubation with 0.6 µM 3'-CDS primer A (12 µM, Clontech) at 72 °C for 5 minutes.

2.7.2.3 Synthesis of RACE ready cDNA using First Choice®RLM-RACE

Five prime RACE ready cDNA from 2 µg total RNA was prepared according to the protocol for small reactions recommended by the supplier (Ambion). Generation of 5' RACE ready cDNA included treatment with alkaline phosphatase, phenol chloroform

extraction and isopropanol precipitation as recommended. The RNA pellet was dissolved in 5 μ l of provided 1 x TAP buffer. One μ l served as minus-Tap control, while 4 μ l were further processed by incubation with pyrophosphatase and ligation with 5' RACE adapter. Two third of the ligation reaction as well as the minus-Tap control were used for reverse transcription (+RT) according to the supplied protocol. One third of the ligation reaction was used as negative control by incubation without reverse transcriptase (-RT). The volume of the +RT and -RT reactions were adjusted with dH₂O to 50 ng initially used RNA per μ l and stored at -20 °C.

Generation of 3' RACE ready cDNA was carried out as recommended (Ambion). Therefore 1 μ g of total RNA was directly used for reverse transcription using a 3' adaptor (+RT), while 0.5 μ g of total RNA served as a negative control for reverse transcription incubated without reverse transcriptase (-RT). The volume of the +RT and -RT reactions were adjusted to 50 ng initially used RNA per μ l and stored at -20 °C.

2.7.3 Quantification

Concentrations of DNA solutions was determined by measuring the absorption at 260 (A_{260}) and 280 (A_{280}) nm using a standard spectrophotometer Ultrospec 3100*pro* (Biochrom). For calculation of the concentration a conversion factor was used, taking into account that absorption of one corresponds to 50 μ g/ μ l DNA.

2.7.4 Restriction digest of DNA

Buffer concentration and incubation temperatures for restriction endonucleases were chosen according to the recommendations of the supplier (Fermentas). Analytical restriction digest using 2 μ l of a standard plasmid DNA Miniprep (see 2.7.1) was carried out with 1-3 units of restriction endonuclease(s) for 1-3 hours or overnight. Restricted DNA was analyzed by agarose gel electrophoresis (see 2.7.5). Restriction digested plasmid DNA for *in vitro* transcription (see 2.8.4) or *in vitro* translation (see 2.13) was obtained by incubation of 10 μ g plasmid DNA with 10 units endonuclease over night, in a final volume of 100 μ l. Linearized plasmid DNA was analyzed and purified by agarose gel electrophoresis (see 2.7.5 and 2.7.7). Restriction digested DNA for Southern Blot (see 2.10.3) was obtained by restriction of 1-15 μ g plasmid DNA with 10 units endonucleases over night, in a final volume of 30-40 μ l.

2.7.5 DNA agarose gel electrophoresis

Separation of DNA-fragments was carried out by agarose gel electrophoresis. Depending on expected fragment sizes 1-2 % (w/v) agarose (Serva or Invitrogen) was dissolved in 1 x

TAE buffer (50 x stock solution: 2 M Tris-base, 1 M acetic acid, 50 mM EDTA, pH 8) containing 0.3 µg/ml ethidium bromide (10 mg/ml in dH₂O) by heating in a microwave. Samples were loaded on the gel supplemented with 1 x loading buffer (6 x stock solution: 10 mM Tris-HCl, 60 mM EDTA, 60 % glycerol, 0.03 % bromophenol blue, 0.03 % xylene cyanol FF). For sizing and approximate quantification of DNA a molecular weight marker (GeneRuler™ ladder mix, Fermentas) was used. Electrophoresis was carried out using 1 x TAE as running buffer containing 0.3 µg/ml ethidium bromide at 5 to 7 V/cm. To visualize the DNA the gel was analyzed by exposition to ultraviolet irradiation (312 nm) using a photo documentation system (Syngene).

2.7.6 Polymerase chain reaction (PCR)

PCR was performed in order to amplify gene fragments from cDNA, plasmid DNA or DNA fragments using a T personal, T1 or T Gradient thermocycler (biometra). Each PCR reaction was assembled in 0.2 ml reaction tubes (Eppendorf). Negative control PCR reactions were performed in parallel using dH₂O and/or -RT (see 2.7.2.1) as a template. Five micro liters of the PCR reactions were analyzed using DNA agarose gel electrophoresis (see 2.7.5). See appendix 7.3 for a list of used primers.

2.7.6.1 PCR using FIREPol DNA polymerase

A typical PCR reaction of 25 or 50 µl using FIREPol DNA Polymerase (Solis BioDyne) contained template DNA (50 ng cDNA or 0.05-5 ng plasmid DNA or 50 ng genomic DNA), 1 x BD buffer (10 x, Solis BioDyne), 2 mM MgCl₂ (25 mM, Solis BioDyne), 0.2 mM dNTPs (2.5 mM each, Fermentas), 0.2 µM forward and 0.2 µM reverse primers (Eurofins MWG Operon), 1.5 U FIREPol DNA polymerase (5 U/µl).

Hot start PCR was carried out by addition of the DNA polymerase during 3-5 minutes of the initial denaturing step at 95 °C. Thereafter 25 to 39 cycles of denaturation (30 s at 95 °C), annealing (30 s at 40 °C to 70 °C) and polymerization (0.5 to 3 min at 72 °C) followed. A final annealing step for 5 minutes and polymerization step for 10 minutes completed the reaction. The reaction was then cooled to 4 °C and stored at 4 °C or -20 °C.

2.7.6.2 Colony PCR using FIREPol DNA polymerase

Colony PCR was used to analyze single *E.coli* colonies for the contained plasmid. Therefore a colony was picked with a sterile toothpick and transferred and lysed by stirring the bacterial material in 10 µl dH₂O. The toothpick was immediately transferred into culture medium to prepare an over night culture, while 5 µl of the cell suspension

served as a template for PCR. The initial PCR denaturing step was increased to 10 minutes for additional cell lysis, while other conditions remained as described in 2.7.6.1.

2.7.6.3 PCR using *Pfu* DNA polymerases

Two different proof reading DNA polymerases were used for cloning efforts. These are *Pfu* DNA polymerase from Promega (supplied with 10 x buffer) and *PfuUltra*[™] HF Ultra from Stratagene (supplied with 10 x buffer). A typical PCR reaction of 25 or 50 µl using *Pfu* DNA Polymerases contained 0.05-5 ng template DNA, 1 x *Pfu* buffer, 0.2 mM dNTPs (2.5 mM each, Fermentas), 0.2 µM forward and 0.2 µM reverse primers (Eurofins), 1.25 U DNA polymerase (2.5 U/µl). Hot start PCR was carried as described in 2.7.6.1.

2.7.6.4 PCR using Advantage[®] 2 PCR Kit

Advantage[®] 2 PCR Kit (Takara Bio Europe/Clontech) was used to perform rapid amplification of cDNA ends. A typical PCR reaction of 50 µl using TITANIUM[™] *Taq* DNA polymerase contained template DNA (2.5 µl RACE ready cDNA, see 2.7.2.2), 1 x Advantage 2 PCR buffer, 0.2 mM dNTPs, 0.2 µM gene specific primers (GSP), 1 x universal primer mix and 1 x Advantage 2 Polymerase Mix. The PCR reaction was subjected to a touch down PCR. The initial 5 cycles of denaturing (30 s at 94 °C) and elongation (3 min at 72 °C) were followed by 5 cycles of denaturing (30 s at 94 °C), annealing (30 s at 70 °C) and elongation (3 min at 72 °C). Finally 25 cycles of denaturing (30 s at 94 °C), annealing (30 s at 68 °C) and elongation (3 min at 72 °C) were performed.

In case of no detectable amplification product a secondary 'nested' PCR was carried out. Nested gene specific primers were designed according to predicted or known cDNA sequences. Five prime nested GSP was located upstream of 5' GSP for 5' RACE and 3' nested GSP was located downstream of 3' GSP for 3' RACE. Corresponding forward and reverse nested universal primers were provided by the supplier. Previous to a nested PCR an aliquot of the completed primary PCR reaction was diluted 1 to 50 in dH₂O and subjected to a secondary amplification. This 50 µl nested PCR reaction contained 5 µl template DNA 1 x Advantage 2 PCR buffer, 0.2 mM dNTPs, 0.2 µM gene specific nested primer, 1 x nested universal primer and 1 x Advantage 2 Polymerase Mix. Amplification was carried out using 25 cycles of denaturing (30 s at 94 °C), annealing (30 s at 68 °C) and elongation (3 min at 72 °C).

2.7.6.5 Correction of point mutations of a plasmid by PCR

Standard PCR in a volume of 25 µl was performed as described in 2.7.6.3 using 20 ng of plasmid DNA as a template. To correct the sequence for one nucleotide two

complementary reverse and forward primers of 24 to 29 nucleotides were designed (no. 392, 393, 394, 395; see appendix 7.3). Both primers contained the nucleotide which should be exchanged in the center of the sequence and had a melting temperature of 68 to 70 °C. Hot start PCR was carried out as described in 2.7.6.3, followed by 17 cycles of denaturation, annealing at 60 °C and polymerization. The polymerization time of *PfuUltra*TM HF polymerase (1 kb/min; Stratagene) was adjusted according to the size of the whole plasmid.

Directly after the amplification the methylated and hemi-methylated template DNA was restricted by addition of 10 U *DpnI* and incubation for 1 hour at 37 °C. Two µl of the reaction was used for transformation in chemically competent bacteria (see 2.7.8.3).

2.7.6.6 Preparation of digoxigenin-labeled DNA probes

The reaction was assembled as described in 2.7.6.1, while 0.2 M dNTPs were replaced by 1 x PCR Dig labeling Mix (10 x, Roche). Estimation of probe concentration and analysis of successful labeling was carried out using agarose gel electrophoresis (see 2.7.5) and dot blot (see 2.10.2), respectively. Probes were stored at -20 °C.

2.7.7 Purification of DNA fragments

2.7.7.1 Isolation using agarose gel electrophoresis

Agarose gel electrophoresis was carried out (see 2.7.5) to isolate DNA fragments from a mixture or to purify restricted DNA (see 2.7.4). DNA was visualized with ultraviolet irradiation and the desired fragment was excised from the gel with a cover slip. The DNA was purified with QIAquick Gel Extraction Kit (QIAGEN) following the instructions of the manufacturer. DNA was eluted in 30 µl dH₂O preheated to 70 °C and stored at -20 °C.

2.7.7.2 Isolation using column purification

To purify DNA fragments from PCR, High Pure PCR Product Purification Kit (Roche) was used following the protocol of the manufacturer. The sample was eluted in 50 µl supplied elution buffer and stored at -20 °C.

2.7.8 Cloning of DNA fragments

2.7.8.1 Cloning of DNA polymerase amplicons into a T-overhang vector

PCR fragments were cloned into pCR®2.1-TOPO® vector using TOPO TA cloning® Kit (Invitrogen). Therefore the DNA was purified as described in 2.7.7 or used directly from the PCR reaction. Routinely 3' adenine overhangs were added to the PCR fragments with Firepol DNA polymerase (Solis BioDyne). Therefore 6 µl of PCR product was incubated with 1 x BD buffer (10 x, Solis BioDyne), 2 mM MgCl₂ (25 mM, Solis BioDyne), 2 mM dATP (10 mM, Fermentas) and 0.1 U FIREPol DNA Polymerase (5 U/µl; Solis BioDyne) for

10 min at 72 °C in a final volume of 10 µl. The reaction was stored on ice or at -20 °C until the cloning reaction was assembled. The cloning reaction using pCR®2.1-TOPO® vector (Invitrogen) was prepared as described by the manufacturer, while 4 µl of PCR fragments with 3' A overhangs were used. The reaction was incubated 25 minutes at room temperature and then chilled on ice immediately.

2.7.8.2 Cloning of restricted DNA fragments into dephosphorylated plasmids

Vector dephosphorylation of 5' phosphates from 5'-protruding, 5'-recessive or blunt ends was carried out to prevent reassembling of restricted plasmid vectors (see 2.7.4). 50 ng of the vector was incubated with 1 U shrimp alkaline phosphatase (SAP, 1 U/µl, Roche) in 1 x SAP buffer (10 x, Roche) for 1 hour at 37 °C in a final volume of 9 µl. After inactivation of SAP by heating to 65 °C for 15 minutes the complete reaction was used for subsequent ligation. For ligation of DNA fragments into a dephosphorylated vector Fast-Link™ DNA Ligation Kit (Epicentre Biotechnologies) was used. Taking into account the sizes of vector and insert both were mixed in a ratio of 1:3 and incubated with 1 x Fast link buffer (10 x), 1 mM ATP (10 mM) and 2 U Fast link T4 DNA ligase (2 U/µl) in a final volume of 20 µl. The reaction was incubated 1 hour at room temperature. After inactivation of the ligase by heating to 70 °C for 15 minutes two µl of the reaction was used for transformation in chemically competent bacteria (see 2.7.8.3).

2.7.8.3 Transformation by heat shock

Two µl of the cloning reaction were used for transformation in *E. coli* BIOBlue 10⁹ (Bioline) or *E. coli* One Shot® (Invitrogen) chemically competent cells according to the instructions of the supplier.

2.7.9 Nucleotide sequence analysis

DNA sequencing was performed by Eurofins. Samples were send in a total volume of 15 µl, while 1 µg of plasmid DNA or 30 to 300 ng PCR product were supplied in water as recommended by the company. If sequencing was not performed with provided oligonucleotides (Eurofins) the samples were supplemented with 1 µM gene specific primer (see appendix 7.3). Analysis of the data was carried out using the software package Vector NTI (Invitrogen) and further online available resources provided by the National Center for Biotechnology Information (NCBI; <http://www.ncbi.nlm.nih.gov/>) and the European Bioinformatics Institute (EMBL-EBI; <http://www.ebi.ac.uk/>).

2.8 Standard molecular biological methods: RNA

2.8.1 Isolation of total RNA

Total RNA from C57BL/6 mouse tissue was isolated using TRIzol® Reagent (Invitrogen) following the instructions of the manufacturer. Tissue homogenization was carried out using a glass homogenizer. Phase Lock Gel™ Heavy reaction tubes (Eppendorf) were used for phase separation steps. The air dried RNA pellet was resuspended in 25 - 50 µl dH₂O. The quality of isolated total RNA was investigated by agarose gel electrophoresis (see 2.7.5).

2.8.2 Isolation of mRNA/Poly(A) RNA

Total RNA (see 2.8.1) was further purified from excess salt by precipitation with ammonium acetate (see 2.8.6). Isolation of mRNA (Poly(A) RNA) was achieved with MicroPoly(A)Purist™ Kit (Ambion). 75 µg of purified total RNA was bound to Oligo(dT) Cellulose as recommended by the supplier. Poly(A) RNA was recovered by two times elution with 200 µl supplied storage solution. To concentrate the RNA sample a further ammonium acetate precipitation was carried out dissolving the Poly(A) RNA pellet in 6 µl of supplied storage solution and stored at -80 °C.

2.8.3 Quantification

Concentrations of RNA solutions was determined by measuring the absorption at 260 (A₂₆₀) and 280 (A₂₈₀) nm using a standard spectrophotometer Ultrospec 3100pro (Biochrom). For calculation of the concentration a conversion factor was used, taking into account that absorption of one corresponds to 40 µg/µl RNA.

2.8.4 Synthesis of cRNA for injection in *Xenopus laevis* oocytes

RNA for injection *Xenopus laevis* oocytes was prepared by *in vitro* transcription using mMACHINE® Kit (Ambion). One µg of linearized (see 2.7.4) and agarose gel purified (see 2.7.7.1) plasmid DNA served as a template for *in vitro* transcription using T3 or T7 phage RNA polymerase promotor. The reaction was assembled according to the protocol of the supplier, while a 2 hour incubation time was chosen for maximal yield. To enhance translational efficiency in oocytes *in vivo* a polyadenylation was carried out. The poly(A) tail was added to the 3' termini of the cRNA using the Poly(A) Tailing Kit (Ambion) following the instructions of the manufacturer. To remove nucleotides, proteins and salts from the poly(A) tailed cRNA a final purification step using the MEGAClear™ Kit (Ambion) was performed. Following the protocol of the supplier the cRNA was finally eluted in 50 µl of elution buffer preheated to 95 °C. To maximize the recovery a second elution step into a new reaction tube was carried out. The cRNA synthesis was than

analyzed by denaturing agarose gel electrophoresis (see 2.8.5) and the cRNA was stored at -80 °C.

2.8.5 Preparation of digoxigenin-labeled cRNA probes

Digoxigenin labeled sense and antisense cRNA probes were generated from linearized plasmid DNA (see 2.7.4) site or purified PCR fragments (2.7.7.2) containing a T3 or T7 phage RNA polymerase recognition. PCR templates were generated from plasmid DNA with primers extended by sequences encoding the T3 or T7 phage RNA polymerase promoter. Sense (identical to mRNA sequence) and antisense (complementary to mRNA sequence) RNA probes were generated by *in vitro* transcription with T3 and T7 phage RNA polymerase, respectively. A typical 20 µl reaction contained DNA template (1 µg plasmid DNA or 300 ng purified PCR product), 1 x T3 or T7 reaction buffer (10 x, Roche), 1 x Dig RNA Labeling Mix (10 x, Roche), 10 U RiboLock™ Ribonuclease Inhibitor (40 U/µl, Fermentas) and 35 U T3 or T7 RNA polymerase (20 U/µl, Roche). The reaction was incubated at 37 °C for two hours. Remaining DNA template was digested by addition of 1 U DNase I (1 U/µl, Amp Grade Invitrogen) and additional incubation at 37 °C for one hour. After purification by precipitation with ammonium acetate (see 2.8.6) probes were stored at -80 °C. Analysis and estimation of concentration was carried out using agarose gel electrophoresis (see 2.7.5).

2.8.6 Purification by precipitation with ammonium acetate

Precipitation was carried out to purify RNA samples from nucleotides or to concentrate RNA samples. The RNA solution was supplemented with 1/10 of 5 M ammonium acetate and 2.5 x cold 100 % ethanol and incubated at -20 °C over night or for 30 minutes at -80 °C. A 30 minute centrifugation step at maximum speed was carried out to pellet the RNA. After removal of the supernatant, 500 µl of 75 % ethanol was added to wash the pellet. A second centrifugation step at maximum speed of 15 minutes was used to pellet the RNA again. The ethanol was carefully removed and the pellet was air dried at room temperature for 10 to 30 minutes. The RNA was recovered using 10 - 75 µl dH₂O, depending on the size of the pellet. For digoxigenin labeled RNA probes two precipitation steps were carried out, one at - 20 °C over night and one for 30 minutes at -80 °C.

2.8.7 Denaturing agarose gel electrophoresis

The quality of RNA was analyzed using denaturing agarose gel electrophoresis. For this purpose 1.2 % (w/v) agarose was dissolved in 1 x formaldehyde (FA) buffer (10 x: 200 mM MOPS, 50 mM sodium acetate, 10 mM EDTA, pH 7) by heating in a microwave. After cooling down to approximately 60 °C, formaldehyde (37 %) was added to the gel in a final

concentration of 0.67 % (v/v). Samples containing 1 x loading buffer (5 x: 4 x FA buffer, 0.25 % bromophenol blue (v/v), 4 mM EDTA, 0.9 M formaldehyde, 20 % glycerol (v/v), 30.1 % formamide (v/v)) were denatured for 5 minutes at 65 °C. Samples were immediately chilled on ice and supplemented with 0.02 µg/µl ethidium bromide (10 mg/ml). For sizing and approximate quantification of RNA an appropriate molecular weight marker (0.5-10 kb RNA ladder, Invitrogen) was used. After equilibration of the polymerized gel in 1 x FA buffer containing 0.67 % (v/v) formaldehyde (37 %) for at least 30 minutes gel electrophoresis was carried out for 30 minutes at 70 V. To visualize the RNA the gel was analyzed by ultraviolet irradiation (312 nm) using a photo documentation system (Syngene).

2.9 *In situ* hybridization of digoxigenin labeled RNA probes

2.9.1 Buffers

2 x Buffer 1	0.3 M NaCl; 0.2 M maleic acid; pH 7.5
Buffer 2	1 % blocking reagent (Roche) in 1 x buffer 1
Buffer 3	0.1 M Tris-HCl; 0.1 M NaCl; 50 mM MgCl ₂ ; pH 9.5
10 % blocking reagent	10 % (w/w) blocking reagent (Roche) in 1 x buffer 1
Color substrate	0.175 mg/ml BCIP (Roth); 0.25 mg/ml NBT (Roche); 0.1 M Tris-HCl; 0.1 M NaCl; 50 mM MgCl ₂ ; pH 9.5
50 x Denhardt's reagent	1 % (w/w) BSA; 1 % (w/w) Polyvinylpyrrolidon; 1 % (w/w) Ficoll 400
Hybridization buffer	prehybridization buffer; 100 mg/ml dextranesulphate; RNA probe (20 - 800 ng/µl)
20 x Hybridization salts	3 M NaCl; 0.1 M PIPES; 0.1 M EDTA; pH 6.8
4 % PFA	4 % (w/v) paraformaldehyde; 1 x PBS; 1 mM MgCl ₂ ; pH 7.2
10 x PBS	0.2 M NaHPO ₄ ; 0.8 M Na ₂ HPO ₄ ; 0.65 M NaCl; pH 7.4
Prehybridization buffer	50 % formamide (v/v); 5 x hybridization salts; 5 x Denhardt's reagent; 0.2 % SDS (v/v); 250 µg/ml yeast tRNA; 250 µg/µl salmon sperm DNA
RNase buffer	0.5 M NaCl; 10 mM Tris-HCl; 1 mM EDTA; 10 µg/µl RNase; pH 7.5
10 % SDS	10 % (w/w) SDS in water
20 x SSC	0.3 M sodium citrate; 3 M NaCl; pH 7
TE buffer	10 mM Tris-HCl; 1 mM EDTA; pH 8
Triethanolamine	0.1 M Triethanolamine; 0.25 % (v/v) acetic anhydride; pH 8
10 % TritonX100	10 % (v/v) TritonX100 in 1 x PBS

2.9.2 Tissue sample origin

Human tissue samples from circumvallate and fungiform papillae were purchased from biopsies taken by Dr. Raguse (Charité, Campus Virchow Klinikum). The procedure was approved by the local ethical committee. Human circumvallate biopsies originate from patients with tumors in the tongue or in the oral cavity, while samples were free of

abnormal tissue and patients were not treated with radiotherapy. Human fungiform biopsies originate from voluntary donors. Immediately after the biopsy the tissue was frozen in liquid nitrogen and stored at -80 °C or transferred into the fixative 2 % paraformaldehyde (see 2.11.2).

2.9.3 Cryo sections

Ten µm cross sections of human circumvallate and fungiform papillae without fixative were prepared at -20 °C using the standard cryostat microtom Cryotom HM505 E (Microm). Tissue was removed from -80 °C and embedded in Jung tissue freezing medium (Leica Microsystems). Sections were thaw mounted onto positively charged glass slides SuperFrost/Plus (Microm) and stored at -80 °C.

2.9.4 *In situ* hybridization procedure

Previous to hybridization, sections were fixed for 5 min using 4 % (w/v) PFA. After a short wash with 1 x PBS tissue was permeabilized by incubation in 0.2 M HCl for 10 min and 10 % TritonX100 for 2 min. Remaining TritonX100 was removed by washing the slides in 1 x PBS for 1 minute. Afterwards the tissue was acetylated by incubation in triethanolamine incl. acetic anhydride for 10 minutes. The following incubation in prehybridization buffer was performed in a humid chamber containing 50 % formamide for five hours at 50 °C. Hybridization was carried out over night under equal conditions, while sections were incubated with riboprobes (see 1.8.4) diluted in hybridization buffer. Final concentrations of probes are listed in appendix 7.4. Each hybridization experiment was carried out using sense and antisense probes for the mRNA of interest. The sense probe, which is identical to the mRNA sequence served thereby as a negative control. After hybridization, the slides were washed two times 15 minutes at RT using 2 x SSC. Unbound riboprobes were digested by RNaseA treatment at 37 °C for 30 min in RNase buffer. Subsequently two high-stringency washes for 15 min were performed at 50 °C using 0.4 x SSC.

2.9.5 Colorimetric detection

Sections were equilibrated in 1 x buffer 1 for 5 minutes followed by a blocking step in 1 % blocking solution for one to three hours. Thereafter an anti-digoxigenin antibody (1:750, Roche) diluted in 1 % blocking solution was applied for one hour. Unbound antibody was removed by two washes with 1 x buffer 1 for 30 min each. After equilibration in buffer 3, the color substrate was applied in the dark over night. The color reaction was stopped by incubation in TE buffer for at least five min the next day. Afterwards sections were mounted in an aqueous mounting medium (Dako).

2.9.6 Data analysis

Photomicrographs of sections were taken with the CCD camera RT slider (Diagnostic Instruments) mounted to an Axioplan microscope (Zeiss).

2.10 Filter hybridization of DNA probes: southern blot, colony blot and dot blot

2.10.1 Reagents and equipment

Antisera	see appendix 7.6
Blocking reagent	1-10 % (w/w) blocking reagent (Roche) in maleic acid buffer or Tris-buffer
Color substrate	0.175 mg/ml BCIP (Roth); 0.25 mg/ml NBT (Roche); 0.1 M Tris-HCl; 0.1 M NaCl; 50 mM MgCl ₂ ; pH 9.5
Denaturation solution	0.5 M NaOH; 1.5 M NaCl
Detection buffer	0.1 M Tris-HCl; 0.1 M NaCl; pH 9.5
Prehybridization buffer	50 % (v/v) formamide; 5 x SSC; 0.1 % (w/v) N-lauroyl-sarcosine; 0.02 % (w/v) SDS; 2 % blocking reagent
High stringency buffer	0.5 x SSC; 0.1 % (w/v) SDS
Hybridization buffer	prehybridization buffer; digoxigenin labeled probe
Low stringency buffer	2 x SSC; 0.1 % (w/v) SDS
Maleic acid buffer	0.1 M maleic acid; 0.15 M NaCl; pH 7.5
Neutralization solution	0.5 M Tris-HCl; 1.5 M NaCl; pH 7.5
Nylon membranes	Amersham Hybond TM N ⁺ (GE Healthcare) Nylon membrane for colony hybridization (Roche)
Proteinase K solution	2 mg/ml in 2 x SSC (20 mg/ml stock solution in 1x PBS)
10 % SDS	10 % (w/w) SDS in water
20 x SSC	0.3 M sodium citrate; 3 M NaCl; pH 7
TBS buffer	0.02 M Tris-HCl; 0.15 M NaCl; pH 7.5
TBST buffer	0.02 M Tris-HCl; 0.15 M NaCl; 0.1 % (v/v) Tween20; pH 7.5
TE buffer	10 mM Tris-HCl; 1 mM EDTA; pH 8
Tris buffer	0.1 M Tris-HCl; 0.15 M NaCl; pH 7.5
UV-crosslinker	BIO-Link BLX (254 nm, Biometra), exposition energy: 0.120 J/cm ²
Washing buffer	maleic acid buffer; 0.3 % (v/v) Tween20

2.10.2 Dot Blot

To investigate the labeling of digoxigenin labeled DNA probes (see 2.7.6.6) and as a positive control for southern blot, phage lift and colony blot hybridization, a dot blot was performed. Therefore 1 µl of the probe or 100 ng of the non-labeled template plasmid was spotted onto a positively charged nylon membrane. The DNA was additionally cross linked to the membrane by exposition to UV light in a UV-crosslinker (see 2.10.1). The membrane was than directly used for hybridization and detection as described in 2.10.6, 2.10.7 and 2.10.8.

2.10.3 Southern Blot

Restricted DNA fragments (see 2.7.4) were separated by agarose gel electrophoresis (see 2.7.5). After electrophoresis the DNA fragments were depurinated by a 15 min incubation of the gel in 0.25 M HCl. After a short rinse with deionized water, the DNA in the gel was denatured by incubation two times 15 minutes in denaturation solution. Neutralization was achieved by submerging the gel two times for 15 minutes in neutralization solution, and checked with pH paper (Roth). After equilibration of the gel in the transfer buffer (20 x SSC) the DNA was transferred by capillary transfer over night onto a nylon membrane as described in "DIG application manual for filter hybridization". The DNA transfer was controlled by visual control of the blotted gel by exposition to ultraviolet irradiation (312 nm) using a photo documentation system (Syngene). The transferred DNA was cross linked to the wet membrane by exposition to UV light in a UV-crosslinker (see 2.10.1). The membrane was then directly used for hybridization and detection as described in 2.10.6 and 2.10.7.

2.10.4 Colony Blot

To elucidate colonies directly for contained plasmids of interest, colony blot was performed. Colonies grown on standard LB agar plates (see 0) were pre-cooled for at least 30 minutes at 4 °C. To transfer the colonies onto a nylon membrane, a membrane disc was placed onto the plate and the orientation was labeled. The membrane was allowed to soak to the plate for approximately one minute and carefully removed using forceps. The membrane disc was placed upside up on a filter paper soaked with denaturation solution and left for fifteen minutes. Excess of solution was removed by placing the membrane on a dry filter paper. Neutralization was carried out by placing the membrane on filter paper soaked with neutralization solution for 15 minutes. The membrane was equilibrated in 2 x SSC for ten minutes and the DNA was cross linked to the wet membrane by exposition to UV light in a UV-crosslinker (see 2.10.1). To remove cell debris the membrane was placed into an empty petri dish and incubated with proteinase K solution for one hour at 37 °C. Afterwards cell debris were removed by placing filter papers soaked with deionized water onto the membrane and repetitive pulling-off. To improve sticking of the cell debris to the wet filter, it was applied with pressure on the membrane. The membrane was then directly used for hybridization and detection as described in 2.10.6 and 2.10.7.

2.10.5 Plaque lift

Plaques were plated on petri dishes (ø 9 cm) as described in 2.15.2 or on petri dishes (ø 14.5 cm) using the 3.5 fold volume of bacterial cells and NZY-top agar. Developed

plaques were transferred to nylon membranes as described for colony blot (see 2.10.4). The membranes were treated equally, while denaturation was carried out for five minutes and the proteinase K step was omitted. Hybridization and detection was carried out as described in 2.10.6 and 2.10.7.

2.10.6 Hybridization and stringency washes

Prior to hybridization the membranes were incubated in 10 ml/100 cm² prehybridization solution for one to three hours. This step was carried out using roller-bottles at 42 °C in a hybridization oven (Peqlab). The hybridization temperature was calculated in respect of probe properties and buffer composition according to "DIG application manual for filter hybridization" (Roche). Digoxigenin labeled probes (see 2.7.6.6) were denatured for 5 minutes at 95 °C and chilled on ice prior to addition to prewarmed hybridization solution. After removal of prehybridization solution the membrane was incubated over night in 3.5 ml/100 cm² hybridization solution with a final probe concentration of 25 ng/ml. The hybridization solution was removed on the following day and stored at -20 °C. Stored hybridization solution was reused up to ten times after fresh denaturation for 10 minutes at 65 °C prior to use. To remove excess of unbound probe the membrane was washed in ample low stringency buffer two times for 5 minutes. A high stringency wash was carried out two times for 15 minutes at 68 °C using ample of prewarmed high stringency buffer.

2.10.7 Chromogenic detection

The hybridized and washed membrane (see 2.10.6) was equilibrated in washing buffer for two minutes and subsequently submerged in 1 % blocking solution for one to three hours. The membrane was then incubated for 30 minutes with an anti-digoxigenin antibody coupled to an alkaline phosphatase (no. 17, see 7.6 in 1 % blocking solution). Unbound antibody was washed away by submerging the membrane two times 15 minutes in ample of washing buffer. After equilibration in detection buffer, the color substrate was applied in the dark. The reaction was stopped when expected signals appeared or after maximal 16 hours by addition of TE buffer. The membrane was air dried and documented by scanning.

2.10.8 Chemiluminescent detection of southern blots

For southern blot (see 2.10.3) quantification chemiluminescent detection was carried out using ECL Western blotting detection reagents (GE Healthcare). The hybridized and washed membrane (see 2.10.6) was equilibrated in washing buffer for two minutes followed by two blocking steps. The membrane was first blocked in 1 % blocking solution in maleic acid buffer for 1-3 hours, followed by 1 hour incubation in 1 % blocking reagent

in Tris-buffer. Thereafter an anti digoxigenin antibody coupled to a horse radish peroxidase (no. 83, see 7.6 in 1 % blocking reagent in Tris-buffer) was applied for 1 hour. Unbound antibody was washed away by submerging the membrane two times for 5 minutes and once for 15 minutes in ample TBST buffer. After washing two times for 5 minutes in TBS the membrane was transferred in a plastic bag. Excess of TBS buffer was removed and exchanged by a 1:1 mixture of detection solution 1 and 2 (GE Healthcare) to a final volume of about 0.125 ml per cm² membrane. After 1-5 minute incubation, excess of detection solution was drained off and developing chemiluminescence was detected with a luminescent analysis system using a CCD camera (LAS-1000; Fujifilm). The membrane was exposed 5 s, 1 min, 5 min, 15 min, 30 min and 60 min. Pictures were taken using an aperture of 0.85 and an integration of 2 x 2 pixel. Signals were quantified by measuring the intensities using ImageJ (Rasband, 1997-2005).

2.11 Immunohistochemistry

2.11.1 Reagents and equipment

Antisera	see appendix 7.6
Antisera dilutions	0.1 % BSA; 0.3 % TritonX100; 1 x PBS
Blocking solution	1 % (w/w) BSA; 0.05 % saponine (w/w); 0.2 % gelatine (w/w); 1 x PBS
DPX	mounting medium (44581, Fluka)
10 x PBS	0.2 M NaHPO ₄ ; 0.8 M Na ₂ HPO ₄ ; 0.65 M NaCl; pH 7.4
Peroxidase substr.	0.5 mg/ml DAB (50 mg/ml); 1 x PBS; 0.01 % H ₂ O ₂
2 % PFA	2 % (w/v) paraformaldehyde; 1 x PBS; 1 mM MgCl ₂ ; pH 7.2
10 x TBS	0.2 M Tris-HCl; 1.5 M NaCl; pH 7.5
Tris-EGTA buffer	1 mM Tris-HCl; 0.5 mM EGTA; pH 9
Washing buffer	0.1 % BSA; 0.5 % saponine; 0.2 % gelatine; 1 x PBS

2.11.2 Paraffin sections

Human sample tissue (see 2.9.2) was removed from -80 °C and prewarmed to -20 °C before 4 °C cold 2 % PFA (see 2.10.1) was added. The tissue was fixed for 24 hours at RT and subsequently embedded in paraffin according to standard protocols. Two µm sections were cut using a standard rotary microtome. Previous to immunohistochemistry the sections were dewaxed by incubation with toluol for two times 3 minutes followed by a downward ethanol row starting with two times 100 % ethanol for 3 minutes and continued with 96 %, 70 % and 40 % ethanol, while each step was carried out once for 2 minutes. Hydration was completed by two times incubation in distilled water for 2 minutes each.

2.11.3 Procedure for immunoperoxidase labeling

Indirect immune labeling using a peroxidase was carried out according to Hager *et al.*, 2001. In a first step the dewaxed sections were incubated for 10 minutes with 0.5 % (v/v) H₂O₂ (30 %) in methanol to block endogenous peroxidases. After two wash steps with distilled water for 5 minutes, heat induced epitope retrieval was carried out using Tris-EGTA buffer. Therefore slides were transferred into a plastic cuvette containing Tris-EGTA buffer and heated two times 5 minutes at 180 W using a microwave oven. After cooling down to room temperature sections were washed twice with distilled water. Non-specific antibody binding was prevented by blocking free aldehyde groups using a 30 minute incubation with 50 mM NH₄Cl in 1 x PBS and saturation of the surface with proteins by incubation with blocking solution for 1 to 3 hours. Blocking solution was drained off and appropriate primary antisera dilutions (no. 107; 108; 109; 116; 269; 270; 271; see appendix 3.4) were added. Specificity of antisera labeling was controlled by incubation omitting the primary antibody and/or by preabsorption of antisera with the appropriate blocking peptide (see 3.4). In each case the sections were incubated over night at 4 °C in a humid chamber with water saturated atmosphere. On the following day the sections were rinsed in washing buffer for 3 times 10 minutes. Secondary biotinylated antibodies (no. 2; 4; 24 in antisera dilution; see appendix 7.6) were applied for one hour at room temperature. Afterwards sections were rinsed by washing 3 times in 1 x PBS for 10 minutes.

2.11.4 Detection with DAB

Detection of biotinylated secondary antibodies with 3',3'-diaminobenzidine (DAB) was carried out using Vectastain® ABC-Kit (Vector Laboratories). ABC solution was prepared by the addition of 1 drop of reagent A (avidin), 1 drop of reagent B (biotinylated peroxidase) and 0.1 % Tween20 to 2.5 ml 1 x PBS. The mixture was incubated for 30 minutes in before it was applied to the sections treated as described in 2.11.3. The sections were incubated for 90 minutes in a humid chamber with water saturated atmosphere and subsequently washed 3 times for 10 minutes in 1 x PBS. The peroxidase substrate was applied to the sections and staining was allowed to develop under visual control using a standard microscope (Olympus CH30). The reaction was stopped by rinsing with distilled water. For long term mounting the sections were dehydrated by incubation with an ascending ethanol row starting with 40 %, continued with 70 %, 90 % and 96 % for 2 minutes each. Afterwards a 3 minute wash in 100 % ethanol was carried out followed by incubation in RotiHistol (Roth) or Histo-Clear (National Diagnostics) for

2 times 5 minutes. Sections were mounted with cover slips using several drops of DPX mounting medium and stored at 4 °C.

2.11.5 Detection with fluorescent dyes

Detection of biotinylated secondary antibodies with fluorescent dyes was carried out using tyramide amplification following the protocol of the supplier (Perkin Elmer). For that approach the protocol described in 2.11.3 was modified by using 1 x TBS instead of 1 x PBS. Subsequently the slides were incubated with streptavidin coupled peroxidase (1:100 in 1 x TBS) for 30 minutes in a humid chamber with water saturated atmosphere. After washing 3 times for 5 minutes with 1 x TBS, tyramide working solution (1:100 in amplification diluent; Perkin Elmer) was applied for 5 minutes. The sections were rinsed in 1 x TBS 3 times for 5 minutes before avidin-conjugated fluorescein (no. 8 see appendix 7.6; in 1 x TBS) was applied for 1 hour in the dark. A final wash step using 1 x TBS 3 times for 5 minutes removed excess of the fluorescent dye. The sections were embedded in aqueous mounting medium containing the counter stain DAPI (Vectashield, Vector Laboratories) and stored at 4 °C in the dark.

2.11.6 Data analysis

Photomicrographs of sections were taken with the CCD camera RT slider (Diagnostic Instruments) mounted to an Axioplan microscope (Zeiss).

2.12 Immunocytochemistry

2.12.1 Cultivation of HEK293T-cells for immunocytochemistry

For immunocytochemistry cells were seeded on poly-D-lysine coated cover slips (ø 12 mm) in 24-well-plates. Therefore sterilized cover slips were placed into 24 well plates and incubated with 10 µg/ml Poly-D-Lysine hydrobromide (1 mg/ml; Sigma) for 15 minutes. The agent was removed by pipetting and each well was washed three times with 500 µl 1 x PBS (see 2.9.1). Wells were allowed to air dry for 15 to 30 minutes and stored at 4 °C or used immediately to seed trypsinated cells to a confluence of 50 to 70 % (see 1.5). Cells were seeded in a final volume of 500 µl per well using DMEM^{plus} medium without the antibiotic G418.

2.12.2 Transient transfection in 24-well plates for immunocytochemistry

Transient transfection of DNA into HEK293 cells grown to a confluence of 50 % to 70 % was performed using Lipofectamine™ 2000 (Invitrogen) according to the manufacturers' protocol. Therefore DMEM^{plus} medium was exchanged by 400 µl serum-free DMEM. Per well, 2 µl of Lipofectamine were diluted in DMEM to a final volume of 50 µl and incubated for 5 minutes. Subsequently 0.8 µg plasmid DNA (no. 59, 60, 62 see 0) diluted in

DMEM in a final volume of 50 μ l was added and the mixture was incubated for 20 minutes. The complex in finally 100 μ l was added to each well containing cells and 400 μ l of DMEM and incubated at 37 °C. After 4 to 6 hours medium was exchanged by DMEM^{plus} without the antibiotic G418 and immunocytochemistry was performed after 48 hours. For comparison to gene encoding plasmids empty plasmid was transfected as a negative control and the cells designated as mock transfected cells.

2.12.3 Procedure

Cells grown in 24-well plates were washed with prewarmed 1 x PBS for 5 minutes followed by two times 5 minutes with 4 °C cold 1 x PBS with 500 μ l per well. After incubation for 30 minutes in cold 1 x PBS, the cells were incubated in 300 μ l biotinylated concanavalin A solution (see appendix 7.6, in cold 1 x PBS) for one hour at 4 °C. Excess of concanavalin was removed by three washes in 1 x PBS for 5 minutes at room temperature. Cells were subsequently fixed in 2 % PFA (see 2.9.1) for 5 minutes and washed again 3 times 5 minutes with 1 x PBS. Thereafter, immunostaining of was carried out as described in 2.11.3. Cells were first treated with 50 mM NH₄Cl in 1 x PBS followed by blocking in blocking solution (see 2.11.1). Primary antibodies were diluted in antisera dilution solution (see 2.11.1) and applied over night at 4 °C in a volume of 150 μ l per well. Cells were washed in washing buffer (see 2.11.1) and detection of primary antisera was carried out by application of fluorescent secondary antibodies (no. 1; 3; 67 see 7.6) for one hour. Biotinylated concanavalin A was detected in parallel by incubation with fluorescent streptavidin (no. 68 see 7.6). Excess of secondary antibody and streptavidin was removed by 3 wash steps in 1 x PBS. Cover slips were transferred on a slide and embedded in aqueous mounting medium (Vectashield, Vector Laboratories) and stored at 4 °C in the dark.

2.12.4 Data analysis

Analysis and documentation of immunocytochemical labeled cells was performed using the inverted confocal microscope Leica DM IRE2 (Leica Microsystems) coupled to appropriate software (Leica Confocal Software).

2.13 *In vitro* translation

For *in vitro* translation of plasmid DNA the “TNT® T7 Quick Coupled Transcription/Translation System” (Promega) was used. Plasmids carrying genes of interest under the control of T7 RNA polymerase promotor were linearized by restriction digest using *NotI* or *NheI* (see 2.7.4) yielding 5'-overhangs. Linearized templates were purified under RNase free conditions via agarose gel electrophoresis and extraction (see

2.7.7). A standard reaction contained 1 µg linearized plasmid template, 0.02 mM methionine, 1 µl T7 TNT® PCR enhancer and 40 µl of TNT® T7 master mix in a final volume of 50 µl. A radio-labeled reaction was assembled using 0.5 µg linearized plasmid template, 20.5 µCi EasyTag™ [³⁵S]methionine (Perkin Elmer), 0.5 µl T7 TNT® PCR enhancer and 20 µl of TNT® T7 master mix in a final volume of 26 µl. A negative control was included using the linearized empty vector. The reactions were incubated for 90 minutes at 30 °C. The *in vitro* translation was completed by the addition of 33 ng RNaseA and 1.2 mM cycloheximide and an additional incubation for 10 minutes at 30 °C. The reactions were stored at -80 °C or -20 °C for short term storage. An aliquot of 2.5 µl was analyzed using denaturing SDS polyacrylamide gel electrophoresis (PAGE) (see 2.14.2). SDS-PAGE of non-radioactive *in vitro* translation reaction in the presence of 40 µM methionine was used for Western Blot analysis (see 2.14). Amount of protein of non-radiolabeled *in vitro* translations was determined using Bio-Rad Protein assay using microassay procedure for microtiter plates. For analysis of incorporated radiolabeled methionines phosphorimager radiography was carried out. Therefore the polyacrylamide gel was fixed and proteins were non-specifically stained using coomassie brilliant blue. For fixation and staining the polyacrylamide gel was incubated coomassie staining solution (0.3 % Coomassie brilliant blue R250, 50 % (w/v) trichloroethanoic acid, 2 % (v/v) methanol) for 45 minutes. Excess of the dye was removed by destaining for 2.5 hours with three changes of the destaining solution (45 % (v/v) methanol, 7.5 % (v/v) acetic acid). Subsequently the gel was submerged in conservation solution (50 ml 100 % glycerole, 125 ml 100 % ethanol, 375 ml distilled water) for 1 hour and dried on a gel dryer (Bio-Rad) at 60 °C for 4 hours. The dry gel was than analyzed by exposure to storage phosphor screen (Amersham Pharmacia Biotech) 72 hours or 3 weeks and subsequent storage phosphor autoradiography using Storm™ Imaging System (Amersham Biosciences).

2.14 Western Blot

2.14.1 Reagents for SDS polyacrylamide gel electrophoresis

AB-3 (49.5 %)	48 g Acrylamide, 1.5 g N,N'-Methylenebisacrylamide ad 100 ml
AB-6 (49.5 %)	46.5 g Acrylamide, 3 g N,N'-Methylenebisacrylamide ad 100ml
10 % APS	(w/v) fresh prepared in water
10 x Anode buffer	1 M Tris, 0.225 M HCl, pH adjusted to 8.9
4 % Collecting gel	4 % (v/v) Acrylamide (AB-3), 1 x gel buffer, 0.075 % (v/v) APS, 0.075 % TEMED
3 x Gel buffer	3 M Tris, 1 M HCl, 0.3 % SDS, pH 8.75
10 x Cathode buffer	1 M Tris, 1 M Tricine, 1 % SDS, pH ~8.3 not adjusted

2 x Sample buffer	8 % SDS, 20 % Glycerole, 100 mM Tris pH 7.0, 0.033 % Coomassie brilliant blue G, stored at -20 °C 4 % (v/v) 2-Mercaptoethanol was added shortly before use
16.5 % Separating gel	16.5 % (v/v) Acrylamide (AB-6), 1 x gel buffer, 0.033 % APS, 0.033 % TEMED
10 % Spacer gel	10 % Acrylamide (AB-3), 1 x gel buffer, 0.05 % (v/v) APS, 0.05 % TEMED

2.14.2 Reducing SDS polyacrylamide gel electrophoresis (SDS-PAGE)

For analysis of protein samples one dimensional SDS polyacrylamide gel electrophoresis was carried out (Schagger, 2006). Therefore a three part polyacrylamide gel (22 x 15.5 x 0.75 cm) made of 3 ml collecting gel, 6 ml spacer gel and 13 ml separating gel was poured. Polymerization of the polyacrylamide gels was started by adding APS and TEMED lastly. Separation and spacer gel were polymerized together for 2 hours, while the surface was covered with water-saturated butanol. Subsequently, the alcohol was removed and the gel surface was rinsed with water and dried using filter paper. The collecting gel was poured and polymerized for an additional hour after a comb was placed between the glass plates. Thereafter, the gel was placed into an electrophoresis apparatus with two distinct buffer tanks, while the top of the gel was submerged in cathode buffer and the bottom in anode buffer. The comb was removed and the slots were rinsed with 1 x cathode buffer. 150 µg of *in vitro* translation (see 2.13) was denatured for 30 minutes at 40 °C in the presence of 1 x sample buffer. The samples were loaded on the collecting gel and electrophoresis was started with 90 V constant. After all samples had migrated out of the slots electrophoresis was carried out for 13 - 14 hours at 30 mA constant. For sizing of samples a protein standard (161-0377, Bio-Rad) was used.

2.14.3 Semi-dry blot of proteins from SDS-polyacrylamide gels

Size separated proteins were transferred on nitrocellulose membrane using a standard semi-dry transfer system for electro blotting (Sammy-Dry; Schleicher & Schuell). Therefore the SDS-polyacrylamide gel, filter paper and Protran™ nitrocellulose membrane (0.1 µm, Whatman) were equilibrated in transfer buffer (0.3 M Tris, 100 mM acetic acid, pH 8.6) before assembling a stack in the following order from anode (+) to cathode (-): 3 filter papers, membrane, gel, 3 filter papers. A constant current of 0.4 mA/cm² was applied at room temperature for 16 - 24 hours. Electro-blotted nitrocellulose membranes were submerged in ponceau S staining solution (0.2 % Ponceau S, 3 % trichloroethanoic acid) to stain the transferred proteins non-specifically. The

membrane was destained with several washes of distilled water and a final wash in TBST (20 mM Tris-HCl, 150 mM NaCl, 0.1 % (v/v) Tween20; pH 7.5).

2.14.4 Immunolabeling of transferred proteins

After electro blotting and Ponceau S staining (see 2.14.3) the nitrocellulose membrane was merged in TBST (20 mM Tris-HCl, 150 mM NaCl, 0.1 % (v/v) Tween20; pH 7.5) and blocked using blocking solution (5 % (w/v) nonfat dry milk (Bio-Rad) in TBST) for 1 to 3 hours with agitation. The primary antiserum was diluted in blocking solution (no. 109, 1:1000) and incubated for over night at 4 °C with agitation. On the following day, excess of antibody was washed by three wash steps for 5 minutes using TBST. The secondary antibody coupled to horseradish peroxidase (no. 326; 1: 10'000 in blocking solution, see appendix 7.6) was applied for 1 hour at room temperature with agitation, followed by two TBST wash steps for 5 minutes and one wash step for 15 minutes. Excess of the detergent Tween20 was removed by two wash steps in ample of TBS. Chemiluminescent detection was carried out using ECL Western blotting detection reagents (GE Healthcare). Excess of TBS buffer was removed and exchanged by a 1:1 mixture of detection solution 1 and 2 to a final volume of about 0.125 ml per cm² membrane. After 5 minute incubation, excess of detection solution was drained off and developing chemiluminescence was detected with a luminescent analysis system using a CCD camera (LAS-1000; Fujifilm). Pictures were taken using an aperture of 0.85 and an integration of 2 x 2 pixel.

2.15 Bacteriophage cDNA library of *macaca foliate papillae*

Complementary DNA library was generated by cooperation partners (University Hohenheim, Dr. R. Hoppe; Unilever, E. Tareilus) using ZAP Express®cDNA Synthesis Kit and ZAP Express® Gigapack®III Gold Cloning Kit (Stratagene).

2.15.1 Sample origin and process status of the library

Poly(A) RNA (18 µg) from foliate papillae (420 mg) of 5 tongues of *Macaca mulatta* served as a template for cDNA synthesis, which finally had an average size of 1.5 to 2 kb. Generated cDNAs larger than 1.5 kb were ligated into the λ-ZAP Express vector (Stratagene) and packaged into *E. coli* XL1-Blue MRF' (Stratagene). Subsequent amplification by plating the library (see 2.15.2) was carried out, while 55'000 independent cDNA clones were divided into pools with approximately 2000 each. This once amplified cDNA library consisting of 26 λ-phage pools was provided by our cooperation partners and was titered in our lab before use as described in 2.15.2. Furthermore a large scale *in vivo* excision (see 2.15.3) was carried out in our lab yielding a finally twice amplified cDNA library consisting of 26 pBK-CMV plasmid pools.

2.15.2 Plating and titering of the cDNA library λ -phages

Bacterial host strain *E. coli* XL1-Blue MRF' (Stratagene) was grown over night using 5 ml LB-broth supplemented with 15 $\mu\text{g/ml}$ tetracycline. Five to 50 μl of this over night culture were used to inoculate a 5 ml LB-broth+ (see 2.2) without selection antibiotic and grown until $\text{OD}_{600} = 0.6 - 1$ (see 2.3.3). Cells were pelleted by centrifugation for 10 minutes at 1000 g and resuspended in 10 mM MgSO_4 to a final OD_{600} of 1. λ -phages of each pool (see 2.15.1) were diluted 1:100, 1:1000 and 1:10'000 in 10 mM MgSO_4 . Ten μl of phage dilution were mixed with 200 μl of *E. coli* XL1-Blue MRF' ($\text{OD}_{600} = 1$ in 10 mM MgSO_4) and incubated for 15 minutes at 37 °C without shaking. Thereafter, 3 ml of NZY-top agar prewarmed to 48 °C was added and the mixture was poured onto NZY-agar plates prewarmed to 37 °C. Plaques were allowed to develop over night at 37 °C. The titer was determined by counting the plaques and calculation of plaque forming units (pfu) per μl (see appendix 7.7, Tab. 7.5).

2.15.3 Large scale *in vivo* excision of pBK-CMV phagemid vector

40'000 pfu of λ -phages of each pool were added to 0.5 μl *E. coli* XL1-Blue MRF' of $\text{OD}_{600} = 1$ in 10 mM MgSO_4 (see 2.15.2), which corresponds to approximately 400'000 cells. Further 4'000'000 ExAssist® interference resistant helper phages (Stratagene, 1×10^8 pfu/ μl) were added and the final volume was adjusted to 50 μl with 10 mM MgSO_4 . Phages were allowed to attach to the cells for 15 minutes at 37 °C without shaking before 500 μl of LB-broth was added and an incubation of 3 hours with shaking followed. λ -phages and cells were lysed by heating to 70 °C for 20 minutes and cell debris were separated by centrifugation at 1000 g for 10 minutes. The supernatant, containing excised phagemids, was removed and stored at 4 °C. For titering, 5 μl of excised phagemids were incubated with 160 μl *E. coli* XL0LR of $\text{OD}_{600} = 1$ (see 2.15.2) for 15 minutes at 37 °C without shaking. Forty μl of 5 x NZY-broth was added to the mixture which was further incubated at 37 °C for 45 minutes. Ten and 100 μl were plated on LB-agar selection plates supplemented with 50 $\mu\text{g/ml}$ kanamycin and incubated over night at 37 °C. The titer was determined by counting the colonies and calculation of colony forming units (cfu) per μl , while $\text{cfu} = \text{pfu}$ of excised phagemids. For *in vivo* excision, at least 20'000 or up to 50'000 cfu phagemids were mixed with *E. coli* XL0LR of $\text{OD}_{600} = 1$ in a final volume of 1.6 ml. The mixture was incubated 15 minutes at 37 °C without shaking before 400 μl of 5 x NZY-broth was added and the cells were incubated with shaking for 45 minutes at 37 °C. The whole suspension was used to inoculate 100 to 200 ml LB-broth selection media supplemented with kanamycin. Over night culture at 37 °C was used for a large scale

plasmid preparation (see 2.7.1) and for preparation of a glycerole stock (see 2.3.2) on the following day.

2.15.4 Scaling down the size of cDNA library pools of *macaca* foliate papillae
Scaling down of plasmid pools made of approximately 2000 individual cDNA clones was done on the basis of the large scale *in vivo* excision (see 2.15.3). Therefore the *E. coli* XL0LR glycerole stock of a pool was titrated regarding to colony forming units (cfu) per volume. A scaling down of a pool by the factor of ten was achieved by splitting 3000 individual cDNA clones to 15 sub-pools. Therefore a definite volume containing 3000 cfu was prepared from the corresponding glycerole stock and used to inoculate 15 LB-kanamycin agar plates with approximately 200 cfu by spreading the bacterial suspension. After incubation at 37 °C overnight the approximately 200 colonies were harvested by floating off with LB medium. The bacterial suspension was either used for direct plasmid DNA isolation or for inoculation of a LB-kanamycin liquid culture. A glycerole stock was prepared in both cases (see 2.3.2).

2.16 Electrophysiology

Oocytes of *Xenopus laevis* were used as a heterologous expression system of *in vitro* generated cRNA (see 2.8) and analyzed by two electrode voltage clamp (TEVC) measurements. TEVC allows measuring the ion flow through the oocyte membrane as an electric current by clamping the membrane potential to a constant voltage. The membrane potential of the oocyte originates from different ion concentrations between the intra- and extracellular fluids as well as from the permeability of the membrane. Heterologously expressed proteins modifying the permeability of the oocyte membrane could therefore be analyzed with TEVC.

2.16.1 Preparation of *Xenopus laevis* oocytes and cRNA injection

2.16.1.1 Buffers and culture media

Culture media were supplemented with 2.5 mM sodium pyruvate, 10 U/ml penicillin G and 10 µg/ml streptomycin.

Anesthetic	0.1 - 0.15 % (w/v) 3-aminobenzoic acid ethyl ester methane-sulfonate; 0.25 M NaHCO ₃
Barth medium	90 mM NaCl; 2 mM KCl; 0.41 mM CaCl ₂ ; 0.33 mM Ca(NO ₃) ₂ ; 0.82 mM MgCl ₂ ; 10 mM HEPES; pH 7.4
Ca ²⁺ -free KulORI	90 mM NaCl; 1 mM KCl; 5 mM HEPES; pH 7.4
Collagenase-buffer KulORI	2 mg/ml collagenase IA or II (Sigma-Aldrich) in Ca ²⁺ -free KulORI 90 mM NaCl; 1 mM KCl; 2 mM CaCl ₂ ; 5 mM HEPES; pH 7.4
Na-Pyruvat	2.5 M in deionized water, filter sterilized
NMDG-KulORI	10 mM NaCl; 1 mM KCl; 2 mM CaCl ₂ ; 5 mM HEPES; 80 mM NMDG; pH 7.4 with HCl

NMDG-Barth	10 mM NaCl; 2 mM KCl; 0.41 mM CaCl ₂ ; 0.33 mM Ca(NO ₃) ₂ ; 0.82 mM MgCl ₂ ; 80 mM NMDG; 10 mM HEPES; pH 7.4 with HCl
Pyruvate	2.5 M in distilled water, filter sterilized
Penicillin G	10000 U/ml (Sigma-Aldrich)
Streptomycin	10 mg/ml (Sigma-Aldrich)

2.16.1.2 Isolation of *Xenopus laevis* oocytes

Female frogs were anesthetized by bathing in anesthetic for 15 minutes. Parts of the ovarian lobes of one of the paired ovaries were removed by survival surgery and transferred to KulORi. Muscle and skin were sutured and the frog was allowed to recover for at least 3 months.

To separate the oocytes from ovarian epithelium and to remove the oocyte surrounding follicle cell layer an enzymatic digestion was carried out. Therefore the removed lobes were transferred into a petri dish containing Ca²⁺-free KulORI and divided into smaller packages of about 10 to 20 oocytes. The oocyte packages were then washed 3 times within 5 minutes and 2 times for 5 minutes in Ca²⁺-free KulORI on a horizontal shaker. The enzymatic digestion was carried out at room temperature using collagenase-buffer and incubation for approximately 40 minutes on a horizontal shaker. The incubation time was critically linked to the collagenase activity and was empirical determined for each batch of collagenase. The progress of the defolliculation was monitored visually using a stereo binocular microscope (Olympus). The digestion was stopped by five wash steps in plenty of Ca²⁺-free KulORI as described before. Isolated oocytes were transferred into KulORI or Barth medium supplemented with penicillin/ streptomycin and pyruvate. For recovery oocytes were stored for at least 1 hour at 18 °C. Afterwards viable oocytes of developmental stages V and VI were selected manually using a glass pasteur pipette for subsequent microinjection of cRNA. All oocytes were maintained at 18 °C.

2.16.1.3 Microinjection of cRNA

In vitro generated cRNA (see 2.8.4) was injected into the bright vegetal pole of selected oocytes using the micro injector Nanoliter 2000 (WPI). Glass micropipettes used for injection were pulled from glass capillaries (4878, 3.5 in., WPI) with a standard pipette puller P-97 (Sutter Instrument). Previous to the injection the micropipette was opened by breaking the tip using RNase free forceps. Each oocyte was microinjected with 64 nl of cRNA solution using the fast injection speed. Amount of injected cRNA depended on the particular approach. For establishment of screening assay 12 pg of human α -ENaC cRNA was functionally expressed with an excess of 16 ng human $\beta\gamma$ -ENaC. Thus, lowest

possible concentration of one macaque cDNA clone in a pool of 2000 cDNA clones was mimicked. For screening of cDNA library for novel salt taste receptors and ENaC interaction partners to 22 to 42 ng of macaque pool cRNA with either 16 ng human $\beta\gamma$ -ENaC or 5 ng human δ -ENaC were injected per oocyte. Thereby expression of *macaca* pool F1-7 with 16 ng human $\beta\gamma$ -ENaC as well as expression of 350 pg human δ -ENaC with 32 pg human $\beta\gamma$ -ENaC served as positive controls. Amount of injected cRNA was determined empirical, leading to reproducible assembly of an amiloride sensitive $\delta\beta\gamma$ -ENaC sodium channel. Heterologous expression of mouse δ -ENaC transcripts was achieved by injection of 32 ng mouse δ -ENaC cRNA with either 16 ng human $\beta\gamma$ -ENaC or 2 ng human $\alpha\beta\gamma$ -ENaC cRNA per oocyte. Oocytes injected with ENaC-subunits were maintained in low-sodium solution (NMDG-KulORi or NMDG-Barth) during the expression phase. Water injected oocytes served as a control for each batch of oocytes and were designated as mock oocytes. After 2 to 3 days the oocytes were analyzed using two electrode voltage clamp as described in 2.16.2.

2.16.2 Two electrode voltage clamp (TEVC) using OpusXpress 6000A
An automated parallel voltage-clamp screening system (OpusXpress 6000A; Molecular Devices) was used for TEVC analysis of oocytes. The system enables whole cell recordings of 8 oocytes in parallel, while each oocyte is placed in a recording chamber continuously superfused with recording buffer (0.5 ml/min). For TEVC measurements each oocyte was impaled with two silver chloride microelectrodes designated as 'voltage electrode' and 'current electrode'. Electrodes had low capacitance and low resistance, latter ranging from 0.5 to 2.5 M Ω . Glass bodies of these microelectrodes were pulled from glass capillaries (TW150F-6, WPI) and filled with 3 M KCl as an electrolyte. Two further permanent installed bath reference electrodes present in each recording chamber enabled the measurement of the actual membrane potential of an oocyte by setting the extracellular bath potential to 0 mV. This 'virtual ground' is achieved by measuring the potential of the extracellular space with one reference electrode (Ag/AgCl pellet) and passing of current by the second bath electrode (platinum wire) to adjust the command voltage of zero mV. Using that voltage clamp the intracellular potential measured by the voltage electrode corresponds to the actual membrane potential of the oocyte. To measure the ion flow through the oocyte membrane as an electric current this membrane potential is clamped to a command voltage of -40 to -60 mV using the current electrode. The current passed to adjust the command potential is a direct measurement of ion flow through the oocyte membrane. TEVC analysis of cRNA injected oocytes and mock oocytes were performed

by superfusion with test solutions dissolved in recording buffer. To achieve a complete exchange of recording buffer with the test substance, oocytes were superfused with 300 to 500 μl with a flow rate of 1 to 2 ml/min. Application of recording buffer served as a control for each oocyte recorded.

2.16.3 Data recording

Current traces obtained with OpusXpress 6000A were recorded using OpusXpress software (1.1; Molecular Devices). Data sampling and conversion from analog I/V recordings to digital data was performed using the OpusXpress software. It enabled the control and tuning of the amplifier modules and digitizer for each of the 8 channels. Voltage clamp was carried out using ultra high DC gain, while following settings were set for all channels. The voltage sensing V head stage amplifiers were used with a voltage clamp gain of 2000 and a voltage clamp lag of 220 μs . Capacitance was neutralized to maximal 20 pF. The head stage amplifiers were used with an output gain of 2 and a filter cut-off frequency of 2 Hz. All other settings were used as set default (for detailed information see OpusXpress®6000A user's guide). Current traces were analyzed using Clampfit software (9.2; Molecular Devices). No digital filters were used.

2.16.4 Data analysis

For correction of individual oocyte fluctuations and application artifacts the recording buffer application was subtracted from measured responses for each oocyte. To correct for batch specific fluctuations the responses of mock oocytes were additionally subtracted from the measured response. Both correction approaches were carried out manually in Microsoft Excel. The detection limit of membrane current changes was limited to a change of 14 nA. Oocytes with a membrane current change above baseline fluctuation of Δ 14 nA were designated as responsive oocytes. Negative membrane current changes were designated as activation, while positive membrane current change was designated as inhibition. Data for heterologously expressed cRNAs were obtained from at least 2 batches of oocytes with at least 3 measured oocytes each. Statistical significance of responses, e.g. in comparison to mock oocytes, was tested using an independent two-sample (equal variance) and two-tailed Student's t-test.

2.17 Database search, multiple sequence alignment and phylogenetic tree construction

Homology search in NCBI and ENSEMBLE databases for SCNN1D and SCNN1A orthologs was performed using longest known human protein reference sequences NP_001123885 and NP_001153048.1 as templates (Wheeler *et al.*, 2008; Flicek *et al.*, 2007).

Longest orthologous SCNN1D proteins of selected vertebrate species as well as respective SCNN1A paralogue proteins were used to perform a multiple sequence alignment with MEGA software package version 4 (Tamura *et al.*, 2007). Thereby, following full length SCNN1D and SCNN1A protein sequences of mammalian and reptilian species were used: chimpanzee, western gorilla, bornean orangutan, rhesus monkey, white-tufted-ear marmoset, domestic guinea pig, cattle, dog, african savanna elephant, grey short-tailed opossum, chicken and zebra finch. Additionally, longest mouse and rat SCNN1A protein reference sequences were included in the alignment. Phylogenetic tree was calculated by neighbor-joining method and phylogeny was tested with 1000 replications.

To evaluate mouse *Scnn1d* (pseudo)gene, mouse chromosome 4 qE2 was analyzed for homologies to exonic and intronic sequences of human *SCNN1D* located on homologous human chromosome 1 p36.33 (Liddell *et al.*, 1999). Thereby genomic DNA of reference assembly 37.1 of laboratory mouse C57BL/6J was compared with *SCNN1D* (ID 6339). Homology search was carried out using BLASTN (Wheeler *et al.*, 2008) with successive reduction of stringency. Algorithm parameters different from standard settings used for low stringency BLASTN search were; word size: 7, match/mismatch score: 1/-1. Moreover, species specific repeats were filtered and a minimal score of 30 bits was set as cut off from random sequence homologies.

Repetitive sequences were identified using RepeatMasker (Smit *et al.*, 1996-2010) and the interspersed repeat database RepBase (Jurka *et al.*, 2005). Homologous reference sequences of retroviral sequences were identified using homology search (BLASTN).

3 Results

3.1 Possible involvement of ENaC in human salt taste perception

Multiple lines of evidences verify ENaC as amiloride-sensitive salt taste receptor in rodents (see 1.3). Expression analysis of ENaC subunits in human lingual tissue showed presence of all ENaC subunits in fungiform papillae and circumvallate papillae in the rank order $\alpha \sim \beta > \gamma \gg \delta$ (Stähler *et al.*, 2008). However, highest expression levels were found in non-chemosensory tissue, lacking taste papillae. A role in human salt taste perception would require a localization of ENaC subunits to taste bud cells, as it was shown for human bitter taste receptors (Behrens *et al.*, 2007; Chandrashekar *et al.*, 2000; Clapp *et al.*, 2001; Mueller *et al.*, 2005) or sweet taste receptors (Nelson, G. *et al.*, 2001; Zhang, Y. *et al.*, 2003). To evaluate cellular localization of α -, β -, γ - and δ -ENaC subunit mRNAs and proteins, *in situ* hybridization and immunohistochemistry were carried out, respectively.

3.1.1 Localization of ENaC subunit mRNAs in lingual taste tissue

To investigate if ENaC mRNAs are located in taste bud cells *in situ* hybridization (ISH) with digoxigenin-labeled RNA probes was carried out. ENaC-subunit specific probes (see appendix 7.4) were designed according to mRNA reference sequences of α -ENaC (NM_001038); β -ENaC (NM_000336); γ -ENaC (NM_001039) and δ -ENaC (NM_002978) (Wheeler *et al.*, 2008). ENaC subunit specific probes are able to detect virtually all known splice variants (see appendix 7.4, Tab. 7.4), with exception of two short δ -ENaC processed transcripts of 645 bp and 208 bp (Hubbard *et al.*, 2009, Wheeler *et al.*, 2008). *In situ* hybridization analysis included 24 fungiform papillae of 7 donors and 6 circumvallate papillae from 6 donors, while 50 and 60 sections were examined, respectively. Sense probes, identical to the mRNA sequences served as negative control in each experiment. No labeling of β -, γ -, or δ -ENaC mRNAs was detected within taste buds of analyzed circumvallate and fungiform papillae (see Fig. 3.1). However, *in situ* hybridization was sensitive enough to detect β -, γ - and δ -ENaC mRNAs in non-chemosensory epithelial cells (see Fig. 3.1, arrows), which is in accordance with localization of ENaC subunits in rodent tongue epithelium (Kretz *et al.*, 1999). Solely mRNA detected within taste buds was α -ENaC subunit mRNA in circumvallate papillae (see Fig. 3.1, arrowheads). No labeling was observed in the controls using the appropriate sense probes.

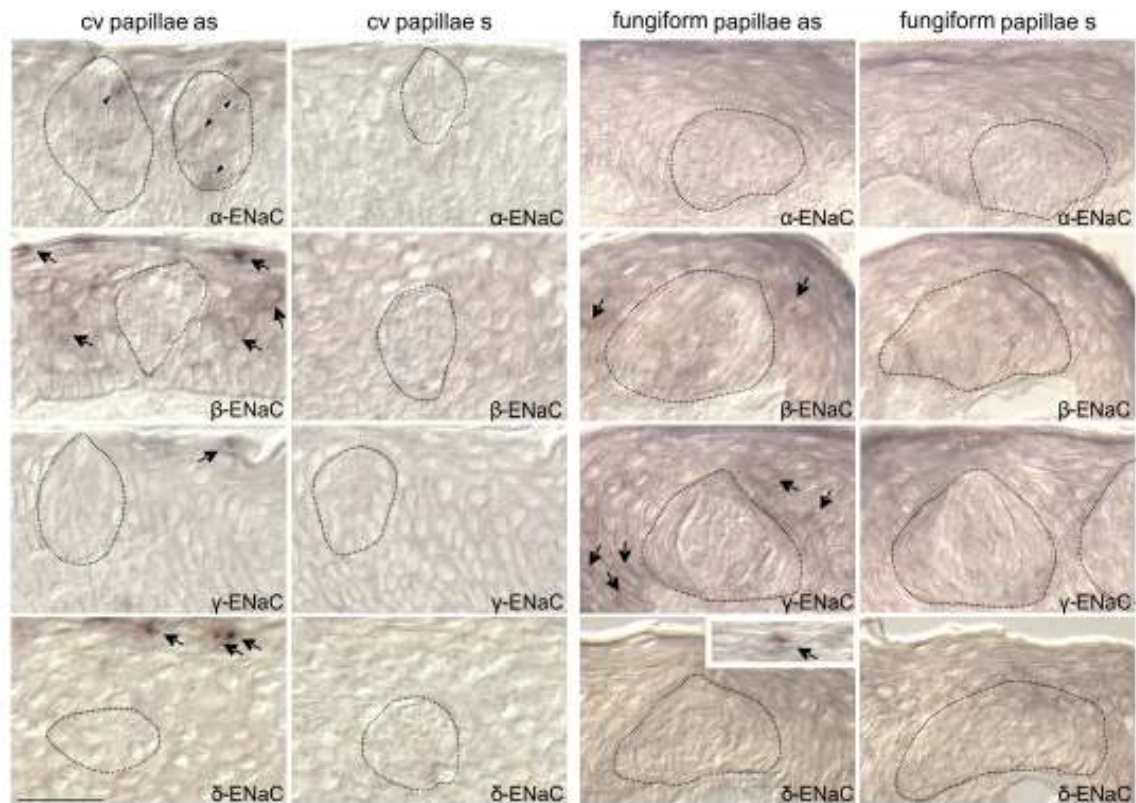


Fig. 3.1: Localization of ENaC subunit mRNAs in circumvallate and fungiform taste papillae by *in situ* hybridization. Brightfield photomicrographs of colorimetric detected 10 μ m cryo-sections of circumvallate (cv) and fungiform papillae hybridized with digoxigenin labeled α -, β -, γ - or δ -ENaC antisense (as) and sense probes (s). Sense probes served as negative control. Taste buds are encircled by dotted lines, while arrow heads point to labeled taste bud cells and arrows point to labeled epithelial cells. The inset in the panel showing the data for δ -ENaC antisense in fungiform papillae representatively shows one labeled epithelial cell. Scale bar of 20 μ m applies for all pictures as well as for the inset.

Quantification was carried out counting positively labeled taste buds in relation to the total amount of taste buds per section and resulted in 56 % labeled taste buds in circumvallate papillae for the α -ENaC antisense probe (see Tab. 3.1, ISH).

Tab. 3.1: Percentage of positive taste buds/total taste buds per section using *in situ* hybridization (ISH) and immunohistochemistry (IHC).

	ISH (RNA)				IHC (protein)			
	circumvallate		fungiform		circumvallate		fungiform	
ENaC	%	positive/total	%	positive/total	%	positive/total	%	positive/total
α	56	47/84	0	0/39	17	12/69	0	0/25
β	0	0/90	0	0/37	9	7/80	75	6/8
γ	0	0/109	0	0/51	97	87/90	81	9/11
δ	0	0/154	0	0/25	25 (100) [#]	28/112 (28/28) [#]	14 (100) #	4/27 (4/4) [#]

[#] all visible taste pores were stained

In conclusion, analyses on RNA level showed α -ENaC mRNA present in taste bud cells of circumvallate papillae, while β -, γ - and δ -ENaC mRNAs were confined to taste bud surrounding epithelial cells in both papillae.

3.1.2 Localization of ENaC subunit proteins in lingual taste tissue

To account for short lived ENaC mRNA and to provide evidence for the lingual presence of ENaC subunits on protein level, indirect immunohistochemistry was carried out. The analysis with specific antisera for ENaC subunits (see appendix 7.6) included 7 fungiform papillae and 5 circumvallate papillae from 5 donors, while 75 and 90 sections per subunit were examined, respectively. All antisera labeled non-chemosensory epithelial cells in circumvallate and fungiform papillae, with exception of the α -ENaC antiserum in fungiform papillae (see Fig. 3.2 A, arrows). Specific antisera for α - and β -ENaC labeled a small subset of taste bud cells in circumvallate papillae with 17 % and 9 % labeled taste buds per section, respectively. More cells were labeled with the γ -ENaC antiserum with 97 % taste buds per section (see Tab. 3.1, IHC). A comparable amount of cells was labeled in fungiform papillae using β - and γ -ENaC antisera with 75 % and 81 % labeled taste buds per section, respectively. In contrast to circumvallate papillae, no labeling was observed for the α -ENaC antiserum in fungiform papillae.

The δ -ENaC antiserum labeled 25 % and 14 % of taste buds in circumvallate and fungiform papillae, respectively (see Tab. 3.1). Remarkably, this antibody labeled all visible taste pores (see Fig. 3.2 A+C, arrowheads and Tab. 3.1). Specificity of antisera was controlled by pre-absorption with the corresponding blocking peptides, resulting in a marked reduction or absence of any labeling (see Fig. 3.2 A). Furthermore specific binding of secondary antibodies was proven by incubation of sections omitting the primary antisera, which resulted in no labeling at all (see Fig. 3.2 B).

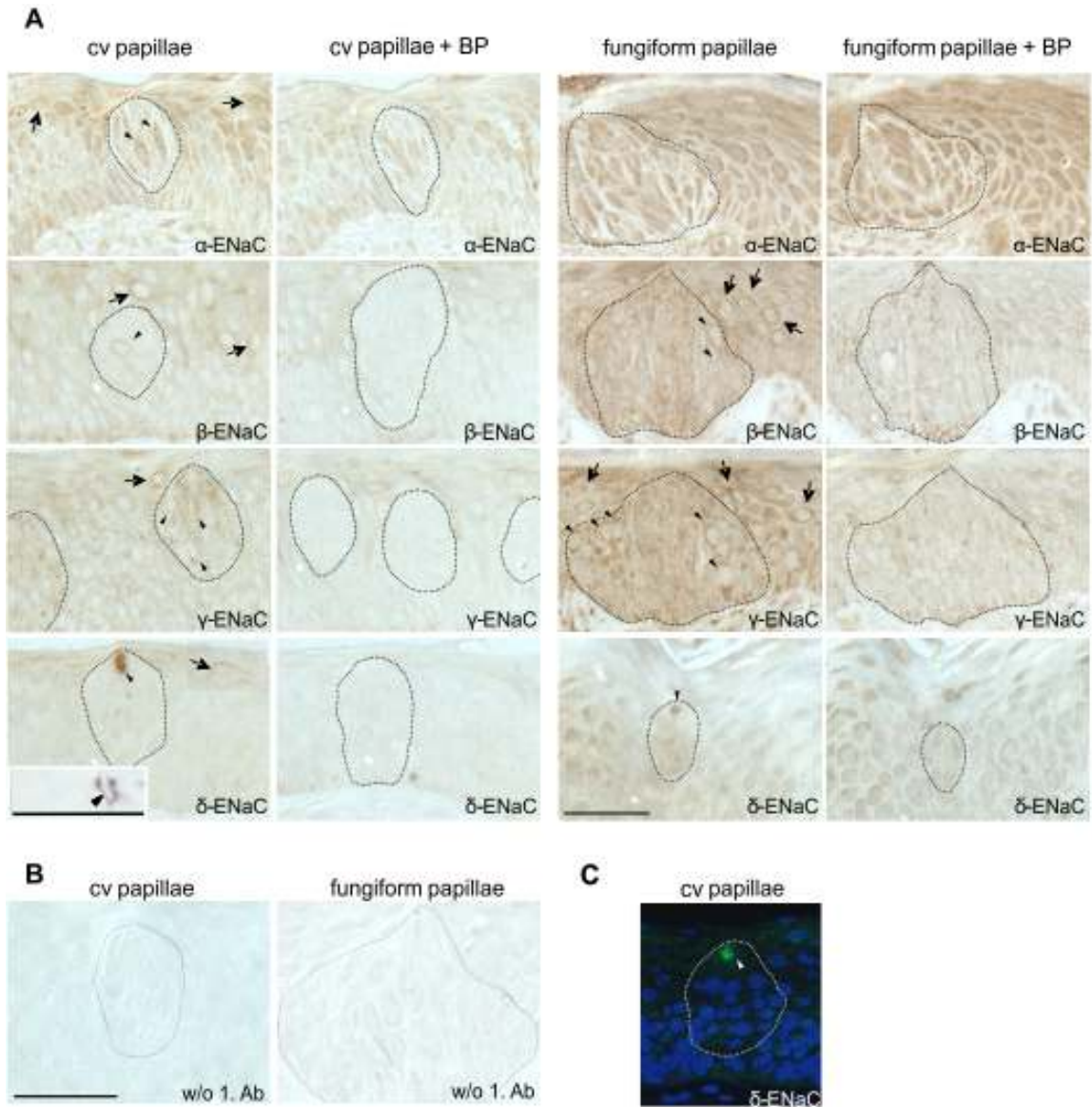


Fig. 3.2: Localization of ENaC subunit proteins in circumvallate and fungiform papillae by immunohistochemistry. **A** Brightfield photomicrographs of DAB-immunoperoxidase labeled 2 μ m paraffin-sections of circumvallate (cv) and fungiform papillae incubated with specific antisera directed against α -, β -, γ - or δ -ENaC. The inset in the panel showing the data for δ -ENaC antiserum in cv demonstrates a stained pore at higher magnification. Pre-absorbed antisera with the corresponding blocking peptide (BP) served as a specificity control. **B** Representative micrographs of cv and fungiform papillae omitting primary antibody. **C** Fluorescence photomicrograph of fluorescence-immunoperoxidase labeled cv taste pore of a 2 μ m paraffin-section incubated with δ -ENaC antiserum (green, excitation at 488 nm). Nuclei are counterstained with DAPI (blue, excitation at 360 nm). Taste buds are encircled by dotted lines, while arrow heads point to labeled taste bud cells and arrows point to labeled epithelial cells. Scale bar in all pictures is 20 μ m.

Taken together RNA and/or protein of all ENaC subunits were shown to be present in human taste buds of circumvallate and fungiform papillae, with the exception of α -ENaC in fungiform taste buds. Immunohistochemical data point to the presence of basolateral α -, β -, and γ -ENaC subunits in circumvallate and β - and γ -ENaC subunits in fungiform

taste bud cells. Strikingly, the δ -ENaC subunit was exclusively located at taste pores of fungiform and circumvallate papillae.

3.1.3 Validation of δ -ENaC protein localization in taste pores

Immunolocalization of δ -ENaC revealed prominent taste pore staining of by δ -ENaC antiserum in both taste papillae. However, this is in conflict to the failed detection of δ -ENaC mRNA by *in situ* hybridization as well as with low expression levels in taste tissue with less than 1 % of those of the other ENaC subunits found by quantitative RT-PCR (Stähler *et al.*, 2008). Possibly δ -ENaC mRNA is short lived and its protein is comparably stable. On the other hand δ -ENaC antiserum purchased from Chemicon might unspecifically stick to taste pore, arising the question whether the antiserum targets δ -ENaC protein at the taste pore. To show further evidence for δ -ENaC protein in human taste pores three additional anti-human δ -ENaC antisera were purchased (Abnova, lab no. 269; Abcam, 270; Santa Cruz, 271, see Fig. 3.3 and Tab. 7.6). Raised in different host species, they were immunized with human δ -ENaC immunogenes distinct from the initially used antiserum purchased from Chemicon (see Fig. 3.3). The exact epitope sequence of Abcam and Santa Cruz antisera are not published, but according to personal correspondence with the supplier the known Chemicon epitope could be excluded (yellow in Fig. 3.3). Prior to immunohistochemistry, specificity of all δ -ENaC antisera was analyzed using immunocytochemistry. Thereby, HEK293T cells transiently transfected with human δ -ENaC were incubated with the four δ -ENaC antisera. Specificity of immunolabeling was controlled by pre-absorption of δ -ENaC antisera with their corresponding blocking peptides. HEK293T cells transiently transfected with empty plasmid DNA served as a negative control. In order to exclude cross reactivity, HEK293T cells were transfected with human α -ENaC, the closest relative of δ -ENaC, sharing 37 % identical amino acids. These α -ENaC expressing cells were further used to control the success of transfection by incubation with α -ENaC antiserum.

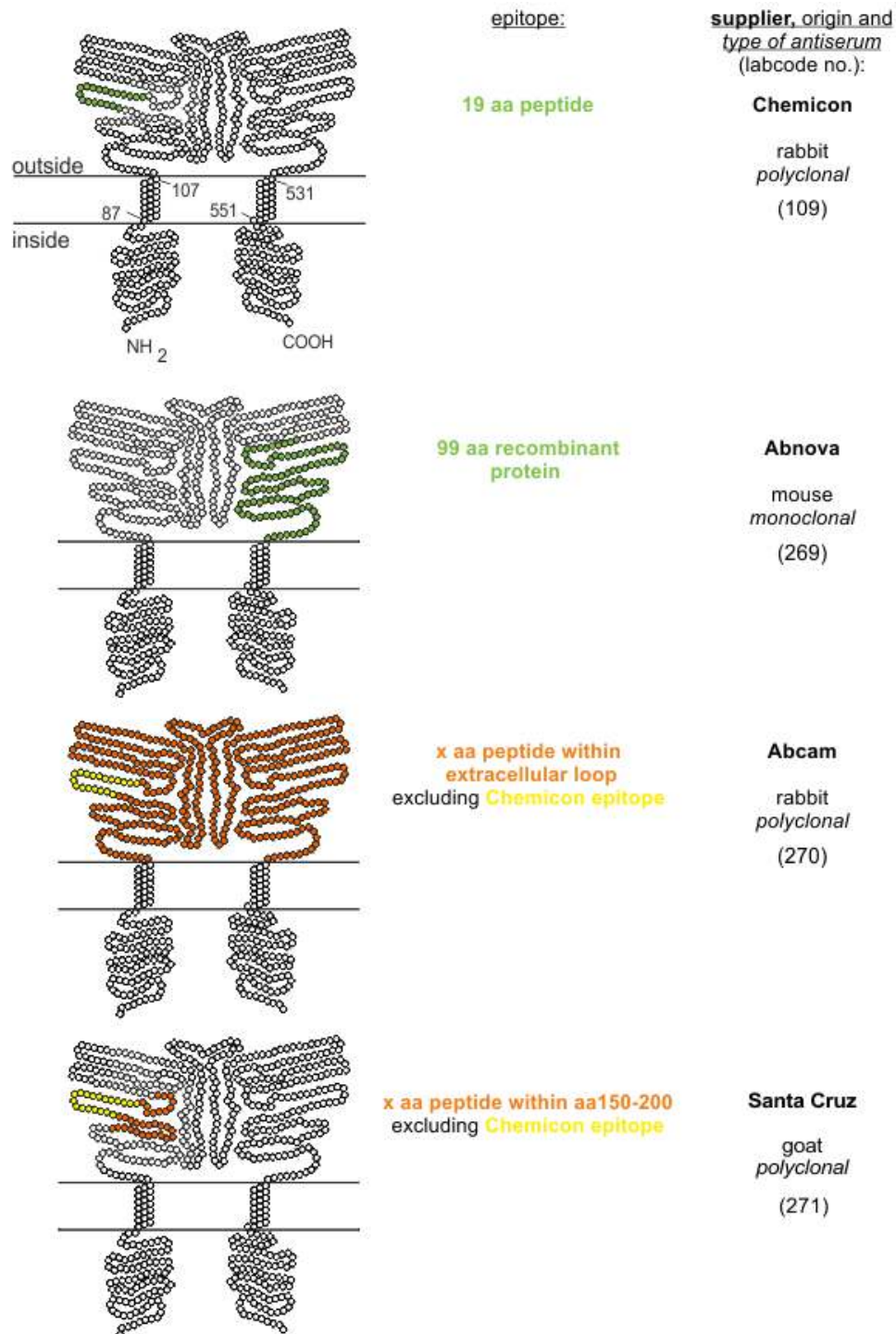


Fig. 3.3 Snake plot representation of human δ -ENaC subunit NP_002969 (638 aa) and δ -ENaC antisera epitope localizations. Each circle corresponds to an amino acid. Transmembrane helices were assigned according to UniProtKB entry P51172, while numbers correspond to transmembrane amino acid positions. Green filled circles indicate the exact localization of the immunogen residues. Orange circles indicate the putative region of an immunogen, while yellow filled circles show the excluded residues (personal correspondence of the supplier). The immunogen localization applies also for δ -ENaC isoform NM_001130413.1 (704 aa) which has a longer N-terminus.

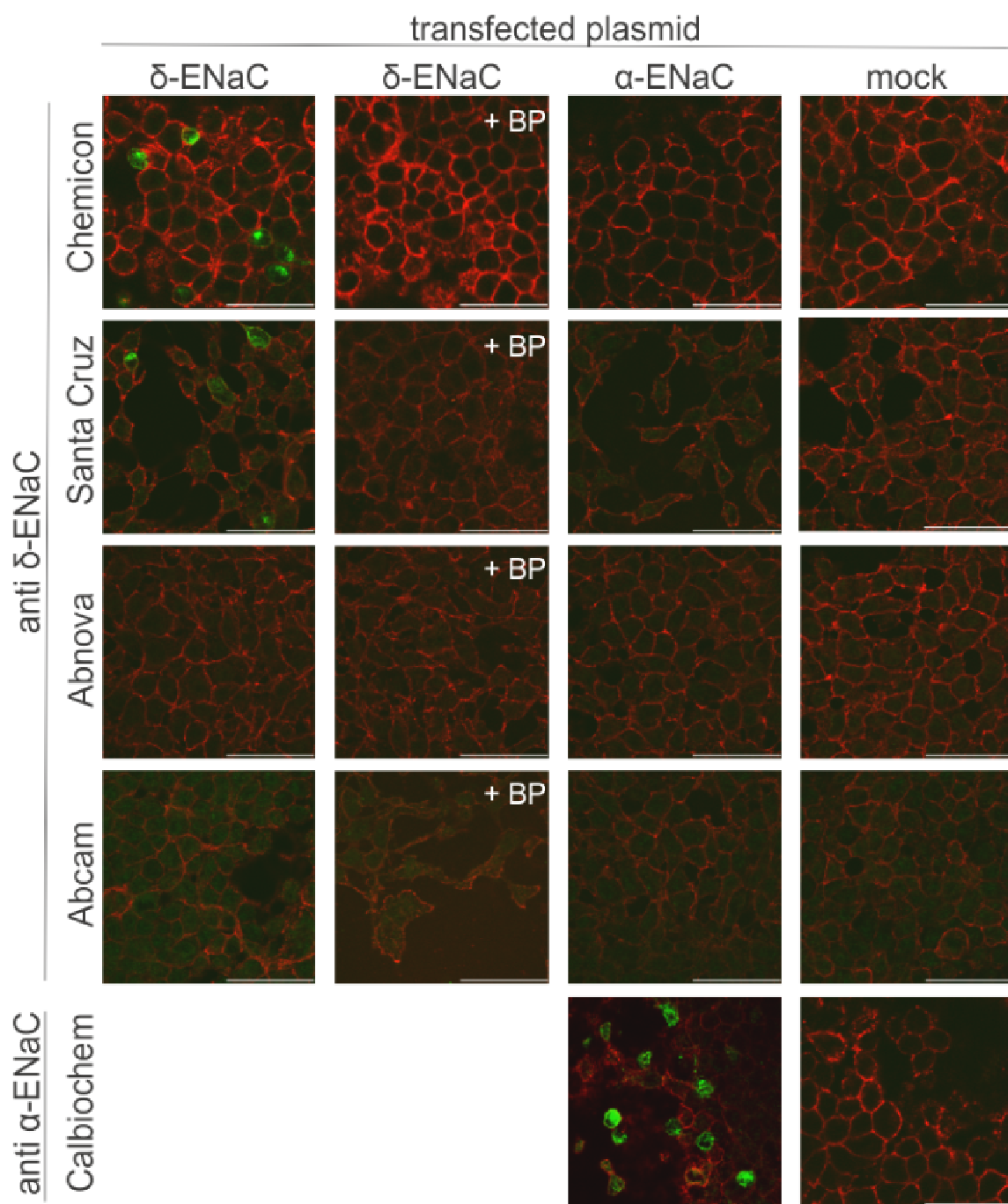


Fig. 3.4: Immunocytochemistry of human α -ENaC, human δ -ENaC and mock transfected HEK293T cells. Fluorescence photomicrographs of HEK293T cells transiently transfected with α -ENaC, δ -ENaC or empty plasmid DNA (mock). Cells were incubated with specific antisera directed against α -ENaC or δ -ENaC or without (w/o 1. Ab) and detected with fluorescent secondary antisera (green; excitation at 488 nm). Antisera pre-absorbed with the appropriate blocking peptide (BP) served as a specificity control. Glycoproteins of cell membranes were labeled by incubation with biotinylated concanavalin A and detected with fluorescent avidin (red; excitation at 633 nm). See Tab. 7.6 for applied antisera concentrations. Scale bar is 50 μ m.

Success of transfection was ensured by incubation of α -ENaC transfected cells with α -ENaC antiserum (Tab. 7.6). Green fluorescence of cells provided evidence for successful transfection in each experiment (see Fig. 3.4). Green fluorescence of cells heterologous expressing human δ -ENaC confirmed specific labeling by anti δ -ENaC antiserum purchased from Chemicon (see Fig. 3.4). Pre-absorption of antiserum as well as

application to α -ENaC transfected cells resulted in no staining at all. Thus, anti δ -ENaC antiserum purchased from Chemicon specifically detects human δ -ENaC (see Fig. 3.4). The same was true for anti δ -ENaC antiserum purchased from Santa Cruz, which specifically detected heterologously expressed human δ -ENaC in immunocytochemistry. However, antisera purchased from Abnova and Abcam failed to detect heterologously expressed δ -ENaC under applied conditions and were therefore excluded from further analyses. Incubation of mock transfected cells with primary antisera specific for δ -ENaC or α -ENaC showed no green fluorescence at all, showing that antisera do not unspecifically detect proteins of mock transfected cells (see Fig. 3.4). In conclusion, heterologously expressed human δ -ENaC protein is a specific target of antisera purchased from Chemicon and Santa Cruz. Thus, Santa Cruz antiserum was used to validate presence of δ -ENaC in human taste bud cells. In accordance with previous results obtained using antiserum purchased from Chemicon, application of Santa Cruz δ -ENaC antiserum to human circumvallate taste tissue resulted in apical labeling of taste bud cells as well as epithelial cells (see Fig. 3.5).

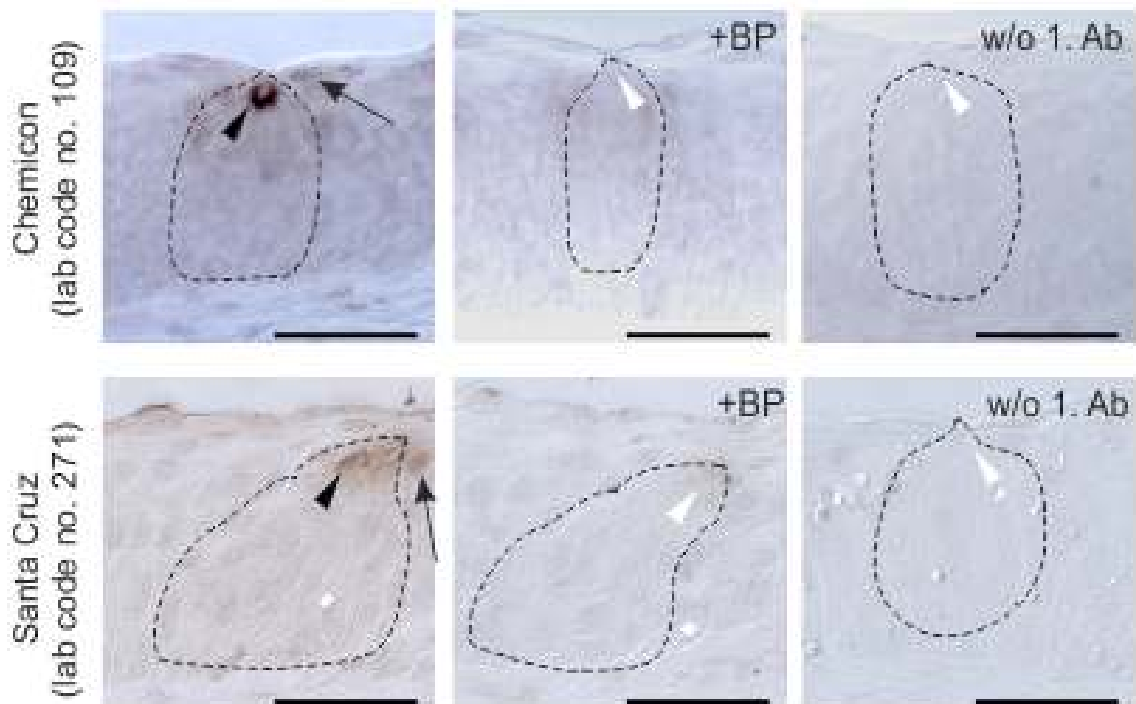


Fig. 3.5: Localization of δ -ENaC subunit proteins in human circumvallate papillae by immunohistochemistry. Brightfield photomicrographs of DAB-immuno-peroxidase labeled 2 μ m paraffin-sections of circumvallate papillae incubated with specific antisera from Chemicon or Santa Cruz directed against human δ -ENaC. Pre-absorbed antisera with the corresponding blocking peptide (BP) and omitted primary antibody (w/o 1. Ab) served as a specificity control. Taste buds are encircled by dashed lines. Black arrow heads point to labeled taste bud pores, arrows to labeled epithelial cells. White arrow heads point to non-labeled taste pores. Scale bar is 20 μ m.

Specificity, of the labeling was evident by its absence in controls without and with pre-absorbed primary antibody. Notably, staining pattern obtained with Santa Cruz δ -ENaC antiserum is consistent with immunolabeling by Chemicon antibody (see Fig. 3.5), validating the presence of δ -ENaC protein in human taste bud cells. Thus, two antisera raised in distinct host species using distinct immunogenes give evidence for the apical presence of δ -ENaC protein in human taste bud cells.

3.2 A role for delta-ENaC in rodent taste transduction?

Localization of δ -ENaC in taste pores strongly suggests a role in human taste transduction. In contrast, δ -ENaC is annotated as pseudogene in mouse (NG_011905) showing 94 % sequence identity over 51 nucleotides to human δ -ENaC (NM_002978) (Hubbard *et al.*, 2009). However, δ -ENaC mRNA was detected in mouse spermatids and pleural tissue (Hernandez-Gonzalez *et al.*, 2006, Nie *et al.*, 2009). Moreover, sperm membranes showed immunoreactivity to human anti- δ -ENaC antiserum, providing evidence for mouse δ -ENaC protein (Hernandez-Gonzalez *et al.*, 2006). To elucidate a possible role of δ -ENaC in rodent taste transduction mouse taste papillae were analyzed using human δ -ENaC antisera purchased from Chemicon and Santa Cruz previously validated for human lingual tissue (see 3.1.3). As shown in Fig. 3.6 the human δ -ENaC antiserum purchased from Chemicon specifically labeled the pore of mouse vallate taste buds and surrounding epithelial cells in a similar manner as observed for human taste buds (see Fig. 3.5).

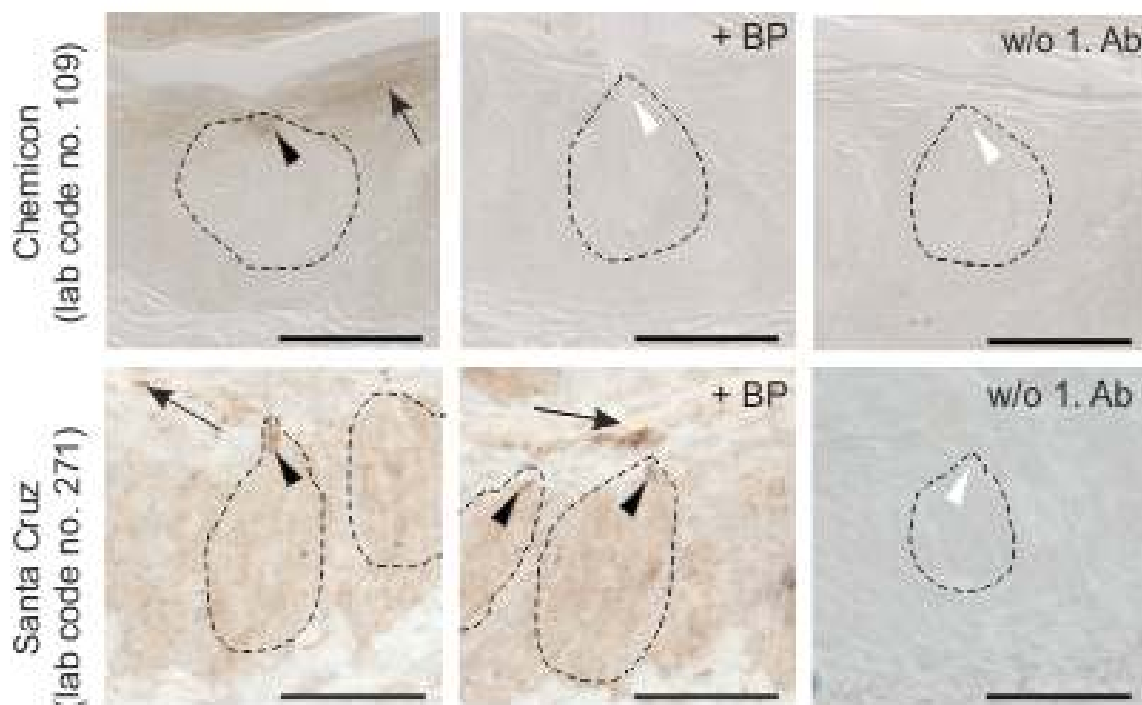


Fig. 3.6: Localization of δ -ENaC subunit proteins in mouse vallate papillae by immunohistochemistry. Brightfield photomicrographs of DAB-immuno-peroxidase labeled 2 μ m paraffin-sections of mouse vallate papillae incubated with antisera purchased from Chemicon or Santa Cruz specifically recognizing heterologously expressed human δ -ENaC. Pre-absorbed antisera with the corresponding blocking peptide (BP) and omitted primary antibody (w/o 1. Ab) served as a specificity control. Taste buds are encircled by dotted lines. White arrow heads point to taste pores. Black arrow heads and arrows indicate labeled taste pores and epithelial cells, respectively. Scale bar is 20 μ m.

Consistent with the immunolabeling in human lingual tissue all visible taste pores were stained. Specificity was controlled by pre-absorption with the corresponding blocking peptide as well as omitting the primary antibody, which both resulted in the absence of any labeling (see Fig. 3.6). In contrast, staining of mouse vallate taste pores and surrounding epithelium by anti human δ -ENaC antiserum purchased from Santa Cruz was unspecific, as pre-absorption of primary antibody with the corresponding blocking peptide resulted in persistent binding (see Fig. 3.6). However, the staining could be ascribed to the anti δ -ENaC antiserum, as no labeling occurred omitting the primary antibody. Thus, no clear evidence for the presence of δ -ENaC orthologue in mouse taste tissue could be provided on protein level, using human anti δ -ENaC antisera.

3.3 Evolution of epithelial sodium channel subunit delta in mice

Up to date, neither sequences of experimental detected mRNA nor protein of mouse δ -ENaC are annotated (Hubbard *et al.*, 2009; Wheeler *et al.*, 2008). Interestingly mouse δ -ENaC was classified as pseudogene by automated genome annotation (Wheeler *et al.*,

2008), while parts of δ -ENaC mRNAs were detected by RT-PCR in BALB/c and CD1 mice (Hernandez-Gonzalez *et al.*, 2006; Nie *et al.*, 2009). However, no experimental data about possible function of mouse δ -ENaC or its evolutionary origin are available (Sayers *et al.*, 2011). Thus, it is not clear if δ -ENaC is a gene, coding for functional protein product, or a transcribed pseudogene in mice. In order to elucidate if mice possess δ -ENaC protein, possibly detected by human anti δ -ENaC in vallate taste pores, mouse δ -ENaC pseudogene was analyzed.

3.3.1 Vertebrate δ -ENaC proteins and genetic organization of the mouse ortholog

In order to clarify if mouse δ -ENaC is a gene, coding for functional protein product, or a pseudogene, evolution of mouse δ -ENaC was investigated. To distinguish between human and mouse δ -ENaC genes, latter are indicated italic and termed *SCNN1D* and *Scnn1d* (sodium channel, non-voltage gated 1, delta), respectively. Respective proteins of both species are given in large letters (SCNN1D). This nomenclature is used from now on to differentiate genes and proteins. To determine if possible *Scnn1d* pseudogenization is a unique feature of mice, BLAST homology screen was used to analyze evolutionary conservation of SCNN1D among vertebrates. Thereby, human SCNN1D amino acid sequence served as template to identify vertebrate protein orthologs (Flicek *et al.*, 2011; Sayers *et al.*, 2011). This led to identification of SCNN1D in various species, as for example chicken, opossum, elephant, dog and the rodent guinea pig (Flicek *et al.*, 2011; Sayers *et al.*, 2011). In order to prove that identified SCNN1D proteins are species orthologs, multiple sequence alignment with corresponding SCNN1A paralogs was carried out and a phylogenetic tree was calculated (see appendix 7.7, Fig. 7.1 and Fig. 3.7A). Fig. 3.7 shows a clear separation of identified SCNN1A and SCNN1D proteins in two tree branches, demonstrating their paralog character. The presence of SCNN1D in reptiles, mammals and in particular in guinea pig implies evolutionary conservation of SCNN1D in vertebrates including rodents. Close evolutionary relation of mouse and guinea pig, which diverged 75 million years ago, is illustrated in the evolutionary tree (see Fig. 3.7B). However, no SCNN1D ortholog protein was found for mouse, while SCNN1A paralogs were easily identified (see Fig. 3.7). Thus, pseudogenization of *Scnn1d* might be species dependent and is possibly not a unique feature of the genus rodents. Interestingly, evolutionary tree illustrates larger amino acid divergences between SCNN1D protein orthologs than for SCNN1A (Fig. 3.7B).

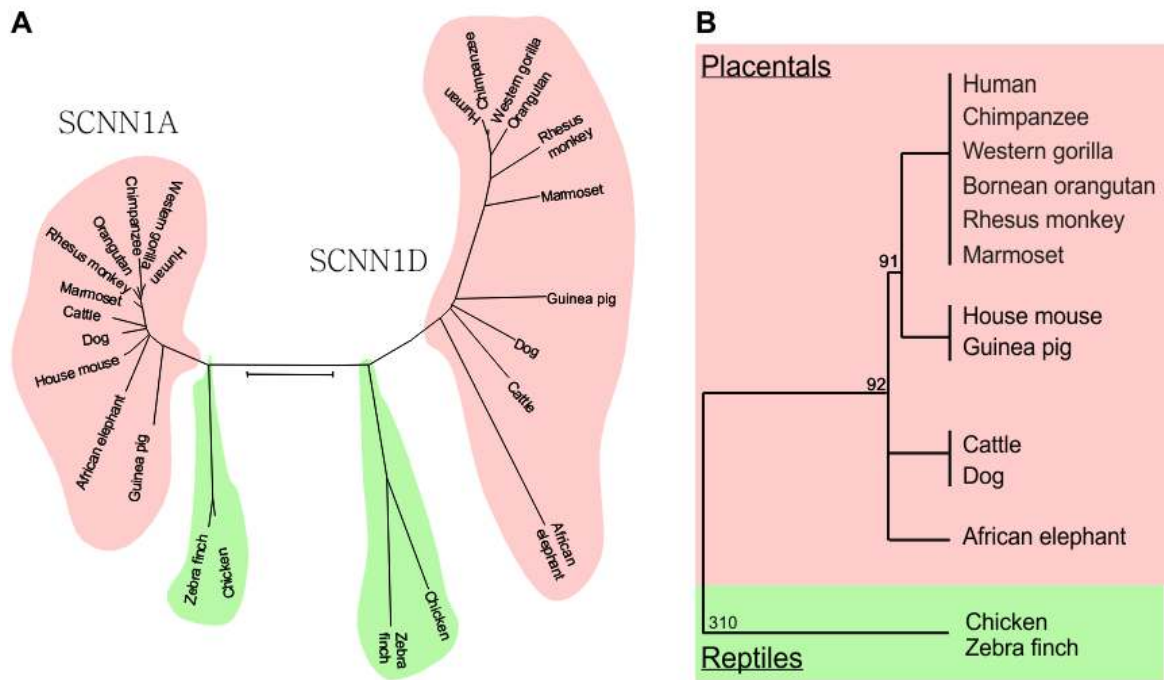


Fig. 3.7: Phylogenetic tree of SCNN1D and SCNN1A protein sequences and taxonomic relationship of species. **A** Phylogenetic tree based on multiple sequence alignment of SCNN1D and SCNN1A protein sequences referring to position 202 to 631 of human SCNN1D reference sequence NM_002978 (see appendix 7.7, Fig. 7.1). Dendrogram was calculated by neighbor-joining method and phylogeny was tested with 1000 replications. Scale bar indicates 10 % amino acid divergence in protein sequences. For accession numbers see appendix 7.7, legend of Fig. 7.1. **B** Evolutionary dendrogram of vertebrate species shown in A (Hedge 2002; Koina *et al.* 2006). Vertebrate classes placentals and reptiles are highlighted in red and green, respectively. Numbers indicate divergence time in millions of years ago. Branch lengths are not proportional to time.

Absence of mouse SCNN1D protein from databases is in accordance with classification of *Scnn1d* as pseudogene in laboratory mouse strain C57BL/6J (NG_011905.1, Sayers *et al.*, 2011). In order to get insight into possible SCNN1D protein loss in mice, genetic organization of mammalian SCNN1D was investigated. Thus, closest neighboring genes locating on the same chromosomal strand were evaluated. Virtually all eutherian SCNN1D are flanked by *PUSL1* and *B3GALT6*, exemplarily shown for human SCNN1D on chromosome 1 p36.33 (see Fig. 3.8, Flicek *et al.*, 2011; Sayers *et al.*, 2011). In fact, annotated mouse *Scnn1d* pseudogene is flanked by ortholog *B3galt6* and *Pusl1* genes on mouse chromosome 4 qE2, which is homolog to human chromosome 1 p36.33 (see Fig. 3.8, Sayers *et al.*, 2011). Moreover, mouse B3GALT6 and PUSL1 proteins are easily identified by BLAST homology search using human ortholog amino acid sequences (Sayers *et al.*, 2011). Thus, neighboring genes code for functional protein products and formation of *Scnn1d* pseudogene was without effect for *B3galt6* and *Pusl1* genes, encoded in proximity. Direct neighborhood of *B3galt6* and *Pusl1* would argue for a loss of *Scnn1d* by deletion. In

contrast, neighboring genes were found in a distance of about 100 kb in mice, which is more than twice of the distance in humans, making a gene loss by deletion highly unlikely. Thus, insertions might be responsible for putative pseudogenization of *Scnn1d* and loss of SCNN1D in mice.

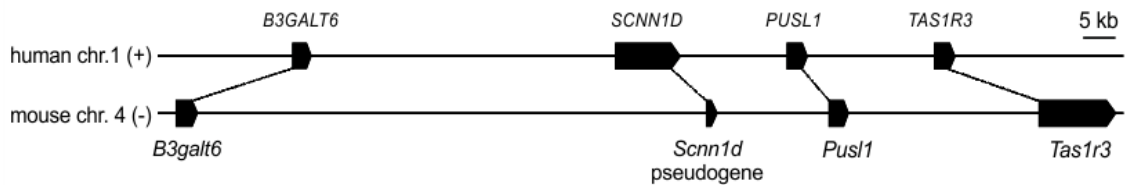


Fig. 3.8: Chromosomal organization of human SCNN1D and mouse *Scnn1d*. Detail of organization of homolog chromosomal regions of human chromosome 1 p36.33 plus (+) strand and mouse chromosome 4 qE2 minus (-) strand. Schematically shown are human genes *B3GALT6* (gene ID: 126792, Sayers *et al.*, 2011), *SCNN1D* (6339), *PUSL1* (126789) and *TAS1R3* (83756) as well as mouse genes *B3galt6* (117592), *Pusl1* (433813), *Tas1r3* (83771) and annotated mouse *Scnn1d* pseudogene (140501). Gene orthologs are connected by dotted lines. Scale is given in kilo bases (kb).

Interestingly, annotated *Scnn1d* spans only 1.6 kb on mouse chromosome 4 qE2, which is six fold less than its human *SCNN1D* ortholog (Sayers *et al.*, 2011). Hence, additional ortholog sequences might be present on mouse chromosome 4 qE2 possibly missed by automated computational genome annotation (Sayers *et al.*, 2011).

3.3.2 Comparative gene mapping of human *SCNN1D* to mouse chromosome 4

In order to reveal complete mouse *Scnn1d* gene structure comparative mapping of human *SCNN1D* to mouse chromosome 4 qE2 was carried out. Therefore BLAST homology search was used to map complete human *SCNN1D* to mouse chromosomal sequence interjacent of mouse *B3galt6* and *Pusl1* genes. Thereby, sixteen mouse sequence regions ortholog to *SCNN1D* exon and intron sequences were identified and termed as “homologies” from now on (see Fig. 3.9A). Mouse chromosomal homologies, ranging from 26 to 228 nucleotides were designated consecutively from roman I to XVI (see Fig. 3.9A). Except for human exons 2, 5, and 12, homologies for all fourteen *SCNN1D* exons as well as for intron 1 and 11 were discovered (see Fig. 3.9A). Interestingly, chromosomal homologies I and XVI, ortholog to human exon 1 and 14 are ortholog to known 5' and 3' untranslated (UTR) sequences of *SCNN1D* derived transcripts. This implies the identification of complete mouse *Scnn1d* gene encoding region. Notably, mouse homology V and XIV are ortholog to *SCNN1D* regions encoding highly conserved transmembrane

domains of SCNN1D. Thus, SCNN1D protein encoding domains might be preserved on mouse chromosome 4 qE2.

In total, 15 % of human *SCNN1D* sequence was retrieved on mouse chromosome 4 qE2, spanning 31 kb. This clearly expands the annotated *Scnn1d* sequence by the factor of 17 (Sayers *et al.*, 2011). However, vertebrate *SCNN1D* genes have a mean length of about 10 kb (Flicek *et al.*, 2011; Sayers *et al.*, 2011), which point to an unusual large size of computationally identified mouse *Scnn1d*. To evaluate this, the origin of sequences possibly expanding mouse *Scnn1d*, the chromosomal region encoding *Scnn1d* was analyzed in detail. Thereby, accumulation of repetitive sequences became evident. Using repeat masker software 47 % of 100 kb genomic region interjacent of mouse *B3galt6* and *Pusl1* genes were identified as interspersed repeats (Jurka *et al.*, 2005; Smit *et al.*, 1996-2010). Latter include short and long interspersed nuclear elements (SINE, LINE) as well as long terminal repeat (LTR) elements. In contrast, ortholog 47 kb genomic sequence interjacent of human *B3GALT6* and *PUSL1* genes possess 20 % SINEs, LINEs and LTR elements. The difference between human and mouse becomes impressively obvious comparing *SCNN1D* and *Scnn1d* encoding regions. Strikingly, 31 kb *Scnn1d* encoding region is comprised of 72 % interspersed repeats, while *SCNN1D* encoding region possess negligible 7 %. Masking repetitive elements within *Scnn1d* and *SCNN1D* chromosomal coding regions results in 9 kb free of repetitive sequences for both species. Hence, mouse *Scnn1d* gene was likely expanded by integration of interspersed repeats, providing an explanation for its unusual large size in regard to ortholog vertebrate *SCNN1D* genes, spanning 10 kb in average.

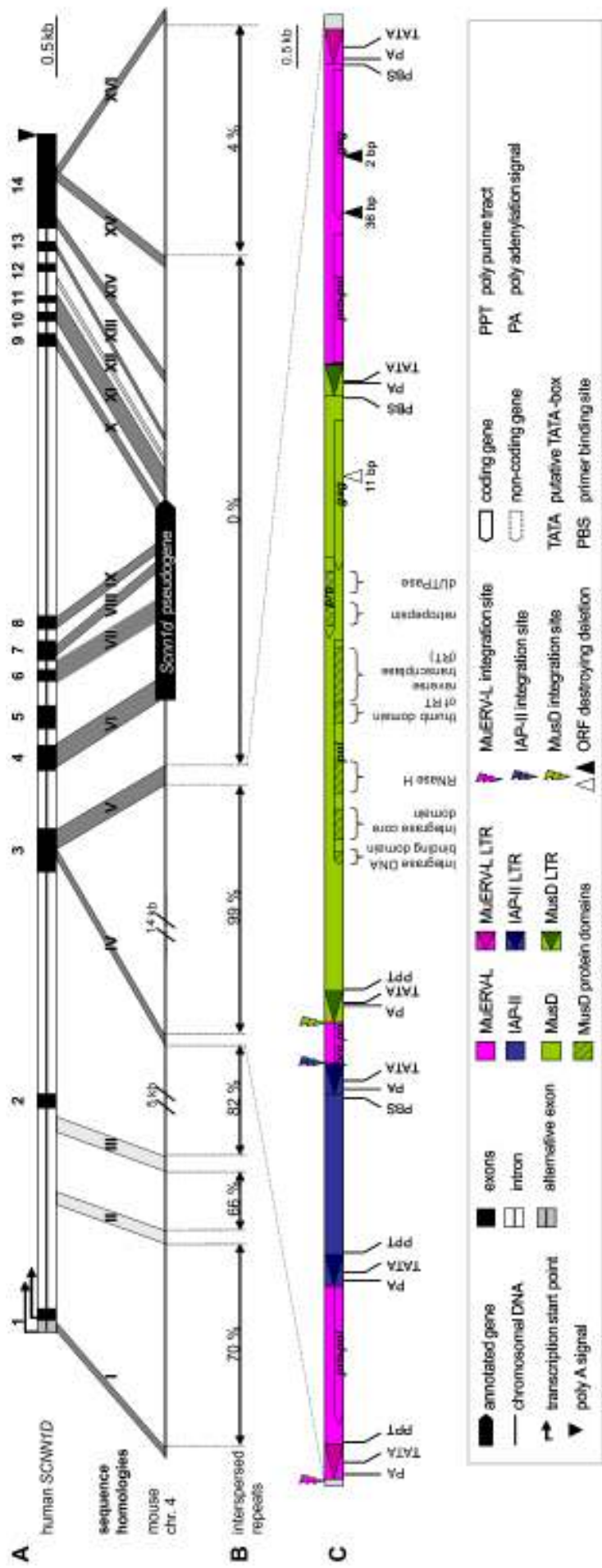


Fig. 3.9: Fine-mapping of human *SCNN1D* to mouse chromosome 4 and analysis for repetitive elements. **A** Schematic illustration of comparative chromosomal mapping of human *SCNN1D* reference gene (gene ID: 6339) to ortholog 31 kb section of mouse chromosome 4 qE2. Dashed lines on chromosome 4 qE4 mark shortened sequence by indicated sizes. Mouse chromosomal sequence regions homolog to human *SCNN1D* exons and introns are highlighted by dark and light grey parallelograms, respectively. Ortholog mouse sequences are numbered from roman I to XVI, while human *SCNN1D* exons are numbered from Latin 1 to 14. **B** Analysis of mouse *Scnn1d* homolog region for interspersed repeats. Analyzed sequence region interjacent of *SCNN1D* ortholog sequences is indicated by black arrows and bordered by dashed lines. Amount of identified interspersed repeats using repeat masker software is given in %. **C** Magnification of **B**. Shown is mouse chromosomal region between homology IV and V ortholog to human *SCNN1D* exon 3. Identified endogenous retroviruses MusD, MuERV-L and IAP-II are schematically shown in color code (see figure legend and text for details). Retroviral proteins encoded in *pro* and *pol* genes are given beneath brackets below respective genes. Scale is given in kilo bases (kb).

3.3.3 *Scnn1d* evolution by repetitive elements and identification of retroviral sequences

Interspersed repeats may have contributed to putative pseudogenization of mouse *Scnn1d*. Therefore, origin and distribution of repetitive sequences within identified *Scnn1d* were further investigated. Strikingly, accumulation of repetitive sequences within identified *Scnn1d* encoding region was observed interjacent of mouse homologies I, II, III, IV and V, representing 25 of 31 kb of *SCNN1D* ortholog region (see Fig. 3.9B). In contrast, 6 kb spanning chromosomal region inbetween mouse homologies V to XVI was virtually free of interspersed repeats (see Fig. 3.9B). Notably, this region contains the vast bulk of *SCNN1D* ortholog sequences with twelve of sixteen mouse homologies. Repetitive elements interjacent of mouse homologies I, II, III and IV, spanning 9 kb, are of diverse origin, including 14 % SINEs, 7 % LINEs as well as 56 % fragmentary LTR-like elements. Interestingly, 16 kb sequence between mouse homologies IV and V was exclusively made of large associated LTR-elements integrated inverse, in respect of *Scnn1d* (see Fig. 3.9B+C). Strikingly, mouse homologies IV and V are both ortholog to human exon 3, which codes for the first transmembrane domain of human *SCNN1D* protein (see Fig. 3.9A). Hence, mouse homology IV and V possibly correspond to ancestral mouse *Scnn1d* exon, which was originally homolog to human *SCNN1D* exon 3. Thus, it is highly likely that original *Scnn1d* exon ortholog to *SCNN1D* exon 3 was destroyed by insertion of retroviral sequences and thereby became a pseudogene in mice.

In general, pseudogenes can originate from functional genes by three distinct processes. These are either duplication of parental DNA (Nakano & Gunn, 2001) or retrotransposition of parental RNA intermediates (Peter *et al.*, 1988) or accumulation of mutations, deletions and insertions in functional genes (Vanin, 1985). Thus, pseudogenes can be classified as duplicated, processed and unitary pseudogenes, with respect to their evolutionary origin (Zhang, Z. D. *et al.*, 2008b). BLAST sequence analysis of mouse genome with previously identified *Scnn1d* sequences as well as with annotated *Scnn1d* pseudogene sequence (Sayers *et al.*, 2011) did not identify a further copy of *Scnn1d* within the mouse genome. Hence *in silico* analyses of C57BL/6J genome point to unitary *Scnn1d* pseudogene distributed over 31 kb of mouse chromosome 4 qE4.

3.3.3.1 Evolution of endogenous retrovirus insertion disrupting mouse *Scnn1d*

To track evolution and pseudogenization of mouse *Scnn1d* by repetitive elements, large associated LTR-elements were characterized with respect to their identity and order of chromosomal integration. BLAST homology search against NCBI nucleotide collection

identified three LTR-elements, locating inbetween mouse homologies IV and V, as endogenous retroviruses (ERVs, see Fig. 3.9C). A type L ERV (ERV-L) spans the whole 16 kb sequence inbetween mouse homologies IV and V (pink in Fig. 3.9C). The identified ERV-L element shows 95 % nucleotide identity to MuERV-L previously identified in BALB/c mice (Benit *et al.*, 1997) and was therefore designated as MuERV-L (pink in Fig. 3.9C). Notably, two additional type K ERVs (ERV-K) interrupt its sequence (blue and green in Fig. 3.9C). The more 5' located MuERV-L interrupting element shows 79 % nucleotide identities to renin-2 associated intracisternal A-type particle (IAP), originally identified in DBA/2 mice (Burt *et al.*, 1984). Thus, the 2.5 kb IAP type II retrotransposon was designated as IAP-II (blue in Fig. 3.9C). The more 3' located MuERV-L interrupting element is a 7.5 kb ERV-K element. It shows 98 % nucleotide identity to MusD-1 retrotransposon initially described for C57BL/6 mice and was therefore designated as MusD (green in Fig. 3.9C, Mager & Freeman, 2000).

In order to evaluate mutational evolution of mouse *Scnn1d* by MuERV-L, IAP-II and MusD, evolutionary order of chromosomal integration was determined. Transposition of ERVs includes duplication of target DNA sequence at the integration site, which thereupon flanks LTRs in the host genome as short direct repeats (Wicker *et al.*, 2007). Thus, sequence of short direct repeats gives evidence about integration site of respective ERVs. Interestingly, 3' MuERV-L integration site (AATG) overlaps with previously identified mouse homology IV ortholog to human *SCNN1D* exon 3 (pink flash in Fig. 3.9C). Thus, mouse chromosomal DNA encoding ancestral *Scnn1d* most likely served as DNA target for integration of MuERV-L, causing interruption of *Scnn1d* coding region (see Fig. 3.9C). Integration sites of IAP-II (GTTACA, blue flash in Fig. 3.9C) as well as of MusD (GGACAC, green flash in Fig.3.9C) originate from MuERV-L DNA, verifying their subsequent integration into MuERV-L and latter as the first integrated ERV. Analysis of variations within LTRs, which are initial identical and co-evolve independently with the host genome upon integration (Gifford & Tristem, 2003), revealed MusD as the youngest ERV, with only two nucleotide variations. Thus, ancestral mouse *Scnn1d* was interrupted by integration of MuERV-L, followed by insertion of IAP-II and recently MusD.

3.3.3.2 Analysis of mutagenicity of *Scnn1d* disrupting endogenous retroviruses

Mouse mobile elements are known for their persistent activity, responsible for 10 % of *de novo* insertional mutagenesis (Maksakova *et al.*, 2006, Zhang, Y. *et al.*, 2008a). Autonomous replication of LTR-elements requires transcription machinery of their hosts as well as

retroviral signal sequences for reverse transcription. To predict mutagenicity of MuERV-L, IAP-II and MusD sequence analysis was carried out.

In order to give evidence about ERV gene expression by mouse transcription machinery, LTR sequences were analyzed for eukaryotic transcription signals as TATA-box and polyadenylation signal. Five prime and 3' LTRs of MuERV-L and IAP-II contained consensus sequences of putative TATA-boxes (see Fig. 3.9C). Putative TATA-box of MusD LTRs possess a nucleotide exchange from T to C, when compared to TATA-box of first described MusD element (Mager & Freeman, 2000), resulting in suboptimal consensus sequence. However, retrotransposition active element MusD-1 possesses identical suboptimal TATA-box (Ribet *et al.*, 2004), suggesting possible transcription of identified MusD variant locating within *Scnn1d*. Polyadenylation signals are conserved in all LTRs of MuERV-L, IAP-II and MusD elements (see Fig. 3.9C). Thus, eukaryotic transcription signals are present and might enable LTR-driven gene expression.

Additional retroviral signal sequences are required for reverse transcription of ERVs, as tRNA primer binding site (PBS) downstream of 5'-LTR and purine-rich sequence (PPT) upstream of 3'-LTR. These signal sequences are present in MuERV-L, IAP-II as well as MusD allowing reverse transcription by retroviral proteins. In accordance with their classification into ERV-L and ERV-K type elements, MuERV-L possess a leucine (L) tRNA and MusD possess a lysine (K) tRNA PBS. Consistent with literature IAP-II element possess a phenylalanine tRNA primer binding site (Hawley *et al.*, 1984, Burt *et al.*, 1984; Christy *et al.*, 1985). Taken together, essential transcription signals for host transcription machinery as well as retroviral signal sequences are present in all three identified ERVs.

Autonomous replication and transposition of LTR-elements require functional retroviral proteins for reverse transcription. These requisite viral enzymes are protease, reverse transcriptase and integrase encoded in retroviral *pro* and *pol* genes. Further retroviral genes are *gag* and *env*, which encode structural proteins necessary for packaging of viral RNA into progeny virions. In accordance with described ERV elements *env* gene is absent in all identified ERVs pointing to a strict intracellular life cycle (Benit *et al.*, 1999, Ribet *et al.*, 2007). Thus, horizontal transmission from cell to cell is not feasible for MuERV-L, IAP-II and MusD.

ERVs can be still active for intracellular retrotransposition if coding competent *pro* and *pol* genes are encoded (Ribet *et al.*, 2007). MuERV-L lacks intact retroviral *pro* and *pol* genes due to integration of IAP-II and MusD retrotransposons (see Fig. 3.9C). Moreover,

MuERV-L *gag* gene is disrupted by two frame shift inserting deletions (black arrowhead in Fig 3.9C). Similarly, identified IAP-II lacks intact retroviral *gag*, *pro* and *pol* genes, due to large internal deletions, which is in accordance with other IAP-II elements (Horie *et al.*, 2007). Therefore, MuERV-L as well as IAP-II are not coding competent for protease, reverse transcriptase and integrase proteins and are therefore not able to transpose autonomously. Similarly, no functional *gag* gene is encoded in MusD sequence, caused by frame shift inserting deletion (see white arrowhead in Fig. 3.9C). Interestingly and in contrast to MuERV-L and IAP-II, MusD encodes complete *pro* and *pol* genes. MusD *pro* gene is coding competent for a 318 aa protein, which is 99 % identical to MusD-1 protease (DAA01917.1, Ribet *et al.*, 2004). According to protein reference sequence, identified MusD protease encompasses trimeric dUTP diphosphatase as well as pepsin like aspartate protease (see Fig. 3.9C). MusD *pol* gene is coding competent for 868 aa protein, which is 99 % identical to MusD-1 *pol*-derived proteins (DAA01918.1, Ribet *et al.*, 2004). Identified MusD *pol*-derived proteins include reverse transcriptase, thumb domain of reverse transcriptase, RNaseH as well as integrase core and integrase DNA binding domains (see Fig. 3.9C). Thereby, identified MusD variant integrated within *Scnn1d* is theoretically able for autonomous intracellular retrotransposition. However as revealed before, 5' and 3' LTRs of MusD differ in 2 nucleotides. Taken into account that autonomous retrotransposition was only evident for MusD elements possessing identical LTR sequences (Ribet *et al.*, 2004), identified MusD is most likely inactive concerning retrotransposition. However, MusD is coding competent for retroviral proteins which are possibly present *in vivo*. Taken together, MuERV-L, IAP-II and MusD, disrupting mouse *Scnn1d* are most likely not able to retrotranspose autonomously.

3.3.4 Expression analysis and characterization of mouse *Scnn1d*

3.3.4.1 RT-PCR analysis

In silico analyses point to unitary *Scnn1d* pseudogene, challenging the presence of protein coding *Scnn1d* transcripts in C57BL/6 mice. However, 80 % of *SCNN1D* ortholog sequences locate 3' of integrated ERVs identified and are virtually free of interspersed repeats. Thus, a truncated *Scnn1d* transcript coding for truncated mouse SCNN1D protein seems possible. One prerequisite for a possible function of *Scnn1d* is the existence of messenger RNA (mRNA). Interestingly, parts of *Scnn1d* transcripts were previously detected in BALB/c and CD-1 mice (Hernandez-Gonzalez *et al.*, 2006; Nie *et al.*, 2009). To assess the presence of *Scnn1d* derived mRNAs in C57BL/6 mice, RT-PCR with *Scnn1d*

specific primers was carried out. Mouse homology VI, ortholog to human *SCNN1D* exon 4, represents the largest exon ortholog sequence with 194 bp (see Fig. 3.9A). Therefore homology VI was chosen as template for primer specifically directed against *Scnn1d*. In addition to vallate papillae, presence of *Scnn1d* derived mRNAs was investigated in kidney and testis, which are representative expression sites for rodent *Scnn1* subunits (Lingueglia *et al.*, 1996; Waldmann *et al.*, 1995, Kretz *et al.*, 1999, Hernandez-Gonzalez *et al.*, 2006). Moreover, tissues represent distinct physiological functions including sodium regulation and taste transduction (Kellenberger, S. & Schild, 2002, Chandrashekar *et al.*, 2010, Stähler *et al.*, 2008). In fact, RT-PCR products of expected 143 base pairs were amplified from all tissues analyzed (see Fig. 3.10).

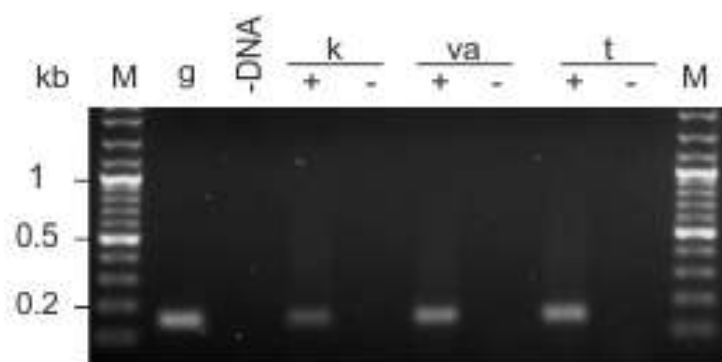


Fig. 3.10: *Scnn1d* expression analysis and derived mouse *Scnn1d* transcripts. RT-PCR analysis of cDNA generated from total RNA isolated from testis (t), kidney (k) and vallate papillae (va) of mouse strain C57BL/6 was carried out with *Scnn1d* specific primers. An expected 143 bp PCR product was amplified from all tissues analyzed. Genomic DNA (g) served as positive control. Reaction for cDNA synthesis was assembled with (+) or without (-) reverse transcriptase. Negative control (-DNA) contained all PCR components except DNA template. M: DNA molecular weight marker, kb: kilo bases

Thus, in accordance with literature *Scnn1d* transcripts exist (Hernandez-Gonzalez *et al.*, 2006; Nie *et al.*, 2009). Here, *Scnn1d* transcripts were localized to circumvallate papillae, kidney and testis *in vivo*, implying a possible function in C57BL/6 mice.

3.3.4.2 Identification of *Scnn1d* transcripts by rapid amplification of cDNA ends

In order to assess nucleotide sequence of complete *Scnn1d* mRNAs, *Scnn1d* transcripts were amplified using rapid amplification of cDNA ends (RACE). Based on PCR products obtained by initial RT-PCR (see Fig. 3.10), gene specific primers (GSP) and nested GSPs for 3' as well as 5' RACE were designed (see appendix 7.3, Tab. 7.2). RACE RT-PCR resulted in several 5' as well as 3' RACE amplicons from cDNA of C57BL/6 vallate papillae, kidney and testis were obtained by RT-PCR (see Fig. 3.11). To ensure the amplification of complete 3' and 5' cDNA ends, additional GSPs locating close to the initially identified

5'- or 3'-ends of amplified and sequenced RACE-PCR products were used (grey arrows in Fig. 3.12B). Subsequent RACE RT-PCR revealed no additional PCR products for the 5'-ends, arguing that the 5'-end was identified by initially used GSP. For 3'-ends additional PCR products were obtained for all tissues analyzed (see asterisks in Fig. 3.11). Tissue specific assembly of obtained RT-PCR products led to 9 distinct *Scnn1d* transcripts with a length of 2.9, 3.2, 1.9, 1.8, 2.8, 4.1, 3.5, 3.2 and 2.6 kb, consecutively numbered from 1 to 9 (see Fig. 3.11). Thereof, transcript 1 and 2 were amplified from vallate papillae, transcript 3 to 5 from kidney and transcript 6 to 9 from testis, respectively (see Fig. 3.11). To validate that identified transcripts are derived from mature mRNAs, sequences were analyzed for posttranscriptional modifications. All *Scnn1d* transcripts are spliced mRNAs, with exception of transcript 2 and 5, amplified from vallate papillae and kidney, respectively (see Fig. 3.12). Consensus splice donor and acceptor sites were identified for virtually all intron-exon boundaries. Moreover, alternative polyadenylation signals AAGAAA and AACTAAA (Graber *et al.*, 1999) are located at the 3'-end of transcript 1 to 7 (see Fig. 3.12), which were possibly used for 3'-end processing of these transcripts (Sastre-Garau *et al.*, 2000, Liu *et al.*, 2007). Additional to polyadenylation signal, consensus cleavage site and T/G rich regions are present at the 3'-end of transcripts 1 to 5, which are typical for 3'-end of mature mRNAs. Testis transcripts 8 and 9 lacked 3'-end processing signals. However, amplification from polyA RNA implies the presence of polyA tail and thereby 3'-end processing is assumed. In summary, assembled *Scnn1d* transcripts 1 to 9 are tissue specific and posttranscriptional processed, implying an active transcription of *Scnn1d* to mature mRNAs in C57BL/6 mice.

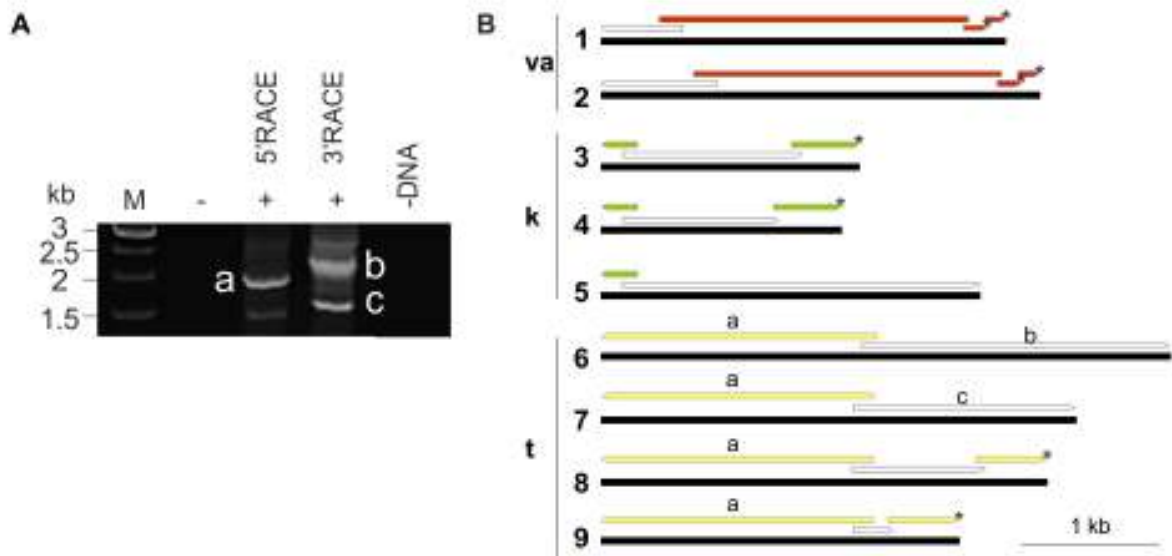


Fig. 3.11: Mouse *Scnn1d* transcripts obtained by RACE-RT-PCR. **A** Representative PCR products obtained by 3'RACE, 5'RACE from cDNA generated from testis poly A RNA. PCR products indicated by a, b and c are schematically depicted in B. Reaction for cDNA synthesis was assembled with (+) or without (-) reverse transcriptase. Negative control (-DNA) contained all PCR components except DNA template. M: DNA molecular weight marker. Genomic DNA (g) served as positive control. **B** Schematically shown are theoretically longest possible *Scnn1d* transcripts 1-9 (black rectangles) assembled in respect of tissue origin. Five prime and 3' RACE PCR products are shown as left and right orientated arrows, respectively. RT-PCR product using two gene specific primers (GSP) amplified from vallate papilla is shown as rectangle. Three prime RACE PCR products obtained by subsequent RACE PCR using 3' RACE amplicon derived primers are labeled with asterisks (*). RACE PCR products identical in sequence and used for the assembly of several transcript variants are highlighted by color code: red (va), green (k) and yellow (t). RACE PCR products differing in sequence within tissues are shown as white arrows. kb: kilo bases

Identified *Scnn1d* transcripts 1-9 were used to derive C57BL/6 *Scnn1d* gene structure by alignment to mouse chromosome 4qE2. Thus, consensus *Scnn1d* gene sequence, encompassing 4.6 kb was found (see Fig. 3.12B). This experimental derived *Scnn1d* gene does not encompass whole 31 kb spanning unitary *Scnn1d* pseudogene predicted by previously conducted *in silico* analyses. However, it enlarges annotated pseudogenic *Scnn1d* sequence by 3 kb in total (Sayers *et al.*, 2011). More precisely the annotated pseudogene sequence is expanded by 1.8 kb upstream and 1.2 kb downstream. It includes retroviral MuERV-L sequence at the 5' end as well as *SCNN1D* ortholog sequence homologies V-XIV. Notably, three alternative and tissue specific transcription start sites were identified for testis, vallate papillae and kidney (see Fig. 3.12). Relative localization of experimental identified *Scnn1d* in comparison to sequence homologies to human *SCNN1D*, MuERV-L and annotated *Scnn1d* on mouse chromosome 4qE2 is illustrated in Fig. 3.12A.

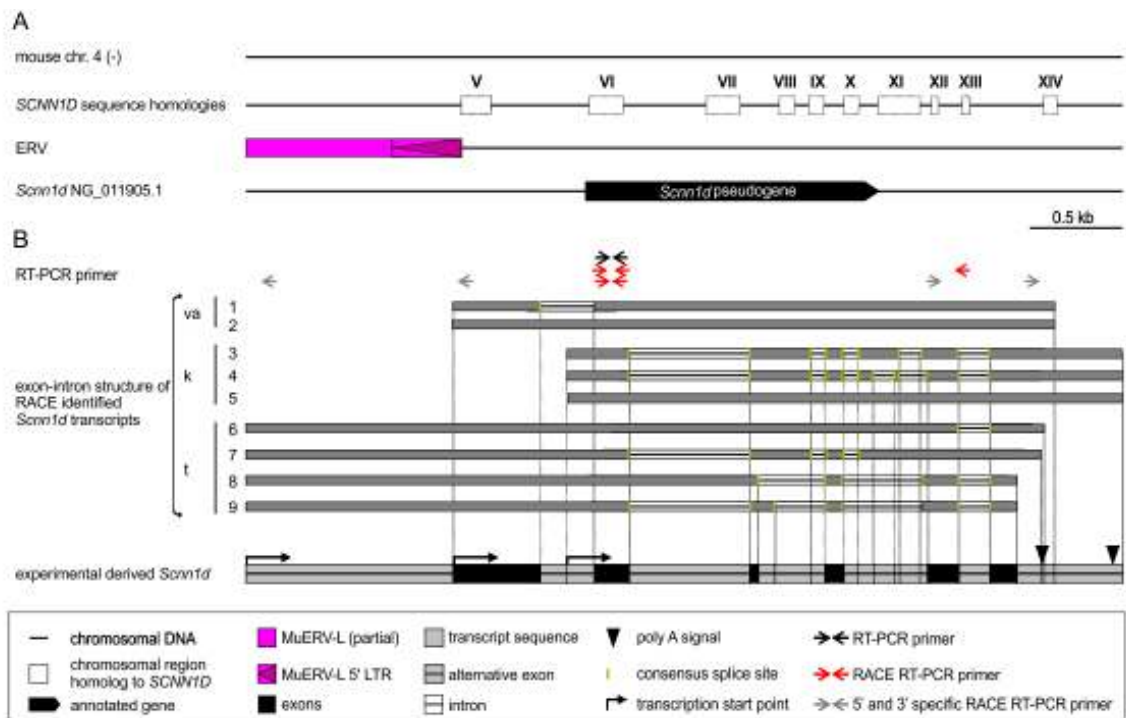


Fig. 3.12: Experimentally identified *Scnn1d* gene structure in comparison to mouse chromosome 4. **A** Detail of mouse chromosome 4 is shown schematically in respect of homologies to human *SCNN1D*, present ERVs and annotated *Scnn1d*. **B** Exon-intron structure of *Scnn1d* transcripts 1-9 identified by RACE RT-PCR from vallate papillae (va), kidney (k) and testis (t) as well as RT-PCR primers are shown (see figure legend and text for details). Exon-intron boundaries are indicated by dashed lines. Derived *Scnn1d* gene structure is illustrated beneath. A and B are depicted in same scale, primer and consensus splice sites are not. kb: kilo base

In order to identify putative promoters, chromosomal sequence upstream of *Scnn1d* transcription start sites were analyzed for TATA boxes. No consensus TATA-box could be identified within 100 bp upstream of RACE identified *Scnn1d* transcription start sites, corresponding to transcript start in testis, vallate papillae and kidney, respectively. Notably, 5'-LTR sequence of MuERV-L is located 30 bp upstream of vallate *Scnn1d* transcript start site (see Fig. 3.12). Thus, LTR-driven transcription by antisense promotor activity might be responsible for transcription of *Scnn1d* in vallate papillae (Maksakova *et al.*, 2006).

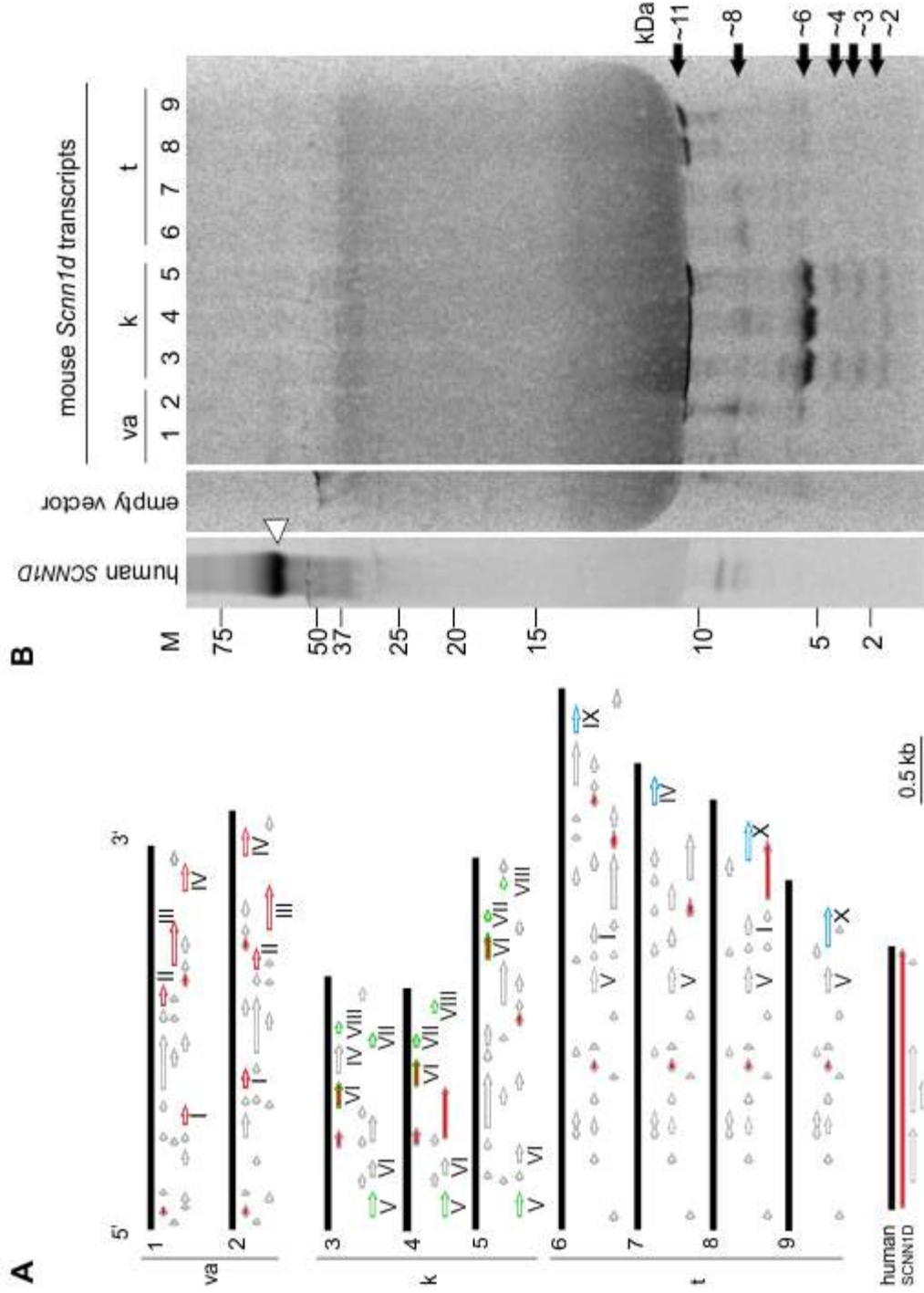
3.3.4.3 Analysis of *Scnn1d* transcripts for coding competence

Experimental identified *Scnn1d* gene enlarges automatically annotated mouse *Scnn1d* from 1.8 to 4.6 kb (see Fig. 3.12). Notably, expanded *Scnn1d* gene sequence includes SCNN1D sequence homologies V to XV ortholog to human exons 3 to 14 (see Fig. 3.9). As these encode 90 % of human SCNN1D protein, truncated mouse SCNN1D polypeptide might be encoded by *Scnn1d* transcripts. Notably, *Scnn1d* transcripts from testis and vallate papillae include retroviral sequences at their 5'-end, while kidney transcripts are

free of repetitive sequences (see Fig. 3.12). In order to investigate Scnn1d transcripts revealed by RACE analysis, latter were analyzed for open reading frames (ORFs) by computational translation of all nine Scnn1d transcripts in all three phases of the direct strand. Thereby, no main ORF coding for mouse SCNN1D was identified. In contrast, numerous premature stop codons lead to multitude small ORFs, while largest had a size of 432 bp and 144 aa, respectively (see Fig. 3.13A). In total, 57 distinct ORFs, with a size ranging from 30 to 432 bp are encoded within identified nine Scnn1d transcripts (see Fig. 3.13A). Thus, Scnn1d does most likely not code for full length SCNN1D protein, which has a size of 638 aa in humans (Wheeler et al., 2008). Seven of 57 ORFs present in transcripts from vallate papillae, kidney and testis, showed sequence homologies to human SCNN1D on amino acid level (red filled arrows in Fig. 3.13A). Thus, short SCNN1D peptides might be present in C57BL/6 mice.

In order to elucidate if Scnn1d transcripts are coding competent for polypeptides, radio labeled in vitro translation was carried out. Human plasmid DNA encoding SCNN1D was used as positive control and revealed successful in vitro translated SCNN1D protein detected at an expected size of about 70 kDa (see Fig. 3.13B). Smaller protein bands of about 8 kDa can be explained by ORFs additionally encoded on SCNN1D transcript (see Fig. 3.13B). In vitro translation of Scnn1d transcripts resulted in detection of polypeptides ranging from 2 to 11 kDa, while estimation of protein size within 10-15 kDa region is difficult, due to protein cloud of reticulocyte lysate used for in vitro translation (see Fig. 3.13B).

Fig. 3.13: Schematic representation of open reading frames derived from mouse *Scnn1d* transcripts and autoradiogram of *in vitro* translated *Scnn1d* transcripts 1-9. A Identified mouse *Scnn1d* transcript variants 1-9 from vallate papillae (va), kidney (k) and testis (t) are illustrated as black rectangles. Computationally derived open reading frames (ORFs) with a minimal length of 30 bp are depicted as block arrows for all three phases of the direct strand. Red filled block arrows label ORFs with homology to human SCNN1D. Transcript of human SCNN1D used as positive control is shown below *Scnn1d* transcripts. ORFs possibly translated by *in vitro* translation and detected by autoradiography (see B) are numbered from I to X and indicated as red (va), green (k) or blue (t) outlined arrows (see Tab. 1). Estimated sizes of potentially translated ORFs (kDa) are: ORF I (5), II (5), III (7), IV (12), V (6), VI (7), VII (4), VIII (3), IX (7), X (11). Kb: kilo bases. **B** *In vitro* translation using rabbit reticulocyte lysate was carried out in the presence of [³⁵S] methionine.



Human SCNN1D transcript, mouse *Scnn1d* transcripts 1-9 and empty vector served as templates. Products were separated using reducing tricine-SDS PAGE and exposed to phosphorimager screen. *In vitro* translation product of SCNN1D is depicted with modified intensity balance and served as positive control with an expected *in vitro* translated protein size of about 70 kDa (white arrowhead). Empty vector served as negative control and showed no protein bands. Black arrows indicate *in vitro* translation products from mouse *Scnn1d* transcripts, while estimated protein sizes are indicated on the right in kDa. Marker (M) bands from 2 to 75 kDa are depicted on the left. Broad cloud between 10 and 15 kDa is due to proteins of rabbit reticulocyte lysate.

However, detection of polypeptides by in vitro translation arise the possibility of presence of Scnn1d derived proteins in vivo. In order to correlate polypeptides to ORFs present on Scnn1d transcripts, computed molecular weights of ORFs as well as distribution of ORFs among transcripts was analyzed. Moreover, ORFs were analyzed for strength of Kozak sequence as well as homology to human SCNN1D on protein level (see Tab. 3.2). In vitro translation of vallate Scnn1d transcripts 1 and 2 result in detection of proteins at 8 kDa for both transcripts. These are likely derived from ORF IV, which is restricted to these transcripts and encodes a polypeptide of estimated 7 kDa (see Fig. 3.13A). Scnn1d transcript 2 led to detection of additional proteins detected at 6 and 11 kDa. ORFs potentially encoding 6 kDa proteins are ORF I and II with an estimated molecular weight of 5 kDa (see Fig. 3.13A). ORF III, coding for 12 kDa protein might be translated to a protein detected at 11 kDa (see Fig. 3.13A). However, ORF I, II and III are also present on Scnn1d transcript 1, lacking 6 and 11 kDa protein on autoradiography. Scnn1d transcripts 3, 4 and 5 revealed a nearly identical protein pattern after in vitro translation with proteins detected at about 2, 3, 4, 6, 8 and 11 kDa (see Fig. 3.13B). Possibly translated ORFs encoded in all kidney transcripts with an estimated size of 3, 4, 6 and 7 kDa are ORF VIII, VII, V and VI, respectively (see A). ORF VI is the largest ORF restricted to all three kidney transcripts. Hence, this ORF might be responsible for proteins detected at about 8 and 11 kDa. Interestingly, predicted ORF VI shows homology to human SCNN1D protein, with 20 % identities over 60 aa, while none of the other ORFs possess homology to human SCNN1D (see Tab. 3.2). Strong protein band at 6 kDa is most likely due to ORF V, as this is the first ORF encoded on kidney Scnn1d transcripts, strongly suggesting a transcription (see Fig. 3.13A). Although ORF VIII and VII are candidate ORFs for proteins detected at 3 and 4 kDa, these might be degradation products of 6 kDa protein. Latter is likely due for protein detected at 2 kDa, as no ORF restricted to Scnn1d transcripts 3, 4 and 5 could be correlated. Thus, small proteins from 2 to 4 kDa are likely degradation products of 6 kDa protein encoded by ORF V.

Tab. 3.2: Possibly *in vitro* translated open reading frames from *Scnn1d* transcripts 1-9.

ORF	length (nt)	length (aa)	protein size (kDa)	tissue	encoded by transcript no.	strong Kozak	homology to human SCNN1D
I	135	44	5	vallate	1, 2	-	-
				testis	6, 8		
II	147	48	5	vallate	1,2	-	-
III	324	107	12	vallate	1,2	-	-
				kidney	5		
IV	198	65	7	vallate	1, 2	-	-
				kidney	3		
				testis	7		
V	180	59	6	kidney	3, 4, 5	-	-
				testis	6, 7, 8, 9		
VI	183	60	7	kidney	3, 4, 5	-	20 % over 60 aa 3 % over 638 aa
VII	99	32	4	kidney	3, 4, 5	-	-
VIII	84	27	3	kidney	3, 4, 5	+	-
IX	198	65	7	testis	6	+	-
X	288	95	11	testis	8, 9	+	-

ORF, open reading frame; nt, nucleotides; kDa, kilo Dalton; no., number

In vitro translation of testis *Scnn1d* transcripts 6 to 9 showed distinct protein patterns. Proteins detected at 8 kDa were derived from transcripts 6 and 7, while 11 kDa proteins were translated from transcripts 8 and 9. Potential ORFs translated from *Scnn1d* transcripts 6 and 7 are ORF IX and ORF IV with 7 kDa each (see Fig. 3.13A). An ORF of about 8 kDa is not encoded in these transcripts. Protein of about 11 kDa, derived from *Scnn1d* transcript 8 and 9, originate most likely from ORF X, which has a computed molecular weight of 11 kDa (see Fig. 3.13A). This is substantiated by strong Kozak sequence of this ORF (see Tab. 3.2). Taken together short polypeptides are possibly present in all tissues analyzed, while proteins with homology to human SCNN1D might be present in kidney.

In order to reveal if *Scnn1d* derived polypeptides are recognized by human SCNN1D antiserum, which labeled vallate taste pores (see 3.2), western blot was carried out. However, analysis of all possible reading frames encoded in *Scnn1d* transcripts for homology to anti SCNN1D epitope revealed a maximal identity of 37 %, with maximal two positions side by side, pointing to the lack of adequate epitope similarity to human SCNN1D. Thus, only full size human SCNN1D was detected at expected size of 70 kDa, which derives from same *in vitro* translation experiment (white arrowhead in Fig. 3.14). Transfer of small proteins was ensured by processing of anti-SCNN1D control peptide made of 19 amino acids and predicted molecular weight of about 2 kDa. As shown by arrows in Fig. 3.14, small peptide was easily detected. Thus, *in vitro* translated protein

products from *Scnn1d* transcripts are not a target of anti human SCNN1D antiserum purchased from Chemicon. In conclusion, immunoreactivity of vallate taste pores is not due to *Scnn1d* protein products (see Fig. 3.6). Thus, human SCNN1D antibody purchased from Chemicon likely recognizes an unknown protein in taste pores of mice in addition to human SCNN1D. Moreover, this invalidates specific binding of human SCNN1D antiserum purchased from Chemicon to mouse taste pores of vallate papillae (see Fig. 3.6).

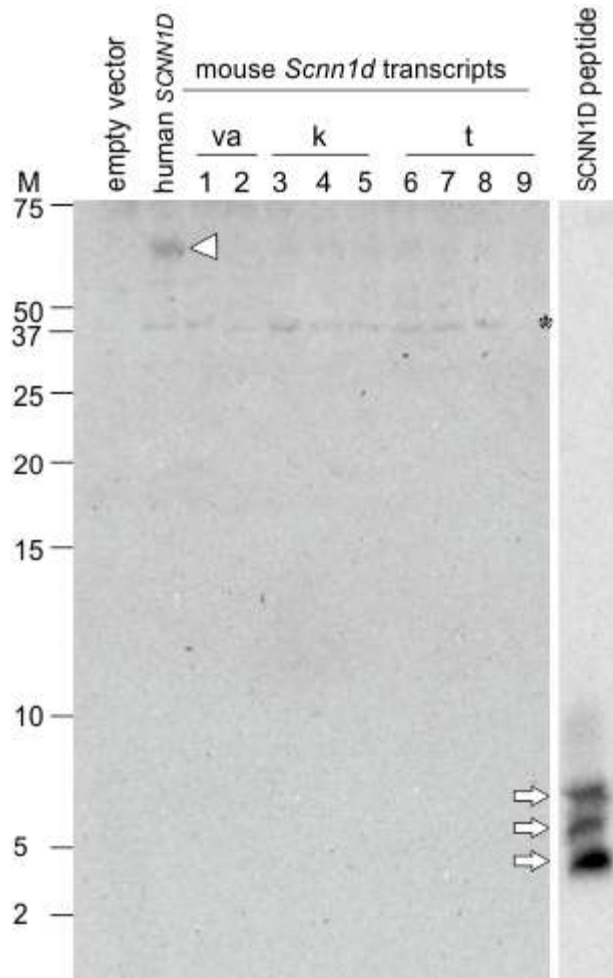


Fig. 3.14: Western blot analysis of *in vitro* translated *Scnn1d* transcripts. *In vitro* translation using rabbit reticulocyte lysate was carried out using human SCNN1D transcript, mouse *Scnn1d* transcript variants 1-9 from vallate papillae (va), kidney (k) and testis (t) and empty vector as templates. Equal protein amounts were separated using reducing tricine-SDS PAGE. A 70 kDa (white arrowhead) protein band representing full size human SCNN1D protein was detected with anti human SCNN1D antiserum. Empty vector and control peptide (white arrows) served as specificity controls. Asterisk labels nonspecific bands from the rabbit reticulocyte lysate, present in all lanes. M: molecular weight standard in kDa.

3.3.4.4 Analysis *Scnn1d* derived polypeptides for ion channel like function

Active transcription of *Scnn1d* transcripts implies physiological function of its transcripts. Moreover, they are coding competent for several short peptides from 2 to 11 kDa, including peptides with similarities to human SCNN1D. A function seems possible, taking various physiological functions of small polypeptides into account. The 10 kDa membrane

protein phospholemman for example can assemble into functional ion channels and is implicated in ion channel regulation (Moorman *et al.*, 1995; Wang *et al.*, 2010). Moreover, *Scnn1d* transcripts were detected in tissues known for SCNN1 expression (Kellenberger, S. & Schild, 2002), which makes an interaction of *Scnn1d* derived peptides with SCNN1A, SCNN1B and SCNN1G possible. In order to evaluate if *Scnn1d* derived peptides have an ion channel like function similar to human epithelial sodium channel, *Scnn1d* transcripts were heterologously expressed in oocytes of *Xenopus laevis*. Taking into account that interaction of human SCNN1D with SCNN1B and SCNN1G leads to assembly into functional $\delta\beta\gamma$ -ENaC ion channels, oocytes were microinjected with cRNA of *Scnn1d* transcripts in combination with cRNA derived from *SCNN1B* and *SCNN1G*. Protein products of *SCNN1B* and *SCNN1G* ($\beta\gamma$ -ENaC) are not able to assemble into a functional ion channel *in vitro* (McDonald *et al.*, 1995). Thus, ion channels assembled by polypeptides derived from *Scnn1d* transcripts alone as well as ion channels assembled by interaction with $\beta\gamma$ -ENaC will be detected by two-electrode voltage clamp analyses. If a functional ion channel is assembled, membrane current changes are detectable upon ion stimulation. Taking into account that $\alpha\beta\gamma$ - and $\delta\beta\gamma$ -ENaC differ significantly in their pharmacological properties, ion channels assembled by *Scnn1d* protein products might have distinctive properties. In order to account for possibly rendered ion selectivity several salt solutions should be applied. In order to determine adequate concentrations mock oocytes were exposed to sodium-, calcium-, ammonium-, potassium- and chloride-ions in a concentration range of 10 to 60 mM represented by NaCl, Na₂CO₃, CaCl₂, NH₄Cl, and KCl. Taking into account that 40 mM NaCl is a potent stimulus for human $\alpha\beta\gamma$ -ENaC or $\delta\beta\gamma$ -ENaC expressing oocytes, this was the concentration of choice for the NaCl stimulus (Stähler *et al.*, 2008). Thus, assay concentrations for Na₂CO₃, CaCl₂, KCl and NH₄Cl should evoke a maximal membrane current change as 40 mM NaCl in mock oocytes (dashed line in Fig. 3.15). In regard to that, the final assay concentrations were 40 mM NaCl, 10 mM Na₂CO₃, 10 mM CaCl₂ and 10 mM KCl. NH₄Cl was excluded from the analysis as endogenous responses of mock oocytes were strong in all tested concentrations (see Fig. 3.15). Mock and buffer application corrected membrane current changes mediated by oocytes functional expressing mouse δ -ENaC-like cRNAs 1 to 9 together with human $\beta\gamma$ -ENaC is depicted in Fig. 3.16. In accordance with literature $\beta\gamma$ -ENaC behaved like water injected control oocytes, showing no membrane current change upon salt application (see Fig. 3.16A). In contrast, $\delta\beta\gamma$ -ENaC positive control led to expected $\delta\beta\gamma$ -ENaC mediated sodium current changes from -0.7 to -1.2 μ A upon application of

Na₂CO₃ and NaCl, respectively. However, no membrane current changes of oocytes heterologous expressing *Scnn1d* transcripts in combination with βγ-ENaC were detected upon application of salt solutions (see Fig. 3.16A).

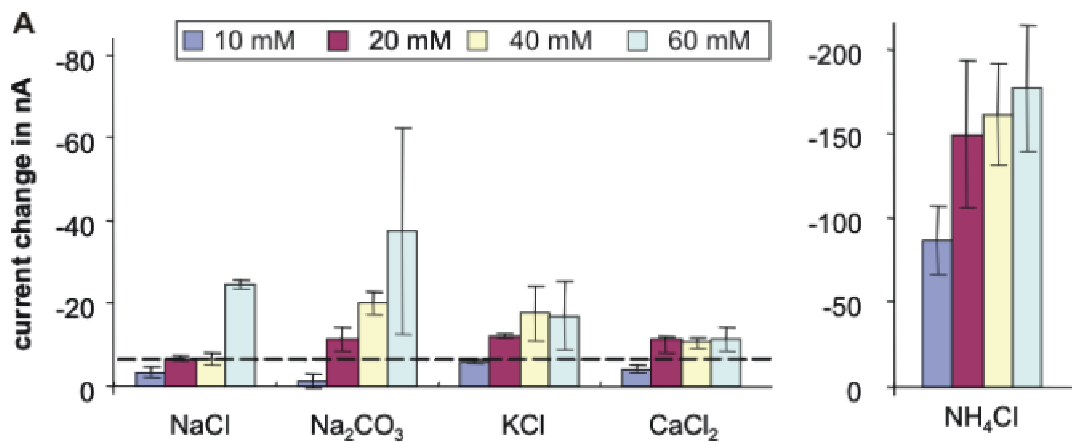


Fig. 3.15 Two-electrode voltage clamp analysis of mock oocytes. Amplitude of membrane current changes of water injected mock oocytes in nano ampere (nA) challenged with NaCl, Na₂CO₃, CaCl₂ and KCl. Dashed line indicates mean membrane current change induced by application of 40 mM NaCl. All salt solutions were diluted in NMDG-KulORi oocyte perfusion buffer. Two batches of oocytes with at least 3 individual oocytes each were measured. Response of every oocyte was corrected for individual responses to buffer application and the mean response of mock oocytes. Error bars indicate standard deviation.

Thus, protein products of *Scnn1d* are not able to assemble into a functional channel, neither alone nor by interaction with βγ-ENaC using electrophysiological recording conditions optimized for ENaC measurements (Stähler *et al.*, 2008). Identification of *Scnn1d* transcripts in vallate papillae, kidney and testis, which are known expression sites for mouse αβγ-ENaC (Hernandez-Gonzalez *et al.*, 2006; Kretz *et al.*, 1999; Lingueglia *et al.*, 1994), makes a modulatory role possible.

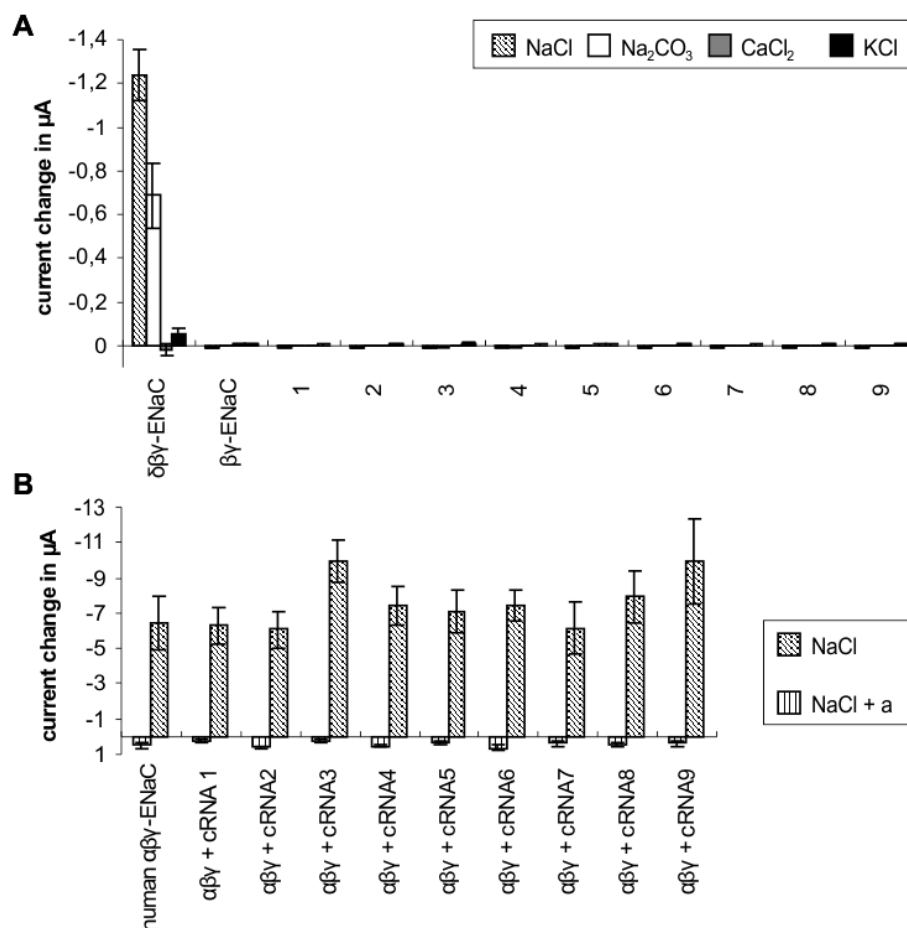


Fig. 3.16 Two-electrode voltage clamp measurements of oocytes functional expressing mouse *Scnn1d* transcripts. Membrane current changes were corrected for membrane current changes induced in water injected mock oocytes. Two batches of oocytes with at least 3 individual oocytes each were measured. Response of every oocyte was corrected for individual responses to buffer application and the mean response of mock oocytes. Error bars indicate \pm standard error of the mean. **A** Co-expression of cRNA from *Scnn1d* transcripts 1-9 with cRNA of human $\beta\gamma$ -ENaC subunits in oocytes of *Xenopus laevis*. Human $\delta\beta\gamma$ -ENaC and $\beta\gamma$ -ENaC served as positive and negative control, respectively. Shown are mean membrane current changes upon application of 40 mM NaCl, 10 mM Na₂CO₃, 10 mM CaCl₂ and 10 mM KCl diluted in perfusion buffer NMDG-KuLORi. **B** Mean membrane current changes of oocytes heterologous expressing *Scnn1d* transcript variants 1-9 in combination with human $\alpha\beta\gamma$ -ENaC exposed to 40 mM NaCl with or without 30 μ M amiloride (a) are depicted. Oocytes functional expressing human $\alpha\beta\gamma$ -ENaC served as positive control.

In order to assess a putative modulatory role of *Scnn1d* transcripts and translation products on sodium membrane currents induced by heterologous expression of $\alpha\beta\gamma$ -ENaC cRNAs, *Scnn1d* transcripts were co-injected with human $\alpha\beta\gamma$ -ENaC cRNA. Electrophysiological analysis showed neither a significant effect on $\alpha\beta\gamma$ -ENaC mediated sodium membrane currents, nor on $\alpha\beta\gamma$ -ENaC amiloride sensitivity (see Fig. 3.16B). Thus, a modulatory function of *Scnn1d* transcripts and derived polypeptides is not evident. Taken together a physiological function of polypeptides derived from *Scnn1d* transcripts could not be shown.

3.4 Taste tissue cDNA library screening for ENaC interaction partners & novel salt taste receptor candidates

Immunohistochemical data confined human δ -ENaC to apical taste pores of circumvallate as well as fungiform papillae, strongly suggesting a role in taste transduction. However, human δ -ENaC subunit alone is not able to form an efficient sodium channel (Waldmann *et al.*, 1995), making an apical sodium channel unlikely. Native interaction partner β - and γ -ENaC, essential for sodium channel assembly *in vitro* (Waldmann *et al.*, 1995), were localized basolateral in fungiform papillae and circumvallate papillae. This regional separation of δ -ENaC and $\beta\gamma$ -ENaC in both taste papillae makes assembly of apical sodium taste receptor candidate $\delta\beta\gamma$ -ENaC highly unlikely and indicates the presence of unknown interaction partner of apical δ -ENaC in circumvallate and fungiform taste buds. Additional absence of basolateral α -ENaC in fungiform papillae suggests presence unknown $\beta\gamma$ -ENaC interaction partners, as $\beta\gamma$ -ENaC are not able to assemble a functional sodium channel on their own *in vitro* (McDonald *et al.*, 1995). Interaction of $\beta\gamma$ -ENaC with unknown polypeptides seems likely, concerning versatile interaction with δ -ENaC, α -ENaC or both leading to sodium channel assembly (Waldmann *et al.*, 1995; McDonald *et al.*, 1995; Ji, H. L. *et al.*, 2006).

In order to identify polypeptides which might assemble into functional channels with $\beta\gamma$ -ENaC or δ -ENaC a functional expression assay using *Xenopus laevis* oocytes was established. Thereby a cDNA library of *Macaca mulatta* foliate papillae was used to search for polypeptides that in combination with $\beta\gamma$ -ENaC or δ -ENaC could form functional ion channels for sodium and/or various cations. On the one hand, screening cDNAs from rhesus monkey should lead to identification of macaque polypeptides, allowing identification of human ortholog salt taste receptor candidates involving ENaC subunits. Moreover, the assay would lead to identification of ion channels independent from ENaC subunits. Thereby, potential sodium taste receptor candidates as well as cation unspecific salt taste receptor candidates could be identified.

3.4.1 Characterization of cDNA library from *Macaca mulatta* foliate papillae

To identify potential salt taste receptor candidates a taste tissue cDNA library, generated from foliate papillae of *Macaca mulatta* and packaged in λ -phages, was used (see 2.15.1). Quality of cDNA was confirmed by PCR amplification of marker genes and amplification of 5'-ends of transcripts up to 6 kb. The library was once amplified and the gained 55'000 independent cDNA clones with an average size of 1.5 to 2 kb were divided into 26 pools,

namely F1-1 to F1-26. These λ -phage pools with approximately 2000 individual cDNA clones each were provided by Dr. R. Hoppe (University Hohenheim, Stuttgart) and E. Tareilus (Unilever Research Center, Vlaardingen) and processed as described in 2.15. Heterogeneity of the pools and size of inserts was confirmed by restriction analysis of 10 representative single clones of each pool (data not shown). No obvious accumulation of restriction patterns was observed, implying high complexity of the library. This cDNA library should be used to screen for novel human ENaC interaction partners as well as to identify ENaC-independent ion channels.

In order to exclude false positive results by interaction of $\beta\gamma$ -ENaC or δ -ENaC with known interaction partners α -ENaC and $\beta\gamma$ -ENaC, respectively, cDNA library pools were examined for the presence of α -, β -, γ - and δ -ENaC cDNA clones. Thereby, no full length β -, γ - or δ -ENaC cDNA was amplified from the cDNA pools. However, using primers specific for a short internal sequence of respective ENaC subunits, several pools were found to contain partial cDNAs. Such amplicons for β -, γ - and δ -ENaC cDNAs were detected in 12, 6 and 8 pools, respectively, verified by sequencing of representative PCR products. In contrast to δ -, β - or γ -ENaC cDNA clones lacking full length coding sequence, α -ENaC with an expected full length coding sequence of 2 kb was amplified in 7 cDNA pools, namely pool F1-7, -10, -12, -14, -15, -24 and -26 (see Fig. 3.17). Sequence analysis of PCR products generated from pool F1-26 confirmed both PCR products as macaque α -ENaC subunit. The smaller PCR product obtained from pool F1-26 was identified as macaque α -ENaC splice variant missing exon 3 of macaque reference sequence XM_001103017.2 (Wheeler *et al.*, 2008). In conclusion, 7 of 26 cDNA pools likely assemble a $\alpha\beta\gamma$ -ENaC sodium channel when co-expressed with human $\beta\gamma$ -ENaC, as human $\alpha\beta\gamma$ -ENaC is known to form a functional sodium channel *in vitro* (McDonald *et al.*, 1995). Notably, co-expression with δ -ENaC will not lead to sodium channel assembly, as $\alpha\delta$ -ENaC do not form efficient sodium channels (Waldmann *et al.*, 1995).

In order to exclude false positive results, macaque α -ENaC was disabled prior to use of cDNA pools for functional screening in combination with human $\beta\gamma$ -ENaC as described next. For functional expression *Macaca mulatta* cDNA library plasmid pools have to be linearized with a restriction endonuclease prior to cRNA generation and injection into oocytes of *Xenopus laevis*. Thus, restriction endonuclease *NotI* was chosen for linearization, as macaque α -ENaC (XM_001103017.2) possesses an internal *NotI* site, which leads to the generation of truncated cRNA. Thereby, truncated macaque α -ENaC cRNA is generated,

lacking full length coding sequence. This facilitates the use of all macaque α -ENaC PCR positive pools within the screening for interaction partners of human $\beta\gamma$ -ENaC.

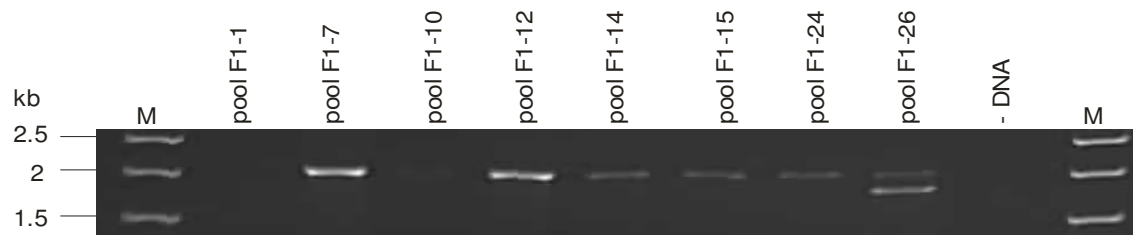


Fig. 3.17 PCR amplification of α -ENaC from *macaca mulatta* cDNA library pools. Shown are all PCR positive pools, as well as F1-1 as one representative negative pool. PCR was performed on 10 ng pool plasmid DNA using α -ENaC specific primers. The predicted size of the full length α -ENaC PCR product was 2094 bp. A PCR reaction omitting DNA template (-DNA) served as negative control. M: molecular weight marker.

In order to further assess quality and complexity of the cDNA library, macaque α -ENaC positive pools were representatively analyzed for insert lengths and sequences. To examine insert sizes of macaque α -ENaC cDNA clones southern blot analysis was carried out. In accordance with PCR analysis, southern blot confirmed presence of α -ENaC cDNAs in pool F1-7, -10, -12, -14, -15, -24 and -26 (see Fig. 3.18). Moreover, presence of cDNA clones with distinct insert lengths became evident (see Fig. 3.18). Six of 11 cDNA variants designated as F1-7b, F1-10, F1-12b, F1-14, F1-24, and F1-26b showed a size of about 3.2 kb (see Fig. 3.18), which is in accordance with database reference sequence of macaque α -ENaC mRNA (XM_001103017.2, Wheeler *et al.*, 2008). In contrast, variants F1-7a, F1-12a, F1-15a, F1-15b and F1-26 were detected at about 7, 3.6, 8, 2.2 and 3.6 kb, respectively (see Fig. 3.18). Notably, processing of α -ENaC PCR negative pool F1-1 resulted in no staining at all, confirming specific binding of macaque α -ENaC probe (see Fig. 3.17).

To evaluate the sequence of different α -ENaC cDNA variants representatively, α -ENaC cDNA clones F1-7a, F1-7b, F1-12a, F1-12b and F1-15b were isolated via phage or colony blot. All isolated cDNA clones were confirmed as macaque α -ENaC, showing 80 to 98 % nucleotide identity to macaque reference sequence XM_001103017.2 (Wheeler *et al.*, 2008). Clone F1-7a was revealed as cDNA library artifact. Latter contains macaque α -ENaC cDNA inserted inverse into the cloning vector, leading to incomplete restriction and detection at about 7 kb in the southern blot analysis (see Fig. 3.18). Sequence analysis of variant F1-7b, F1-12a, F1-12b and F1-15b revealed correct orientated macaque α -ENaC cDNAs with lengths estimated from southern blot analyses (see Fig. 3.18). Variants F1-7b, F1-12a, F1-12b differed in 5'UTR sequence and thereby in N-termini of encoded α -ENaC

proteins of 689, 727 and 714 aa, respectively (see Fig. 3.19). Clone F1-15b, detected at about 2.2 kb in the southern blot analysis (see Fig. 3.18) contains a 5'-truncated α -ENaC cDNA, leading to an open reading frame coding for 370 aa α -ENaC protein.

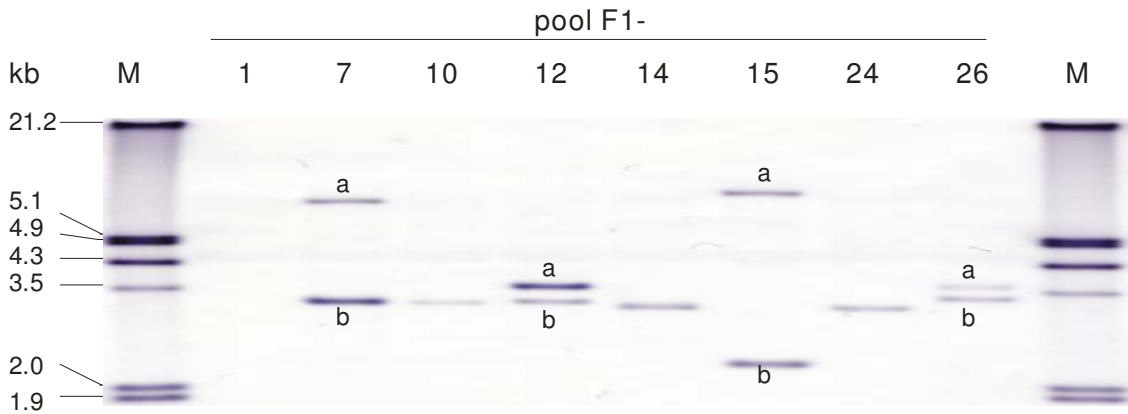


Fig. 3.18 Southern blot analysis of selected cDNA library plasmid pools. Pool F1-1, -7, -10, -12, -14, -15, -24 and -26 were restricted with *EcoRI/XhoI* and resolved on a 1% agarose gel. The gel was blotted to a positively charged nylon membrane and hybridized with digoxigenin labelled *macaca* α -ENaC DNA probe, which corresponds to nt 1145 to 1653 of *macaca* α -ENaC (XM_001103017.2). Distinct *macaca* α -ENaC cDNA variants within one pool were designated as 'a' and 'b'. F1-1 served as control for specific binding of the α -ENaC probe, while all other analyzed were PCR-positive for α -ENaC (see Fig. 3.17). M: Digoxigenin labeled DNA molecular weight marker, kb: kilo bases.

Taken together, various sizes of cDNAs detected in southern blot analysis could be explained by the presence of distinct macaque α -ENaC cDNA variants differing in the 5'UTR as well as of cDNA library artifacts.

Species	Clone/Seq	Length (aa)	Sequence	Position
human	isoform 1	669	-----MEGNKL	6
	isoform 2	728	MGHARGSLTRVPGVMGEGTQGPPELSLDPDPCSPQSTPGLMKGNKLEEQDPRPLQFIPGLMEGNKL	65
	isoform 3	692	-----MSSIKGNKLEEQDPRPLQFIPGLMEGNKL	29
macaca	ref. seq.	692	-----MSSIKGNKLEEQDPRPLQFTAGLMEGNKL	29
	F1-7b	689	-----MKGNKLEEQDPRPLQFTAGLMEGNKL	26
	F1-12a	726	--MARGNLTWVPGVMGEGTQGPPELSLDPDPCSPQSAPGLMKGNKLEEQDPRPLQFTAGLMEGNKL	63
	F1-12b	714	-----MGEQTQGPPELSLDPDPCSPQSAPGLMKGNKLEEQDPRPLQFTAGLMEGNKL	51

Fig. 3.19 N-termini of macaque α -ENaC proteins. Protein reference sequences of human and macaque α -ENaC as well as putative macaque α -ENaC proteins derived from cDNA clones F1-7b, F1-12a and F1-12b were aligned with ClustalW using Mega 4.0. The N-terminal part of the alignment was depicted using Genedoc (Nicholas *et al.*, 1997). The degree of conservation is shown in shades. Black corresponds to 100% conservation, dark grey with white characters to 80% conservation, grey with black letters to 60% and black letters on white background to less conservation. Accession numbers: human α -ENaC isoform 1-3: NP_001029.1, NP_001153048.1, NP_001153047.1; macaque α -ENaC reference sequence: XP_001103017.2 (Wheeler *et al.*, 2008).

In conclusion, most of analyzed cDNA clones contain a full length macaque α -ENaC cDNA with a maximal size of 3.6 kb, arguing for quality of the cDNA used to generate the macaque cDNA library. However, full length δ -, β - or γ -ENaC cDNAs with reference mRNA lengths up to 3.5 bp (see Tab. 7.4) were not detected within cDNA library, although transcripts with lengths up to 6 kb are present (see Fig. 3.23).

3.4.2 Development of functional expression assay for cDNA library screening

Each cDNA library pool contains approximately 2000 individual cDNA clones. In order to evaluate if functional expression in *Xenopus laevis* oocytes is sensitive enough to detect a single cDNA clone out of 2000 clones, human α -ENaC was diluted 1:2000 and co-injected with cRNA of human $\beta\gamma$ -ENaC. Notably, human α -ENaC cRNA was diluted within cRNA of macaque α -ENaC negative pool F1-1 to mimic a pool of 2000 distinct cRNAs within one oocyte (see 2.16.1.3). Co-expression with human $\beta\gamma$ -ENaC led to assembly of functional sodium channel, as significant sodium current changes with a mean of -114 nA were detectable upon application of 40 mM NaCl (see Fig. 3.20). In contrast and consistent with the literature (McDonald *et al.*, 1995), no sodium channel was assembled by functional expression of human $\beta\gamma$ -ENaC (see Fig. 3.20). In conclusion, the assay is sensitive enough to detect one cRNA out of approximately 2000 cRNAs by functional expression in *Xenopus laevis* oocytes.

In order to validate that species interaction between macaque and human cDNA clones takes place macaque α -ENaC was heterologously expressed in combination with human $\beta\gamma$ -ENaC. Thereby, pool F1-7 was representatively chosen for co-expression experiments. Notably, cRNA of pool F1-7 was generated from *Xba*I linearized plasmid pool DNA which does not affect macaque α -ENaC cDNA. Pool cRNA derived from *Xba*I linearized pool F1-7 is subsequently termed as F1-7[#]. A functional sodium channel was assembled by heterologous expression of pool F1-7 in combination with human $\beta\gamma$ -ENaC leading to activatory membrane current changes with a mean of -107 nA (see Fig. 3.20), representatively illustrated for individual oocytes in Fig. 3.20B. Notably, negative membrane current changes correspond to cation entry or anion efflux under used electrophysiologic measuring conditions. These inward directed membrane current changes are termed 'activatory currents' from now on. Likewise, positive membrane current changes correspond to net efflux of cations or influx of anions and were termed 'inhibitory currents'.

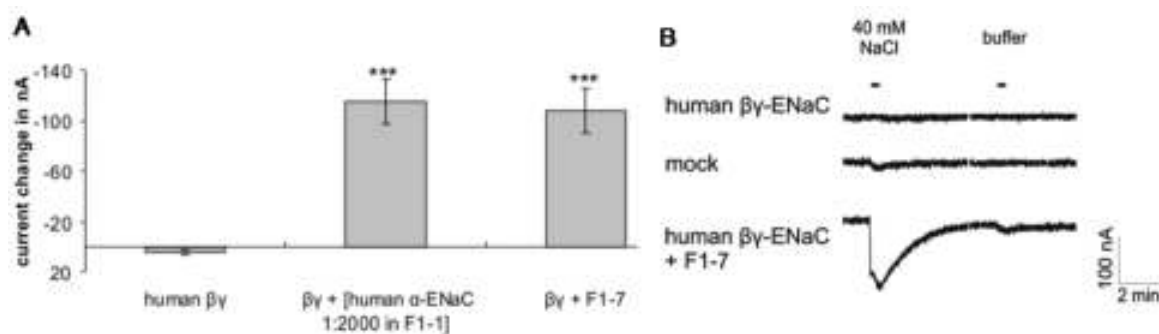


Fig. 3.20 Functional expression of human $\beta\gamma$ -ENaC subunits with human α -ENaC diluted 1:2000 or *macaca* α -ENaC PCR-positive pool F1-7. **A Whole cell membrane current changes of oocytes induced by 40 mM NaCl in NMDG-KulORi. Oocytes were injected with 16 ng human $\beta\gamma$ -ENaC cRNA, 16 ng human $\beta\gamma$ -ENaC cRNA in combination with 12 pg human α -ENaC cRNA diluted in macaque pool F1-1 as well as with 16 ng human $\beta\gamma$ -ENaC cRNA in combination with 34 ng pool cRNA F1-7. Membrane current changes of individual oocytes were corrected for their response to perfusion buffer (NMDG-KulORi) application. Moreover the mean membrane current change of mock oocytes induced by 40 mM NaCl was subtracted. Two batches of oocytes with at least 3 individual oocytes were measured. Standard error is indicated by error bars. Significance was tested with an independent two sample student's t-test. *** $p < 0.001$. **B** Representative current traces of two-electrode voltage clamp measurements. Exemplary current traces of oocytes functional expressing 16 ng human $\beta\gamma$ -ENaC, 16 ng human $\beta\gamma$ -ENaC in combination with 34 ng F1-7-control, as well as mock oocytes challenged with 40 mM NaCl and perfusion buffer. Bar indicates duration of application.**

In accordance with literature no membrane current changes were observed for expression of human $\beta\gamma$ -ENaC alone or mock injected oocytes (Waldmann *et al.*, 1995). Remarkably, it could be ensured that the induced membrane current change is mediated by macaque α -ENaC, as co-expression F1-7 cRNA generated using macaque α -ENaC targeting *NotI* linearized plasmid pool did not show any membrane current change upon sodium application. Notably, heterologously expressed macaque pool F1-7 leads to comparable activatory current changes as human α -ENaC in a dilution of 1:2000, which is in good accordance with expected 2000 cDNA clones per pool.

In conclusion, heterologous expression assay is feasible to detect novel macaque interaction partners for human ENaC subunits as well as novel polypeptides using *Macaca mulatta* cDNA library.

3.4.3 Screening for interaction partners of human $\beta\gamma$ -ENaC and novel ion channels potential involved in salt taste transduction

In order to identify novel salt taste receptor candidates as well as polypeptides which might assemble into functional channels with $\beta\gamma$ -ENaC, sodium and non-sodium salts perceived as salty in humans (Perty, 1838; von Skramlik, 1933; Cardello, 1978; van der Klaauw & Smith, 1995) were used in functional assay. Therefore, adequate assay concentrations of NaCl, Na₂CO₃, CaCl₂ and KCl were previously determined using mock oocytes (see 3.3.4.4, Fig. 3.15), which were 40 mM NaCl, 10 mM Na₂CO₃, 10 mM CaCl₂ and 10 mM KCl. Sufficient expression level of oocytes as well as sensitivity of electrophysiological measurement was verified by heterolog expression of macaque α -ENaC containing pool F1-7[#] for each oocyte batch. Application of NaCl and Na₂CO₃ to this positive control resulted in significant activating membrane current changes of -121 and -118 nA, respectively, verifying assembly of sodium channels (see Tab. 3.3). Significant inhibitory and outward directed mean current change of 33 nA induced by the application of CaCl₂ is consistent with an inhibitory effect of Ca²⁺ on $\alpha\beta\gamma$ -ENaC (Ismailov *et al.*, 1997). Consistent with virtual impermeability of $\alpha\beta\gamma$ -ENaC to potassium ions (Kellenberger, S. *et al.*, 1999), application of KCl did not lead to significant membrane current changes when applied to functionally expressed F1-7[#] (see Tab. 3.3). Responses were recorded and normalized as described in 2.16.4, while oocytes with a membrane current change above baseline fluctuation of +/- 14 nA were designated as responsive oocytes.

Functional expression of F1-1 to F1-26 pool cRNA in combination with human $\beta\gamma$ -ENaC did not result in the assembly of a sodium channel, as no significant sodium current changes were detected upon application of NaCl and/or Na₂CO₃ (see Tab. 3.3). In contrast, significant activatory and inward directed membrane current changes upon application of 10 mM CaCl₂ were detected for pool F1-4, F1-12, F1-15, F1-25 and F1-26, with mean membrane current change of -27 nA (see Tab. 3.3), pointing to presence of polypeptides enabling entry of calcium ions. Furthermore, significant activatory inward directed membrane current changes upon application of 10 mM KCl were detected for pool F1-3 and F1-15 with mean membrane current changes of -27 and -63 nA, respectively. This suggests presence of proteins facilitating potassium entry via oocyte membrane. Remarkably, pool F1-15 responded significantly to CaCl₂ as well as to KCl, which implies the presence of a cation-nonspecific ion channel permeable for both cations (see Fig. 3.21).

Pools responding significantly to at least two applied salts point to the presence of cation nonspecific ion channel, which could be a cation non-specific salt taste receptor candidate. Thus, pool F1-15 was representatively chosen for further analysis. Interestingly, pool F1-6 showed activatory responses to all applied salt solutions. Although these were not significant, F1-6 was the solely pool responding to both sodium salts and was therefore further analyzed with respect to cation unspecific ion channels (see Tab. 3.3).

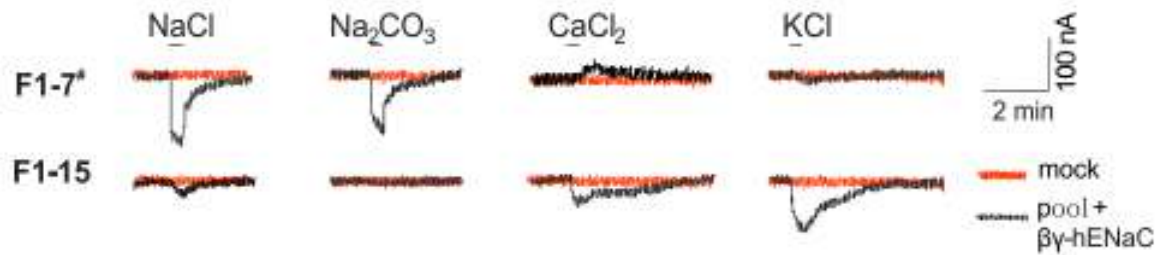


Fig. 3.21 Representative current traces of oocytes functional expressing F1-7# and pool F1-15. Exemplary current traces of oocytes functional expressing 16 ng human βγ-ENaC in combination with 34 ng F1-7# or 36 ng pool F1-15 cRNA challenged with 40 mM NaCl, 10 mM Na₂CO₃, 10 mM CaCl₂ and 10 mM KCl. Representative trace of mock oocyte from the same batch is indicated in red. Bar indicates duration of application.

Tab. 3.3: Electrophysiologic recordings of oocytes functional expressing macaque cDNA library pools F1-1 to F1-26 in combination with human $\beta\gamma$ -ENaC. Shown are number of responsive oocytes and batches as well as normalized membrane current changes. Significant membrane current changes are highlighted in yellow.

human $\beta\gamma$ -ENaC + F1-	40 mM NaCl						10 mM Na ₂ CO ₃						10 mM CaCl ₂						10 mM KCl					
	current change of responsive oocytes +/- SD [nA]	significance p	current change of total oocytes +/- SD [nA]	no. of oocytes (total, responsive)	batches (total, responsive)	current change of responsive oocytes +/- SD [nA]	significance p	current change of total oocytes +/- SD [nA]	no. of oocytes (total, responsive)	batches (total, responsive)	current change of responsive oocytes +/- SD [nA]	significance p	current change of total oocytes +/- SD [nA]	no. of oocytes (total, responsive)	batches (total, responsive)	current change of responsive oocytes +/- SD [nA]	significance p	current change of total oocytes +/- SD [nA]	no. of oocytes (total, responsive)	batches (total, responsive)				
7#	-121 +/- 113	**	-85 +/- 110	70	28	40	78	-91 +/- 116	**	40	78	**	13 +/- 26	33	5	44 +/- 24	**	13 +/- 26	33	1	8			
1	-	n.s.	0	12	0	12	8	-26 +/- 86	n.s.	1	12	n.s.	-18 +/- 61	8	1	-220	n.s.	-18 +/- 61	8	0	2			
2	-	n.s.	1 +/- 4	14	0	14	0	0	n.s.	0	14	n.s.	0	0	0	-	n.s.	0	0	2	2			
3	-	n.s.	0	14	0	14	0	0	n.s.	0	14	n.s.	-10 +/- 7	7	1	-16	n.s.	-10 +/- 7	7	1	2			
4	-	n.s.	0	14	0	14	0	0	n.s.	0	14	n.s.	-5 +/- 10	21	1	-23 +/- 8	**	-5 +/- 10	21	1	2			
5	-	n.s.	0	14	0	14	0	0	n.s.	0	14	n.s.	0	0	0	-	n.s.	0	0	2	2			
6	-27 +/- 8	n.s.	-4 +/- 10	32	16	32	6	-4 +/- 14	n.s.	2	4	n.s.	0 +/- 4	3	1	-22	n.s.	0 +/- 4	3	2	4			
7	-	n.s.	0	12	0	12	0	0	n.s.	0	12	n.s.	0	0	0	-	n.s.	0	0	2	2			
8	-	n.s.	0	12	0	12	0	0	n.s.	0	12	n.s.	-2 +/- 6	8	1	-20	n.s.	-2 +/- 6	8	0	2			
9	-	n.s.	0	12	0	12	0	0	n.s.	0	12	n.s.	0	0	0	-	n.s.	0	0	0	2			
10	-	n.s.	0	13	0	13	0	0	n.s.	0	13	n.s.	0	0	0	-	n.s.	0	0	0	2			
11	-	n.s.	-1 +/- 4	26	0	26	8	-4 +/- 12	n.s.	1	4	n.s.	-2 +/- 6	8	2	-23 +/- 0	n.s.	-2 +/- 6	8	2	4			
12	-18	n.s.	-1 +/- 4	24	4	24	4	0	n.s.	2	4	*	5 +/- 11	17	2	-31 +/- 1	*	5 +/- 11	17	1	4			
13	-	n.s.	0	16	0	16	0	0	n.s.	0	16	n.s.	0	0	0	-	n.s.	0	0	0	3			
14	-	n.s.	0	14	0	14	0	0	n.s.	0	14	n.s.	-2 +/- 8	7	1	-32	n.s.	-2 +/- 8	7	1	3			
15	-65 +/- 39	n.s.	-6 +/- 12	23	9	23	9	-4 +/- 17	n.s.	1	4	n.s.	-8 +/- 13	27	1	-29 +/- 8	**	-8 +/- 13	27	2	4			
16	-	n.s.	0	14	0	14	0	0	n.s.	0	14	n.s.	0	0	0	-	n.s.	0	0	0	3			
17	-	n.s.	0	10	0	10	0	0	n.s.	0	10	n.s.	0	0	0	-	n.s.	0	0	0	2			
18	-20	n.s.	-2 +/- 6	11	9	11	9	0	n.s.	0	11	n.s.	0	0	0	-	n.s.	0	0	0	2			
19	-	n.s.	0	12	0	12	0	0	n.s.	0	12	n.s.	0	0	0	-	n.s.	0	0	0	2			
20	-	n.s.	0	11	0	11	0	0	n.s.	0	11	n.s.	0	0	0	-	n.s.	0	0	1	3			
21	-	n.s.	0	10	0	10	0	0	n.s.	0	10	n.s.	0	0	0	-	n.s.	0	0	1	2			
22	-	n.s.	0	14	0	14	0	-1 +/- 5	n.s.	0	14	n.s.	0	0	0	-	n.s.	0	0	1	3			
23	-	n.s.	0	24	0	24	4	-2 +/- 8	n.s.	1	4	n.s.	1 +/- 4	4	1	-18	n.s.	1 +/- 4	4	2	3			
24	-	n.s.	0	13	0	13	0	0	n.s.	0	13	n.s.	0	0	0	-	n.s.	0	0	0	3			
25	-	n.s.	0	27	0	27	0	0	n.s.	0	27	n.s.	-7 +/- 15	22	2	-31 +/- 15	*	-7 +/- 15	22	2	4			
26	-	n.s.	0	19	0	19	0	0	n.s.	0	19	n.s.	-3 +/- 7	16	2	-19 +/- 4	*	-3 +/- 7	16	2	4			

#, F1-7 containing intact macaca α -ENaC cRNA; SD, standard deviation; gray, pools chosen for fractionation; n.s., not significant; *, p < 0.05; **, p < 0.01

To validate and isolate potential cation unspecific ion channel detected within pool F1-6 and pool F1-15, cDNA clone pools have to be subsequently reduced in size. In order to establish an adequate scaling down procedure, fractionation of pool F1-7 containing two α -ENaC cDNA clones F1-7a and F1-7b (see 3.4.2) was used as a control. Thereby, parental pool F1-7 was scaled down by the factor of ten to 15 sub-pools with 200 cDNA clones each. Subsequent PCR analysis of F1-7 sub-pools confirmed the presence of macaque α -ENaC in five of 15 sub-pools (see Fig. 3.22), showing that the scaling down procedure is suitable to recover single cDNA clones.

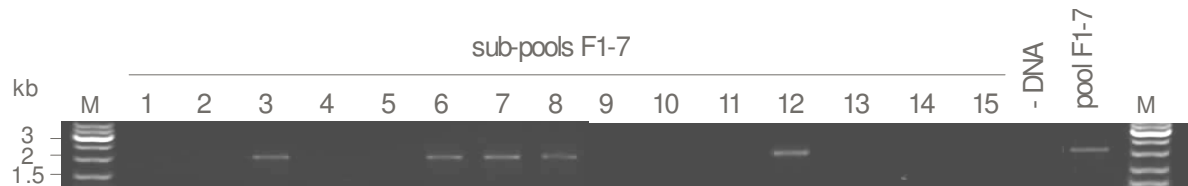


Fig. 3.22 PCR amplification of α -ENaC from sub-pools generated from parental pool F1-7 of *Macaca mulatta* cDNA library. PCR was carried out using F1-7 sub-pool plasmid DNA and *macaca* α -ENaC specific primers. Predicted size of full length α -ENaC is 2094 kb. PCR reaction assembled without DNA template (-DNA) served as negative control. M: DNA molecular weight markers.

The established fractionation procedure was applied to pool F1-6 and F1-15. Fifteen 2.15.4 sub-pools with approximately 200 cDNA clones were generated for each parental pool (see 2.15.4) and functionally expressed in combination with human $\beta\gamma$ -ENaC.

Activatory responses of parental pool F1-6 to NaCl, Na₂CO₃ and KCl were not recovered within F1-6 sub-pools (see Tab. 3.4), suggesting that initially noticed but non-significant responses of parental pool were non-specific. However, activating membrane current change induced by CaCl₂ was found in F1-6 sub-pool 5 (see Tab. 3.4). Anyway, F1-6 sub-pool 5 was not further investigated as the lack of response to other salts makes a cation unspecific ion channel unlikely. Significant activatory membrane current changes detected upon application of CaCl₂ and KCl to functionally expressed parental pool F1-15 (see Fig. 3.21), were not recovered in sub-pools (see Tab. 3.5).

In order to investigate if failed recovery is due to a strong reduction in plasmid heterogeneity, qualitative control of sub-pool heterogeneity in comparison to the parental pool was carried out by restriction analysis. Thereby, expected reduction of complexity as well as accumulation of cDNA clones within sub-pools was evident by lacking or stronger insert bands, respectively, when compared to the parental pool (see white arrows Fig. 3.23). Assembly of all sub-pools showed slightly reduced heterogeneity in total (see Fig.

3.23). Thus, cDNA clones could be lost during scaling down procedure which might be one reason for failed recovery of responses detected using the parental pool F1-15.

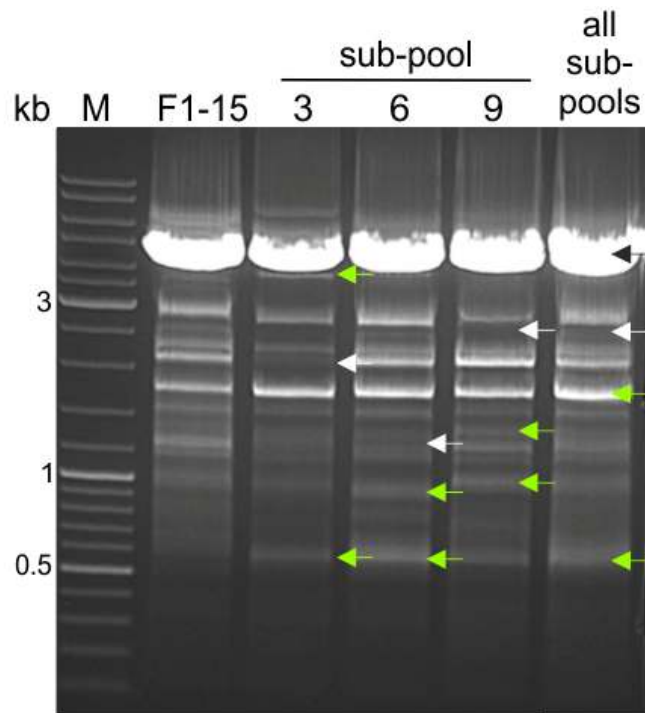


Fig. 3.23 Restriction analysis of parental pool F1-15 and representative sub-pools. Restriction was carried out with *EcoRI* and *XhoI*, used for generation of macaque cDNA library. Pool F1-15 as well as sub-pool 3, 6 and 9, were restricted and separated using agarose gel electrophoresis. Black arrow indicates excised cloning vector pBK-CMV at about 4.5 kb. White and green arrows indicate representative bands, which are lacking or accumulated in sub-pools. Assembly of all sub-pools is shown in the right lane. M, DNA molecular weight marker: 10, 8, 6, 5, 4, 3.5, 3, 2.5, 2, 1.2, 1, 0.9, 0.8, 0.7, 0.6, 0.5, 0.4, 0.3, 0.2, 0.1 kilo bases (kb)

In conclusion, screening of macaque cDNA library pools F1-1 to F1-26 as well as sub-pools of F1-6 and F1-15 by co-expression with human $\beta\gamma$ -ENaC did not reveal an interaction partner of human $\beta\gamma$ -ENaC. Moreover, this means that no ENaC-independent salt taste receptor candidate was detected in macaque cDNA library using the established functional screening assay.

Tab. 3.4: Electrophysiologic recordings of oocytes functional expressing macaque cDNA library pool F1-6 sub-pools in combination with human $\beta\gamma$ -ENaC. Shown are number of responsive oocytes and batches as well as normalized membrane current changes. Significant membrane current changes are highlighted in yellow.

40 mM NaCl		10 mM Na ₂ CO ₃		10 mM CaCl ₂		10 mM KCl		F1-6 sub-pools		
$\beta\gamma$ -ENaC +	current change of responsive oocytes +/- SD [nA]	significance p	current change of total oocytes +/- SD [nA]	no. of oocytes	batches	current change of responsive oocytes +/- SD [nA]	significance p	current change of total oocytes +/- SD [nA]	no. of oocytes	batches
F1-7 [#]	-148 +/- 79	**	-148 +/- 79	100	5	36 +/- 43	*	-34 +/- 48	56	2
F1-6 [#]	-27 +/- 8	n.s.	-4 +/- 10	16	3	-22	n.s.	-7	13	2
F1-6 sub-pools										
1	1	3	1	11	9	-	n.s.	0	0	3
2	0	3	0	11	0	-	n.s.	0	0	3
3	0	2	0	8	0	-	n.s.	0	0	2
4	0	3	0	13	0	-	n.s.	0	0	3
5	1	4	1	13	8	-20	n.s.	0	0	4
6	0	3	0	8	0	-	n.s.	0	0	3
7	0	2	0	6	0	-	n.s.	0	0	2
8	1	4	1	14	7	-24	n.s.	-18 +/- 76	64	4
9	1	3	1	13	8	-35	n.s.	0	0	3
10	0	2	0	6	0	-	n.s.	0	0	2
11	0	2	0	8	0	-	n.s.	0	0	2
12	0	3	0	11	0	-	n.s.	0	0	3
13	0	2	0	8	0	-	n.s.	0	0	2
14	0	2	0	8	0	-	n.s.	0	0	2
15	0	3	0	10	0	-	n.s.	0	0	3

#, F1-7 containing intact macaca α -ENaC cRNA; SD, standard deviation; gray, pools chosen for fractionation; n.s., not significant, $p > 0.05$; *, $p < 0.05$; **, $p < 0.01$

Tab. 3.5: Electrophysiologic recordings of oocytes functional expressing macaque cDNA library pool F1-15 sub-pools in combination with human $\beta\gamma$ -ENaC. Shown are number of responsive oocytes and batches as well as normalized membrane current changes. Significant membrane current changes are highlighted in yellow.

$\beta\gamma$ -ENaC +	40 mM NaCl						10 mM Na ₂ CO ₃						10 mM CaCl ₂						10 mM KCl						F1-15 sub-pools								
	current change of responsive oocytes +/- SD [nA]	significance p	current change of total oocytes +/- SD [nA]	no. of oocytes total	responsive	batches total	responsive	current change of responsive oocytes +/- SD [nA]	significance p	current change of total oocytes +/- SD [nA]	no. of oocytes total	responsive	batches total	responsive	current change of responsive oocytes +/- SD [nA]	significance p	current change of total oocytes +/- SD [nA]	no. of oocytes total	responsive	batches total	responsive	current change of responsive oocytes +/- SD [nA]	significance p	current change of total oocytes +/- SD [nA]		no. of oocytes total	responsive	batches total	responsive				
F1-7 [#]	-165 +/- 196	**	-165 +/- 196	11	100	3	3	-197 +/- 210	**	-197 +/- 210	11	100	3	3	107 +/- 78	**	64 +/- 80	11	6	3	3	11	36	12 +/- 30	n.s.	31 +/- 41	F1-7 [#]	1					
F1-15 ^{##}	-65 +/- 39	n.s.	-6 +/- 12	23	9	2	4	-4 +/- 17	n.s.	-67	15	27	1	4	-29 +/- 8	**	-8 +/- 13	15	4	1	4	4	43	-27	44	-63 +/- 47	F1-15 ^{##}	2					
F1-15 sub-pools																																	
1	-	n.s.	0	8	0	0	2	0	n.s.	-	8	0	0	0	-	n.s.	0	8	0	0	2	0	0	0	0	-	n.s.	0	8	0	1		
2	-	n.s.	0	7	0	0	3	0	n.s.	-	6	0	0	1	-26	n.s.	-4 +/- 9	7	14	1	3	1	6	17	-5 +/- 11	n.s.	-30	n.s.	1	3	1	2	
3	-	n.s.	0	9	0	0	2	3	n.s.	-31 +/- 5	9	11	1	3	-18	n.s.	-2 +/- 6	9	11	1	3	1	9	22	-5 +/- 5	n.s.	21 +/- 5	n.s.	2	3	2	3	
4	-	n.s.	0	6	0	0	0	2	n.s.	-	6	0	0	0	-	n.s.	0	6	0	0	2	0	6	0	0	-	n.s.	-	n.s.	0	2	0	4
5	-	n.s.	0	7	0	0	0	2	n.s.	-	7	0	0	0	-	n.s.	0	7	0	0	2	0	7	0	0	-	n.s.	-	n.s.	0	2	0	5
6	-28	n.s.	-3 +/- 8	11	9	1	3	-11 +/- 20	n.s.	-42 +/- 14	11	27	1	3	41 +/- 7	n.s.	8 +/- 16	11	18	1	3	2	11	18	-6 +/- 15	n.s.	-35 +/- 12	n.s.	1	3	2	6	
7	-	n.s.	0	8	0	0	1	3	n.s.	27 +/- 4	8	13	1	3	31	n.s.	4 +/- 10	8	13	1	3	1	8	0	0	-	n.s.	-	n.s.	0	3	0	7
8	-31	n.s.	-3 +/- 9	10	10	2	3	-6 +/- 19	n.s.	-17 +/- 29	9	33	0	3	-	n.s.	0	10	10	0	3	0	10	11	-9 +/- 24	n.s.	-77	n.s.	1	3	1	8	
9	-	n.s.	0	8	0	0	0	3	n.s.	-	8	0	0	0	-	n.s.	0	8	0	0	3	0	8	0	0	-	n.s.	-	n.s.	0	0	0	9
10	-	n.s.	0	9	0	0	0	2	n.s.	-	9	0	0	0	-	n.s.	0	9	0	0	2	0	9	11	2 +/- 5	n.s.	17	n.s.	1	2	1	10	
11	20	n.s.	3 +/- 7	7	14	0	2	0	n.s.	-	6	0	0	1	55 +/- 26	*	16 +/- 28	7	29	1	2	2	7	29	0	0	-	n.s.	0	2	0	11	
12	19	n.s.	2 +/- 5	12	8	2	3	-3 +/- 13	n.s.	-11 +/- 25	12	25	0	3	-	n.s.	0	12	17	0	3	0	12	17	2 +/- 11	n.s.	9 +/- 26	n.s.	1	3	2	12	
13	-	n.s.	0	6	0	0	0	3	n.s.	-	6	0	0	0	-	n.s.	0	6	0	0	3	0	6	0	0	-	n.s.	-	n.s.	0	3	0	13
14	-	n.s.	0	10	0	0	1	2	n.s.	-15	10	10	0	2	-	n.s.	0	10	10	0	1	2	1	10	2 +/- 5	n.s.	17	n.s.	1	2	1	14	
15	-	n.s.	0	8	0	0	0	2	n.s.	-	8	0	0	0	-	n.s.	0	8	0	0	0	2	0	8	0	0	-	n.s.	0	2	0	15	

#, F1-7 containing intact macaca α -ENaC cRNA; SD, standard deviation; gray, pools chosen for fractionation; n.s., not significant, $p > 0.05$; *, $p < 0.05$; **, $p < 0.01$

3.4.4 Screening for novel interaction partners of human δ -ENaC potential involved in human salt taste transduction

In order to identify polypeptides which might assemble into functional channels with δ -ENaC, the established functional expression assay using *Xenopus laevis* oocytes was used (see 3.4.2). An internal control similar to macaque pool F1-7 including α -ENaC cDNA was not feasible here, as no full length clones of macaque $\beta\gamma$ -ENaC were present in the cDNA library. Therefore, heterologously expressed human $\delta\beta\gamma$ -ENaC was used to control stable expression level of oocytes (see Fig. 3.24). In agreement with literature (Waldmann *et al.*, 1995), expression of human δ -ENaC alone showed detectable responses to application of sodium salts in some oocyte batches (see batch 1 in Fig. 3.24) or was indistinguishable from mock injected oocytes (see batch 2 in Fig. 3.24). In order to correct for background originating from intrinsic δ -ENaC sodium channels mean responses of human δ -ENaC expressing oocytes were used for normalization of batch specific fluctuations in addition to buffer normalization of individual oocytes as described in 2.16.4.

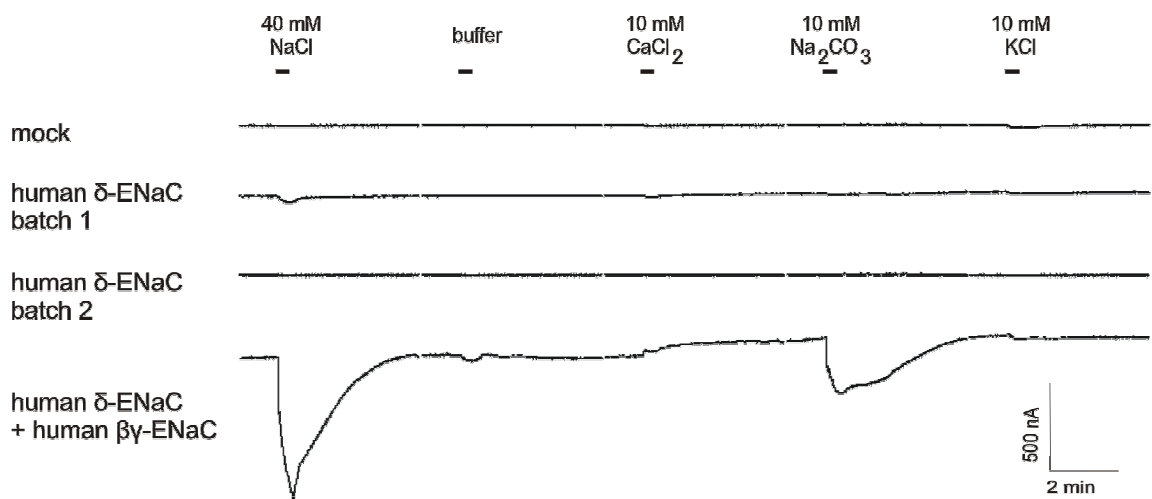


Fig. 3.24 Representative current traces of two-electrode voltage clamp measurements. Exemplary current traces of oocytes functional expressing 320 pg human δ -ENaC, 320 pg human δ -ENaC in combination with 32 pg human β and 32 pg human γ -ENaC, as well as mock oocytes challenged with 40 mM NaCl, 10 mM Na₂CO₃, 10 mM CaCl₂, 10 mM KCl and perfusion buffer. Bar indicates duration of application. Two distinct batches for oocytes functional expressing 320 pg human δ -ENaC are shown (batch 1 and batch 2).

Fig. 3.24 illustrates that a functional $\delta\beta\gamma$ -ENaC sodium channel was assembled by co-expression of human δ -ENaC in combination with human $\beta\gamma$ -ENaC, showing significant activating and inward directed sodium membrane current changes with a mean of -751 nA and -871 nA by application of 40 mM NaCl and 10 mM Na₂CO₃, respectively

(see Tab. 3.6). In accordance with literature functionally expressed human $\delta\beta\gamma$ -ENaC channel showed expected membrane current changes in response to sodium salts (Waldmann *et al.*, 1995). As observed for of $\alpha\beta\gamma$ -ENaC chimera a significant inhibitory and outward directed mean membrane current change of 53 nA induced by the application of 10 mM CaCl_2 was observed (see 3.4.3). Consistent with virtual impermeability of $\delta\beta\gamma$ -ENaC to potassium ions (Waldmann *et al.*, 1995), the application of 10 mM KCl did not lead to a significant membrane current change (see Tab. 3.6).

Functional expression of pool F1-1 to F1-26 in combination with human δ -ENaC resulted in significant inhibitory membrane current changes in oocytes challenged with sodium salts (see Tab. 3.6). These outward directed membrane current changes of oocytes were observed by functional expression of 17 out of 26 pool cRNAs (see Tab. 3.6). Representative membrane current changes of oocytes functional expressing pool F1-3, challenged with NaCl, Na_2CO_3 , CaCl_2 and KCl, are shown in Fig. 3.25. To elucidate if the inhibitory sodium currents are due to intrinsic human δ -ENaC activity, which was used for normalization of membrane current changes (see 2.16.4), pool F1-3 was chosen for further analysis by fractionation.

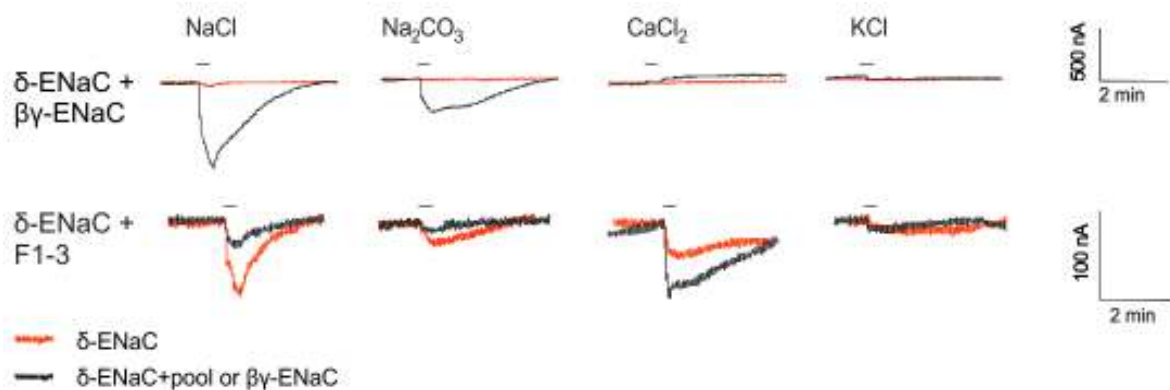


Fig. 3.25 Representative current traces of oocytes functional expressing pool F1-3. Exemplary current traces of oocytes functional expressing 320 pg human δ -ENaC in combination with 22 ng F1-3 cRNA or 16 ng human $\beta\gamma$ -ENaC challenged with 40 mM NaCl, 10 mM Na_2CO_3 , 10 mM CaCl_2 and 10 mM KCl. Representative membrane current change of oocytes injected with 320 pg human δ -ENaC alone from the same batch of oocytes is shown as red trace. Pool F1-3 and human $\beta\gamma$ -ENaC are shown in different scales. Bar indicates duration of application.

Tab. 3.6: Electrophysiologic recordings of oocytes functional expressing macaque cDNA library pools F1-1 to F1-26 in combination with human δ -ENaC. Shown are number of responsive oocytes and batches as well as normalized membrane current changes. Significant membrane current changes are highlighted in yellow.

human δ -ENaC + F1-	$\beta\gamma^{\#}$	10 mM KCl						10 mM CaCl ₂						10 mM Na ₂ CO ₃						40 mM NaCl							
		current change of responsive oocytes [nA]	significance p	current change of total oocytes [nA]	no. of oocytes responsive (%)	total	responsive	batches total	responsive	current change of responsive oocytes [nA]	significance p	current change of total oocytes [nA]	no. of oocytes responsive (%)	total	responsive	batches total	responsive	current change of responsive oocytes [nA]	significance p	current change of total oocytes [nA]	no. of oocytes responsive (%)	total	responsive	batches total	responsive		
1	1	-11 +/- 106	n.s.	-8 +/- 88	69	16	11	7	53 +/- 96	*	41 +/- 88	88	17	7	871 +/- 860	***	-871 +/- 860	100	17	751 +/- 1144	***	751 +/- 1144	100	17	751 +/- 1144	***	
2	2	16	n.s.	1 +/- 4	5	19	1	3	10 +/- 25	n.s.	3 +/- 15	32	19	3	46 +/- 4	**	36 +/- 19	79	15	100 +/- 6	***	100 +/- 6	79	15	78 +/- 41	***	
3	3	17 +/- 2	n.s.	3 +/- 7	20	20	4	3	45 +/- 2	n.s.	2 +/- 7	10	20	1	34 +/- 16	**	26 +/- 20	75	15	73 +/- 34	***	73 +/- 34	80	16	58 +/- 42	***	
4	4	11 +/- 20	n.s.	2 +/- 10	21	38	8	4	-21 +/- 47	n.s.	-9 +/- 32	42	43	6	25 +/- 45	n.s.	15 +/- 37	59	22	73 +/- 60	**	73 +/- 60	63	27	46 +/- 59	**	
5	5	24 +/- 11	n.s.	8 +/- 13	14	22	3	4	-35 +/- 63	n.s.	-14 +/- 43	38	24	3	-10 +/- 74	n.s.	-7 +/- 62	67	16	3 +/- 181	n.s.	3 +/- 181	75	18	2 +/- 157	n.s.	
6	6	10 +/- 13	n.s.	3 +/- 8	25	20	5	2	11 +/- 24	n.s.	3 +/- 14	30	20	3	25 +/- 22	n.s.	15 +/- 21	60	12	71 +/- 19	**	71 +/- 19	65	13	46 +/- 37	**	
7	7	19 +/- 3	n.s.	3 +/- 7	17	29	5	2	1 +/- 31	n.s.	1 +/- 21	48	29	6	25 +/- 25	n.s.	13 +/- 22	52	14	52 +/- 55	*	52 +/- 55	59	17	30 +/- 49	*	
8	8	17 +/- 0	n.s.	4 +/- 7	23	13	3	2	22 +/- 30	n.s.	13 +/- 11	62	13	2	61 +/- 16	**	33 +/- 33	54	7	149 +/- 27	**	149 +/- 27	54	13	80 +/- 77	**	
9	9	-15	n.s.	-2 +/- 5	10	10	1	2	2 +/- 53	n.s.	1 +/- 29	30	10	2	43 +/- 54	*	35 +/- 51	80	8	106 +/- 97	**	106 +/- 97	90	10	95 +/- 97	**	
10	10	15 +/- 0	n.s.	2 +/- 5	14	14	2	2	7 +/- 11	n.s.	6 +/- 10	86	14	2	68 +/- 22	***	39 +/- 34	57	8	160 +/- 3	***	160 +/- 3	57	14	91 +/- 79	***	
11	11	-	n.s.	0 +/- 0	0	14	0	2	18 +/- 1	n.s.	14 +/- 8	79	14	2	70 +/- 2	***	40 +/- 35	57	8	167 +/- 2	***	167 +/- 2	57	14	96 +/- 83	***	
12	12	15 +/- 0	n.s.	2 +/- 5	14	14	2	2	19 +/- 3	n.s.	9 +/- 10	50	14	2	65 +/- 7	***	37 +/- 33	57	8	163 +/- 6	***	163 +/- 6	57	14	93 +/- 81	***	
13	13	1 +/- 8	n.s.	1 +/- 8	83	12	10	2	13 +/- 8	n.s.	13 +/- 8	100	12	2	63 +/- 16	***	48 +/- 31	75	9	165 +/- 4	***	165 +/- 4	67	12	110 +/- 78	***	
14	14	-29	n.s.	-2 +/- 8	8	13	1	2	20 +/- 3	n.s.	8 +/- 10	38	13	2	68 +/- 2	***	45 +/- 32	69	9	162 +/- 2	***	162 +/- 2	69	13	112 +/- 75	***	
15	15	18 +/- 4	n.s.	5 +/- 9	30	10	3	1	26 +/- 12	n.s.	14 +/- 7	80	10	2	69 +/- 1	**	41 +/- 34	60	6	162 +/- 6	***	162 +/- 6	60	10	97 +/- 80	***	
16	16	16 +/- 1	n.s.	3 +/- 6	17	12	2	1	17 +/- 2	n.s.	10 +/- 9	58	12	2	68 +/- 1	***	45 +/- 32	67	8	164 +/- 2	***	164 +/- 2	67	12	109 +/- 77	***	
17	17	18 +/- 26	n.s.	5 +/- 19	29	14	4	3	20 +/- 3	n.s.	20 +/- 3	100	14	3	61 +/- 4	**	35 +/- 34	57	8	119 +/- 81	**	119 +/- 81	57	14	68 +/- 86	**	
18	18	-69 +/- 84	n.s.	-14 +/- 46	18	11	2	2	19 +/- 3	n.s.	9 +/- 10	45	11	2	65 +/- 7	***	48 +/- 30	73	8	164 +/- 2	***	164 +/- 2	67	12	110 +/- 78	***	
19	19	18 +/- 2	n.s.	#6 +/- 9	36	11	4	4	42 +/- 47	*	38 +/- 46	92	12	4	-87 +/- 0	n.s.	-7 +/- 24	8	1	154 +/- 100	n.s.	154 +/- 100	17	4	26 +/- 70	n.s.	
20	20	28 +/- 9	**	17 +/- 15	61	18	11	2	3 +/- 19	n.s.	1 +/- 10	28	18	2	-45 +/- 53	**	-28 +/- 47	61	3	-96 +/- 146	**	-96 +/- 146	18	13	-69 +/- 131	**	
21	21	22 +/- 10	*	18 +/- 12	83	12	10	4	20 +/- 4	n.s.	3 +/- 8	17	12	1	25 +/- 6	n.s.	11 +/- 13	42	5	80 +/- 29	n.s.	80 +/- 29	38	13	31 +/- 43	n.s.	
22	22	30 +/- 10	*	15 +/- 17	46	13	6	2	18 +/- 1	n.s.	4 +/- 7	20	15	2	32 +/- 11	n.s.	12 +/- 17	38	5	50 +/- 41	n.s.	50 +/- 41	15	10	33 +/- 41	n.s.	
23	23	15	n.s.	1 +/- 4	9	11	1	1	57 +/- 29	**	57 +/- 29	100	11	3	-	n.s.	0	0	0	-	n.s.	-	0	0	0	0	n.s.
24	24	-35 +/- 3	n.s.	-6 +/- 13	17	12	2	1	66 +/- 34	**	60 +/- 38	92	12	3	18	n.s.	2 +/- 5	8	1	26	n.s.	26	8	2 +/- 7	n.s.		
25	25	-21 +/- 24	n.s.	-6 +/- 16	31	16	5	2	69 +/- 32	***	52 +/- 10	75	16	2	17 +/- 1	n.s.	3 +/- 7	19	3	-45 +/- 5	n.s.	-45 +/- 5	20	10	-5 +/- 14	n.s.	
26	26	26 +/- 4	*	17 +/- 13	64	11	7	1	17 +/- 2	n.s.	8 +/- 9	45	11	2	20	n.s.	2 +/- 6	9	1	-11 +/- 35	n.s.	-11 +/- 35	11	5	-6 +/- 26	n.s.	
		19 +/- 4	n.s.	4 +/- 8	20	10	2	3	16 +/- 26	n.s.	11 +/- 23	70	10	3	18	n.s.	2 +/- 5	10	1	39 +/- 5	n.s.	39 +/- 5	10	2	8 +/- 16	n.s.	

#, human $\beta\gamma$ -ENaC; SD, standard deviation; gray, pools chosen for fractionation; n.s., not significant; *, p < 0.05; **, p < 0.01; ***, p < 0.001

Pool F1-3 was fractionated to 15 sub-pools with 200 cDNA clones each to validate this inhibitory response and to isolate potential inhibitory cDNA clone(s). Functional expression of 15 sub-pools together with human δ -ENaC and exposition to NaCl, Na₂CO₃, CaCl₂ and KCl did not verify significant inhibitory response of parental pool F1-3 to NaCl (see Tab. 3.7). Notably, significance was determined with respect to parental pool F1-3.

A significant activatory response to CaCl₂ with a mean of -64 and -41 nA was detected in F1-3 sub-pool 6 and 7, which possibly confirms initial not significant activatory response of parental pool F1-3. Thus, responsible cDNA clone(s) might be accumulated within F1-3 sub-pool 6 and 7. However, sub-pools do not respond to potassium chloride or sodium salts, suggesting ion channel(s) specific for calcium ions. Thus, this or these ion channels either independently or by interaction with human δ -ENaC are no cation unspecific ion channels as it would be expected for cation unspecific salt taste receptor candidates. Therefore, F1-3 sub-pool 6 and 7 were not subject of further investigations.

Tab. 3.7: Electrophysiologic recordings of oocytes functional expressing macaque cDNA library pool F1-3 sub-pools in combination with human δ -ENaC. Shown are number of responsive oocytes and batches as well as normalized membrane current changes. Significant membrane current changes are highlighted in yellow.

human δ -ENaC +	$\beta V^{\#}$	40 mM NaCl										10 mM Na ₂ CO ₃										10 mM CaCl ₂										10 mM KCl									
		batches		no. of oocytes		current change of total oocytes [nA]	significance p	current change of responsive oocytes [nA]	batches		no. of oocytes		current change of total oocytes [nA]	significance p	current change of responsive oocytes [nA]	batches		no. of oocytes		current change of total oocytes [nA]	significance p	current change of responsive oocytes [nA]	batches		no. of oocytes		current change of total oocytes [nA]	significance p	current change of responsive oocytes [nA]	batches		no. of oocytes		current change of total oocytes [nA]	significance p	current change of responsive oocytes [nA]					
F1-3 [#]		4	4	9	9	-1131 +/- 1524		-1131 +/- 1524			4	4	9	100	-659 +/- 695	***	-659 +/- 695		25 +/- 45			4	4	7	9	78	-122 +/- 196	*	-156 +/- 209		4	4	6	67	-14 +/- 60	n.s.	-14 +/- 60				
F1-3 sub-pool		4	6	27	43	63	**	73 +/- 60			4	6	22	37	15 +/- 37	n.s.	15 +/- 37		25 +/- 45			6	6	18	43	42	-9 +/- 32	n.s.	-21 +/- 47		4	6	8	38	2 +/- 10	n.s.	2 +/- 10				
1		2	2	9	16	56		-9 +/- 53			2	2	10	12	-17 +/- 40	n.s.	-17 +/- 40		-27 +/- 47			1	2	8	16	50	-25 +/- 28	*	-50 +/- 17		1	2	1	12	-2 +/- 6	n.s.	-2 +/- 6				
2		2	2	7	11	64		-48 +/- 68			2	2	8	10	-6 +/- 35	n.s.	-8 +/- 41		-8 +/- 41			2	2	5	11	45	-23 +/- 31	n.s.	-50 +/- 26		2	2	4	8	-3 +/- 21	n.s.	-6 +/- 29				
3		2	2	8	9	89		-25 +/- 85			2	2	6	9	-3 +/- 19	n.s.	-5 +/- 24		-5 +/- 24			2	2	8	9	89	-48 +/- 73	n.s.	-54 +/- 75		1	2	1	9	-4 +/- 10	n.s.	-26				
4		1	3	3	9	33		24 +/- 36			2	3	5	9	4 +/- 42	n.s.	7 +/- 55		7 +/- 55			1	3	1	7	14	-2 +/- 5	n.s.	-131 +/- 140		1	3	1	7	-2 +/- 5	n.s.	-15				
5		2	2	5	11	45		8 +/- 26			2	2	7	11	-3 +/- 41	n.s.	-5 +/- 41		-5 +/- 41			2	2	6	11	55	-45 +/- 74	n.s.	-83 +/- 83		1	2	1	11	-2 +/- 5	n.s.	-16				
6		2	2	5	11	45		24 +/- 36			2	2	8	11	-1 +/- 43	n.s.	-1 +/- 51		-1 +/- 51			2	2	7	11	64	-41 +/- 50	*	-64 +/- 49		1	2	2	10	4 +/- 7	n.s.	19 +/- 1				
7		2	2	7	9	78		14 +/- 30			2	2	5	9	-4 +/- 31	n.s.	-8 +/- 42		-8 +/- 42			2	2	7	9	78	-32 +/- 36	*	-41 +/- 36		1	2	1	7	-4 +/- 9	n.s.	-26				
8		1	2	1	7	14		9 +/- 22			1	2	1	7	7 +/- 17	n.s.	48		48			1	2	2	7	29	-4 +/- 7	n.s.	-16 +/- 0		1	2	1	7	2 +/- 5	n.s.	15				
9		2	2	5	10	50		4 +/- 70			1	2	4	10	10 +/- 42	n.s.	22 +/- 61		22 +/- 61			1	2	2	10	20	-10 +/- 25	n.s.	-50 +/- 33		0	2	0	10	0 +/- 0	n.s.	-				
10		2	2	4	7	57		-60 +/- 88			1	2	2	7	-8 +/- 27	n.s.	-28 +/- 44		-28 +/- 44			2	2	2	7	29	-12 +/- 20	n.s.	-41 +/- 17		0	2	0	6	0 +/- 0	n.s.	-				
11		1	2	1	7	14		-3 +/- 7			0	2	0	7	0 +/- 0	n.s.	-		-		2	2	3	7	43	-2 +/- 11	n.s.	-4 +/- 17		1	2	2	7	5 +/- 8	n.s.	18 +/- 0					
12		1	2	6	10	60		-47 +/- 143			1	2	5	10	-13 +/- 50	n.s.	-27 +/- 68		-27 +/- 68			1	2	4	10	40	-16 +/- 23	n.s.	-41 +/- 19		2	2	2	8	-5 +/- 22	n.s.	-20 +/- 40				
13		1	2	4	9	44		31 +/- 36			1	2	5	9	25 +/- 25	*	45 +/- 14		45 +/- 14			0	2	0	9	0	0 +/- 0	n.s.	-		0	2	0	9	0 +/- 0	n.s.	-				
14		1	2	2	6	33		24 +/- 36			1	2	2	6	19 +/- 27	n.s.	56 +/- 5		56 +/- 5			0	2	0	6	0	0 +/- 0	n.s.	-		0	2	0	6	0 +/- 0	n.s.	-				
15		2	2	4	7	57		-37 +/- 50			1	2	3	7	27 +/- 31	n.s.	63 +/- 1		63 +/- 1			1	2	1	7	14	-4 +/- 11	n.s.	-32		0	2	0	7	0 +/- 0	n.s.	-				

[#], human β -ENaC; SD, standard deviation; gray, pools chosen for fractionation; n.s., not significant; p > 0.05; *, p < 0.05; **, p < 0.01; ***, p < 0.001

Remarkably, pool F1-19 was the solely pool showing an activating inward directed sodium current change upon application of NaCl as well as Na₂CO₃, when co-expressed with human δ -ENaC (see Fig. 3.26 and Tab. 3.6). The mean membrane current change induced by application of NaCl and Na₂CO₃ was -96 nA and -45 nA, respectively (see Tab. 3.6). Additionally, a significant inhibitory response, with a mean of 28 nA was detected by application of KCl.

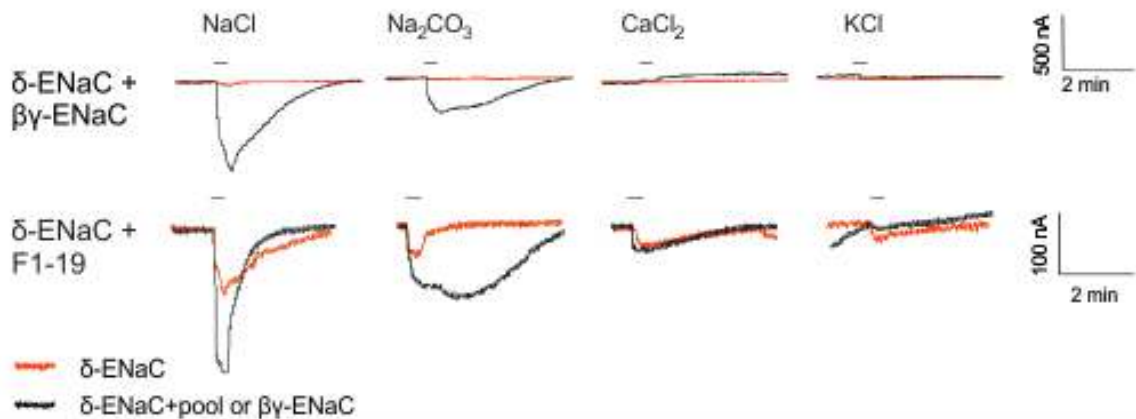


Fig. 3.26 Representative current traces of oocytes functional expressing pool F1-19. Exemplary current traces of oocytes functional expressing 320 pg human δ -ENaC in combination with 32 ng F1-19 cRNA or 16 ng human $\beta\gamma$ -ENaC challenged with 40 mM NaCl, 10 mM Na₂CO₃, 10 mM CaCl₂ and 10 mM KCl. Representative membrane current change of oocytes injected with 320 pg human δ -ENaC alone from the same batch of oocytes is shown as red trace. Pool F1-19 and human $\beta\gamma$ -ENaC are shown in different scales. Bar indicates duration of application.

Notably, pool F1-19 was not noticed during screening of cDNA pools interactionpartners of $\beta\gamma$ -ENaC. This strongly suggests that activatory sodium responses are an effect of interaction of pool F1-19 cDNA clone(s) in combination with human δ -ENaC. To validate activatory response upon sodium application and to isolate potential δ -ENaC interaction partner, pool F1-19 was fractionated to 15 sub-pools as described before (see 3.4.3). Sub-pools were functionally expressed in combination with human δ -ENaC and challenged with NaCl, Na₂CO₃, CaCl₂ and KCl as the parental pool before. Significant membrane current change of pool F19 upon sodium salts was not recovered within F1-19 sub-pools (see Tab. 3.8). Thus, responsible cDNA clone(s) was not accumulated in sub-pools and cannot be isolated. In conclusion, no human δ -ENaC interaction partner could be identified by screening of cDNA library pools F1-1 to F1-26. Moreover and in accordance with $\beta\gamma$ -ENaC screening no ENaC-independent salt taste receptor candidate was detected.

Tab. 3.8: Electrophysiologic recordings of oocytes functional expressing macaque cDNA library pool F1-19 sub-pools in combination with human δ -ENaC. Shown are number of responsive oocytes and batches as well as normalized membrane current changes. Significant membrane current changes are highlighted in yellow.

40 mM NaCl			10 mM Na ₂ CO ₃			10 mM CaCl ₂			10 mM KCl			F1-19 sub-pool						
human δ -ENaC +	$\beta\gamma^{\#}$	19 $\#$	current change of responsive oocytes +/- SD [nA]	significance p	current change of total oocytes +/- SD [nA]	no. of oocytes (%)	batches	current change of responsive oocytes +/- SD [nA]	significance p	current change of total oocytes +/- SD [nA]	no. of oocytes (%)	batches	current change of responsive oocytes +/- SD [nA]	significance p	current change of total oocytes +/- SD [nA]	no. of oocytes (%)	batches	
			-295 +/- 308	*	-240 +/- 110	100	2 2 8 8	42 +/- 19	**	31 +/- 24	75	2 2 6 8	0 +/- 16	n.s.	0 +/- 13	40	1 2 2 5	1 2 3
			-96 +/- 146	**	-28 +/- 47	61	2 3 11 18	3 +/- 19	n.s.	1 +/- 10	28	2 3 5 18	28 +/- 9	**	17 +/- 15	61	2 3 11 18	2 3 3
F1-19 sub-pools																		
1	0	2	0	7	0	0	1	22 +/- 1	n.s.	2 +/- 2	0	0	6 +/- 3	n.s.	6 +/- 3	7	0	2
2	0	2	0	8	0	0	0	-	n.s.	1 +/- 3	0	0	6 +/- 5	n.s.	6 +/- 5	8	0	2
3	0	2	0	8	0	0	0	-	n.s.	3 +/- 5	13	1	3 +/- 3	n.s.	3 +/- 3	8	0	2
4	0	3	0	8	0	0	0	-	n.s.	0 +/- 3	8	0	3 +/- 5	n.s.	3 +/- 5	8	0	2
5	0	2	0	8	0	13	1	-18	n.s.	-4 +/- 14	13	1	6 +/- 5	n.s.	6 +/- 5	18	1	2
6	0	2	0	7	0	0	0	-	n.s.	0 +/- 4	7	0	1 +/- 5	n.s.	1 +/- 5	7	0	2
7	0	2	0	8	0	0	0	-	n.s.	1 +/- 6	8	0	3 +/- 5	n.s.	3 +/- 5	8	0	2
8	0	2	0	8	0	0	0	-	n.s.	5 +/- 2	8	0	6 +/- 2	n.s.	6 +/- 2	8	0	2
9	0	2	0	8	0	0	0	-	n.s.	3 +/- 2	8	0	6 +/- 4	n.s.	6 +/- 4	8	0	2
10	0	2	0	8	0	0	0	-	n.s.	2 +/- 3	8	0	4 +/- 3	n.s.	4 +/- 3	8	0	2
11	1	2	1	8	13	0	0	-	n.s.	2 +/- 5	8	0	3 +/- 6	n.s.	3 +/- 6	13	0	2
12	0	2	0	8	0	0	0	-	n.s.	3 +/- 7	13	1	4 +/- 3	n.s.	4 +/- 3	8	0	2
13	0	2	0	8	0	0	0	-	n.s.	0 +/- 2	8	0	5 +/- 3	n.s.	5 +/- 3	8	0	2
14	1	2	1	8	13	13	1	-19	n.s.	4 +/- 4	8	0	3 +/- 4	n.s.	3 +/- 4	8	0	2
15	1	2	1	7	14	0	0	-	n.s.	2 +/- 4	7	0	5 +/- 4	n.s.	5 +/- 4	7	0	2

#, human $\beta\gamma$ -ENaC; SD, standard deviation; gray, pools chosen for fractionation; n.s., not significant; p > 0.05; *, p < 0.05; **, p < 0.01; ***, p < 0.001

4 Discussion

4.1 Involvement of epithelial sodium channel in human salt taste transduction

Verification of ENaC as amiloride sensitive sodium taste receptor in rodents (Chandrashekar *et al.*, 2010) suggests the conclusion that ENaC plays a role in human salt taste perception, too. However, rodent and human salt taste transduction differs considerably so that an involvement of ENaC in human salt perception is not trivial (see 1.3 and 1.4) and has to be substantiated. Evidence for presence of all four human ENaC subunits, namely α -, β -, γ - and δ -ENaC, in taste papillae and non-chemosensory epithelium was found by RT-PCR (Huque *et al.*, 2002; Stähler *et al.*, 2008; Huque *et al.*, 2009). This confirms previous studies in rodents (Kretz *et al.*, 1999; Lin *et al.*, 1999; Shigemura *et al.*, 2005), extending them by detection of δ -ENaC mRNA in lingual tissue. A prerequisite for an involvement of ENaC in human salt taste transduction is expression of ENaC subunits in taste bud cells, as shown for rodents (Kretz *et al.*, 1999; Lin *et al.*, 1999; Shigemura *et al.*, 2005; Yoshida *et al.*, 2009a; Chandrashekar *et al.*, 2010). In order to validate or invalidate presence of ENaC subunit mRNAs and proteins in taste bud cells, localization studies using *in situ* hybridization and immunohistochemical analyses were carried out in this study. In accordance with RT-PCR data (Stähler *et al.*, 2008) and consistent with a role in taste transduction, all ENaC subunits were detected in taste bud cells as well as non-chemosensory cells by immunohistochemistry, with exception of α -ENaC in fungiform taste bud cells (see Fig. 3.2). Although *in situ* hybridization was sensitive enough to detect β -, γ - and δ -ENaC mRNAs in non-chemosensory epithelial cells surrounding taste buds, α -ENaC mRNA was solely detected ENaC subunit mRNA within circumvallate taste cells (see Fig. 3.1). Notably, it was ensured that *in situ* hybridization probes were able to detect virtually all known β -, γ - and δ -ENaC splice variants (see Tab. 7.4). Concerning permanent cell renewal and short life time of a taste bud cell with an average of about ten days (Beidler & Smallman, 1965; Farbman, 1980), ENaC mRNAs may be short-lived or confined to transient sets of developing taste bud cells, whereas polypeptides are present in mature cells and comparatively stable. This would explain that ENaC detection by antibodies might be considerably more sensitive than detecting ENaC mRNA by *in situ* hybridization. Additionally, exclusive detection of α -ENaC mRNA is likely due to its high abundance, which is in accordance with RT-PCR results revealing α -ENaC as most frequent mRNA in taste tissue (Stähler *et al.*, 2008). This is in accordance

with studies in rodents showing high abundance of α -ENaC mRNA in circumvallate taste bud cells compared to other ENaC subunits (Kretz *et al.*, 1999; Lin *et al.*, 1999). Immunoreactivity of α -, β - and γ -ENaC was found to be associated with basolateral parts of taste bud cells. This suggests the presence of basolateral $\alpha\beta\gamma$ -ENaC ion channels in circumvallate papillae possibly involved in basolateral sodium entry. An observation, which has also been made in rodents (Kretz *et al.*, 1999; Shigemura *et al.*, 2005). Notably, number of taste buds and cells within taste buds that are labeled with the various antibodies varied (see Tab. 3.1), raising the question about ENaC subunit composition *in vivo*. Anti- β -ENaC antiserum labeled much fewer buds in the circumvallate papillae than in fungiform papillae, while the anti- γ -ENaC antiserum labelled comparable proportions of taste buds in both types of papillae. Topographical differences between anterior and posterior taste papillae was previously observed in rats (Kretz *et al.*, 1999, Lin *et al.*, 1999), and might be responsible for amiloride sensitivity of sodium taste signals arising from fungiform papillae and amiloride insensitivity of sodium taste signals arising from vallate papillae in rodents (Formaker & Hill, 1991; Hill *et al.*, 1990). Moreover, presence of basolateral amiloride sensitive $\alpha\beta\gamma$ -ENaC in human circumvallate papillae is in accordance with submucosal amiloride sensitivity previously shown for rat lingual epithelium (Mierson *et al.*, 1996). Possibly, basolateral $\alpha\beta\gamma$ -ENaC in human circumvallate taste cells might be stimulated by sodium ions, entering paracellularly via tight junctions. Interestingly, amiloride cannot penetrate through tight junctions (Kitada *et al.*, 2001) and has thereby no access to basolateral $\alpha\beta\gamma$ -ENaC in circumvallate papillae. Thus, sodium taste mediated by basolateral $\alpha\beta\gamma$ -ENaC would be amiloride insensitive and might account for observed amiloride-insensitivity of sodium taste in human sensory studies (Halpern & Darlington, 1998) as well as for amiloride insensitivity of sodium taste signals arising from vallate papillae in rodents (Formaker & Hill, 1991; Hill *et al.*, 1990). Another option for human amiloride insensitivity might be lacking co-localization of ENaC subunits hindering assembly of functional $\alpha\beta\gamma$ -ENaC ion channels in circumvallate papillae, as assumed for mouse vallate taste bud cells showing separate cell populations for α - and β -ENaC (Chandrashekar *et al.*, 2010).

Notably, neither α -ENaC immunoreactivity, nor mRNA was found in human fungiform taste bud cells, which might be due to individual differences among human subjects (Huque *et al.*, 2002) or to species differences in human and rodent sodium taste transduction. A lack of α -ENaC in fungiform taste bud cells is in strong contrast to studies in mice, revealing α -ENaC as essential subunit for mediation of amiloride sensitive

sodium taste via fungiform taste bud cells (Chandrashekar *et al.*, 2010). However, this might substantiate species differences of strong amiloride sensitivity of mouse sodium taste (Brand *et al.*, 1985; Hill *et al.*, 1990; Spector *et al.*, 1996) and largely amiloride insensitive human sodium taste perception (Feldman *et al.*, 2003; Halpern, 1998; Ossebaard & Smith, 1995). A lack of α -ENaC in human fungiform taste bud cells means absence of functional amiloride sensitive $\alpha\beta\gamma$ -ENaC ion channels and might explain amiloride insensitivity of human sodium taste perception.

Intriguingly, δ -ENaC showed most prominent immunoreactivity, localized to the pore region of every taste bud analyzed, strongly suggesting a role in taste transduction (see Fig. 3.2 and Tab. 3.1). This prominent apical localization of δ -ENaC was confirmed by two antisera raised in different host species and against distinct δ -ENaC epitopes (see Fig. 3.5). However, one of these antisera likely recognizes an unknown protein in mouse vallate taste pores (see Fig. 3.6). Hence, specificity of antisera to heterologously expressed human δ -ENaC protein was confirmed using immunocytochemistry, suggesting a specific binding of both antisera to human δ -ENaC without cross-reactivity to human α -ENaC (see Fig. 3.4). Moreover, β - or γ -ENaC antisera raised in the same species did not stick to taste pores. Therefore, a non-specific sticky binding of anti δ -ENaC to taste pores is unlikely. Localization of δ -ENaC in the taste pore of fungiform and circumvallate taste buds appears similar as observed for other taste receptors (Hoon *et al.*, 1999), substantiating a potential role in taste transduction. Thus, an apical sodium ion entry involving δ -ENaC is highly likely. Remarkably, taste pore labeling by anti- δ -ENaC antiserum resembles immunohistochemical staining of tight junction proteins (Gao *et al.*, 2009; Michlig *et al.*, 2007). Thus, alternatively to apical entry of sodium ions into taste bud cells, δ -ENaC might be additionally involved in paracellular sodium entry via tight junctions. Participation of δ -ENaC in sodium taste transduction might further explain human amiloride-insensitivity of human sodium taste (Halpern & Darlington, 1998), as $\delta\beta\gamma$ -ENaC is more than 50 fold less sensitive against the diuretic amiloride than $\alpha\beta\gamma$ -ENaC *in vitro* (Ji, H.-L. *et al.*, 2004, Ji, H. L. *et al.*, 2006).

However, regional separation of δ -ENaC from its basolateral localized native interaction partner β - and γ -ENaC makes assembly of efficient apical $\delta\beta\gamma$ -ENaC unlikely in fungiform and circumvallate taste buds. *In vitro*, functional channels formed by δ -subunits have little channel activity, which can largely be enhanced through coexpression with β - and γ -ENaC (Waldmann *et al.*, 1995). Notably, basolateral localized $\beta\gamma$ -ENaC in

fungiform papillae cannot assemble a functional sodium channel *in vitro* too (Waldmann *et al.*, 1995), raising the question about identity of ion channels allowing basolateral sodium entry in fungiform taste bud cells. Thus, unknown polypeptides might be present to assemble a functional ion channel in human fungiform taste bud cells involving apical δ -ENaC and basolateral $\beta\gamma$ -ENaC, respectively. Alternatively, translocation of $\beta\gamma$ -ENaC to apical located δ -ENaC upon certain physiological conditions can be assumed (Lin *et al.*, 1999). However, existence of unknown δ -ENaC interaction partners is additionally likely in human brain, where δ -ENaC is expressed without detection of β - and/or γ -ENaC (Giraldez *et al.*, 2007). Notably, ion channel properties are likely rendered by unknown interaction partner assembling with δ -ENaC in fungiform and circumvallate taste pores or $\beta\gamma$ -ENaC in basolateral compartments of fungiform taste bud cells. Thus, novel properties may further affect sensitivity towards amiloride and ion selectivity (Ji, H. L. *et al.*, 2006). Thus, δ -ENaC is a potential candidate involved in transduction of sodium specific as well as cation unspecific salt taste transduction. Further, modified ion channel properties and composition of a putative human salt taste receptor involving δ -ENaC might explain why some potent $\delta\beta\gamma$ -ENaC enhancer found *in vitro* fail to increase saltiness perception *in vivo* (Stähler *et al.*, 2008).

Taken together, ENaC likely plays a role in human taste transduction in particular involving apical δ -ENaC in fungiform and circumvallate taste bud cells as well as basolateral $\alpha\beta\gamma$ -ENaC in circumvallate taste bud cells. This is consistent with salt taste enhancing potential of compounds increasing sodium currents mediated by $\alpha\beta\gamma$ - and $\delta\beta\gamma$ -ENaC *in vitro* (Stähler *et al.*, 2008). However, definite ENaC subunit compositions in fungiform taste bud cells remain elusive for apical δ -ENaC ion channels on the one hand and basolateral $\beta\gamma$ -ENaC ion channels on the other hand. In accordance with literature, modified subunit composition alters sodium channel properties, as shown for $\alpha\beta\gamma$ - and $\delta\beta\gamma$ -ENaC (Waldmann *et al.*, 1995). Thus, interaction of δ -ENaC and $\beta\gamma$ -ENaC subunits with probably unknown polypeptides in fungiform and circumvallate papillae are promising sodium and salt taste receptor candidates. However, latter does not rule out existence of unknown and ENaC independent salt taste receptor candidates.

4.2 Taste tissue cDNA library screening for salt taste receptor candidates

In order to resolve subunit composition of ion channels involving human $\beta\gamma$ -ENaC or δ -ENaC in taste bud cells a taste tissue specific cDNA library from rhesus monkey was used to identify putative ENaC interaction partners. Thereby, ENaC independent salt taste receptor candidates might be identified as well, as human δ -ENaC or $\beta\gamma$ -ENaC alone do not form efficient sodium channels.

Representatively, cDNA library was characterized for *macaca* α -ENaC cDNA inserts. In accordance with macaque α -ENaC data base entries XM_001103017, XM_001103097 and XM_001103409 (Wheeler *et al.*, 2008), at least three coding and full length α -ENaC cDNA variants with a maximal size of 3.6 kb are included within cDNA library pools (see Fig. 3.18 and Fig. 3.19). Thus, cDNA library inserts are heterogen arguing for high quality of the cDNA library, enabling isolation of full length genes. However, no full length clones of macaque δ -, β - and γ -ENaC were detected by RT-PCR, while full length α -ENaC was found in 7 of 26 cDNA library pools. This confirms high α -ENaC mRNA expression levels found in human taste tissue (Stähler *et al.*, 2008), pointing to short lived or less strong expressed mRNAs of macaque δ -, β - and γ -ENaC. This comparably strong expression of human α -ENaC in respect of other subunits is in accordance with observations in this thesis (see Fig. 3.1) as well as with α -ENaC expression levels in rodents (Kretz *et al.*, 1999; Shigemura *et al.*, 2005). Thus, cDNA library made from macaque foliate papillae represents molecular state of ENaC mRNA expression observed for human circumvallate and fungiform papillae. Consequently, used cDNA library is an adequate source to screen for novel taste related polypeptides, while some short lived mRNAs might be not represented by the cDNA library.

To find salt taste receptor candidates, oocytes heterologous expressing cDNA pools in combination with human $\beta\gamma$ -ENaC or δ -ENaC were challenged with two sodium salts as well as calcium chloride and potassium chloride. Established screening assay was shown to be sensitive enough to detect single cDNA clones from a mixture of 2000 (see Fig. 3.20), showing its feasibility to identify macaque polypeptides interacting with human ENaC subunits or assembling novel salt taste receptor candidates. Under chosen assay conditions activatory, inward directed membrane current changes point to potential salt taste receptor candidates, enabling cation entry into the cell. Significant activatory membrane current changes upon salt application were detected for two pools. Pool F1-19 showed a significant activatory inward directed membrane current change in response to

sodium salts, when co-expressed with human δ -ENaC (see Fig. 3.26). This points to expression of sodium specific ion channels and a potential sodium salt taste receptor. Notably, activity of functionally expressed pool F1-19 was not noticed, when co-expressed with $\beta\gamma$ -ENaC (see Tab. 3.3), pointing to a specific interaction with human δ -ENaC. Second responding pool, pool F1-15 showed significant activatory responses to calcium chloride as well as potassium chloride, when co-expressed with $\beta\gamma$ -ENaC (see Fig. 3.21). This points to presence of cation unspecific ion channels. Accordingly, neither polypeptides which assemble into sodium channels with $\beta\gamma$ -ENaC nor ENaC-independent sodium or cation unspecific channels were detected. Moreover, none of potential cDNA clones interacting with δ -ENaC or $\beta\gamma$ -ENaC could be recovered within generated sub-pools, although scaling down procedure was feasible to recover single cDNA clones, representatively shown for macaque α -ENaC from pool F1-7 (see Fig. 3.22). Thus, heterologous expression of macaque cDNA library pools did neither reveal ENaC interaction partners nor novel ENaC-independent salt taste receptor candidates.

A possible reason for rare detection of pools leading to activatory membrane current changes upon salt application might be underrepresentation of putative macaque interaction partners, leading to exceedance of the detection limit of the functional assay. In respect of generation of cDNA library taste related genes might be underrepresented, as tissue source were whole macaque foliate papillae including taste bud cells, non-chemosensory epithelial cells as well as connective tissue. Thus taste bud cells are underrepresented and this might be also due for some taste related mRNAs. This cDNA library redundancy has also been observed for human cDNA library made from fungiform papillae (Rossier, O. *et al.*, 2004). Amplification of cDNA library clones necessary to build sub-pools may lead to further enrichment of overrepresented cDNAs. Although heterogeneity of sub-pools seems not to be reduced extremously, cDNA clones might be lost during scaling down procedure (see Fig. 3.23). This underrepresentation or loss of cDNA clones might explain failed recovery of parental pool activity in sub-pools. A subtracted and taste specific cDNA library, which can be achieved by differential PCR, selective hybridization, or selective isolation of taste bud mRNA would be a powerful target to identify ENaC interaction partners and novel salt taste receptor candidates. However, this approach will identify taste bud cell specific targets only. Targets expressed in taste bud cells as well in surrounding epithelium, as ENaC subunits found in chemosensory as well as non-chemosensory cells (see Fig. 3.2), would be missed.

Alternatively and additional to cDNA library redundancy, separation of interacting polypeptides in distinct sub-pools is imaginable. Thereby, polypeptides mediating membrane current changes by multiple interactions in parental pools might be not recovered in sub-pools. Further, initial detected membrane current changes might be non-specific due to fluctuations in expression profile of endogenous ion channels of different oocyte batches or single oocytes and therefore not recovered in sub-pools. However, endogenous responses were minimized by normalization of membrane current changes to perfusion buffer application and mock injected oocytes. Thus, batch or single oocyte dependent statistical spikes are rare, which is in accordance with limited numbers of responsive pools. Beyond screening source further critical conditions could influence detection of ion channels using functional expression in *Xenopus laevis* oocytes. Thus, functional assay was established to detect ENaC-like constitutive active ion channels using TEVC with defined holding potential. No voltage steps or voltage ramps were carried out, which would activate voltage gated ion channels. Thus, these types of ion channels were not detectable at constant holding potential conditions used in the established assay. Additionally, critical buffer conditions, which were optimal for ENaC-like sodium channels, might led to hindered detection of novel ion channels. Still another option would be lacking interaction between human and macaque polypeptides. However, species interaction is expected as primate ortholog proteins are highly homolog and was verified by functional expression of pool F1-7 including macaque α -ENaC in combination with human $\beta\gamma$ -ENaC (see Fig. 3.20). Thus, lacking interaction between human and macaque polypeptides is unlikely but cannot be excluded.

Taken together, screening of a macaque taste tissue cDNA library did neither reveal polypeptides assembling into a functional cation channel by interaction with δ -ENaC or $\beta\gamma$ -ENaC nor ENaC independent salt taste receptor candidates. Thus, exact composition and identity of amiloride sensitive and insensitive human salt taste receptors could not be clarified within this study and stay exciting questions for further research.

4.3 Evolution of delta-ENaC in mice

Potential involvement of δ -ENaC in human taste transduction raises the question about physiological role of the rodent ortholog. Interestingly and in contrast to α -ENaC (SCNN1A), β -ENaC (SCNN1B), and γ -ENaC (SCNN1G), no murine δ -ENaC (SCNN1D) ortholog protein is annotated, so far (Flicek *et al.*, 2011; Sayers *et al.*, 2011). Phylogenetic

analyses showed evolutionary conservation of SCNN1D within various vertebrates, as known for its paralog SCNN1A. However, mouse SCNN1D protein is absent from databases (Flicek *et al.*, 2011; Sayers *et al.*, 2011). Thus, neither computationally predicted mouse SCNN1D protein record nor any experimental evidence for mouse SCNN1D is available. Taking high coverage of mouse genome sequence as well as completed automated annotation into account this points to loss of SCNN1D in mice (Sayers *et al.*, 2011). Remarkably, protein homology search identified SCNN1D from closely related guinea pig, a member of the same taxonomic order rodentia (see Fig. 3.7). Thus, loss of SCNN1D protein is not a unique feature of rodents and must have happened after divergence of guinea pig and mice 75 million years ago (Adkins *et al.*, 2001). Notably, multiple sequence alignment shows larger amino acid divergences between vertebrate SCNN1D protein orthologs when compared to its SCNN1A paralog (see Fig. 3.7). Thus, it is highly likely that SCNN1D evolved more divergent, while SCNN1A evolved under higher purifying selection pressure. This hypothesis is substantiated by the essential role of SCNN1A in sodium homeostasis and osmoregulation, which cannot be compensated by other proteins, unavoidable leading to early postnatal death in knock out mice lacking SCNN1A (Hummler *et al.*, 1996). Compared to this severe phenotype, putative loss of SCNN1D seems to have no obvious effect in mice. Absence of mouse SCNN1D protein from databases is in accordance with classification of *Scnn1d* as pseudogene in laboratory mouse strain C57BL/6J by computational prediction (Sayers *et al.*, 2011). Closer look to genetic localization of *Scnn1d* pseudogene revealed similar genetic organization as known for vertebrate SCNN1D genes (Sayers *et al.*, 2011). In particular, *Scnn1d* is located on distal mouse chromosome 4, which is syntenic to human chromosome 1 encoding SCNN1D (see Fig. 3.8; Liddell *et al.*, 1999). Protein products of *Scnn1d* adjacent genes were easily identified (Sayers *et al.*, 2011), pointing to functional genes encoded in proximity (see Fig. 3.8). Notably, neighboring genes are located more distant from each other than their human paralogs, making a *Scnn1d* pseudogenization by deletion unlikely.

Gene mapping of human SCNN1D to mouse chromosomal DNA revealed insights into evolution of mouse *Scnn1d*. Thereby, 31 kb spanning region, partially ortholog to SCNN1D, was identified on mouse chromosome 4 (see Fig. 3.9A). Latter contains annotated 1.6 kb *Scnn1d* pseudogene sequence but revealed 17 fold more ancestral *Scnn1d* sequences than annotated so far. It is highly likely that virtually complete *Scnn1d* was identified, as ortholog sequences to human SCNN1D include similarities to known 5' and 3' untranslated sequences of SCNN1D derived human transcripts. Despite comparable

gene lengths are known for paralog *Scnn1a*, *Scnn1b* and *Scnn1g* with 24, 53 and 34 kb, respectively, computationally identified mouse *Scnn1d* coding region possess an unusual large size in respect of ortholog vertebrate *SCNN1D* genes, spanning 10 kb in average (Flicek *et al.*, 2011; Sayers *et al.*, 2011). Further *in silico* analyses of C57BL/6J genome identified mutational evolution of *Scnn1d* by interspersed repeats, responsible for distribution of *SCNN1D* homolog sequences over 31 kb (see Fig. 3.9B). Insertional mutagenesis of *Scnn1d* was in particular due to subsequent integration of three endogenous retroviral elements (ERVs), namely MuERV-L, IAP-II and MusD (see Fig. 3.9C). It is highly likely that initial integration of MuERV-L led to pseudogenization of *Scnn1d*, leading to disruption of *Scnn1d* and destroying its coding competence for a functional *SCNN1D* gene product. Further, subsequent integration of IAP-II and MusD led to additional disruption of *Scnn1d*. Notably, insertional mutagenesis as well as absence of a functional *Scnn1d* counterpart in the mouse genome point to unitary character of *Scnn1d* pseudogene.

Retroviral elements are present in all vertebrates, inducing genetic diversity by species specific vertical as well as interspecies horizontal transmission to host genomes (Coffin *et al.*, 1997). Known ERVs showing nucleotide sequence identities of 95, 79 and 98 % to identified MuERV-L, IAP-II and MusD, respectively, enabled insights into their evolutionary origin (Benit *et al.*, 1997; Burt *et al.*, 1984; Ribet *et al.*, 2004). ERV-L related sequences are widespread in mammals, while they are not able to transfer horizontally (Benit *et al.*, 1999). MuERV-L is derived from a recent amplification burst within *Mus musculus* strains less than 2 million years ago and is absent in rat (Benit *et al.*, 1997; Benit *et al.*, 1999). Thus, identified ERV-L integrated into *Scnn1d* is most likely *Mus musculus* specific retroviral element. IAP elements are well known endogenous genomic mutagens in mice (Zhang, Y. *et al.*, 2008a) not able to transfer horizontally as well (Graham *et al.*, 2000). IAP amplification events occurred independently during evolution of *Mus* and *Rattus*, implying strain specificity for *Mus musculus* (Lueders & Kuff, 1983, Kuff & Lueders, 1988, Coffin *et al.*, 1997). Notably, MusD elements are solely reported for *Mus* genus, unable to transfer horizontally (Ribet *et al.*, 2004, Baillie *et al.*, 2004). Thus, identified ERVs responsible for mutational evolution of *Scnn1d* are restricted to the *Mus* genus, which diverged 5 to 10 million years ago from other murinae (Sonigo *et al.*, 1987, Coffin *et al.*, 1997). Thus, germ line entry of retroviruses, and thereby pseudogenization of *Scnn1d* happened by infection of a murinae ancestor maximal 10 million years ago. This

genus specificity is substantiated by presence of SCNN1D protein in guinea pig (Sayers *et al.*, 2011), demonstrating that SCNN1D loss is not a unique feature of rodents.

ERVs are known for their persistent activity and impact on host genome evolution (Kazazian, 2004). Analysis of integrated ERVs concerning host transcription signals revealed putative transcription of MuERV-L, IAP-II and MusD by host transcription machinery. However, autonomous replication and transposition of LTR-elements requires functional retroviral proteins for reverse transcription encoded in *env*, *gag*, *pro* and *pol* genes. In accordance with described ERV elements *env* gene is absent in all identified ERVs verifying a strict intracellular life cycle of MuERV-L, IAP-II and MusD (Benit *et al.*, 1999, Ribet *et al.*, 2007). Thus, horizontal transmission from cell to cell is not feasible for MuERV-L, IAP-II and MusD. Moreover, autonomous intracellular transposition is unlikely for MuERV-L, which lacks intact *gag*, *pro* and *pol* genes due to deletions and integration of IAP-II and MusD retrotransposons. In accordance with related IAP-elements (Horie *et al.*, 2007), autonomous transposition is not feasible for IAP-II as well, as *gag*, *pro* and *pol* genes are disrupted by large internal deletions. In contrast, MusD was found to be fully coding competent for *pro* and *pol* genes requisite for reverse transcription. Thus, autonomous intracellular transposition seems likely. However, *ex vivo* assays showed restriction of autonomous mobility to MusD elements possessing intact *gag*, *pro* and *pol* genes as well as identical LTRs (Ribet *et al.*, 2004). Beside a frame shift inserting deletion within *gag* gene of identified MusD, 5' and 3' LTRs are not identical as well. Thus, similarly to *Scnn1d* associated MuERV-L and IAP-II, MusD is most likely not competent for autonomous retrotransposition. However, MusD belongs to most active ERV families, making transcription and possibly functional retroviral gene products likely (Ribet *et al.*, 2007). Thus potential mutagenicity of identified MusD variant has to be further evaluated using transposition and infectivity assays as described by Ribet and co-workers (Ribet *et al.*, 2007). Moreover, MusD *pro* and *pol* protein products are possibly used to mobilize other non-MusD transcripts as described for early transposon elements (Ribet *et al.*, 2004), which is an interesting phenomenon for further research.

In regard to *in silico* analyses active transcription of *Scnn1d* to protein coding mRNA seems unlikely. However, 80 % of mouse SCNN1D homologies locate 3' of integrated ERVs and are virtually free of interspersed repeats (see Fig. 3.9B). Hence, a truncated *Scnn1d* transcript coding for truncated mouse SCNN1D protein appears possible. Independent evidence was shown by detection of partial *Scnn1d* transcripts in BALB/c

and CD1 mice, pointing to existence of *Scnn1d* mRNA in mice (Hernandez-Gonzalez *et al.*, 2006; Nie *et al.*, 2009). Strikingly, we were able to confirm presence of *Scnn1d* transcripts for C57BL/6 mouse strain. Conventional RT-PCR analyses showed presence of *Scnn1d* mRNA in vallate papillae, kidney and testis, implying transcription of *Scnn1d* (see Fig. 3.10). RACE RT-PCR analysis validated the presence of *Scnn1d* transcripts and enabled identification of nine distinct putative transcript variants (see Fig. 3.11). Sequence analysis revealed tissue specific transcription start sites and posttranscriptional processing implying active transcription of *Scnn1d* in C57BL/6 mice. This extends previous studies, which lacked analysis of complete *Scnn1d* transcript and point to a physiological role of *Scnn1d* transcripts. Additional gene specific primers located close to the initially identified 5' ends did not lead to further amplicons, implying that complete *Scnn1d* transcripts were amplified by RACE. Further, alternative polyA signals were identified for transcripts from vallate papillae, kidney and testis. However, no consensus TATA boxes were identified upstream of three tissue specific transcription start sites, pointing to TATA-less promoters. Identified *Scnn1d* transcripts enabled deduction of 4.6 kb *Scnn1d* gene, which includes MuERV-L sequence at the 5' end. Notably, 5'-LTR sequence of MuERV-L is located 30 bp upstream of second *Scnn1d* transcription start site, specific for vallate papillae. Thus, LTR-driven transcription by antisense promotor activity might be responsible for transcription of *Scnn1d* in vallate papillae, as previously observed for LTR elements (Maksakova *et al.*, 2006). LTR-driven transcription of *Scnn1d* in kidney and testis is unlikely as potential LTRs are located far upstream of transcription start sites in kidney and testis.

Transcript-deduced *Scnn1d* gene does not encompasses complete 31 kb *SCNN1D* ortholog region on mouse chromosome 4 found by comparative mapping (see Fig. 3.9 and Fig. 3.12). Notably, latter encompasses complete sequence annotated as *Scnn1d* pseudogene within NCBI database but enlarges the same about 3 times (Sayers *et al.*, 2011). Strikingly, 10 out of 16 *SCNN1D* ortholog sequence homologies are part of experimental identified *Scnn1d* (see Fig. 3.12A). These ten homolog sequences are ortholog to human *SCNN1D* exons 3 to 14, encoding 90 % of human *SCNN1D* protein. However, *Scnn1d* transcripts were not coding competent for one large open reading frame, but for numerous short polypeptides, including peptides with similarity to human *SCNN1D* (see Fig. 3.13A). *In vitro* translation experiments showed that *Scnn1d* transcripts are indeed coding competent for small polypeptides from 2 to 11 kDa, possibly including proteins with similarities to human *SCNN1D* (see Fig. 3.13 and Tab. 3.2). Although correlation of predicted open

reading frames to *in vitro* translated proteins is not absolute conclusive, short mouse SCNN1D polypeptides might be present at least in kidney. *In vitro* translated protein products from *Scnn1d* transcripts are not a target of applied human SCNN1D antiserum purchased from Chemicon (see Fig. 3.14), which was shown to specifically detect human SCNN1D in immunocytochemistry (see Fig. 3.4). With exception of one presumably translated mouse *Scnn1d* ORF, homologies to human SCNN1D are lacking (see Tab. 3.2). Thus, failed detection of *in vitro* translated *Scnn1d* by immunolabeling is highly likely due to lacking epitope homology of the antiserum raised against a 19 amino acids of human SCNN1D. However, human SCNN1D antiserum purchased from Chemicon specifically detects a protein localized to the pore of mouse vallate taste bud cells (see Fig. 3.6). Results of *in vitro* translation experiments and western blot analyses gave evidence that this is not a *Scnn1d* derived protein. This is in contrast to findings of Hernandez-Gonzalez and colleagues, showing immunoreactivity of mouse sperm membranes using the same antiserum (Hernandez-Gonzalez *et al.*, 2006). However, distinct results might be due to experimental setup, as Hernandez-Gonzales used outbred mouse strain CD-1. Possibly CD-1 *Scnn1d* gene was subjected to distinct mutational evolution by retroviruses than C57BL/6 mice, which cannot be resolved due to lacking CD-1 genome data. However, both mouse strains belong to *Mus* genus and originate from a common ancestor, so that a similar mutational evolution by retroviral integration is expected. Thus, anti human SCNN1D antiserum likely recognized a mouse epitope distinct from SCNN1D in C57BL/6 and CD-1.

Ion channel function and modulatory roles are well known for small polypeptides, as for example 72 aa phospholemman peptide (Moorman *et al.*, 1995; Wang *et al.*, 2010). Thus, possible ion channel function of *Scnn1d* transcript derived polypeptides as well as interaction with known SCNN1 subunits was tested by heterologous expression. Electrophysiological analysis showed that *Scnn1d* protein products are not able to assemble into a functional ion channel, neither alone nor by interaction with human SCNN1B and SCNN1G. Thus, *Scnn1d* transcripts and thereby *Scnn1d* gene does likely not code for sodium channel like polypeptide. Moreover, a modulating action with respect to human sodium channel made of SCNN1A, SCNN1B and SCNN1G was not evident. However, experimental setup was optimized for sodium current measurements, which cannot exclude distinct function of *Scnn1d* derived polypeptides.

In summary, *Mus* specific pseudogenization of mouse *Scnn1d* by integration of retroviral sequences extending annotated *Scnn1d* sequences is evident. Moreover, *Scnn1d* pseudogene is actively transcribed in mouse vallate papillae, kidney and testis and codes for numerous polypeptides possibly present *in vivo*. However, neither sodium channel like function, nor modulatory effects on $\alpha\beta\gamma$ -ENaC could be shown for *Scnn1d* derived transcripts or polypeptides. Thus, mouse *Scnn1d* is a transcribed unitary pseudogene not coding competent for functional proteins with SCNN1D-like function. Therefore, a role of *Scnn1d* in salt taste transduction of mice is highly unlikely. Taking into account that SCNN1D derived human δ -ENaC likely plays a role in human sodium taste transduction, *Mus* specific pseudogenization of δ -ENaC in mice substantiates putative species specific differences in salt taste transduction mechanisms. Moreover, these probably distinct transduction mechanisms might account for distinct amiloride sensitivity of mice and human subjects in sensory studies.

5 Summary

Salty taste has evolved to maintain electrolyte homeostasis, serving as a detector for salt containing food. In rodents, salty taste involves at least two transduction mechanisms. One is sensitive to the drug amiloride and specific for Na⁺, involving epithelial sodium channel (ENaC). A second rodent transduction, which is triggered by various cations, is amiloride insensitive and not almost understood to date. Studies in primates showed amiloride-sensitive as well as amiloride-insensitive gustatory responses to NaCl, implying a role of both salt taste transduction pathways in humans. However, sensory studies in humans point to largely amiloride-insensitive sodium taste perception. An involvement of ENaC in human sodium taste perception was not shown, so far. In this study, ENaC subunit protein and mRNA could be localized to human taste bud cells (TBC). Thus, basolateral $\alpha\beta\gamma$ -ENaC ion channels are likely present in TBC of circumvallate papillae, possibly mediating basolateral sodium entry. Similarly, basolateral $\beta\gamma$ -ENaC might play a role in fungiform TBC. Strikingly, δ -ENaC subunit was confined to taste bud pores of both papillae, likely mediating apical or paracellular gustatory sodium entry in TBC. However, regional separation of δ -ENaC and $\beta\gamma$ -ENaC in fungiform and circumvallate TBC indicate the presence of unknown interaction partner necessary to assemble into functional ion channels. However, screening of a macaque taste tissue cDNA library did neither reveal polypeptides assembling into a functional cation channel by interaction with δ -ENaC or $\beta\gamma$ -ENaC nor ENaC independent salt taste receptor candidates. Thus, ENaC subunits are likely involved in human taste transduction, while exact composition and identity of an amiloride (in)sensitive salt taste receptors remain unclear.

Localization of δ -ENaC in human taste pores strongly suggests a role in human taste transduction. In contrast, δ -ENaC is classified as pseudogene in mouse. However, no experimental detected sequences are annotated, while evidences for parts of *Scnn1d* derived mRNAs exist. In order to elucidate if *Scnn1d* is possibly involved in rodent salt taste perception, *Scnn1d* gene was evaluated in this study. Comparative mapping of *SCNN1D* to mouse chromosome 4 revealed complete *Scnn1d* sequence as well as its pseudogenization by *Mus* specific endogenous retroviruses. Moreover, tissue specific transcription of unitary *Scnn1d* pseudogene was found in mouse vallate papillae, kidney and testis and led to identification of nine *Scnn1d* transcripts. *In vitro* translation experiments showed that *Scnn1d* transcripts are coding competent for short polypeptides, possibly present *in vivo*. However, no sodium channel like function or sodium channel modulating activity was evident for *Scnn1d* transcripts and derived polypeptides. Thus, an involvement of mouse δ -ENaC in sodium taste transduction is unlikely and substantiates species specific differences in salt taste transduction mechanisms.

6 Zusammenfassung

Der Salzgeschmack ermöglicht elektrolytreiche Nahrungsquellen zu erkennen und ist eine essentielle Komponente für den Erhalt des Elektrolythaushalts. In Nagern sind bisher zwei Mechanismen bekannt, welche an der Vermittlung des Salzgeschmacks beteiligt sind. Ein Natrium-spezifischer, Amilorid-sensitiver Signaltransduktionsweg wird über den epithelialen Natriumkanal (ENaC) vermittelt. Ein weiterer, bisher ungeklärter Transduktionsweg, ist Amilorid-unempfindlich und wird durch verschiedene Kationen vermittelt. Während Studien in Primaten Amilorid-sensitive als auch -insensitive gustatorische Signaltransduktionswege nachweisen konnten, weisen human-sensorische Studien auf eine Amilorid-Unempfindlichkeit des Natrium-spezifischen Salzgeschmacks hin. Eine Beteiligung des ENaC bei der Vermittlung des menschlichen Salzgeschmacks wurde bislang nicht gezeigt. In dieser Arbeit konnte die mRNA als auch Proteine von ENaC Untereinheiten in menschlichen Geschmacksrezeptorzellen (GRZ) lokalisiert werden. Demzufolge, könnten $\alpha\beta\gamma$ -ENaC Ionenkanäle an einem basolateralen Natriumeinstrom in circumvallaten GRZ beteiligt sein. Die basolaterale Lokalisation von $\beta\gamma$ -ENaC in fungiformen GRZ weist auf eine gleichartige Funktion hin. Die außergewöhnliche Lokalisation der δ -ENaC Untereinheit ausschließlich in der Porenregion von Geschmacksknospen legt eine Beteiligung dieser ENaC Untereinheit bei der Vermittlung geschmacksrelevanter apikaler bzw. transzellulärer Natriumströme nahe. Gleichwohl weist die räumliche Trennung von apikalen δ -ENaC und basolateralen $\beta\gamma$ -ENaC auf die Existenz unbekannter Interaktionspartner hin, da beide getrennt voneinander nicht in der Lage sind effektive Natriumkanäle zu assemblieren. Die Durchmusterung einer geschmacksrelevanten cDNA Bibliothek führte weder zur Identifikation von ENaC Interaktionspartnern, noch von ENaC unabhängigen Polypeptiden, welche in der Lage sind einen Kationenkanal zu bilden. Die genaue Zusammensetzung humaner Amilorid-(in)sensitiver Salzrezeptoren bleibt daher unklar und ein spannendes Feld für weitere Untersuchungen.

Die Poren assoziierte Lokalisation der δ -ENaC Untereinheit impliziert eine wichtige Rolle bei der gustatorischen Signaltransduktion. Erstaunlicherweise ist die orthologe δ -ENaC Untereinheit der Maus als *Scnn1d* Pseudogen klassifiziert. Neben dieser automatischen Annotierung sind keine experimentell ermittelten Sequenzen in Datenbanken hinterlegt obwohl *Scnn1d* abgeleitete mRNA nachgewiesen werden konnte. Im Rahmen dieser Arbeit wurde *Scnn1d* untersucht, um eine mögliche Beteiligung an der murinen Salzgeschmackstransduktion zu klären. Durch Sequenzabgleich mit humanen *SCNN1D* konnte das vollständige *Scnn1d* Gen der Maus identifiziert werden, wobei sich dessen Pseudogenisierung durch *Mus* spezifische endogene Retroviren zeigte. Darüber hinaus wurden neun gewebsspezifische *Scnn1d* Transkripte nachgewiesen, welche für kurze Polypeptide kodieren. Eine mögliche Funktion derselben als Ionenkanal bzw. eine modulatorische Funktion konnte nicht gezeigt werden. Eine Beteiligung des pseudogenisierten δ -ENaC an der Vermittlung des Salzgeschmacks der Maus ist daher unwahrscheinlich und deutet auf Speziesunterschiede bei der Salzgeschmacksvermittlung hin.

7 Appendix

7.1 Abbreviations

A, nA	ampere, nano ampere
APS	ammonium persulfate
BCIP	5-bromo-4-chloro-3-indoyl-phosphate
DAPI	4',6-diamidino-2-phenylindole dihydrochloride
dNTP	deoxyribonucleosidtriphosphate
DTT	dithiothreitol
dH ₂ O	deionized water
EDTA	ethylenediaminetetraacetic acid
EGTA	ethylene glycol-bis(2-aminoethylether)-N,N,N',N'-tetraacetic acid
HEPES	4-(2-hydroxyethyl)piperazine-1-ethanesulfonic acid
I	current
KulORi	Kultur Oocyten Ringer
min	minute
MOPS	3-[N-morpholino]propanesulfonic acid
NBT	(3,3' - (3,3' - dimethoxy - 4,4' - biphenylen) - bis - [2 - (p-nitrophenyl) - 5 - phenyl- 2H-tetrazolium chloride]
NMDG	N-methyl-D-glucamine
nt	nucleotides
NZ amine	casein hydrolysate
PIPES	1,4-Piperazinediethanesulfonic acid, Piperazine-1,4-bis(2-ethanesulfonic acid), Piperazine-N,N'-bis(2-ethanesulfonic acid)
RT	room temperature or reverse transcriptase
SDS	sodium dodecyl sulfate
TAE	tris-acetate-edta
TEMED	N,N,N',N'-tetramethylethylenediamine
TEVC	two electrode voltage clamp
Tris	tris(hydroxymethyl)aminomethane
U	unit
V	volt
v/v	volume/volume
w/v	weight/volume
w/w	weiht/weight

7.2 Plasmids

Tab. 7.1: Plasmids.

lab code	vector	insert	application					
			cloning routine	sequence analysis	ISH	ICC	<i>in vitro</i> transcription/ functional assay	<i>in vitro</i> translation
8	pUC	hENaC gamma, NM 001039			X			
14	pGEMHE5	hENaC alpha, NM 001039					X	
15	pGEMHE5	hENaC beta, NM 000336					X	
16	pGEMHE5	hENaC gamma, NM 001039					X	
23	pGEMHE5	empty	X					
25	p Bluescript KS	hENaC beta, NM 000336, nt 1050 - nt 1554			X			
26	p Bluescript KS	hENaC beta, NM 000336, nt 50 - nt 479			X			
27	p Bluescript KS	hENaC beta, NM 000336, nt 474 - nt 1055			X			
50	pUC	hENaC alpha, NM 001039, nt 1481 - nt 2259			X			
57	pBK-CMV	hENaC beta, NM 000336					X	
58	pBK-CMV	hENaC gamma, NM 001039					X	
59	pBK-CMV	empty	X			X		
60	pBK-CMV	hENaC alpha, NM 001038				X	X	
61	pGEMHE5	hENaC delta, NM 002978			X		X	X
62	pBK-CMV	hENaC delta, NM 002978				X		
71	pBK-CMV	macENaC alpha F1-12a from pool F1-12	X					
74	pBK-CMV	macENaC alpha F1-26b from pool F1-26	X					
135	pBK-CMV	macENaC alpha F1-15b from pool F1-15	X					
137	pBK-CMV	macENaC alpha F1-7b from pool F1-7	X					
138	pBK-CMV	macENaC alpha F1-7a from pool F1-7	X					
140	pBK-CMV	macENaC alpha F1-12b from pool F1-12	X					
161	pGEMHE5	mENaC delta, transcript 7					X	X
162	pGEMHE5	mENaC delta, transcript 8					X	X
163	pGEMHE5	mENaC delta, transcript 6					X	X
164	pGEMHE5	mENaC delta, transcript 5					X	X
165	pGEMHE5	mENaC delta, transcript 3					X	X

ISH, *in situ* hybridization; ICC, immunocytochemistry; hENaC, human ENaC; macENaC, macaque ENaC; mENaC, mouse ENaC

7.3 Primers

Primers for a DNA sequence were picked using “primer3” available online at <http://frodo.wi.mit.edu/primer3/#disclaimer> (Rozen & Skaletsky, 2000). General primer picking conditions were used as default or required for the individual application. Usually consecutive G and C at the 3' end of primer (‘CG-clamp’) was limited to one to prevent primer dimerization. Melting temperature, GC-content, secondary structure and primer dimers were predicted using “DNA calculator” available online from Sigma-Aldrich Life Science (<http://www.sigma-agenosys.com/calc/DNAcalc.asp>).

Tab. 7.2: Primers.

lab code	target	sequence (5' - 3')	application				
			5' modification	ISH	RT-PCR	mouse ENaC delta: RACE	cloning mouse ENaC delta
5	hENaC beta	TGAGCAGGAAGGGAATTGTC			X		
9	hENaC delta	ACCTCCCTCTGCTGTCCAC			X		
21	hENaC gamma	CCCTCCTCGTCTTCTCCTTC			X		
22	hENaC gamma	TTCTCCACCATCTTTGTCTGG			X		
25	hENaC beta	GCAGACGCAGGGAGTCATAG			X		
84	hENaC gamma	CATGGCACCCGGAGAGAAGAT	T7	X			
85	hENaC gamma	GGACTCTGAAAGCCATAC	T3	X			
86	hENaC gamma	GTCTGGAACCTCCGTCTCAG	T7	X			
87	hENaC gamma	AGTGGAGGACACGAGGAATG	T3	X			
88	hENaC gamma	CTCTACCTCCTGCAGCCAAC	T7	X			
89	hENaC gamma	AGAAGAAGTCAATGAAGAAGAC	T3	X			
186	hENaC delta	AGTFACGATGGCCTGGACTG	T7	X			
187	hENaC delta	GAGGCGGTAGAAGCAGTGTGTC	T3	X			
188	hENaC delta	AGCTGCTCACCTTCTTCTGC	T7	X			
189	hENaC delta	CGTGTAGCCTCGGTAAGGC	T3	X			
190	hENaC delta	TGCATTCAAGCTCTCCACTG	T7	X			
191	hENaC delta	CAGCTCTTTCGGCTGAGAC	T3	X			
201	macENaC delta	GAGCGGTAGTTGAGCTCCTG			X		
220	hENaC alpha	ATGGAGGGGAACAAGCTGGA			X		
222	hENaC beta	ATGCACGTGAAGAAGTACCTG			X		
224	macENaC alpha	CAAGGAACCTCTCCTCTCAGG			X		
225	macENaC gamma	GAGTCCCGTCCACAGTCC			X		
226	macENaC gamma	TCTGTGCGAGTTGGCTTGTT			X		
229	macENaC delta	ACAGGCTCCATCCTGCTTC			X		
230	macENaC delta	GACCAGGCCGAGAGATCA			X		
300	mENaC delta	CCAGACCTCATTTGCCAACATCTG				X	
301	mENaC delta	GCCTGGGAAAACATCAATGCTCTC				X	
302	mENaC delta	ACTCAGATGCTGCAGATGAATCCC				X	
303	mENaC delta	AGCCCACTTCGTAAGTACTGTCCA				X	
331	mENaC delta	AGATGGAGATGTGGGCTGAC				X	
333	mENaC delta	TTTGTTCCTCACTGGCTGTGTG				X	
334	mENaC delta	TCCTTGGAGGACCTGTTTCAGAGT				X	
384	mENaC delta	ACTCTGAAACAGGTCTCCAAGGA					X
385	mENaC delta	GCTGGAATCAAGTCATGTTTCGT					X
386	mENaC delta	ACGAACCATGACCTTGATTCCAGC					X
387	mENaC delta	GGTGGGGAGGTGCTGCTC					X
388	mENaC delta	GAGATGGTTCCCGCACCACA					X
389	mENaC delta	GGGACACTGACGCCACATAGT					X
390	mENaC delta	GTGTAGAAGTACCCCTTCACACATGA					X
391	mENaC delta	GAATCTGAAGATTCAAAATTCAGCTTC					X

SH, *in situ* hybridization; hENaC, human ENaC; macENaC, macaque ENaC; mENaC, mouse ENaC

7.4 Riboprobes for *in situ* hybridization

Tab. 7.3: Digoxigenin labeled riboprobes as (antisense), s (sense)

gene of interest (human ref. sequence)	template for ivT with lab code no.	length of probe in bp	probe sequence	final conc. for ISH (ng/ml)
ENaC alpha (NM_001038; 3345 bp)	<i>Hind</i> III (as) or <i>Nde</i> I (s) linearized vector no. 50	779	nt 1481 - nt 2259	75
ENaC beta (NM_000336; 2597 bp)	linearized vectors	430; 505; 582; 580		∑ 200
	no. 26 with <i>Spe</i> I (as) or <i>Bam</i> HI (s)	430	nt 50 - nt 479	50
	no. 27 with <i>Xba</i> I (as) / <i>Hind</i> III (s)	582	nt 474 - nt 1055	50
	no. 25 with <i>Hind</i> III (as) or <i>Bst</i> X (s)	505	nt 1050 - nt 1554	50
	with <i>Bst</i> XI (as) or <i>Eco</i> RI (s)	580	nt 1549 - nt 2129	50
ENaC gamma (NM_001039; 3516 bp)	PCR products from plasmid no. 8	552; 402; 412		∑ 500
	primer 86/87	402	nt 139 - nt 541	167
	primer 84/85	552	nt 562 - 1114	167
	primer 88/89	412	nt 1402 - nt 1814	167
ENaC delta (NM_002978; 2503 bp)	PCR products from plasmid no. 61	519; 497; 507		∑ 800
	primer 186/187	519	nt 957 - nt 1475	267
	primer 188/189	497	nt 340 - nt 836	267
	primer 190/191	507	nt 1541 - nt 2047	267

for primer details see Tab. 7.2

Tab. 7.4: Human α -, β -, γ - and δ -ENaC transcript splice variants.

ENaC	accession number	length (bp)	ORF (aa)	detectable via ISH
α	NM_001038 [#]	3345	669	+
	ENST00000338748 ^{##}	3284	245	±
	ENST00000358945 ^{##}	3541	691	+
	ENST00000360168 ^{##}	3475	728	+
	ENST00000396966 ^{##}	3475	669	+
β	NM_000336 [#]	2597	640	+
	ENST00000307331 ^{##}	2556	685	+
γ	NM_001039 [#]	3516	649	+
	NM_002978 [#]	2503	638	+
	NM_001130413 [#]	2693	704	+
δ	ENST00000338555 ^{##}	3475	638	+
	ENST00000379101 ^{##}	2268	-	+
	ENST00000325425 ^{##}	2679	704	+
	ENST00000379099 ^{##}	923	308	+
	ENST00000470022 ^{##}	645	139	-
	ENST00000467651 ^{##}	208	-	-
	ENST00000379110 ^{##}	2007	668	+
	ENST00000379116 ^{##}	1163	302	+
	ENST00000400928 ^{##}	2590	638	+

[#]Wheeler *et al.*, 2008; ^{##}Hubbard *et al.*, 2009; aa, amino acids; bp, base pairs; ORF, open reading frame; ISH, *in situ* hybridization

7.5 *Macaca mulatta* cDNA library pools

Tab. 7.5: Pool titer and concentration of derived cRNA

Pool	final Titer used for <i>in vivo</i> excision	cRNA ng/ μ l
F1-1	57750	752
F1-2	50050	732
F1-3	23980	681
F1-4	50003	791
F1-5	49820	802
F1-6	50161	760
F1-7	45500	1054
F1-8	50005	1018
F1-9	50126	1073
F1-10	49951	1043
F1-11	29703	1125
F1-12	25697	1220
F1-13	46925	1294
F1-14	40221	1261
F1-15	37100	1141
F1-16	49878	1136
F1-17	19935	1115
F1-18	28800	1139
F1-19	21000	1003
F1-20	49000	1088
F1-21	29000	1140
F1-22	53410	1118
F1-23	57225	1047
F1-24	87200	1136
F1-25	51150	870
F1-26	50403	1300

7.6 Antisera, blocking peptides and avidin reagents

Tab. 7.6: Antisera, blocking peptides and avidin reagents.

lab-no.	type	dilution (detection method)	epitope/specificity	origin	conjugate	supplier (catalog no)
1	ab	1:1000	mouse	goat (polyclonal)	Alexa Fluor 488	Molecular Probes (A-11029)
2	ab	1:400	mouse	horse (polyclonal)	biotin	Vector Laboratories (BA-2001)
3	ab	1:1000	rabbit	goat (polyclonal)	Alexa Fluor 488	Molecular Probes (A-11034)
4	ab	1:400	rabbit	goat (polyclonal)	biotin	Vector Laboratories (BA-1000)
8	av	1:200	specific for biotin	-	fluorescein	Vector Laboratories (A-2001)
17	ab	1:5000	digoxigenin	sheep (polyclonal)	alkaline phosphatase	Roche (1093274)
24	ab	1:400	goat	rabbit (polyclonal)	biotin	Vector Laboratories (BA-5000)
67	ab	1:1000	goat	donkey (polyclonal)	Alexa Fluor 488	Molecular Probes (A-11055)
68	av	1:1000	specific for biotin	-	Alexa Fluor 633	Molecular Probes (S21375)
83	ab	1:1000	digoxigenin	sheep (polyclonal)	HRP	Roche (11207733910)
107	ab	1:200	rat β -epithelial sodium channel (epitope 81 % conserved in human)	rabbit (polyclonal)	-	Millipore (AB3532P)
108	ab	1:200	rat γ -epithelial sodium channel (epitope 93 % conserved in human)	rabbit (polyclonal)	-	Millipore (AB3534P)
109	ab	1:100 (DAB) 1:1000 (TSA) 1:100 (ICC)	human δ -ENaC; aa 171-189 (NP_002969.2)	rabbit (polyclonal)	-	Millipore (AB3536P)
112	p	1:2000	Concanavalin A	<i>Canavalia ensiformis</i>	biotin	Sigma (C2272)
116	ab	1:250 (IHC) 1:50 (ICC)	human α -ENaC aa 627-643 (NP_001029)	rabbit (polyclonal)	-	Calbiochem (324906)
125	cp	1:100	specific for ab no. 107	-	-	Chemicon (AG380)
126	cp	1:100	specific for ab no. 108	-	-	Chemicon (AG340)
128	cp	1:100	specific for ab no. 116	-	-	Peptides & Elephants (EP11028)
143	cp	1:100	specific for ab no. 109	-	-	Chemicon (AG981)
269	ab	1:100	recomb. human δ -ENaC aa 217-530 (NP_002969)	mouse (monoclonal)	-	Abnova (H0006339-M02)
270	ab	1:300 (ICC) 1:1000 (IHC)	human δ -ENaC, epitope extracellular and \neq epitope ab109	rabbit (polyclonal)	-	Abcam (ab65708)
271	ab	1:100	human δ -ENaC NP_002969 aa 150-200 and \neq epitope ab no. 109	goat (polyclonal)	-	Santa Cruz (sc-22246)
272	cp	1:20	specific for ab no. 271	-	-	Santa Cruz (sc-22246P)
279	cp	1:100	specific for ab no. 270	-	-	Abcam (ab83047)
280	cp (p)	1:10 (IHC) 1:50 (ICC)	specific for ab no. 269	-	-	Abnova (H0006339-Q01)
326	ab	1:10000 (WB)	rabbit	goat (polyclonal)	HRP	Dianova (111-035-003)

ab, antibody; av, avidin; cp, control peptide; p, protein; IHC, immunohistochemistry; ICC, immunocytochemistry; WB, western blot, HRP, horse radish peroxidase

7.7 Multiple sequence alignment

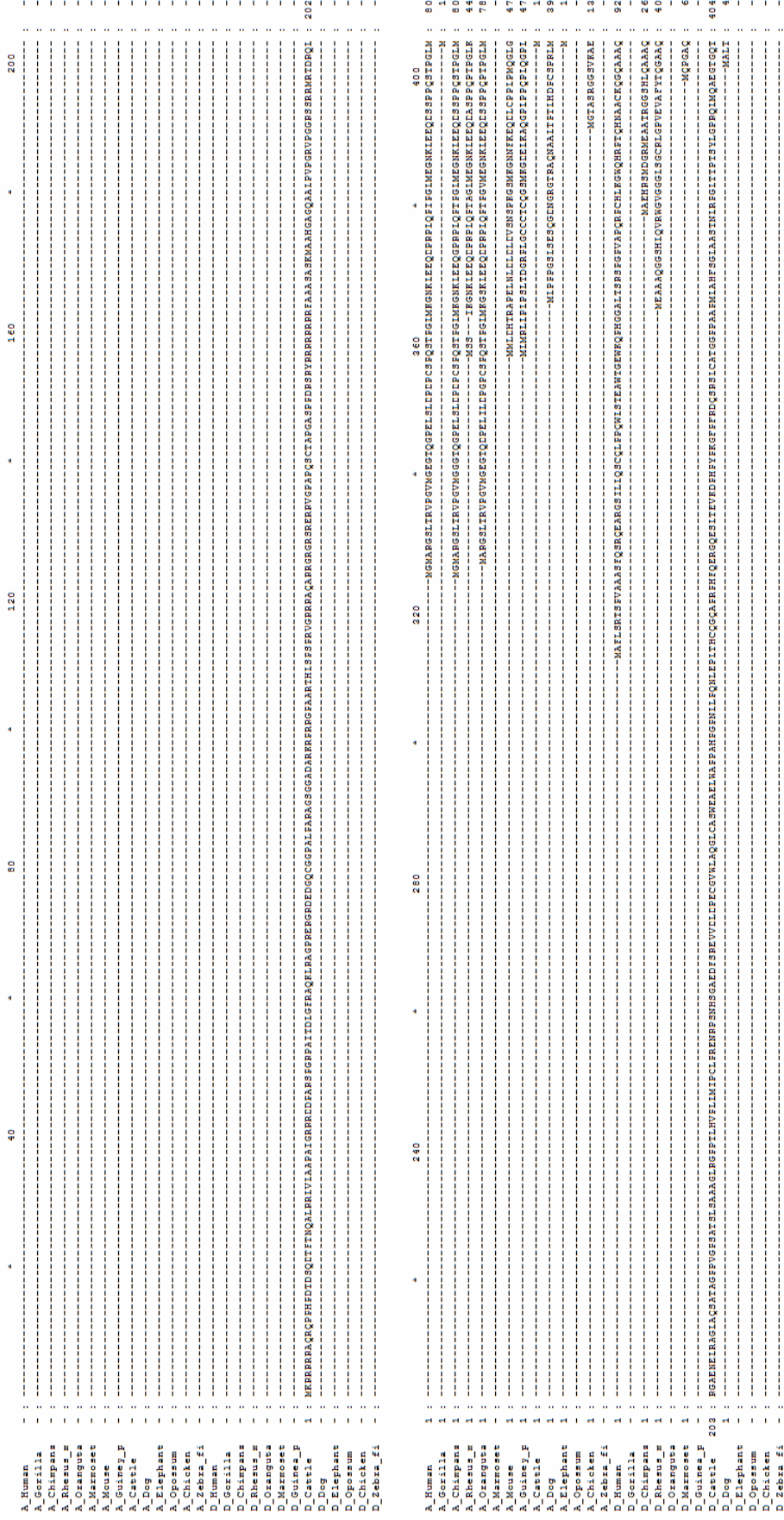


Fig. 7.1: Multiple sequence alignment of vertebrate SCNN1D and SCNN1A protein sequences. Multiple sequence alignment of longest annotated SCNN1D (D) and SCNN1A (A) proteins was carried out using ClustalW and Mega 4.0. Alignment corresponding to aa 202 to 631 of human SCNN1D reference sequence was used to calculate phylogenetic tree (see Fig. 3.7). Degree of conservation is shown in shades. Black corresponds to 100 % conservation, dark grey with white characters to 80 % conservation, grey with black letters to 60 % and black letters on white background to less conservation. For accession numbers see next pages.

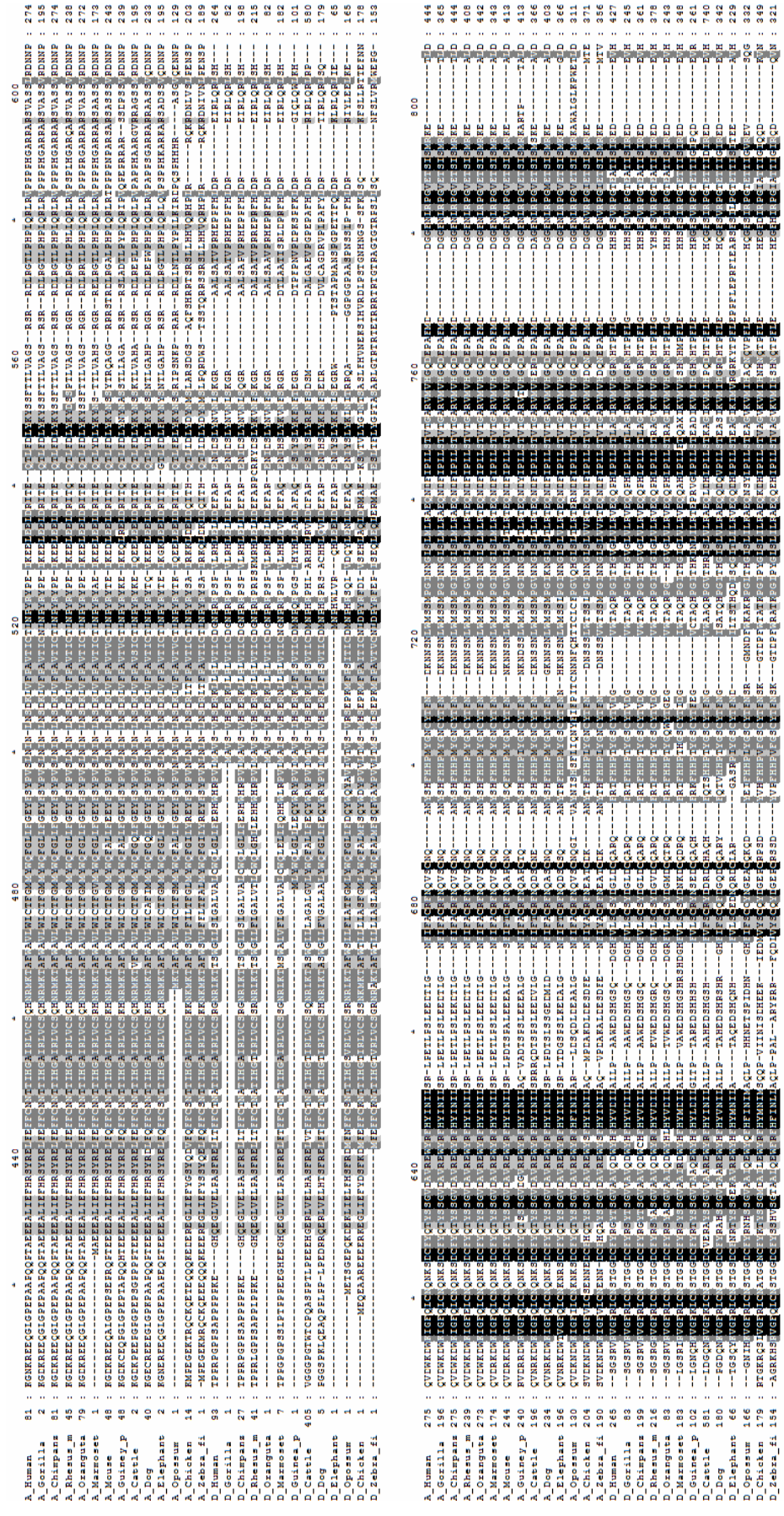


Fig. 7.1 (continued): Multiple sequence alignment of vertebrate SCNN1A and SCNN1A protein sequences. Accession numbers SCNN1D: Human (NP_002969.2), Chimpanzee (NP_001009072.1), Western gorilla (ENSGGOP00000005234), Bornean orangutan (ENSPYP00000002332), Rhesus monkey (ENSMUMUP00000040692), Marmoset (ENSCJAP00000002082), Guinea pig (ENSCPOP00000010513), Dog (XP_546718.2), Cattle (XP_607245.3), African elephant (ENSLAFP00000017298), Opossum (XP_001376284.1), Zebra finch (ENSTGUP00000004254), Chicken (XP_425742). For accession numbers of SCNN1A proteins see next page.

```

840
A.Human 445: HGGDENGSLG...
A.Gorilla 366: HGGDENGSLG...
A.Chimpanzee 445: HGGDENGSLG...
A.Rhesus_m 409: HGGDENGSLG...
A.Oranguta 443: HGGDENGSLG...
A.Marmoset 344: HGGDENGSLG...
A.Mouse 414: HGGDENGSLG...
A.Guinea_P 414: HGGDENGSLG...
A.Cattle 967: HGGDENGSLG...
A.Dog 404: HGGDENGSLG...
A.Opossum 327: HGGDENGSLG...
A.Elephant 312: HGGDENGSLG...
A.Chicken 372: HGGDENGSLG...
A.Zebra_f1 357: HGGDENGSLG...
D.Human 428: SPKAGGEG...
D.Gorilla 246: SPKAGGEG...
D.Chimpanzee 362: SPKAGGEG...
D.Rhesus_m 379: SPKAGGEG...
D.Oranguta 344: SPKAGGEG...
D.Marmoset 345: SPKAGGEG...
D.Cattle 741: SPKAGGEG...
D.Dog 343: SPKAGGEG...
D.Elephant 330: SPKAGGEG...
D.Chicken 350: SPKAGGEG...
D.Zebra_f1 322: SPKAGGEG...

1040
A.Human 567: PNNVYNNRN...
A.Gorilla 488: PNNVYNNRN...
A.Chimpanzee 571: PNNVYNNRN...
A.Rhesus_m 531: PNNVYNNRN...
A.Oranguta 438: PNNVYNNRN...
A.Marmoset 468: PNNVYNNRN...
A.Mouse 536: PNNVYNNRN...
A.Guinea_P 536: PNNVYNNRN...
A.Dog 489: PNNVYNNRN...
A.Elephant 489: PNNVYNNRN...
A.Opossum 494: PNNVYNNRN...
A.Chicken 494: PNNVYNNRN...
A.Zebra_f1 479: PNNVYNNRN...
D.Human 550: PNNVYNNRN...
D.Gorilla 548: PNNVYNNRN...
D.Chimpanzee 584: PNNVYNNRN...
D.Oranguta 566: PNNVYNNRN...
D.Marmoset 571: PNNVYNNRN...
D.Cattle 562: PNNVYNNRN...
D.Dog 464: PNNVYNNRN...
D.Elephant 522: PNNVYNNRN...
D.Chicken 476: PNNVYNNRN...
D.Zebra_f1 443: PNNVYNNRN...

1080
A.Human 1100: VVHKKESREG...
A.Gorilla 1000: VVHKKESREG...
A.Chimpanzee 1100: VVHKKESREG...
A.Rhesus_m 1000: VVHKKESREG...
A.Oranguta 1000: VVHKKESREG...
A.Marmoset 1000: VVHKKESREG...
A.Mouse 1000: VVHKKESREG...
A.Guinea_P 1000: VVHKKESREG...
A.Cattle 1000: VVHKKESREG...
A.Dog 1000: VVHKKESREG...
A.Opossum 1000: VVHKKESREG...
A.Elephant 1000: VVHKKESREG...
A.Chicken 1000: VVHKKESREG...
A.Zebra_f1 1000: VVHKKESREG...

1120
A.Human 1120: LLRRFRVRS...
A.Gorilla 1120: LLRRFRVRS...
A.Chimpanzee 1120: LLRRFRVRS...
A.Rhesus_m 1120: LLRRFRVRS...
A.Oranguta 1120: LLRRFRVRS...
A.Marmoset 1120: LLRRFRVRS...
A.Mouse 1120: LLRRFRVRS...
A.Guinea_P 1120: LLRRFRVRS...
A.Cattle 1120: LLRRFRVRS...
A.Dog 1120: LLRRFRVRS...
A.Elephant 1120: LLRRFRVRS...
A.Opossum 1120: LLRRFRVRS...
A.Chicken 1120: LLRRFRVRS...
A.Zebra_f1 1120: LLRRFRVRS...

1160
A.Human 1160: LLRRFRVRS...
A.Gorilla 1160: LLRRFRVRS...
A.Chimpanzee 1160: LLRRFRVRS...
A.Rhesus_m 1160: LLRRFRVRS...
A.Oranguta 1160: LLRRFRVRS...
A.Marmoset 1160: LLRRFRVRS...
A.Mouse 1160: LLRRFRVRS...
A.Guinea_P 1160: LLRRFRVRS...
A.Cattle 1160: LLRRFRVRS...
A.Dog 1160: LLRRFRVRS...
A.Elephant 1160: LLRRFRVRS...
A.Opossum 1160: LLRRFRVRS...
A.Chicken 1160: LLRRFRVRS...
A.Zebra_f1 1160: LLRRFRVRS...

1200
A.Human 1200: LLRRFRVRS...
A.Gorilla 1200: LLRRFRVRS...
A.Chimpanzee 1200: LLRRFRVRS...
A.Rhesus_m 1200: LLRRFRVRS...
A.Oranguta 1200: LLRRFRVRS...
A.Marmoset 1200: LLRRFRVRS...
A.Mouse 1200: LLRRFRVRS...
A.Guinea_P 1200: LLRRFRVRS...
A.Cattle 1200: LLRRFRVRS...
A.Dog 1200: LLRRFRVRS...
A.Elephant 1200: LLRRFRVRS...
A.Opossum 1200: LLRRFRVRS...
A.Chicken 1200: LLRRFRVRS...
A.Zebra_f1 1200: LLRRFRVRS...

566
567
568
569
570
571
572
573
574
575
576
577
578
579
580
581
582
583
584
585
586
587
588
589
590
591
592
593
594
595
596
597
598
599
600
601
602
603
604
605
606
607
608
609
610
611
612
613
614
615
616
617
618
619
620
621
622
623
624
625
626
627
628
629
630
631
632
633
634
635
636
637
638
639
640
641
642
643
644
645
646
647
648
649
650
651
652
653
654
655
656
657
658
659
660
661
662
663
664
665
666
667
668
669
670
671
672
673
674
675
676
677
678
679
680
681
682
683
684
685
686
687
688
689
690
691
692
693
694
695
696
697
698
699
700
701
702
703
704
705
706
707
708
709
710
711
712
713
714
715
716
717
718
719
720
721
722
723
724
725
726
727
728
729
730
731
732
733
734
735
736
737
738
739
740
741
742
743
744
745
746
747
748
749
750
751
752
753
754
755
756
757
758
759
760
761
762
763
764
765
766
767
768
769
770
771
772
773
774
775
776
777
778
779
780
781
782
783
784
785
786
787
788
789
790
791
792
793
794
795
796
797
798
799
800

```

Fig. 7.1 (continued): Multiple sequence alignment of vertebrate SCNNID and SCNNIA protein sequences. Accession numbers SCNNIA: Human (NP_001153048.1), Chimpanzee (XP_508948.2), Western gorilla (ENSGGOP00000010565), Bornean orangutan (ENSPYP00000004767), Rhesus monkey (XP_001103017.2), Marmoset (ENSCJAP00000001207), Guinea pig (ENSCPOP000000016986), Dog (XP_534912.2), Cattle (NP_777023.1), African elephant (ENSLAFP00000000612), Opossum (ENSMODP000000035866), Zebra finch (ENSTIGUP00000013734), Chicken (NP_990476.2), House mouse (NP_035454.2).

7.8 Companies and Kit specifications

Ambion/Applied Biosystems (Austin, TX, USA)	Perkin Elmer (Waltham, MA, USA)
MicroPoly(A)Purist™ Kit (AM1919)	TSA™ BIOTIN SYSTEM (NEL700)
mMESSAGE mMACHINE® (AM1344, AM1348)	Promega (Madison, WI, USA)
Poly(A) tailing Kit® (AM1350)	TNT T7 Quick Coupled
MEGAclear™ Kit (AM1908)	Transcription/Translation System (L1171)
FirstChoice® RML-RACE (AM1700)	Qiagen (Hilden, GER)
Amersham Pharmacia Biotech, now GE Healthcare	QIAquick gel extraction Kit (28704)
Biochrom (Cambridge, UK)	Roche (Mannheim, GER)
Bioline (Luckenwalde, GER)	High Pure PCR Product Purification (11 732 676 001)
Bio-Rad (Hercules, CA, USA)	Roth GmbH & Co. KG (Karlsruhe, GER)
Bio-Rad Protein Assay	Schleicher & Schuell; now: Whatman
Biometra (Göttingen, GER)	Serva Electrophoresis GmbH (Heidelberg, GER)
Chemicon, now Millipore	Sigma-Aldrich Chemie GmbH (Munich, GER)
Dako	Solis BioDyne (Tartu, EST)
Diagnostic Instruments (Sterling Heights, MI)	Stratagene (La Jolla, CA, USA)
Epicentre Biotechnologies (Madison, WI, USA)	ZAP Express®cDNA Synthesis Kit (200403)
Fast-Link™ DNA Ligation Kit (LK11025)	ZAP Express® Gigapack®III Gold Cloning Kit (200451)
Eppendorf (Hamburg, GER)	Sutter Instrument (Novato, CA, USA)
Eurofins MWG Operon (Ebersberg, GER)	Syngene (Cambridge, UK)
Fujifilm (Tokyo, JPN)	Takara Bio Europe/Clontech (Saint-Germain-en-Laye, FRA)
Fermentas (St. Leon-Rot, A)	Advantage®2 PCR Kit (PT3281-2)
GE Healthcare (Buckinghamshire, UK)	SMART RACE cDNA Amplification Kit (634914)
ECL Western blotting detection reagents and analysis system (RPN2109)	Vector Laboratories (Burlingame, CA, USA)
GENOMED (Löhne, GER)	Vectastain® ABC Kit (PK-4000)
JETquick Plasmid Miniprep Spin Kit (400250)	Whatman, now part of GE Healthcare
Invitrogen (Carlsbad, CA, USA)	VWR International (Darmstadt, GER)
TOPO TA cloning® Kit (K4500-01)	WPI: World Precision Instruments (Sarasota, FL, USA)
Leica Microsystems (Nussloch, Wetzlar, GER)	Zeiss (Oberkochen, GER)
Macherey-Nagel (Düren, GER)	
NucleoBond (PC 100, PC 500)	
Merck KGaA (Darmstadt, GER)	
Microm (Heidelberg, GER)	
Millipore (Billerica, MA, USA)	
Molecular Devices (Sunnyvale, CA, USA)	
Molecular Probes; now Invitrogen	
National Diagnostics (Atlanta, GA, USA)	
Olympus (Hamburg, GER)	
Peptides&elephants (Potsdam, GER)	
Peqlab LLC (Wilmington, DE, USA)	

8 Literature

- Adkins, R. M., Gelke, E. L., Rowe, D., and Honeycutt, R. L. (2001), 'Molecular phylogeny and divergence time estimates for major rodent groups: evidence from multiple genes', *Mol Biol Evol*, 18 (5), 777-91.
- Ahn, Y. J., Brooker, D. R., Kosari, F., Harte, B. J., Li, J., Mackler, S. A., and Kleyman, T. R. (1999), 'Cloning and functional expression of the mouse epithelial sodium channel', *Am J Physiol*, 277 (1 Pt 2), F121-9.
- Arey, L., Tremaine, M., and Monzingo, F. (1935), 'The numerical and topographical relation of taste buds to human circumvallate papillae throughout the life span.' *Anat Rec*, 64, 9-25.
- Avenet, P. (1992), 'Role of amiloride-sensitive sodium channels in taste', *Soc Gen Physiol Ser*, 47, 271-9.
- Avenet, P. & Lindemann, B. (1988), 'Amiloride-blockable sodium currents in isolated taste receptor cells', *J Membr Biol*, 105 (3), 245-55.
- Azzali, G., Gennari, P. U., Maffei, G., and Ferri, T. (1996), 'Vallate, foliate and fungiform human papillae gustatory cells. An immunocytochemical and ultrastructural study', *Minerva Stomatol*, 45 (9), 363-79.
- Baer, J. E., Jones, C. B., Spitzer, S. A., and Russo, H. F. (1967), 'The potassium-sparing and natriuretic activity of N-amidino-3,5-diamino-6-chloropyrazinecarboxamide hydrochloride dihydrate (amiloride hydrochloride)', *J Pharmacol Exp Ther*, 157 (2), 472-85.
- Baillie, G. J., van de Lagemaat, L. N., Baust, C., and Mager, D. L. (2004), 'Multiple groups of endogenous betaretroviruses in mice, rats, and other mammals', *J Virol*, 78 (11), 5784-98.
- Bangel-Ruland, N., Sobczak, K., Christmann, T., Kentrup, D., Langhorst, H., Kusche-Vihrog, K., and Weber, W. M. (2010), 'Characterization of the epithelial sodium channel delta-subunit in human nasal epithelium', *Am J Respir Cell Mol Biol*, 42 (4), 498-505.
- Bartel, D. L., Sullivan, S. L., Lavoie, E. G., Sevigny, J., and Finger, T. E. (2006), 'Nucleoside triphosphate diphosphohydrolase-2 is the ecto-ATPase of type I cells in taste buds', *J Comp Neurol*, 497 (1), 1-12.
- Baum, B. J. (1993), 'Principles of saliva secretion', *Ann N Y Acad Sci*, 694, 17-23.
- Behrens, M. & Meyerhof, W. (2010), 'Oral and extraoral bitter taste receptors', *Results Probl Cell Differ*, 52, 87-99.
- Behrens, M., Meyerhof, W., Hellfritsch, C., and Hofmann, T. (2011), 'Sweet and umami taste: natural products, their chemosensory targets, and beyond', *Angew Chem Int Ed Engl*, 50 (10), 2220-42.
- Behrens, M., Foerster, S., Staehler, F., Raguse, J. D., and Meyerhof, W. (2007), 'Gustatory expression pattern of the human TAS2R bitter receptor gene family reveals a heterogenous population of bitter responsive taste receptor cells', *J Neurosci*, 27 (46), 12630-40.
- Beidler, L. M. & Smallman, R. L. (1965), 'Renewal of cells within taste buds', *J Cell Biol*, 27 (2), 263-72.
- Benit, L., Lallemand, J. B., Casella, J. F., Philippe, H., and Heidmann, T. (1999), 'ERV-L elements: a family of endogenous retrovirus-like elements active throughout the evolution of mammals', *J Virol*, 73 (4), 3301-8.
- Benit, L., De Parseval, N., Casella, J. F., Callebaut, I., Cordonnier, A., and Heidmann, T. (1997), 'Cloning of a new murine endogenous retrovirus, MuERV-L, with strong similarity to the human HERV-L element and with a gag coding sequence closely related to the Fv1 restriction gene', *J Virol*, 71 (7), 5652-7.
- Benos, D. J. & Stanton, A. (1999), 'Functional domains within the degenerin/epithelial sodium channel (Deg/ENaC) superfamily of ion channels', *J Physiol*, 520 (3), 631-44.
- Bernstein, I. L. & Hennessy, C. J. (1987), 'Amiloride-sensitive sodium channels and expression of sodium appetite in rats', *Am J Physiol*, 253 (2 Pt 2), R371-4.

- Bezencon, C., le Coutre, J., and Damak, S. (2007)**, 'Taste-signaling proteins are coexpressed in solitary intestinal epithelial cells', *Chem Senses*, 32 (1), 41-9.
- Brand, J. G., Teeter, J. H., and Silver, W. L. (1985)**, 'Inhibition by amiloride of chorda tympani responses evoked by monovalent salts', *Brain Res*, 334 (2), 207-14.
- Breslin, P. A. & Beauchamp, G. K. (1997)**, 'Salt enhances flavour by suppressing bitterness', *Nature*, 387 (6633), 563.
- Brown, I. J., Tzoulaki, I., Candeias, V., and Elliott, P. (2009)**, 'Salt intakes around the world: implications for public health', *Int J Epidemiol*, 38 (3), 791-813.
- Burt, D. W., Reith, A. D., and Brammar, W. J. (1984)**, 'A retroviral provirus closely associated with the Ren-2 gene of DBA/2 mice', *Nucleic Acids Res*, 12 (22), 8579-93.
- Canessa, C. M., Horisberger, J. D., and Rossier, B. C. (1993)**, 'Epithelial sodium channel related to proteins involved in neurodegeneration', *Nature*, 361 (6411), 467-70.
- Canessa, C. M., Schild, L., Buell, G., Thorens, B., Gautschi, I., Horisberger, J. D., and Rossier, B. C. (1994)**, 'Amiloride-sensitive epithelial Na⁺ channel is made of three homologous subunits', *Nature*, 367 (6462), 463-7.
- Cardello, A. V. (1978)**, 'Chemical stimulation of single human fungiform taste papillae: sensitivity profiles and locus of stimulation', *Sens Processes*, 2 (3), 173-90.
- Chandrashekar, J., Hoon, M. A., Ryba, N. J. P., and Zuker, C. S. (2006)**, 'The receptors and cells for mammalian taste', *Nature*, 444, 288-94.
- Chandrashekar, J., Kuhn, C., Oka, Y., Yarmolinsky, D. A., Hummler, E., Ryba, N. J., and Zuker, C. S. (2010)**, 'The cells and peripheral representation of sodium taste in mice', *Nature*.
- Chandrashekar, J., Mueller, K. L., Hoon, M. A., Adler, E., Feng, L., Guo, W., Zuker, C. S., and Ryba, N. J. (2000)**, 'T2Rs function as bitter taste receptors', *Cell*, 100 (6), 703-11.
- Chang, S. S., Grunder, S., Hanukoglu, A., Rosler, A., Mathew, P. M., Hanukoglu, I., Schild, L., Lu, Y., Shimkets, R. A., Nelson-Williams, C., Rossier, B. C., and Lifton, R. P. (1996)**, 'Mutations in subunits of the epithelial sodium channel cause salt wasting with hyperkalaemic acidosis, pseudohypoaldosteronism type 1', *Nat Genet*, 12 (3), 248-53.
- Chaudhari, N. & Roper, S. D. (2010)**, 'Review series: The cell biology of taste', *J Cell Biol*, 190 (3), 285-96.
- Christy, R. J., Brown, A. R., Gourlie, B. B., and Huang, R. C. (1985)**, 'Nucleotide sequences of murine intracisternal A-particle gene LTRs have extensive variability within the R region', *Nucleic Acids Res*, 13 (1), 289-302.
- Clapp, T. R., Stone, L. M., Margolskee, R. E., and Kinnamon, S. C. (2001)**, 'Immunocytochemical evidence for co-expression of type III IP3 receptor with signaling components of bitter taste transduction', *BMC Neurosc*, 2:6 (1471-2202/2/6).
- Coffin, J. M., Hughes, S. H., and Varmus, H. E. (eds.) (1997)**, *Retroviruses* (New York: Cold Spring Harbor Laboratory Press).
- Daniels, D. & Fluharty, S. J. (2004)**, 'Salt appetite: a neurohormonal viewpoint', *Physiol Behav*, 81 (2), 319-37.
- DeFazio, R. A., Dvoryanchikov, G., Maruyama, Y., Kim, J. W., Pereira, E., Roper, S. D., and Chaudhari, N. (2006)**, 'Separate populations of receptor cells and presynaptic cells in mouse taste buds', *J Neurosci*, 26 (15), 3971-80.
- DeSimone, J. A. & Lyall, V. (2006)**, 'Taste receptors in the gastrointestinal tract III. Salty and sour taste: sensing of sodium and protons by the tongue', *Am J Physiol Gastrointest Liver Physiol*, 291 (6), G1005-10.
- DeSimone, J. A., Heck, G. L., and DeSimone, S. K. (1981)**, 'Active ion transport in dog tongue: a possible role in taste', *Science*, 214 (4524), 1039-41.
- DeSimone, J. A., Heck, G. L., Mierson, S., and Desimone, S. K. (1984)**, 'The active ion transport properties of canine lingual epithelia in vitro. Implications for gustatory transduction', *J Gen Physiol*, 83 (5), 633-56.

- DeSimone, J. A., Lyall, V., Heck, G. L., Phan, T. H., Alam, R. I., Feldman, G. M., and Buch, R. M. (2001), 'A novel pharmacological probe links the amiloride-insensitive NaCl, KCl, and NH₄Cl chorda tympani taste responses', *J Neurophysiol*, 86 (5), 2638-41.
- Diamond, J. M. (1965), 'The mechanism of isotonic water absorption and secretion', *Symp Soc Exp Biol*, 19, 329-47.
- Diamond, J. M. (1966), 'Non-linear osmosis', *J Physiol*, 183 (1), 58-82.
- Doolin, R. E. & Gilbertson, T.A. (1996), 'Distribution and characterization of functional amiloride-sensitive sodium channels in rat tongue', *J Gen Physiol*, 107, 545-54.
- Dvoryanchikov, G., Tomchik, S. M., and Chaudhari, N. (2007), 'Biogenic amine synthesis and uptake in rodent taste buds', *J Comp Neurol*, 505 (3), 302-13.
- Dvoryanchikov, G., Sinclair, M. S., Perea-Martinez, I., Wang, T., and Chaudhari, N. (2009), 'Inward rectifier channel, ROMK, is localized to the apical tips of glial-like cells in mouse taste buds', *J Comp Neurol*, 517 (1), 1-14.
- Dvoryanchikov, G., Huang, Y. A., Barro-Soria, R., Chaudhari, N., and Roper, S. D. (2011), 'GABA, Its Receptors, and GABAergic Inhibition in Mouse Taste Buds', *J Neurosci*, 31 (15), 5782-91.
- Elliott, E. J. & Simon, S. A. (1990), 'The anion in salt taste: a possible role for paracellular pathways', *Brain Res*, 535 (1), 9-17.
- Farbman, A. I. (1980), 'Renewal of taste bud cells in rat circumvallate papillae', *Cell Tissue Kinet*, 13 (4), 349-57.
- Farbman, A. I., Hellekant, G., and Nelson, A. (1985), 'Structure of taste buds in foliate papillae of the rhesus monkey, *Macaca mulatta*', *Am J Anat*, 172 (1), 41-56.
- Feldman, G. M., Heck, G. L., and Smith, N. L. (2009), 'Human Salt Taste and the Lingual Surface Potential Correlate', *Chem Senses*.
- Feldman, G. M., Mogyorósi, A., Heck, G. L., DeSimone, J. A., Santos, C. R., Clary, R. A. , and Lyall, V. (2003), 'Salt-evoked lingual surface potential in humans', *J Neurophysiol*, 90, 2060-64.
- Finger, T. E. (2005), 'Cell types and lineages in taste buds', *Chem Senses*, 30 Suppl 1, i54-5.
- Finger, T. E., Danilova, V., Barrows, J., Bartel, D. L., Vigers, A. J., Stone, L., Hellekant, G., and Kinnamon, S. C. (2005), 'ATP signaling is crucial for communication from taste buds to gustatory nerves', *Science*, 310 (5753), 1495-9.
- Flicek, P., et al. (2011), 'Ensembl 2011', *Nucleic Acids Res*, 39 (Database issue), D800-6.
- Flicek, P., et al. (2007), 'Ensembl 2008', *Nucleic Acids Res*.
- Formaker, B. K. & Hill, D. L. (1988), 'An analysis of residual NaCl taste response after amiloride', *Am J Physiol*, 255 (6 Pt 2), R1002-7.
- Formaker, B. K. & Hill, D. L. (1991), 'Lack of amiloride sensitivity in SHR and WKY glossopharyngeal taste responses to NaCl', *Physiol Behav*, 50 (4), 765-9.
- Frank, M. E. (1991), 'Taste-responsive neurons of the glossopharyngeal nerve of the rat', *J Neurophysiol*, 65 (6), 1452-63.
- Frost, C. D., Law, M. R., and Wald, N. J. (1991), 'By how much does dietary salt reduction lower blood pressure? II--Analysis of observational data within populations', *Bmj*, 302 (6780), 815-8.
- Galindo, M. M., Voigt, N., Stein, J., van Lengerich, J., Raguse, J. D., Hofmann, T., Meyerhof, W., and Behrens, M. (2011), 'G Protein-Coupled Receptors in Human Fat Taste Perception', *Chem Senses*.
- Gao, N., Lu, M., Echeverri, F., Laita, B., Kalabat, D., Williams, M. E., Hevezi, P., Zlotnik, A., and Moyer, B. D. (2009), 'Voltage-gated sodium channels in taste bud cells', *BMC Neurosci*, 10, 20.
- Garty, H. (1994), 'Molecular properties of epithelial, amiloride-blockable Na⁺ channels', *Faseb J*, 8 (8), 522-8.

- Geran, L. C. & Spector, A. C. (2007)**, 'Amiloride-insensitive units of the chorda tympani nerve are necessary for normal ammonium chloride detectability in the rat', *Behav Neurosci*, 121 (4), 779-85.
- Gifford, R. & Tristem, M. (2003)**, 'The evolution, distribution and diversity of endogenous retroviruses', *Virus Genes*, 26 (3), 291-315.
- Gilbertson, T. A. (1993)**, 'The physiology of vertebrate taste reception', *Curr Opin Neurobiol*, 3 (4), 532-9.
- Gilbertson, T. A. & Margolskee, R. F. (2003)**, 'Molecular physiology of gustatory transduction', in Doty, R. L. (ed.), *Handbook of olfaction and gustation* (2 edn.; New York, Basel: Dekker), 707-30.
- Gilbertson, T. A., Avenet, P., Kinnamon, S. C., and Roper, S. D. (1992)**, 'Proton currents through amiloride-sensitive Na channels in hamster taste cells. Role in acid transduction', *J Gen Physiol*, 100 (5), 803-24.
- Giraldez, T., Afonso-Oramas, D., Cruz-Muros, I., Garcia-Marin, V., Pagel, P., Gonzalez-Hernandez, T., and Alvarez de la Rosa, D. (2007)**, 'Cloning and functional expression of a new epithelial sodium channel delta subunit isoform differentially expressed in neurons of the human and monkey telencephalon', *J Neurochem*, 102 (4), 1304-15.
- Graber, J. H., Cantor, C. R., Mohr, S. C., and Smith, T. F. (1999)**, 'In silico detection of control signals: mRNA 3'-end-processing sequences in diverse species', *Proc Natl Acad Sci U S A*, 96 (24), 14055-60.
- Graham, K. M., Ko, C., Park, K. S., Sarge, K., and Park-Sarge, O. K. (2000)**, 'Expression of an intracisternal A-particle-like element in rat ovary', *Biochem Biophys Res Commun*, 278 (1), 48-57.
- Guth, L. (1957)**, 'The effects of glossopharyngeal nerve transection on the circumvallate papilla of the rat', *Anat Rec*, 128 (4), 715-31.
- Hager, H., Kwon, T.-H., Vinnikova, A. K., Masilamani, S., Brooks, H. L., Frokiaer, J., Knepper, M. A., and Nielsen, S. (2001)**, 'Immunocytochemical and immunoelectron microscopic localization of alpha-, beta- and gamma-ENaC in rat kidney', *Am J Physiol Renal Physiol*, 280, F1093-F1106.
- Halpern, B. P. (1998)**, 'Amiloride and vertebrate gustatory responses to NaCl', *Neurosci Biobehav Rev*, 23 (1), 5-47.
- Halpern, B. P. & Darlington, R. B. (1998)**, 'Effects of amiloride on gustatory quality descriptions and temporal patterns produced by NaCl', *Chem Senses*, 23 (5), 501-11.
- Hawley, R. G., Shulman, M. J., and Hozumi, N. (1984)**, 'Transposition of two different intracisternal A particle elements into an immunoglobulin kappa-chain gene', *Mol Cell Biol*, 4 (12), 2565-72.
- Heck, G. L., Mierson, S., and DeSimone, J. A. (1984)**, 'Salt taste transduction occurs through an amiloride-sensitive sodium transport pathway', *Science*, 223 (4634), 403-5.
- Hellekant, G., Ninomiya, Y., and Danilova, V. (1997a)**, 'Taste in chimpanzees II: single chorda tympani fibers', *Physiol Behav*, 61 (6), 829-41.
- Hellekant, G., Danilova, V., and Ninomiya, Y. (1997b)**, 'Primate sense of taste: behavioral and single chorda tympani and glossopharyngeal nerve fiber recordings in the rhesus monkey, *Macaca mulatta*', *J Neurophysiol*, 77 (2), 978-93.
- Hernandez-Gonzalez, E. O., Sosnik, J., Edwards, J., Acevedo, J. J., Mendoza-Lujambio, I., Lopez-Gonzalez, I., Demarco, I., Wertheimer, E., Darszon, A., and Visconti, P. E. (2006)**, 'Sodium and epithelial sodium channels participate in the regulation of the capacitation-associated hyperpolarization in mouse sperm', *J Biol Chem*, 281 (9), 5623-33.
- Herness, S. & Zhao, F. L. (2009)**, 'The neuropeptides CCK and NPY and the changing view of cell-to-cell communication in the taste bud', *Physiol Behav*, 97 (5), 581-91.
- Hill, D. L., Formaker, B. K., and White, K. S. (1990)**, 'Perceptual characteristics of the amiloride-suppressed sodium chloride taste response in the rat', *Behav Neurosci*, 104 (5), 734-41.

- Hodgkin, A. L. & Huxley, A. F. (1952)**, 'A quantitative description of membrane current and its application to conduction and excitation in nerve', *J Physiol*, 117 (4), 500-44.
- Hoon, M. A., Adler, E., Lindemeier, J., Battey, J. F., Ryba, N. J., and Zuker, C. S. (1999)**, 'Putative mammalian taste receptors: a class of taste-specific GPCRs with distinct topographic selectivity', *Cell*, 96 (4), 541-51.
- Horie, K., Saito, E. S., Keng, V. W., Ikeda, R., Ishihara, H., and Takeda, J. (2007)**, 'Retrotransposons influence the mouse transcriptome: implication for the divergence of genetic traits', *Genetics*, 176 (2), 815-27.
- Huang, Y. A., Maruyama, Y., Stimac, R., and Roper, S. D. (2008)**, 'Presynaptic (Type III) cells in mouse taste buds sense sour (acid) taste', *J Physiol*, 586 (Pt 12), 2903-12.
- Huang, Y. J., Maruyama, Y., Dvoryanchikov, G., Pereira, E., Chaudhari, N., and Roper, S. D. (2007)**, 'The role of pannexin 1 hemichannels in ATP release and cell-cell communication in mouse taste buds', *Proc Natl Acad Sci U S A*, 104 (15), 6436-41.
- Hubbard, T. J., et al. (2009)**, 'Ensembl 2009', *Nucleic Acids Res*, 37 (Database issue), D690-7.
- Hummler, E., Barker, P., Gatzky, J., Beermann, F., Verdumo, C., Schmidt, A., Boucher, R., and Rossier, B. C. (1996)**, 'Early death due to defective neonatal lung liquid clearance in aENaC-deficient mice', *Nature Genetics*, 12, 325-28.
- Huque, T., Wysocki, L., Bayley, D., Breslin, P. A., Spielman, A., and Brand, J. (2002)**, 'Expression of epithelial sodium channels (ENaCs) in human fungiform papillae', *24. Meeting of AChemS*.
- Huque, T., Cowart, B. J., Dankulich-Nagrudny, L., Pribitkin, E. A., Bayley, D. L., Spielman, A. I., Feldman, R. S., Mackler, S. A., and Brand, J. G. (2009)**, 'Sour ageusia in two individuals implicates ion channels of the ASIC and PKD families in human sour taste perception at the anterior tongue', *PLoS One*, 4 (10), e7347.
- Intersalt (1988)**, 'An international study of electrolyte excretion and blood pressure. Results for 24 hour urinary sodium and potassium excretion. Intersalt Cooperative Research Group', *Bmj*, 297 (6644), 319-28.
- Ismailov, II, Berdiev, B. K., Shlyonsky, V. G., and Benos, D. J. (1997)**, 'Mechanosensitivity of an epithelial Na⁺ channel in planar lipid bilayers: release from Ca²⁺ block', *Biophys J*, 72 (3), 1182-92.
- Jahnke, K. & Baur, P. (1979)**, 'Freeze-fracture study of taste bud pores in the foliate papillae of the rabbit', *Cell Tissue Res*, 200 (2), 245-56.
- Jang, H. J., Kokrashvili, Z., Theodorakis, M. J., Carlson, O. D., Kim, B. J., Zhou, J., Kim, H. H., Xu, X., Chan, S. L., Juhaszova, M., Bernier, M., Mosinger, B., Margolskee, R. F., and Egan, J. M. (2007)**, 'Gut-expressed gustducin and taste receptors regulate secretion of glucagon-like peptide-1', *Proc Natl Acad Sci U S A*, 104 (38), 15069-74.
- Jensen, D. (1980)**, *The principles of physiology* (2nd edn.; New York: Appleton-Century-Crofts).
- Ji, H.-L., Bishop, L. R., Anderson, S. J., Fuller, C. M., and Benos, D. J. (2004)**, 'The role of pre-H2 domains of alpha- and delta-epithelial Na channels in ion permeation, conductance, and amiloride sensitivity', *J Biol Chem*, 279 (9), 8428-40.
- Ji, H.-L. & Benos, D. J. (2004)**, 'Degenerin sites mediate proton activation of deltabetagamma-epithelial sodium channel', *J Biol Chem*, 279 (26), 26939-47.
- Ji, H. L., Su, X. F., Kedar, S., Li, J., Barbry, P., Smith, P. R., Matalon, S., and Benos, D. J. (2006)**, 'Delta-subunit confers novel biophysical features to abg-human epithelial sodium channel (ENaC) via a physiological interaction', *J Biol Chem*, 281 (12), 8233-41.
- Jurka, J., Kapitonov, V. V., Pavlicek, A., Klonowski, P., Kohany, O., and Walichiewicz, J. (2005)**, 'Rebase Update, a database of eukaryotic repetitive elements', *Cytogenet Genome Res*, 110 (1-4), 462-7.
- Kazazian, H. H., Jr. (2004)**, 'Mobile elements: drivers of genome evolution', *Science*, 303 (5664), 1626-32.

- Kellenberger, S., Hoffmann-Pochon, N., Gautschi, I., Schneeberger, E., and Schild, L. (1999), 'On the molecular basis of ion permeation in the epithelial Na⁺ channel', *J Gen Physiol*, 114 (1), 13-30.
- Kellenberger, S. & Schild, L. (2002), 'Epithelial sodium channel/degenerin family of ion channels: a variety of functions for a shared structure', *Physiol Rev*, 82, 735-67.
- Khan, N. A. & Besnard, P. (2009), 'Oro-sensory perception of dietary lipids: New insights into the fat taste transduction', *Biochim Biophys Acta*.
- Kitada, Y., Mitoh, Y., and Hill, D. L. (1998), 'Salt taste responses of the IXth nerve in Sprague-Dawley rats: lack of sensitivity to amiloride', *Physiol Behav*, 63 (5), 945-9.
- Kitada, Y., Okuda-Akabane, K., and Mitoh, Y. (2001), 'Effects of amiloride on gustatory neural responses to salts in the frog', *Chem Senses*, 26 (9), 1203-10.
- Kretz, O., Barbry, P., Bock, R. , and Lindemann, B. (1999), 'Differential expression of RNA and protein of the three pore-forming subunits of the amiloride-sensitive epithelial sodium channel in taste buds of the rat', *J Histochem Cytochem*, 47 (1), 51-64.
- Kuff, E. L. & Lueders, K. K. (1988), 'The intracisternal A-particle gene family: structure and functional aspects', *Adv Cancer Res*, 51, 183-276.
- Lalonde, E. R. & Eglitis, J. A. (1961), 'Number and distribution of taste buds on the epiglottis, pharynx, larynx, soft palate and uvula in a human newborn', *Anat Rec*, 140, 91-5.
- Law, M. R., Frost, C. D., and Wald, N. J. (1991a), 'By how much does dietary salt reduction lower blood pressure? III--Analysis of data from trials of salt reduction', *Bmj*, 302 (6780), 819-24.
- Law, M. R., Frost, C. D., and Wald, N. J. (1991b), 'By how much does dietary salt reduction lower blood pressure? I--Analysis of observational data among populations', *Bmj*, 302 (6780), 811-5.
- Lawes, C. M., Rodgers, A., Bennett, D. A., Parag, V., Suh, I., Ueshima, H., and MacMahon, S. (2003), 'Blood pressure and cardiovascular disease in the Asia Pacific region', *J Hypertens*, 21 (4), 707-16.
- Lawton, D. M., Furness, D. N., Lindemann, B., and Hackney, C. M. (2000), 'Localization of the glutamate-aspartate transporter, GLAST, in rat taste buds', *Eur J Neurosci*, 12 (9), 3163-71.
- Liddell, R. A., Hirano, M. C., and Mock, B. A. (1999), 'Mouse chromosome 4', *Mamm Genome*, 10 (10), 943.
- Lin, W., Finger, T. E., Rossier, B. C., and Kinnamon, S. C. (1999), 'Epithelial Na⁺ channel subunits in rat taste cells: localization and regulation by aldosterone', *J Comp Neurol*, 405, 406-20.
- Lindemann, B. (1996), 'Taste reception', *Physiol Rev*, 76 (3), 718-66.
- Lindemann, B. (2001), 'Receptors and transduction in taste', *Nature*, 413, 219-25.
- Lingueglia, E., Voilley, N., Lazdunski, M., and Barbry, P. (1996), 'Molecular biology of the amiloride-sensitive epithelial Na⁺ channel', *Exp Physiol*, 81 (3), 483-92.
- Lingueglia, E., Voilley, N., Waldmann, R., Lazdunski, M., and Barbry, P. (1993), 'Expression cloning of an epithelial amiloride-sensitive Na⁺ channel. A new channel type with homologies to *Caenorhabditis elegans* degenerins', *FEBS Lett*, 318 (1), 95-9.
- Lingueglia, E., Renard, S., Waldmann, R., Voilley, N., Champigny, G., Plass, H., Lazdunski, M. , and Barbry, P. (1994), 'Different homologous subunits of the amiloride-sensitive Na⁺ channel are differently regulated by aldosterone', *J Biol Chem*, 269, 13736-39.
- Liu, D., Brockman, J. M., Dass, B., Hutchins, L. N., Singh, P., McCarrey, J. R., MacDonald, C. C., and Graber, J. H. (2007), 'Systematic variation in mRNA 3'-processing signals during mouse spermatogenesis', *Nucleic Acids Res*, 35 (1), 234-46.
- Lueders, K. K. & Kuff, E. L. (1983), 'Comparison of the sequence organization of related retrovirus-like multigene families in three evolutionarily distant rodent genomes', *Nucleic Acids Res*, 11 (13), 4391-408.
- Lyall, V., Heck, G. L., Vinnikova, A. K., Ghosh, S., Phan, T.-H. P., Alam, R. I., Russell, O. F., Malik, S. A., Bigbee, J. W., and DeSimone, J. A. (2004), 'The mammalian amiloride-

- insensitive non-specific salt taste receptor is a vanilloid receptor-1 variant', *J Physiol*, 558, 147-59.
- Mager, D. L. & Freeman, J. D. (2000)**, 'Novel mouse type D endogenous proviruses and ETn elements share long terminal repeat and internal sequences', *J Virol*, 74 (16), 7221-9.
- Mahnensmith, R. L. & Aronson, P. S. (1985)**, 'The plasma membrane sodium-hydrogen exchanger and its role in physiological and pathophysiological processes', *Circ Res*, 56 (6), 773-88.
- Maksakova, I. A., Romanish, M. T., Gagnier, L., Dunn, C. A., van de Lagemaat, L. N., and Mager, D. L. (2006)**, 'Retroviral elements and their hosts: insertional mutagenesis in the mouse germ line', *PLoS Genet*, 2 (1), e2.
- Margolskee, R. F. (2002)**, 'Molecular mechanisms of bitter and sweet taste transduction', *J Biol Chem*, 277 (1), 1-4.
- Margolskee, R. F., Dyer, J., Kokrashvili, Z., Salmon, K. S., Ilegems, E., Daly, K., Maillet, E. L., Ninomiya, Y., Mosinger, B., and Shirazi-Beechey, S. P. (2007)**, 'T1R3 and gustducin in gut sense sugars to regulate expression of Na⁺-glucose cotransporter 1', *Proc Natl Acad Sci U S A*, 104 (38), 15075-80.
- McDonald, F. J., Snyder, P. M., McCray, P. B., Jr., and Welsh, M. J. (1994)**, 'Cloning, expression, and tissue distribution of a human amiloride-sensitive Na⁺ channel', *Am J Physiol*, 266 (6 Pt 1), L728-34.
- McDonald, F. J., Price, M. P., Snyder, P. M., and Welsh, M. J. (1995)**, 'Cloning and expression of the beta- and gamma-subunits of the human epithelial sodium channel', *Am J Physiol*, 268 (5 Pt 1), C1157-63.
- Medler, K. F., Margolskee, R. F., and Kinnamon, S. C. (2003)**, 'Electrophysiological characterization of voltage-gated currents in defined taste cell types of mice', *J Neurosci*, 23 (7), 2608-17.
- Merillat, A. M., Charles, R. P., Porret, A., Maillard, M., Rossier, B., Beermann, F., and Hummler, E. (2009)**, 'Conditional gene targeting of the ENaC subunit genes Scnn1b and Scnn1g', *Am J Physiol Renal Physiol*, 296 (2), F249-56.
- Michlig, S., Damak, S., and Le Coutre, J. (2007)**, 'Claudin-based permeability barriers in taste buds', *J Comp Neurol*, 502 (6), 1003-11.
- Mierson, S., Olson, M. M., and Tietz, A. E. (1996)**, 'Basolateral amiloride-sensitive Na⁺ transport pathway in rat tongue epithelium', *J Neurophysiol*, 76 (2), 1297-309.
- Miller, I. J., Jr. & Reedy, F. E., Jr. (1990a)**, 'Quantification of fungiform papillae and taste pores in living human subjects.' *Chem Senses*, 15 (3), 281-94.
- Miller, I. J., Jr. & Reedy, F. E., Jr. (1990b)**, 'Variations in human taste bud density and taste intensity perception', *Physiol Behav*, 47 (6), 1213-9.
- Mochizuki, Y. (1939)**, 'Studies on the papilla foliata of Japanese.' *Okajimas Folia Anat. Jpn.*, 18, 334-69.
- Moorman, J. R., Ackerman, S. J., Kowdley, G. C., Griffin, M. P., Mounsey, J. P., Chen, Z., Cala, S. E., O'Brian, J. J., Szabo, G., and Jones, L. R. (1995)**, 'Unitary anion currents through phospholemman channel molecules', *Nature*, 377 (6551), 737-40.
- Morris, M. J., Na, E. S., and Johnson, A. K. (2008)**, 'Salt craving: the psychobiology of pathogenic sodium intake', *Physiol Behav*, 94 (5), 709-21.
- Mueller, K. L., Hoon, M. A., Erlenbach, I., Chandrashekar, J., Zuker, C. S., and Ryba, N. J. (2005)**, 'The receptors and coding logic for bitter taste', *Nature*, 434 (7030), 225-9.
- Munch, F. (1896)**, 'Die Topographie der Papillen der Zunge des Menschen und der Säugethiere.' *Morph. Arbeit*, 6, 605-84.
- Murphy, C., Cardello, A. V., and Brand, J. (1981)**, 'Tastes of fifteen halide salts following water and NaCl: anion and cation effects', *Physiol Behav*, 26 (6), 1083-95.
- Murray, R. G. (1973)**, 'The ultrastructure of taste buds', in Friedman, I. (ed.), *The ultrastructure of sensory organs* (North Holland, Amsterdam), 1-81.

- Murray, R. G., Murray, A. , and Fujimoto, S. (1969)**, 'Fine structure of gustatory cells in rabbit taste buds', *J Ultrastruct Res*, 27 (5), 444-61.
- Nakano, H. & Gunn, M. D. (2001)**, 'Gene duplications at the chemokine locus on mouse chromosome 4: multiple strain-specific haplotypes and the deletion of secondary lymphoid-organ chemokine and EBI-1 ligand chemokine genes in the plt mutation', *J Immunol*, 166 (1), 361-9.
- Nelson, G., Hoon, M. A., Chandrashekar, J., Zhang, Y., Ryba, N. J. P., and Zuker, C. S. (2001)**, 'Mammalian sweet taste receptors', *Cell*, 106, 381-90.
- Nelson, G. M. & Finger, T. E. (1993)**, 'Immunolocalization of different forms of neural cell adhesion molecule (NCAM) in rat taste buds', *J Comp Neurol*, 336 (4), 507-16.
- Nicholas, K. B., Nicholas, H. B. Jr., and Deerfield, D. W. (1997)**, 'GeneDoc: Analysis and Visualization of Genetic Variation', *EMBNEW.NEWS*, 4 (14).
- Nie, H. G., Tucker, T., Su, X. F., Na, T., Peng, J. B., Smith, P. R., Idell, S., and Ji, H. L. (2009)**, 'Expression and regulation of epithelial Na⁺ channels by nucleotides in pleural mesothelial cells', *Am J Respir Cell Mol Biol*, 40 (5), 543-54.
- O'Shaughnessy, K. M. & Karet, F. E. (2006)**, 'Salt handling and hypertension', *Annu Rev Nutr*, 26, 343-65.
- Oakley, B. (1970)**, 'Reformation of taste buds by crossed sensory nerves in the rat's tongue', *Acta Physiol Scand*, 79 (1), 88-94.
- Oakley, B., Lawton, A., Riddle, D. R., and Wu, L. H. (1993)**, 'Morphometric and immunocytochemical assessment of fungiform taste buds after interruption of the chordal-lingual nerve', *Microsc Res Tech*, 26 (3), 187-95.
- Ossebaard, C. A. & Smith, D. V. (1995)**, 'Effect of amiloride on the taste of NaCl, Na-gluconate and KCl in humans: implications for Na⁺ receptor mechanisms', *Chem Senses*, 20 (1), 37-46.
- Paran, N., Mattern, C. E., and Henkin, R. I. (1975)**, 'Ultrastructure of the taste bud of the human fungiform papilla', *Cell Tissue Res*, 161 (1), 1-10.
- Perty, M. (1838)**, *Allgemeine Naturgeschichte* (2; Bern: Fischer).
- Peter, B., Man, Y. M., Begg, C. E., Gall, I., and Leader, D. P. (1988)**, 'Mouse cytoskeletal gamma-actin: analysis and implications of the structure of cloned cDNA and processed pseudogenes', *J Mol Biol*, 203 (3), 665-75.
- Prospective study (1995)**, 'Cholesterol, diastolic blood pressure, and stroke: 13,000 strokes in 450,000 people in 45 prospective cohorts. Prospective studies collaboration', *Lancet*, 346 (8991-8992), 1647-53.
- Rapoport, S. I. (1970)**, 'The sodium-potassium exchange pump: relation of metabolism to electrical properties of the cell. I. Theory', *Biophys J*, 10 (3), 246-59.
- Rapoport, S. I. (1971)**, 'The sodium-potassium exchange pump. II. Analysis of Na⁺ -loaded frog sartorius muscle', *Biophys J*, 11 (8), 631-47.
- Rasband, W.S. (1997-2005)**, 'ImageJ', *National Institutes of Health* (version 1.42q edn.; Bethesda, Maryland, USA), <http://rsb.info.nih.gov/ij/>.
- Reutter, K. & Witt, M. (1993)**, 'Morphology of vertebrate taste organs and their nerve supply', in Simon, S. A. & Roper, S. D. (eds.), *Mechanisms of taste transduction* (Boca Raton: CRC Press), 29-82.
- Ribet, D., Dewannieux, M., and Heidmann, T. (2004)**, 'An active murine transposon family pair: retrotransposition of "master" MusD copies and ETn trans-mobilization', *Genome Res*, 14 (11), 2261-7.
- Ribet, D., Harper, F., Dewannieux, M., Pierron, G., and Heidmann, T. (2007)**, 'Murine MusD retrotransposon: structure and molecular evolution of an "intracellularized" retrovirus', *J Virol*, 81 (4), 1888-98.
- Riva, A., Loffredo, F., Puxeddu, R., and Testa Riva, F. (1999)**, 'A scanning and transmission electron microscope study of the human minor salivary glands', *Arch Oral Biol*, 44 Suppl 1, S27-31.

- Rodgers, A., Vaughan, P., Prentice, T., Tan-Torres Edejer, T., Evans, D., and Lowe, J. (2002), *World health report*, eds Campanini, B. & Haden, A. (Geneva, Switzerland: World Health Organization).
- Romanov, R. A., Rogachevskaja, O. A., Bystrova, M. F., Jiang, P., Margolskee, R. F., and Kolesnikov, S. S. (2007), 'Afferent neurotransmission mediated by hemichannels in mammalian taste cells', *Embo J*, 26 (3), 657-67.
- Roper, S. D. (2007), 'Signal transduction and information processing in mammalian taste buds', *Pflugers Arch*, 454 (5), 759-76.
- Rossier, B. C., Pradervand, S., Schild, L., and Hummler, E. (2002), 'Epithelial sodium channel and the control of sodium balance: interaction between genetic and environmental factors', *Annu Rev Physiol*, 64, 877-97.
- Rossier, O., Cao, J., Huque, T., Spielman, A. I., Feldman, R. S., Medrano, J. F., Brand, J. G., and le Coutre, J. (2004), 'Analysis of a human fungiform papillae cDNA library and identification of taste-related genes', *Chem Senses*, 29, 13-23.
- Royer, S. M. & Kinnamon, J. C. (1991), 'HVEM serial-section analysis of rabbit foliate taste buds: I. Type III cells and their synapses', *J Comp Neurol*, 306 (1), 49-72.
- Rozen, S. & Skaletsky, H. J. (2000), 'Primer3 on the WWW for general users and for biologist programmers', in Krawetz, S. & Misener, S. (eds.), *Bioinformatics Methods and Protocols: Methods in Molecular Biology* (version 0.4.0; edn.; Totowa, NJ: Humana Press), pp 365-86.
- Rozengurt, E. & Sternini, C. (2007), 'Taste receptor signaling in the mammalian gut', *Curr Opin Pharmacol*, 7 (6), 557-62.
- Ruiz, C., Gutknecht, S., Delay, E., and Kinnamon, S. (2006), 'Detection of NaCl and KCl in TRPV1 knockout mice', *Chem Senses*, 31 (9), 813-20.
- Sastre-Garau, X., Favre, M., Couturier, J., and Orth, G. (2000), 'Distinct patterns of alteration of myc genes associated with integration of human papillomavirus type 16 or type 45 DNA in two genital tumours', *J Gen Virol*, 81 (Pt 8), 1983-93.
- Sato, M., Ogawa, H., and Yamashita, S. (1975), 'Response properties of macaque monkey chorda tympani fibers', *J Gen Physiol*, 66 (6), 781-810.
- Sayers, E. W., et al. (2011), 'Database resources of the National Center for Biotechnology Information', *Nucleic Acids Res*, 39 (Database issue), D38-51.
- Schagger, H. (2006), 'Tricine-SDS-PAGE', *Nat Protoc*, 1 (1), 16-22.
- Schiffman, S. S., Lockhead, E. , and Maes, F. W. (1983), 'Amiloride reduces the taste intensity of Na⁺ and Li⁺ salts and sweeteners', *Proc Natl Acad Sci U S A*, 80, 6136-40.
- Schuster, H.-P., Pop, T. , and Weilemann, L. S. (1990), *Checklist intensive care medicine*, eds Sturm, A., Lergiadèr, F., and Wicki, O. (Medical Checklists; New York: Thieme Medical Publishers).
- Shah, A. S., Ben-Shahar, Y., Moninger, T. O., Kline, J. N., and Welsh, M. J. (2009), 'Motile cilia of human airway epithelia are chemosensory', *Science*, 325 (5944), 1131-4.
- Shigemura, N., Islam, A. A. S., Sadamitsu, C., Yoshida, R., Yasumatsu, K. , and Ninomiya, Y. (2005), 'Expression of amiloride-sensitive epithelial sodium channels in mouse taste cells after chorda tympani nerve crush', *Chem Senses*, 30, 531-38.
- Simchowicz, L. & Roos, A. (1985), 'Regulation of intracellular pH in human neutrophils', *J Gen Physiol*, 85 (3), 443-70.
- Simon, S. A. (1992), 'Influence of tight junctions on the interaction of salts with lingual epithelia: responses of chorda tympani and lingual nerves', *Mol Cell Biochem*, 114 (1-2), 43-8.
- Smit, A.F.A. , Hubley, R., and Green, P. (2010), 'RepeatMasker Open-3.0', <<http://repeatmasker.org>>.
- Sollars, S. I. & Bernstein, I. L. (1994), 'Amiloride sensitivity in the neonatal rat', *Behav Neurosci*, 108 (5), 981-7.
- Sonigo, P., Wain-Hobson, S., Bougueleret, L., Tiollais, P., Jacob, F., and Brulet, P. (1987), 'Nucleotide sequence and evolution of ETn elements', *Proc Natl Acad Sci U S A*, 84 (11), 3768-71.

- Spector, A. C., Guagliardo, N. A., and St. John, S. J. (1996)**, 'Amiloride disrupts NaCl versus KCl discrimination performance: implications for salt taste coding in rats', *J Neurosci*, 16 (24), 8115-22.
- Spielman, A. I. (1990)**, 'Interaction of saliva and taste', *J Dent Res*, 69 (3), 838-43.
- St John, S. J. & Hallagan, L. D. (2005)**, 'Psychophysical investigations of cetylpyridinium chloride in rats: its inherent taste and modifying effects on salt taste', *Behav Neurosci*, 119 (1), 265-79.
- Stähler, F., Riedel, K., Demgensky, S., Neumann, K., Dunkel, A., Täubert, A., Raab, B., Behrens, M., Raguse, J.-D., Hofman, T., and Meyerhof, W. (2008)**, 'A role of the epithelial sodium channel in human salt taste transduction?' *Chem Percept*.
- Tamura, K., Dudley, J., Nei, M., and Kumar, S. (2007)**, 'MEGA4: Molecular Evolutionary Genetics Analysis (MEGA) software version 4.0', *Mol Biol Evol*, 24 (8), 1596-9.
- Tomchik, S. M., Berg, S., Kim, J. W., Chaudhari, N., and Roper, S. D. (2007)**, 'Breadth of tuning and taste coding in mammalian taste buds', *J Neurosci*, 27 (40), 10840-8.
- van der Klaauw, N. J. & Smith, D. V. (1995)**, 'Taste quality profiles for fifteen organic and inorganic salts', *Physiol Behav*, 58 (2), 295-306.
- Vandenbeuch, A., Clapp, T. R., and Kinnamon, S. C. (2008)**, 'Amiloride-sensitive channels in type I fungiform taste cells in mouse', *BMC Neurosci*, 9, 1.
- Vanin, E. F. (1985)**, 'Processed pseudogenes: characteristics and evolution', *Annu Rev Genet*, 19, 253-72.
- Voilley, N., Lingueglia, E., Champigny, G., Mattei, M. G., Waldmann, R., Lazdunski, M., and Barbry, P. (1994)**, 'The lung amiloride-sensitive Na⁺ channel: biophysical properties, pharmacology, ontogenesis, and molecular cloning', *Proc Natl Acad Sci U S A*, 91 (1), 247-51.
- von Skramlik, E. (1933)**, 'Physiologie des Geschmacksinnes', in von Bethge, A. & von Bergmann, G. (eds.), *Handbuch der normalen und pathologischen Physiologie* (18; Berlin: Springer), 285.
- Waldmann, R., Champigny, G., Bassilana, F., Voilley, N., and Lazdunski, M. (1995)**, 'Molecular cloning and functional expression of a novel amiloride-sensitive Na⁺ channel', *J Biol Chem*, 270 (46), 27411-14.
- Wang, X., Gao, G., Guo, K., Yarotsky, V., Huang, C., Elmslie, K. S., and Peterson, B. Z. (2010)**, 'Phospholemman modulates the gating of cardiac L-type calcium channels', *Biophys J*, 98 (7), 1149-59.
- Weinberger, M. H. (1996)**, 'Salt sensitivity of blood pressure in humans', *Hypertension*, 27, 481-90.
- Wheeler, D. L., et al. (2008)**, 'Database resources of the National Center for Biotechnology Information', *Nucleic Acids Res*, 36 (Database issue), D13-21.
- Whitehead, M. C., Frank, M. E., Hettinger, T. P., Hou, L. T., and Nah, H. D. (1987)**, 'Persistence of taste buds in denervated fungiform papillae', *Brain Res*, 405 (1), 192-5.
- WHO/FAO (2003)**, 'Diet, nutrition and the prevention of chronic diseases', *World Health Organ Tech Rep Ser*, 916, i-viii, 1-149, backcover.
- Wicker, T., Sabot, F., Hua-Van, A., Bennetzen, J. L., Capy, P., Chalhoub, B., Flavell, A., Leroy, P., Morgante, M., Panaud, O., Paux, E., SanMiguel, P., and Schulman, A. H. (2007)**, 'A unified classification system for eukaryotic transposable elements', *Nat Rev Genet*, 8 (12), 973-82.
- Witt, M., Reutter, K., and Miller, I. J. (2003)**, 'Morphology of the peripheral taste system', in Doty, R. L. (ed.), *Handbook of olfaction and gustation* (2 edn.; New York, Basel: Dekker), 651-77.
- Yamamura, H., Ugawa, S., Ueda, T., Nagao, M., and Shimada, S. (2004)**, 'Protons activate the delta-subunit of the epithelial Na⁺ channel in humans', *J Biol Chem*, 279 (13), 12529-34.
- Yamamura, H., Ugawa, S., Ueda, T., Nagao, M., and Shimada, S. (2008a)**, 'Epithelial Na⁽⁺⁾ channel delta subunit mediates acid-induced ATP release in the human skin', *Biochem Biophys Res Commun*.
- Yamamura, H., Ugawa, S., Ueda, T., Nagao, M., Joh, T., and Shimada, S. (2008b)**, 'Epithelial Na⁺ channel delta subunit is an acid sensor in the human oesophagus', *Eur J Pharmacol*, 600 (1-3), 32-6.

- Ye, Q., Heck, G. L., and DeSimone, J. A. (1991)**, 'The anion paradox in sodium taste reception: resolution by voltage-clamp studies', *Science*, 254 (5032), 724-6.
- Ye, Q., Heck, G. L., and DeSimone, J. A. (1993)**, 'Voltage dependence of the rat chorda tympani response to Na⁺ salts: implications for the functional organization of taste receptor cells', *J Neurophysiol*, 70 (1), 167-78.
- Ye, Q., Heck, G. L., and DeSimone, J. A. (1994)**, 'Effects of voltage perturbation of the lingual receptive field on chorda tympani responses to Na⁺ and K⁺ salts in the rat: implications for gustatory transduction', *J Gen Physiol*, 104 (5), 885-907.
- Yoshida, R., Horio, N., Murata, Y., Yasumatsu, K., Shigemura, N., and Ninomiya, Y. (2009a)**, 'NaCl responsive taste cells in the mouse fungiform taste buds', *Neuroscience*, 159 (2), 795-803.
- Yoshida, R., Miyauchi, A., Yasuo, T., Jyotaki, M., Murata, Y., Yasumatsu, K., Shigemura, N., Yanagawa, Y., Obata, K., Ueno, H., Margolskee, R. E., and Ninomiya, Y. (2009b)**, 'Discrimination of taste qualities among mouse fungiform taste bud cells', *J Physiol*.
- Zhang, Y., Maksakova, I. A., Gagnier, L., van de Lagemaat, L. N., and Mager, D. L. (2008a)**, 'Genome-wide assessments reveal extremely high levels of polymorphism of two active families of mouse endogenous retroviral elements', *PLoS Genet*, 4 (2), e1000007.
- Zhang, Y., Hoon, M. A., Chandrashekar, J., Mueller, K. L., Cook, B., Wu, D., Zuker, C. S., and Ryba, N. J. (2003)**, 'Coding of sweet, bitter, and umami tastes: different receptor cells sharing similar signaling pathways', *Cell*, 112 (3), 293-301.
- Zhang, Z. D., Cayting, P., Weinstock, G., and Gerstein, M. (2008b)**, 'Analysis of nuclear receptor pseudogenes in vertebrates: how the silent tell their stories', *Mol Biol Evol*, 25 (1), 131-43.

9 Acknowledgement/Danksagung

Ein besonderer Dank gilt Prof. Meyerhof. Er ermöglichte mir die Promotion in der Abteilung Molekulare Genetik, sowie die Fortbildung durch die Teilnahme an wissenschaftlichen Kongressen und zahlreichen Seminaren. Darüber hinaus möchte ich mich für konstruktive Diskussionen, als auch für eine stets offene Tür bedanken.

Ganz besonders möchte ich mich bei meiner Betreuerin Dr. Frauke Stähler bedanken. Sie stand mir bei fachlichen Fragen mit Rat und Tat zur Seite und war mir mit Ihrer Begeisterungsfähigkeit und Motivation immer eine große Unterstützung und Ansporn.

Stefanie Demgensky danke ich nicht nur für die Hilfe im Laboralltag, sondern auch für die Unterstützung in allen Lebenslagen. Ganz besonders werde ich die lockere Arbeitsatmosphäre innerhalb der Arbeitsgruppe vermissen für die ich mich bei Frauke, Steffi, Jessica und Jonas bedanken möchte. Darüber hinaus danke ich allen Mitarbeitern der Abteilung Molekulare Genetik für die konstruktive und nette Arbeitsatmosphäre.

Außerdem möchte ich mich bei Erwin Tareillus für die Bereitstellung, als auch bei Maik Behrens, Claudia Reichling, Sabine Schmidt und Jessica Schulz, für ihre Hilfe bei der Aufarbeitung der Makkaken cDNA Bank bedanken. Jan Dirk Raguse möchte ich für die Durchführung der Zungenbiopsien danken, sowie all den freiwilligen und tapferen Spendern.

Ein ganz großer Dank gilt meiner Familie und insbesondere Steffen für die großartige Unterstützung während meines gesamten (Promotions)-Studiums.

10 Statutory declaration/Eidesstattliche Erklärung

Statutory declaration

Herewith I declare that I wrote this thesis independently without any help of third parties and without using any other aids than stated and that I cited all references that were used respecting current academic rules.

Potsdam, 10.10.2011

Katja Riedel

Eidesstattliche Erklärung

Hiermit versichere ich, dass ich die Arbeit selbständig verfasst und keine anderen als die von mir angegebenen Quellen und Hilfsmittel benutzt habe. Die Arbeit wurde noch an keiner anderen Hochschule zur Begutachtung eingereicht.

Potsdam, den 10.10.2011

Katja Riedel